LEABHARLANN CHOLÁISTE NA TRÍONÓIDE, BAILE ÁTHA CLIATH | TRINITY COLLEGE LIBRARY DUBLIN
Ollscoil Átha Cliath | The University of Dublin

Terms and Conditions of Use of Digitised Theses from Trinity College Library Dublin

Copyright statement

All material supplied by Trinity College Library is protected by copyright (under the Copyright and Related Rights Act, 2000 as amended) and other relevant Intellectual Property Rights. By accessing and using a Digitised Thesis from Trinity College Library you acknowledge that all Intellectual Property Rights in any Works supplied are the sole and exclusive property of the copyright and/or other IPR holder. Specific copyright holders may not be explicitly identified. Use of materials from other sources within a thesis should not be construed as a claim over them.

A non-exclusive, non-transferable licence is hereby granted to those using or reproducing, in whole or in part, the material for valid purposes, providing the copyright owners are acknowledged using the normal conventions. Where specific permission to use material is required, this is identified and such permission must be sought from the copyright holder or agency cited.

Liability statement

By using a Digitised Thesis, I accept that Trinity College Dublin bears no legal responsibility for the accuracy, legality or comprehensiveness of materials contained within the thesis, and that Trinity College Dublin accepts no liability for indirect, consequential, or incidental, damages or losses arising from use of the thesis for whatever reason. Information located in a thesis may be subject to specific use constraints, details of which may not be explicitly described. It is the responsibility of potential and actual users to be aware of such constraints and to abide by them. By making use of material from a digitised thesis, you accept these copyright and disclaimer provisions. Where it is brought to the attention of Trinity College Library that there may be a breach of copyright or other restraint, it is the policy to withdraw or take down access to a thesis while the issue is being resolved.

Access Agreement

By using a Digitised Thesis from Trinity College Library you are bound by the following Terms & Conditions. Please read them carefully.

I have read and I understand the following statement: All material supplied via a Digitised Thesis from Trinity College Library is protected by copyright and other intellectual property rights, and duplication or sale of all or part of any of a thesis is not permitted, except that material may be duplicated by you for your research use or for educational purposes in electronic or print form providing the copyright owners are acknowledged using the normal conventions. You must obtain permission for any other use. Electronic or print copies may not be offered, whether for sale or otherwise to anyone. This copy has been supplied on the understanding that it is copyright material and that no quotation from the thesis may be published without proper acknowledgement.

Computational and experimental investigation of bone cell response to mechanical stimuli

by

James Gerard McGarry, B.E.

A thesis submitted to the University of Dublin in partial fulfillment of the requirements for the degree of

Doctor in Philosophy

Trinity College Dublin
September 2005

Supervisor
Prof. P.J. Prendergast
(Trinity Centre for Bioengineering)

Co-supervisor (2004-05)
Prof. S.P. Jarvis
(SFI Nanoscience Laboratory)

External supervisor (2003-04)
Prof. J. Klein-Nulend
(Vrije Universiteit Amsterdam)

External Examiner
Prof. C.R. Jacobs
(Stanford University)

Internal Examiner
Prof. B.C. O'Connell
(Trinity Centre for Bioengineering
& School of Dental Science)

TRINITY COLLEGE
15 MAY 2006
LIBRARY DUBLIN
THOS 18
7898

DECLARATION

I declare that I am the sole author of this thesis and that the work presented in it, unless otherwise referenced, is entirely my own. I also declare that the work has not been submitted, in whole or in part, to any other University as an exercise for a degree or other qualification.

I agree that the library of Trinity College Dublin may lend or copy this thesis upon request.

James G. McGarry

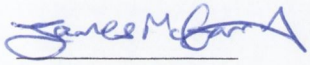

September 2005

ACKNOWLEDGEMENTS

I wish to express my sincere gratitude to my supervisor Professor Patrick Prendergast for his guidance, expertise and inspiration throughout my years at Trinity. I consider myself most fortunate to be one of the many people whom he has helped to realise their potential.

Also I would like to extend my thanks to Professor Jenneke Klein-Nulend for her unlimited support and guidance during my time at the Vrije Universiteit Medical Centre. Working with such a diverse group was a most stimulating and enjoyable experience. Many thanks to Cor, Margriet, Djien, Marlene, Agnes, Lisa, Mel, Jolanda, Aviral, Vincent, Astrid, Ilara, Hein and Chris for their hospitality and friendship.

I would also like to express my sincere appreciation to Professor Suzi Jarvis for her wealth of expertise and for welcoming me so warmly into her research group in the final year of my research at Trinity. Many thanks also to Camille, Michael, Martin, Jason, Alan, Anika and Paula – I look forward to next summer when we can all be glamorous in our Hawaiian shirts again.

The Trinity bioengineering postgraduates and staff with whom I have worked with over these past four years have been great. The camaraderie among fellow postgraduates gives a sense of unity without which one's daily research would be a more daunting pursuit. Many thanks to Kevin, Laoise, Danny, Linda, Triona, John G, John V, Adriele, John B, Alex, Victor, Guisseppe, Niamh, Conor, Oran, Orlaith, John T, Paul, Tadhg, Louise, Emma, Shane, Brianne, Leandro, Jennifer, Mary, Melanie, Luca and Richard.

The final thanks goes to my family, and in particular to my parents, for their support, generosity and encouragement throughout my college years.

CONTENTS

Abstract i

List of acronyms ii

List of figures iv

List of tables xi

Chapter 1 Introduction 1

The fundamental role of mechanical loading in maintaining bone quality throughout life is introduced. The importance of understanding the mechanisms by which the mechanoresponsive cells in bone respond to mechanical stimuli is argued.

Chapter 2 Literature Review 6

Two aspects of bone cell mechanotransduction are reviewed. The first comprises an examination of the structural significance of various organelles, together with a critique of past approaches taken in developing biomechanical models of adherent cells. Secondly, the various biochemical responses of bone cells to *in vitro* mechanical stimuli such as fluid flow, strain or indentation are reviewed.

Chapter 3 Methods 41

The development and application of a computational cell model for use as a mechanobiological tool in investigating bone cell mechanotransduction is described. The experimental methods devised to determine mechanisms of, and cytoskeleton involvement in, osteocyte and osteoblast mechanotransduction of key signalling responses are described.

Chapter 4 Results 72

The structural characteristics and corroboration of the cell model are illustrated. Cell model insights into the physical consequences of fluid flow and strain stimuli on bone cells are presented. Experimentally-determined evidence of cytoskeleton involvement in osteoblast or osteocyte nitric oxide or prostaglandin E_2 response is presented, followed by fluorescent images illustrating single osteoblast mechanotransduction of nitric oxide.

Chapter 5 Discussion 103

The significance of the result that bone cells can distinguish between mechanical stimuli depending on the magnitude of strain caused is interpreted. Based on the experimental results of this thesis and on the literature, subcellular mechanisms by which the actin or microtubule cytoskeleton may influence the signalling pathways for nitric oxide and prostaglandin E_2 response are proposed.

Chapter 6 Conclusions 129

The main results of this thesis are summarised and recommendations for further research arising from these findings are given.

References 135

Appendices 152

ABSTRACT

The importance of mechanical loading in maintaining bone quality is well illustrated by the drastic effects of its absence in, for example, microgravity, cast immobilisation or paraplegia. The mechanisms underlying adaptation of bone to mechanical loading occur on the cellular level. However, it remains unclear how a mechanical stimulus is detected by an osteoblast or an osteocyte to subsequently influence the signalling pathways that would lead to important signalling responses such as nitric oxide (NO) or prostaglandin E_2 (PGE_2) release.

The aim of this thesis is to devise both computational and experimental methods that will yield new insights into the mechanisms of mechanotransduction in bone cells. It is hypothesised that mechanically-induced osteoblast and osteocyte NO and PGE_2 response is dependent on the physical consequences of a mechanical stimulus on the cellular level, and that this mechanotransduction mechanism is mediated by the cytoskeleton.

A computational cell model was developed to serve as a mechanobiological tool to both probe the structural characteristics of cells, and to investigate the physical effects of various magnitudes of fluid flow or strain stimuli on cells. Experimental methods were devised to determine the involvement of actin and microtubule components in mechanotransduction of NO and PGE_2 in both monolayers of bone cells and in single cells.

By extending the results of the cell model to interpreting past *in vitro* experiments, it was concluded that NO and PGE_2 signalling response is dependent not only on the magnitude but also on the nature of cell deformation caused by the stimulus. Experimental results indicate that the cytoskeleton is involved in the mechanotransduction of NO and PGE_2, but differently in osteoblasts and osteocytes. The dynamics and locations of mechanically-induced synthesis and diffusion of NO response occurring in a single osteoblast when stimulated with an indenting force were also determined. Combining these results with what has been reported in literature suggests that mechanotransduction of NO occurs via actin filament regulation of eNOS localised to both caveolae and Golgi membranes. The actin cytoskeleton modulates the PGE_2 pathway in osteocytes via stretch-activated ion channels, whereas in osteoblast PGE_2 response focal adhesions may be the primary mechanosensors.

This information will strengthen the fundamental knowledge required for understanding bone diseases such as osteoporosis, for *in vitro* engineering of bone tissue and for the design of orthopaedic devices that maintain bone health in 'disuse' conditions such as microgravity.

LIST OF ACRONYMS

ADP, adenosine diphosphate;

AFM, atomic force microscopy;

cAMP, cyclic adenosine monophosphate;

CAT-1, cationic amino acid transporter-1;

cGMP, cyclic guanosine monophosphate;

COX-2, cyclooxygenase-2;

CSK, cytoskeleton;

DAF-FM, 4-amino-5-methylamino- 2′,7′ -difluorofluorescein diacetate;

DAG, diacylglycerol;

DNA, deoxyribonucleic acid;

NCP, non-collagenous protein;

EC, endothelial cell;

eNOS, endothelial nitric oxide synthase;

FBS, foetal bovine serum;

MA, micropipette aspiration;

MAPK, mitogen-activated protein kinase;

MC3T3-E1, mouse osteoblastic cell line;

MLO-Y4, murine long bone osteocyte Y4;

MM, microplate manipulation;

mRNA, messenger ribonucleic acid;

MT, microtubule;

MTC, magnetic twisting cytometry;

NCP, non-collagenous protein;

NO, nitric oxide;

OB, osteoblastic cells;

OCY, osteocytic cells;

OFF, oscillatory fluid flow;

PBS, phosphate buffered saline;

PFF, pulsatile fluid flow;

PGE_2, prostaglandin E_2

PI, propidium iodide;

PKC, protein kinase C;

PLA_2, cytosolic phospholipase A_2;

PLC, phospholipase C;

SEM, standard error of the mean;

SMC, smooth muscle cell;

TF, thermal fluctuations;

TNF, tumour necrosis factor

LIST OF FIGURES

1.1 Schematic illustration of the locations of cells in bone tissue. Adapted from www.roche.com/pages/facets/11/ostedefe.htm. **3**

1.2 Schematic of a proposed regulation process in which osteocyte sensing of strain-energy density (SED), mechanical loading and osteoclast resorption regulate bone remodelling. Adapted from Huiskes et al. (2000). **4**

2.1 Schematic illustration of the subcellular components of a typical eukaryotic cell. The intracellular material between the cell membrane and nucleus (i.e. the cytoplasm) contains organelles (including the cytoskeleton) that perform specific functions, and an intracellular liquid cytosol containing soluble nutrients, ions and proteins. Adapted from Bao and Suresh (2003). **8**

2.2 Illustration of the clustering of actin filaments during the formation of adhesion complexes (focal contacts) (A). A detailed view illustrating the structural proteins involved in adhesion bond formation with the fibronectin integrin receptor (B). Adapted from Alberts et al. (1989). **9**

2.3 Images of an adherent fibroblast immunostained for (A) focal adhesion complexes, and (B) actin filaments. Adapted from Alberts et al., 1989. **10**

2.4 Schematic of the components and structure of the cell membrane. Source: www.people.virginia.edu/~rjh9u/cellmemb.html. **12**

2.5 Overview of the elastic properties of cells relative to those of other common materials (the lower scale shows the expanded range for cells). Source: www.biophysik.uni-bremen.de/radmacher/elasticity.html. **15**

2.6 Micropipette aspiration of a chondrocyte 4 s after application of the aspiration pressure. Adapted from Trickey et al. (2004). **16**

2.7 Elasticity map of a section of an osteoblast. Elasticity (E) was calculated from the force-deflection characteristics determined at numerous points using atomic force microscopy. Adapted from Domke et al. (2000). **17**

2.8 Variation in elastic modulus with indentation for an endothelial cell. Note the decreasing stiffness with indentation depth and the dependence of elastic modulus on probe geometry, which becomes less significant at higher indentation depths. **17**

2.9 A three-dimensional model of cell manipulation by magnetocytometry, comprising a membrane/cortex and cytoskeleton both modelled as viscoelastic materials. Source: Karcher et al. (2003). **23**

2.10 Representative structural unit of the open-cell foam network devised by Satcher and Dewey (1996). **25**

2.11 Schematic representation of the percolation model of the cell cytoskeleton. Filaments that form an uninterrupted path from the membrane (outer box) to the nucleus (inner box) are denoted by heavy lines. Shaded circles represent elastic cross-linkers. Adapted from Shafrir and Forgacs (2002). **26**

2.12 A stress-supported tensegrity structure as a representative unit of the cytoskeleton. The grey struts in three orthogonal pairs represent microtubules, while the thinner lines represent actin filaments. Adapted from Stamenovic et al. (1996). **27**

2.13 Apparatus designed to apply longitudinal strains through the substrate to which cells adhere, by (a) uniaxial distension (b) four point bending apparatus. Adapted from Brown (2000). **33**

2.14 Schematic of the parallel plate flow chamber. Adapted from Burger et al. (1998). **35**

2.15 Effect of cyclic strain (CS) and pulsatile fluid flow (PFF) on prostaglandin E_2 (PGE_2) and nitric oxide (NO) release by human bone cells in vitro. Both NO and PGE_2 were significantly increased relative to controls after 60 minutes PFF. Also, collagen type I was increased ~1.6-fold in the CS group, but decreased ~0.6-fold by PFF, as measured after 24 hours of post-incubation (result not shown). Adapted from Mullender et al. (2004). **37**

2.16 Schematic illustration of the principal and components of an atomic force microscope (AFM). The deflection of the AFM cantilever tip (as measured by photodiode detection of laser position) on contact with a sample (such as an adherent cell) is controlled with sub-micron precision by movement of the z-direction piezo. Sample position can be controlled by precise movement of the x-y piezo stage. Adapted from www.asylumresearch.com/Applications /AfmFluo/AfmFluo.pdf **38**

3.1 Images of a spreading chick embryo fibroblast adherent on a glass microplate for (A) 5 minutes, and (B) after 3 hours. The dimensions of the finite element models developed (Table 1) correspond to contact angles (θ) and contact radii (R) highlighted in (B). Adapted from Frisch and Thoumine (1999). **45**

3.2 Three-dimensional computational biomechanical model of an adherent cell. The cell model comprises nucleus (in green), microfilament (blue lines), microtubule (red lines), cytoplasm (internal transparent elements) and membrane (dark blue) components. Half of the cytoplasm and membrane components are omitted for clarity. Cell model dimensions (contact radius, 19.2 μm; height, 7.6 μm) are based on the radius (R) and contact angle (θ) highlighted in Fig. 3.1 and model volume is ~3,000 μm^3. **46**

3.3 A three-dimensional tensegrity network of six compression-bearing struts (two in each orthogonal direction) representing the aggregate behaviour of microtubules (dark lines), surrounded by and connected with 24 tensional cables representing actin

filaments (light lines). The internal cytoskeleton in the cell model (Fig. 3.3) is arrived at by altering the lengths and positioning of the microtubule and actin filament components in order to fit the cytoskeletal network to a more spread configuration (Fig. 3.2). See Section 3.1.1.1 for further explanation. **46**

3.4 Loading conditions used for model confirmation: prescribed displacements and a point load are both applied at location A in a refined area of the surface mesh, to allow comparisons between both methods. Point loads are applied at locations B - D along the model surface (B and D are ~6 and 4 μm respectively from receptor node C). **49**

3.5 Three-dimensional finite element models (A) to (F) of adherent cells at increasingly spread shapes to the final configuration in Fig 2.1. Each model comprises membrane, nucleus, cytoplasm, and cytoskeleton components. The cytoplasm is omitted for clarity in all models. **52**

3.6 Loading conditions applied to the cell model in order to model the effect of substrate strain on a single adherent bone cell. Nodes at the at the cell-substrate interface (see text) are constrained in the y (vertical) direction, and displaced by 0.1% and 0.03% strain in the x and z directions respectively. **55**

3.7 Loading conditions applied to the cell model in order to model the effect of fluid shear stress on a single adherent bone cell. Tangential forces (resolved to x and y components) are applied to each membrane surface node (arrows), based on the area of each surrounding membrane elements. **56**

3.8 Schematic illustration of the apparatus used to apply pulsatile fluid shear stress to osteocytes or osteoblasts by pumping experimental medium through a parallel plate chamber. 37° incubator (A); parallel plate chamber (B); polylysine-coated glass slide containing cells (C); experimental medium (D); H_2O (E); revolving pump (F); 5% CO_2-air mixture (G); flow probe (H); plate with two openings through which experimental medium enters and exits chamber (I). Adapted from Burger and KleinNulend (1995). **58**

3.9 Fluorescent image of intracellular nitric oxide in MC3T3-E1 osteoblastic cells, incubated in DAF-FM fluorescent sensor and buffer solution for 35 mins. Also shown are regions of interest drawn around whole osteoblasts of an internal region of an osteoblast, such that changes in nitric oxide levels within these regions can be precisely quantified. **63**

3.10 Image of a typical cantilever used in each indentation experiment. Prior to each experiment a new cantilever is chosen from three rectangular NSC838 Mikromasch cantilevers and the remaining two (in this case the left and right) cantilevers are removed to prevent uncontrolled contact with other osteoblasts or with the substrate during indentation. This image is taken from below using a 20x objective lens of the

inverted fluorescent microscope. The conical tip extends a height of ~20 μm (out from the page) and has a curvature end-radius of ~14 nm (measurement courtesy of Dr. M. Polcik, SFI Nanoscience Laboratory, TCD). **64**

3.11 Schematic illustration of Hooke's Law - the spring constant (K) of the cantilever must be known to relate the measured deflection (x) to an applied force (F). **65**

3.12 Thermal noise power spectrum – frequency (x-axis: Hz) versus cantilever amplitude (y-axis: nanometres) of a NSC388 Mikromasch cantilever oscillating in air (a) and in liquid medium (b). The characteristic resonant frequency (in kHz), the stiffness (in N/m) and sensitivity (in nm/V) of each cantilever are determined by fitting the various parameters required for implementation of the 'Sader' method to these thermal spectra. **66**

4.1 The effect of prestress on cell model stiffness. The dotted line (stiffness at 0% prestress) illustrates the small increases in stiffness that can also occur when the force is not applied directly to a receptor site. **74**

4.2 Stiffness versus applied force. Note that at 0% prestress in the cytoskeleton there is no strain hardening effect. **74**

4.3 The effect on cell model stiffness of altering the material properties of each cell component from the original values in Table 3.1. **75**

4.4 Variable stiffness on application of vertical indentations of 50 pN along the surface of increasingly spread models A to F (model D is not included as it does not support 50pN at a distance from a receptor site). The dimensions of models A to F are provided in Table 3.2. **75**

4.5 (a) Cell stiffness for increasingly spread configurations from models A to F. Graph (b) shows the corresponding cytoskeleton (CSK) displacements (μm) due to prestress prior to application of horizontal forces that yield stiffness values. **76**

4.6 Reaction force versus indentation displacements for nodes resisting indentation displacements at the apical surface of the computational cell model, for three arbitrary prestress values. **77**

4.7 Illustration of differences in computed cell stiffness due to the point load and probe modelling methods: (a) a point load of 1 pN indents the membrane to ~51.5 nm (0.0515 μm); (b) applied indentation of 60 nm (0.06 μm) is resisted by a reaction force of ~2 pN. **78**

4.8 Elastic modulus versus indentation depth applied to the apical surface of the computational cell model, for three arbitrary prestress values. **79**

4.9 Comparison of displacements in the cell model due to both (A) substrate strain and (B) fluid shear stress loading conditions. The contour legend indicates the magnitude of displacement (μm). The image is exaggerated 30-fold to illustrate the differences in

deformation. Note also the increased resistance to displacement at receptor sites, where the cytoskeleton merges with the membrane. **80**

4.10 Overview of the differences in (A) deformation and (B) displacement of cell model components caused by both fluid flow and substrate strain loading conditions. % deformation is the maximum von Mises stress as a percentage of original elastic properties for each cell model component. Membrane and cytoskeleton displacement (μm) are maximum values. Abbreviations: Cyt-Nuc, the region of the cytoplasm immediately surrounding the nucleus; CSK, cytoskeleton. **81**

4.11 Fluorescent staining of the actin cytoskeleton of osteoblastic (MC3T3-E1) cells illustrating the effect of pulsatile fluid flow (PFF) and disruptors of both actin and microtubule (MT) polymerization (400x magnification). The white arrows indicate examples of cells with parallel alignment of stress fibres. **84**

4.12 Fluorescent staining of the actin cytoskeleton of osteocytic (MLO-Y4) cells illustrating the effect of pulsatile fluid flow (PFF) and disruptors of both actin and microtubule (MT) polymerization. The white arrows indicate examples of cells with parallel alignment of stress fibres. **85**

4.13 The effect of actin and microtubule (MT) cytoskeleton disruption on pulsatile fluid flow-induced (a) NO and (b) PGE_2 release in osteoblastic cells. * Significantly different from 1; # significantly different from untreated. Values are mean ± SEM, $p < 0.05$. **86**

4.14 The effect of actin and microtubule (MT) cytoskeleton disruption on pulsatile fluid flow-induced (a) NO and (b) PGE_2 release in osteocytic cells. * Significantly different from 1; # significantly different from untreated. Values are mean ± SEM, $p < 0.05$. **86**

4.15 Graph of AFM tip indentation force versus piezo movement. The red curve describes how the force changes to reach a maximum 20 nN as the piezo extends the tip into the osteoblast membrane, the blue curve is during piezo retraction. **88**

4.16 Fluorescent images of mitochondrial protein intensity at various time intervals. The point of indentation is indicated by the white arrow. An indentation force of ~20 nN is applied continuously from 31 s until 93 s. **89**

4.17 Images of nitric oxide fluorescence at various time intervals. The point of indentation is indicated by the white arrow. An indentation force of ~20 nN is applied continuously from 57 s until 117 s. **90**

4.18 Normalised fluorescence intensity emitted from regions of interest drawn around the indented osteoblast, and its peri-nuclear region. First successful indentation occurs at 57 s and is continuous until 117 s (as indicated by arrows) after which time the tip is withdrawn. The control values obtained from an accompanying experiment on the same day exhibit a steady decrease in fluorescence due to photobleaching. **91**

4.19 Images of nitric oxide fluorescence at various time intervals. The point of indentation is indicated by the white arrow. An indentation force of ~22 nN is applied continuously from 30 s until 60 s. **93**

4.20 Images of nitric oxide fluorescence at various time intervals. The point of indentation is indicated by the white arrow. An indentation force of ~24 nN is applied continuously from 52 s until 112 s. **94**

4.21 Images of nitric oxide fluorescence at various time intervals. Site of indentation is indicated by the white arrow. The first indentation with a force ranging ~47 nN is applied continuously from 32 s until 93 s. **95**

4.22 Images of nitric oxide fluorescence at various time intervals. Site of indentation is indicated by the white arrow. The first indentation with a force of ~25 nN is applied continuously from 52 s until 112 s. **96**

4.23 Images of nitric oxide fluorescence at various time intervals. Site of indentation is indicated by the white arrow. The first indentation with a force of >60 nN is applied continuously from 140 s until 200 s. **98**

4.24 Images of nitric oxide fluorescence at various time intervals. Site of indentation is indicated by the white arrow. Indentation with a force of ~17 nN is applied continuously from 51 s until 110 s. **99**

4.25 The effect of increasing force (nN), from 1 nN to 400 nN, on cell indentation characteristics. Velocity of indentation is ~ 1.86 $\mu m.s^{-1}$ (0.4 Hz). **101**

4.26 Force curves associated with each osteoblast response to indentation: (a) NO diffusion from localised pools; (b) Increases in NO in the perinuclear region; (c) Increases in intracellular NO then diffusion into extracellular medium; (d) Osteoblast retraction and diffusion of NO from localised pools. Indentation depth (δ) and elasticity (E) and radial strains (in Fig. 4.27) are calculated for each response. **102**

4.27 Comparison of osteoblast membrane radial strains associated with each response to indentation. The force curves referred to for each response are given in Fig. 4.26. **102**

5.1 Schematic diagram illustrating how the cell model explains variation in cell response to fluid flow and strain in terms of cellular deformation. **113**

5.2 Schematic representation of cytoskeleton involvement in signal transduction of mechanical stimulation-induced prostaglandin E_2 release in osteoblasts or osteocytes (see text for explanation). Abbreviations: PKC, protein kinase C; PLA_2, cytosolic phospholipase A_2; COX-2, cyclooxygenase-2; DAG, diacylglycerol; PLC, phospholipase C; PGE_2, prostaglandin E_2. **120**

5.3 Fluorescent image of cells immuno-labelled with antibodies to total eNOS. (a) bovine aortic endothelial cells after stimulation with vascular endothelial growth factor, and

(b) COS-7 cells transfected with eNOS. In both cells total eNOS is localised to the plasma membrane (open arrows) and perinuclear region (arrow heads). Adapted from Fulton et al. (2002). **124**

5.4 Schematic representation of cytoskeleton involvement in signal transduction of mechanical stimulation-induced nitric oxide release in osteoblasts or osteocytes, based on results in this thesis and on several results in the literature (see text). Abbreviations: CAT-1, cationic amino acid transporter-1; eNOS, endothelial nitric oxide synthase; NO, nitric oxide. **125**

LIST OF TABLES

2.1 Summary table of elastic modulus for various cell types. Abbreviations: AFM, atomic force microscopy; MTC, magnetic twisting cytometry; MA, micropipette aspiration; MM, microplate manipulation; EC, endothelial cell; SMC, smooth muscle cell. **18**

2.2 Summary table of elasticity of specific cell components. Note that cytoskeletal components are several orders of magnitude stiffer than the nucleus, cytoplasm or membrane. Abbreviations: microplate manipulation (MM); thermal fluctuations (TF). **21**

3.1 Elastic properties assigned to the components in the model. **47**

3.2 Dimensions of each finite element model A to F in Fig. 3.5. **51**

3.3 Flow characteristics of the applied pulsatile fluid flow regimes. **59**

Chapter 1

Introduction

1.1 Mechanobiology of bone

1.2 Questions of the thesis

1.1 Mechanobiology of bone

Bone is a structural material capable of self-repair and dynamic adaptation of its morphological and structural fitness to serve its functions, which include protection of internal organs, leverage, and structural support under the various loading conditions experienced throughout life. As the continuous adaptation of our bones to the demands of daily usage is not likely pre-programmed in the genes, the most probable explanation lies in the relationship that exists between bone quality and its mechanical usage – the drastic effects of the absence of mechanical loading in microgravity, disuse, and paraplegia include reduced bone mass, deterioration of bone architecture and increased susceptibility to fracture, whereas strenuous exercise results in increased bone mass. The importance of understanding how mechanical forces arising in bone can modulate bone cell activity such that bone mass and architecture remains fit for function throughout life is therefore undeniable, and has been the subject of scientific investigation for many years. Indeed the premise of 'mechanobiology', that *"biological process are regulated by signals to cells generated by mechanical loading"* (van der Meulen and Huiskes, 2002), is a concept that dates back to Roux (1881).

Bone comprises two forms of osseous tissue: cortical bone, a low porosity tissue found primarily in shafts of long bones and vertebrae, and cancellous bone consisting of a high porosity framework of struts and plates called trabeculae that is both light and can withstand multiaxial stresses. Either form of bone tissue comprises a mineral phase and an organic phase, mostly crystals of hydroxyapatite and collagen type I, respectively. This tissue is produced and maintained by the cells within bone, namely the osteocytes, osteoblasts, and osteoclasts (Fig. 1.1). Osteocytes are differentiated osteoblasts that become buried in lacunae within the bone matrix. They connect via canaliculi to osteoblasts and to osteoblast-derived lining cells on the bone surface. Osteocytes exhibit little synthetic activity and may engage in low-level control of local mineralization, and in communicating signals to other cells in bone. The function of osteoblasts is to synthesise, secrete and regulate assembly of the organic matrix, and to facilitate mineral deposition. Osteoclasts are large multi-nucleated cells that are specialised to resorb

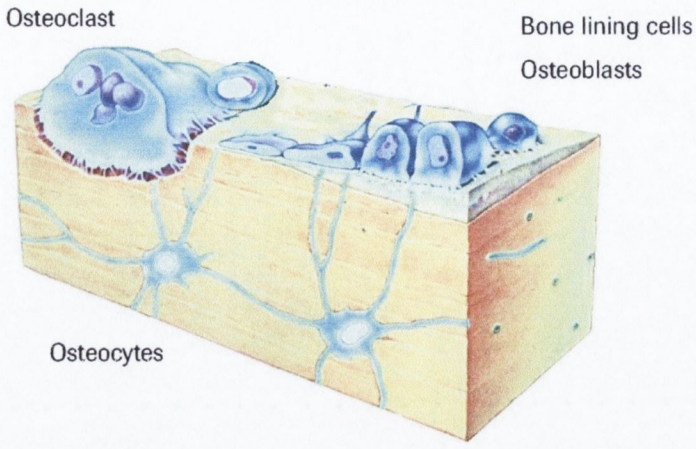

Fig. 1.1 *Schematic illustration of the locations of cells in bone tissue. Adapted from www.roche.com/pages/facets/11/ostedefe.htm.*

bone, which involves dissolution and digestion of the mineral and organic phases. Growth (known as modelling) and continuous renewal of bone (remodelling) occurs via a balance of osteoblast and osteoclast activity.

During physical activity mechanical loads result in strain in the load-bearing matrix, or in strain-derived fluid shear stresses in the bone porosity. As it is known that both osteoblasts and osteocytes are responsive to mechanical forces, a popular hypothesis proposed by Huiskes et al. (2000) is that optimal bone quality is maintained by positive feedback control of bone cell response to the prevailing levels of these stimuli (Fig. 1.2). For example, mechanosensitive osteocytes would respond to bone 'overuse' (an excess level of fluid flow or strain stimuli) by recruiting bone forming osteoblasts via gap-junction communication, or anabolic signalling molecules such as nitric oxide or prostaglandin E_2. Increased osteoblastic activity would cause an increase in bone mass leading to restoration of normal levels of mechanical stimulus. Conversely, a reduction of mechanical loading results in decreased osteoblastic activity and therefore dominant osteoclastic activity, leading to removal of bone mass. Although this hypothesis requires further corroboration, it does emphasise the important fact that any mechanical regulation of bone must occur on the cellular level, via mechanosensitive bone cell (i.e. osteoblast and osteocyte) responses to physiological magnitudes of mechanical stimuli.

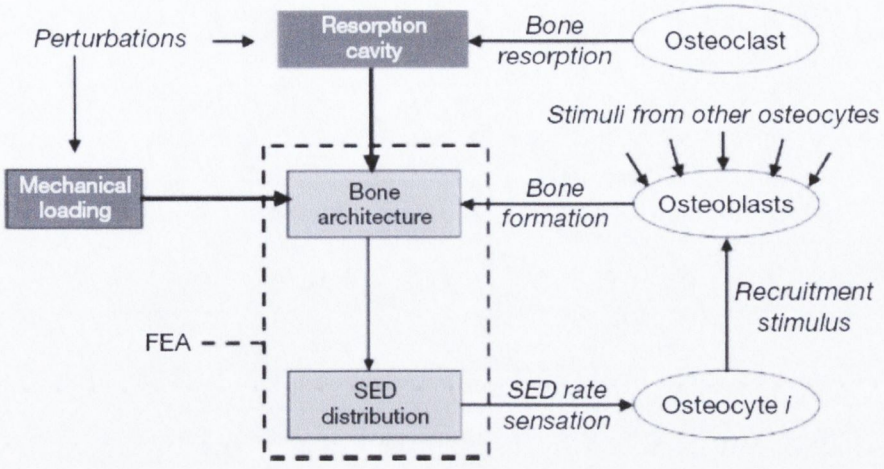

Fig 1.2 *Schematic of a proposed regulation process in which osteocyte sensing of strain-energy density (SED), mechanical loading and osteoclast resorption regulate bone remodelling. Adapted from Huiskes et al. (2000).*

In several *in vitro* experiments, there have been attempts to replicate the *in vivo* environment of *mechanosensitive* bone cells by subjecting cultured osteoblasts and osteocytes to fluid flow or strain *in vitro* and subsequently measuring alterations in specific osteoblast or osteocyte functions. For example, osteopontin and collagen type I (associated with osteoblastic matrix production), nitric oxide and prostaglandin E_2 (both chemical messengers that mediate mechanically-induced bone formation), c-fos (a transcription factor) and cyclooxygenase-2 (an enzyme required for prostaglandin production) have all been reportedly up-regulated by either fluid shear stress or strain of various magnitudes and frequencies. While these results confirm mechanotransduction of important functional responses in osteoblast and osteocyte bone cells, the approach taken in several of these experiments (applying a mechanical stimulus and recording the downstream cell response) does not address the mechanism underlying the conversion of mechanical forces to a biochemical response, that must occur on the cellular level. Interpreting these responses and comparing results from separate experiments is difficult because the physical changes undergone by the cell due to the various applied mechanical stimuli are not known – no theoretical approach has yet been successfully applied to this problem. Furthermore, it is not known what bone cell organelles play a role in

mechanosensitivity, or how a mechanical stimulus is detected and subsequently transduced to signalling responses such as nitric oxide and prostaglandin E_2. Bridging this gap in our understanding of how osteoblasts and osteocytes both detect information regarding the mechanical status of bone, and subsequently transduce the received mechanical stimulus to an appropriate biochemical response, is dependent on the development of new scientific approaches that integrate both theoretical and experimental methods.

1.2 Objectives of this thesis

The aim of this thesis is to investigate the processes whereby mechanosensitive bone cells transduce a mechanical stimulus to a biochemical signalling response. Specifically, two hypotheses are proposed in the thesis:

(i) that osteoblast and osteocyte response to mechanical stimuli includes a magnitude-dependent release of nitric oxide and prostaglandin E_2 signalling molecules; and

(ii) the mechanotransduction mechanism is mediated by the cytoskeleton.

Testing these hypotheses requires that several unresolved aspects of bone cell response to mechanical stimuli be addressed, for example: which organelles are structurally important under imposed mechanical stimuli and in mechanotransduction; what the physical consequences of an applied fluid shear stress or strain are on the cellular level; the nature and magnitude of mechanical stimulus required to activate a signalling response in a single bone cell; whether the cytoskeleton is involved in osteoblast and osteocyte transduction of mechanical forces to nitric oxide and prostaglandin E_2 response. Resolving these primary questions of the thesis will contribute to elucidating the role of mechanical forces in bone adaptation. Such information will strengthen the fundamental knowledge required for understanding biomechanical aspects of bone diseases such as osteoporosis, for determination of the optimal stimuli for *in vitro* engineering of bone tissue, and for the design of orthopaedic devices that may maintain bone health in 'disuse' conditions such as microgravity.

Chapter 2

Literature Review

2.1 Introduction

2.2 Cell biomechanics

2.2.1 Composition and structure of eukaryotic cells

2.2.1.1 The cytoskeleton

2.2.1.2 The cytoplasm and nucleus

2.2.1.3 The membrane and cortical tension

2.2.2 Material behaviour of adherent cells

2.2.2.1 Cell elasticity

2.2.2.2 Cell compressibility

2.2.2.3 Elastic properties of cell organelles

2.3 Computational models of adherent cells

2.3.1 The continuum approach

2.3.2 Discrete models incorporating cell organelles

2.3.2.1 Open-cell foam model

2.3.2.2 Percolation models

2.3.2.3 Tensegrity

2.4 Biochemical responses in mechanically-induced bone adaptation

2.4.1 Introduction

2.4.2 Nitric oxide and prostaglandin E_2

2.5 *In vitro* mechanical stimulation of bone cells

2.5.1 Introduction

2.5.2 Strains applied to substrate to which cells adhere

2.5.3 Fluid flow applied to monolayers of cultured cells

2.5.4 Differences in bone cell response to fluid flow and strain stimuli

2.5.5 Application of mechanical stimuli to single cells

2.6 Conclusions

2.1 Introduction

The purpose of this chapter is to draw attention to many of the unresolved aspects of bone cell response to mechanical forces, thus setting a background for the scientific questions of this thesis. The chapter begins in Section 2.2 with a review of experimental studies investigating the composition and material properties of adherent eukaryotic cells, with a particular emphasis on bone cells. The aim is to establish which organelles are of primary importance within the structural complexity of a living cell. In Section 2.3 theoretical modelling approaches for exploration of mechanotransduction in adherent cells are discussed. In Section 2.4, the biochemical responses of interest in bone adaptation to mechanical loads are discussed. In Section 2.5, experiments involving application of mechanical stimuli to bone cells *in vitro* are reviewed.

2.2 Cell biomechanics

2.2.1 Composition and structure of eukaryotic cells

The organelles in eukaryotic cells (which includes bone cells) of most structural significance due to their function, size or material properties include the cytoskeleton, nucleus, cytoplasm and cell membrane (Fig. 2.1).

2.2.1.1 The cytoskeleton

The cytoskeleton can be viewed as the cell's skeleton. It is a complex interconnected network of various protein filaments that provide strength, flexibility and structure to the overall cell and cytoplasm (Alberts et al., 1989; Martini, 2004). There are three main components of the cytoskeleton: actin filaments, microtubules and intermediate filaments. Due to their mechanical properties, ability to transmit forces, continuously polymerise and reposition, interactions between these interconnected cytoskeletal components dynamically influence cell shape, stiffness, substrate adhesion, and the positioning of other organelles, cell adhesion and overall

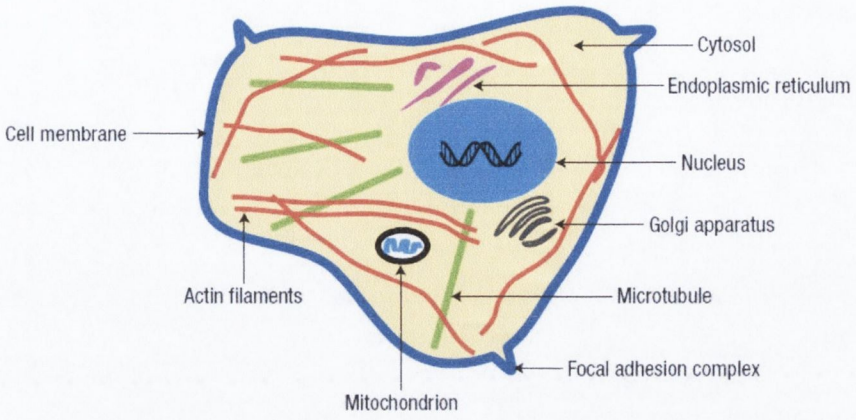

Fig. 2.1 *Schematic illustration of the components of a typical eukaryotic cell. The intracellular material between the cell membrane and nucleus (i.e. the cytoplasm) contains organelles (including the cytoskeleton) that perform specific functions, and an intracellular liquid cytosol containing soluble nutrients, ions and proteins. Adapted from Bao and Suresh (2003).*

cell shape (Maniotis et al., 1997; Martini, 2004). Next the structural characteristics of each cytoskeletal component are introduced.

- Actin filaments are solid thread-like fibres ~3 to 6 nm in diameter distributed throughout the cell cytoplasm and generally arranged in an interconnected network. Most 'rigid' adherent cells (including fibroblasts, osteoblasts, osteocytes and chondrocytes) have a dense sub-membranous network of actin filaments that contributes to maintaining cell shape, and also transmits contractile forces generated by actomyosin sliding mechanisms (Alberts et al., 1989) (Fig. 2.2). Actomyosin is a protein complex of both actin and myosin (motor enzymes that interact with actin) that is also the contractile substance of muscles. It is generally accepted that these contractile forces give rise to a membrane tension that is balanced by microtubules forming interconnected networks with actin, by the cytosol (Wang and Ingber, 1994; Pourati et al., 1998), and by cytoskeletal attachments to the extracellular matrix. These contractile forces have often been referred to as a pre-tension or

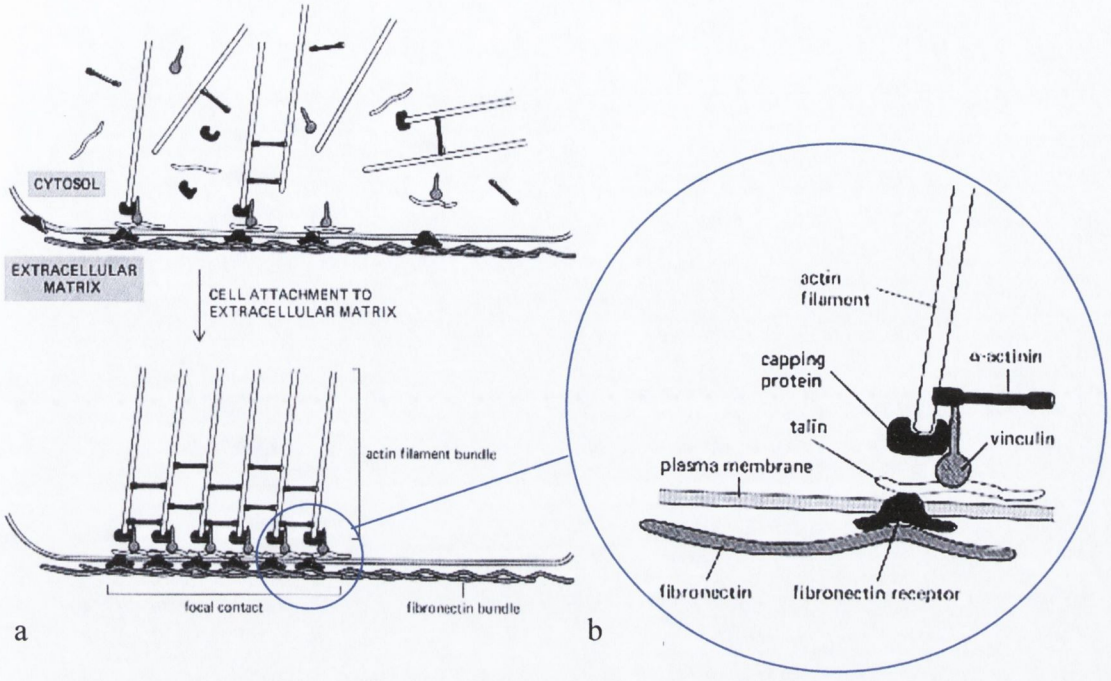

Fig. 2.2 *(a) Illustration of the clustering of actin filaments during the formation of focal adhesion complexes. (b) A detailed view illustrating the structural proteins involved in formation of an adhesion bond with the fibronectin integrin receptor. Adapted from Alberts et al. (1989).*

prestress, the effects of which (on cell structure) have been observed in several studies (Sato et al., 1990; Wang et al., 1993; Shroff et al., 1995; Hubmayr, 1996; Wang et al., 2002). During adhesion bond formation, integrins and intracellular proteins found in adhesion plaques serve as transmembrane links between actin filament bundles (stress fibres) that form inside the cell (Fig. 2.2), and the extracellular matrix or substrate (Alberts et al., 1989). In this way actin cytoskeleton organisation, cell shape, and the number of focal adhesion complex formed are linked (Fig. 2.3). This may explain why a highly spread cell is much stiffer than when rounded (Thoumine et al., 1999). It has been speculated that forces acting on adhesive contacts contribute not only to cell shape and viability, but also to mechanical signal transduction (Chen et al., 1997; Galbraith and Sheetz, 1998; Chen and Ingber, 1999).

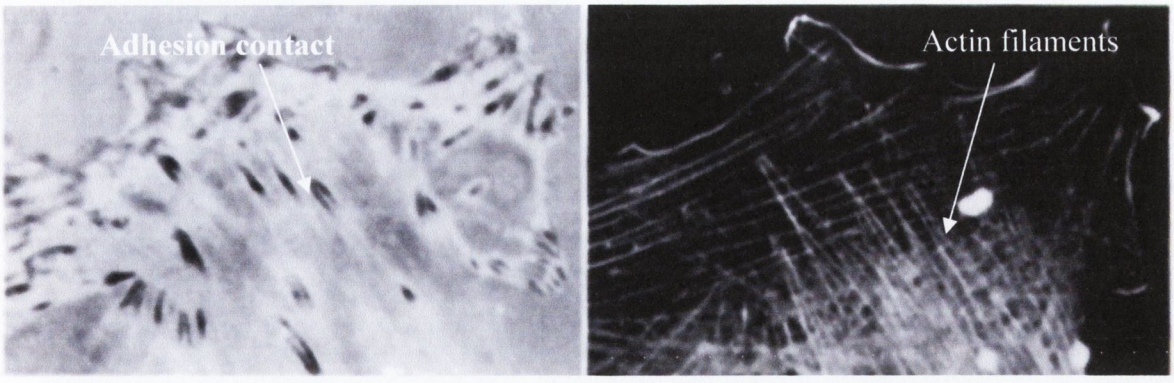

a b

Fig. 2.3 *Images of an adherent fibroblast immunostained for (a) focal adhesion complexes, and (b) actin filaments. Adapted from Alberts et al. (1989).*

- Microtubules are 20 to 25 nm diameter cylindrical tubes composed of units of the protein tubulin, that radiate outward from centrosomes. A centrosome (also known as a 'microtubule organising centre') is a region of the cytoplasm near the nucleus that contains a pair of centrioles oriented at right angles, each consisting of nine microtubule triplets. It is now generally accepted that in several cell types microtubules resist cell compression (Alberts et al., 1989; Martini, 2004). Danowski (1989) reports that treating fibroblasts with microtubule disrupting toxins results in a rapid strengthening of fibroblast contractility, suggesting that microtubules inhibit transmission of contractile forces generated by the sub-membranous actin filament bundles. Microtubules have strength and rigidity, influence the positioning of other organelles, act as tracks for the movement of vesicles by molecular motor proteins, and due to their continuous polymerisation influence such diverse functions as cell migration, and spindle formation in cell mitosis (Martini, 2004).

- Intermediate filaments are durable, insoluble protein fibres of intermediate diameter, 8 to 11 nm. These filaments are arranged in a network surrounding the nucleus and, as such, influence the positioning of other organelles, particularly the nucleus (Alberts et al., 1989). Wang and Stamenovic (2000) report that endothelial

cell stiffness is significantly reduced when intermediate filaments are disrupted. Intermediate filaments are thought to contribute largely to the mechanical support of the cell, particularly at higher strains (Janmey et al., 1991). A specific tensile or compressive role for intermediate filaments has not been established, nor has it been established if they form an interconnected network for force transmission with the other cytoskeletal components. For this reason, the contribution of intermediate filaments to cellular stiffness does not necessarily require distinction from that of the material properties of the cytoplasm.

2.2.1.2 The cytoplasm and nucleus

The cytoplasm is essentially the intracellular material between the cell membrane and the nucleus. It contains the organelles (including the cytoskeleton) and the liquid cytosol which contains soluble nutrients, ions and a high concentration of proteins (Martini, 2004). Because it is mainly a liquid, the cytoplasm is often considered to be incompressible. The degree of incompressibility and material properties of the cytoplasm are dealt with in Section 2.2.2. A reasonable approximation to the structural complexity of the cytoplasm could involve treating the cytosol and internal organelles as a continuum with the appropriate degree of compressibility, provided that the highly significant dynamic role of the various cytoskeletal components in maintaining cell structure is explicitly accounted for.

The nucleus is the largest and most visible organelle within an eukaryotic cell. It is the control centre for cellular operations and stores information required for protein synthesis. The nucleus also contains a fluid nucleoplasm containing a network of fine filaments (the nuclear matrix) and nucleoli. As the largest organelle in the cytosol, the nucleus and its complex internal matrix comprise a most significant part of cell structure.

2.2.1.3 The membrane and cortical tension

The cell membrane is the outer boundary of the cell that physically separates the cytoplasm from the extracellular environment (Fig. 2.4). A phospolopid bilayer through which water and

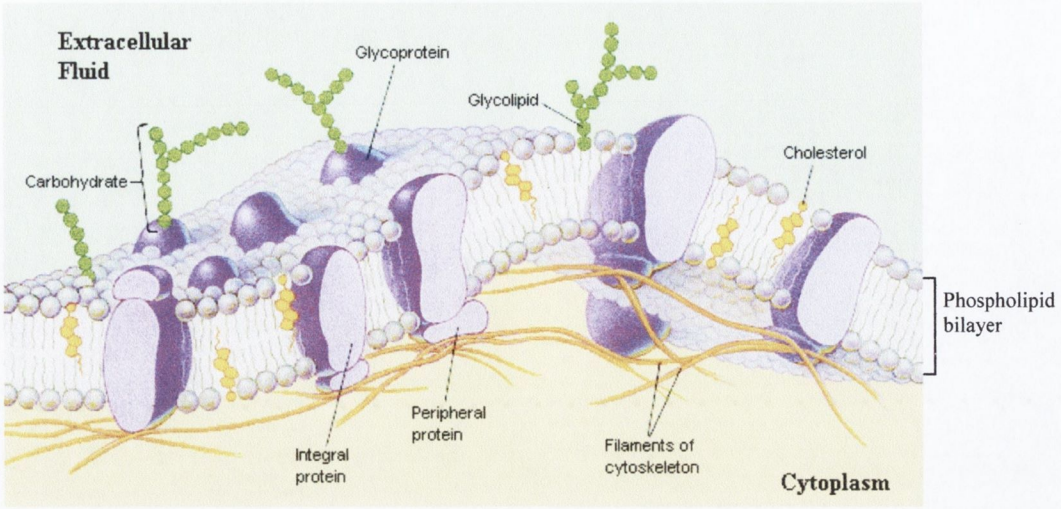

Fig. 2.4 *Schematic of the components and structure of the cell membrane. Source: www.people.virginia.edu/~rjh9u/cellmemb.html.*

solutes cannot pass forms a large part of the membrane structure. Both integral and peripheral proteins that account for 55% of membrane weight are embedded in the bilayer of the membrane (Alberts et al., 1989). Besides acting as a physical barrier, the membrane regulates entry of ions and nutrients and the elimination of waste, exhibits receptor-mediated sensitivity to changes in concentration or composition of the extracellular fluid and to specific molecules, and provides a stable site for binding and catalysis of enzymes. Membrane proteins have specialised functions such as: anchoring the membrane to other cells or to the cytoskeleton, sensitivity to specific molecules called ligands, transport of solutes across the membrane, and selective passage of ions through channels or pores in integral proteins (Martini, 2004). These various functions may be influenced by perturbation of the membrane structure (Janmey, 1998). Although the membrane is neither rigid nor uniform with many proteins free to drift across the surface, the membrane does form a structural barrier (Martini, 2004) and is thus considered an important structural component of adherent eukaryotic cells. There are numerous studies in the literature (as discussed below) documenting the structural importance of the membrane, with many also reporting that membrane tension has a large bearing on cell shape. This membrane tension originates in the sub-membranous (cortical) network of contractile actin filaments anchored to the membrane (Alberts et al., 1989).

Albrecht-Buehler (1987) investigated the role of cortical membrane tension in fibroblast shape and movement. The technique involved drawing a part of the membrane to a point on the substrate a short distance from the cell and observing the consequences. As the membrane retracted rapidly when released, it was concluded that fibroblast shape is partly regulated by membrane tension.

Raucher et al. (1999) used a laser tweezers to pull on the fibroblast membrane. They obtained force versus cell extension characteristics. Resistance to increased displacement was found to be high initially, but decreased exponentially with time. Raucher et al. (1999) noted that this behaviour may be due to the gradual depletion of a membrane reservoir that unfolds to buffer against changes in membrane tension.

Frisch and Thoumine (2002) have predicted the kinetics of spreading fibroblasts in a biomechanical model. Three main parameters were used: adhesion energy, cytoplasmic viscosity, and cortical tension. The value determined for cortical tension was 0.2 – 0.4 mN/μm, which was considered a significant contribution to cell structure. In his observations of spread fibroblasts, Frisch and Thoumine (2002) suggest that cells reach their final degree of spreading when the membrane is pulled taut by depletion of a tension-buffering reservoir.

Using a microneedle, Pourati et al. (1998) reports that adherent endothelial cells immediately retracted (or rounded up) when detached from a substrate. On disruption of the actin cytoskeleton there was no retraction. Furthermore, using magnetic twisting cytometry, application of a 5% strain to the cells resulted in a ~30 % increase in cell stiffness, which did not occur when the actin cytoskeleton was disrupted. Both these results suggested that contractile forces in actin filaments have a significant influence on cell shape and on dynamic alterations in cell stiffness in response to mechanical strain.

2.2.2 Material behaviour of adherent cells

In this Section the various studies in the literature involving experimental characterisation of the material properties of osteoblasts or other morphologically similar cell types, such as fibroblasts, chondrocytes, and endothelial cells are discussed.

2.2.2.1 Cell elasticity

It has been proposed by Radmacher and co-workers (e.g. Radmacher, 2002) that living cell elastic properties range from 1 kPa to 100 kPa, as illustrated in Fig. 2.5. A more extensive examination of the literature reveals that cell elasticity varies considerably depending on the cell type, and on the nature of the experimental methods used in their determination. An overview of the elastic properties of various cell types obtained using micropipette aspiration, atomic force microscopy, magnetic twisting cytometry and other techniques will now be discussed. An overview of this cell elasticity data is presented in Table 2.1 at the end of this Section.

In micropipette aspiration a suction pressure is applied to a suspended cell, and the resultant cell deformation into the suction pipette is recorded (Fig. 2.6). Guilak et al. (2000) quantified the mechanical properties of articular chondrocytes using micropipette aspiration in conjunction with a theoretical viscoelastic model. It was determined that chondrocytes exhibited an instantaneous elastic modulus of ~0.7 kPa. Using a similar approach, Trickey et al. (2000) determined an instantaneous elastic modulus of 0.41 ± 0.17 kPa for chondrocytes. In that study the stiffness of chondrocytes derived from osteoarthritic tissue was significantly higher (increased to 0.63 kPa) and it was proposed that, based on the observed effect of actin-disrupting drugs, the altered biomechanical properties of osteoarthritic cartilage are due to reorganisation of the chondrocyte actin cytoskeleton. Freeman et al. (1994) applied a uniaxial compressive load to deform isolated chondrocytes. A finite element model was used to determine that the chondrocytes deformed with an elastic modulus of ~4 kPa. Hochmuth (2000) also using micropipette aspiration on rigid adherent cells, such as chondrocytes and endothelial cells, and determined that their material behaviour corresponded to an overall elastic modulus on the order of 0.5 kPa.

Atomic force microscopy (AFM) indentation can yield interesting insight into cell elasticity and the importance of cytoskeleton effects on cell stiffness. AFM can be used to obtain force-indentation characteristics at localised points across the cell topography. This data can yield local elasticity estimates by applying the classical Hertz contact relation. Charras and Horton (2002b) report an average elastic modulus of 2.1 kPa for an osteoblast, which can

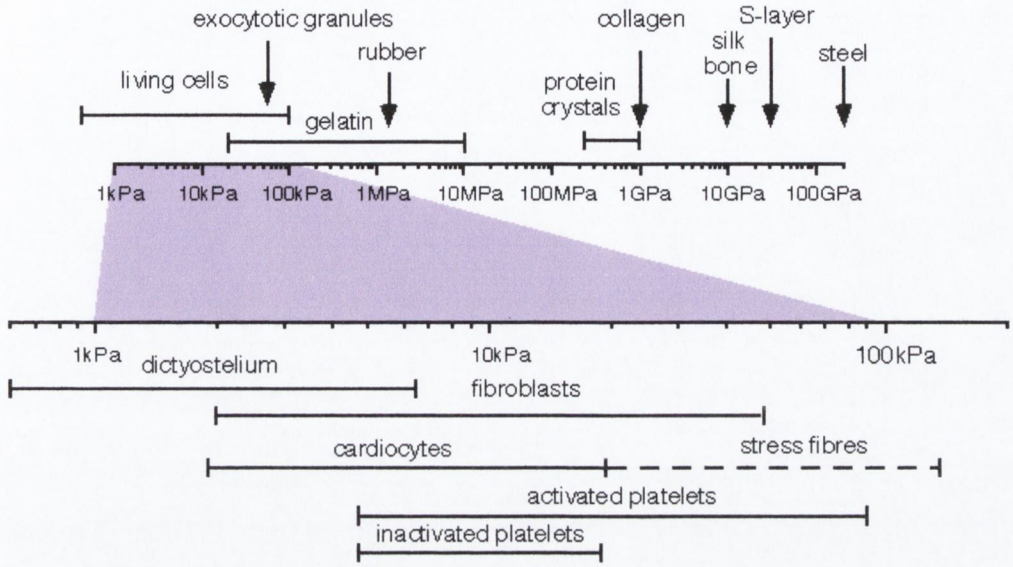

Fig. 2.5 *Overview of the elastic properties of cells relative to those of other common materials (the lower scale shows the expanded range for cells). Source: www.biophysik.uni-bremen.de/radmacher/elasticity.html.*

increase ~100-fold if the AFM tip indents above cytoskeletal components such as stress fibres (actin bundled into long fibres). Domke et al. (2000) found that elasticity values are highest if the cell is indented over the underlying cytoskeleton, as illustrated in Fig. 2.7. In that study it was also reported that osteoblast elasticity varies with underlying substrate material properties – osteoblasts were most stiff on titanium (~8.8 kPa), least stiff on titanium-vanidium (~2.1 kPa), and exhibited intermediate values on polystyrene. This suggested that the cytoskeleton has a large influence on osteoblast stiffness, and that the influence of the degree of cell adhesion on cell stiffness may be related to the number and strength of cytoskeletal attachments that can form on a particular extracellular surface.

Mathur et al. (2001) report a wide range of elasticity values for various cell types: cardiac muscle were stiffest (~100kPa), endothelial were least stiff (~6 kPa), while skeletal muscle cells exhibited intermediate values. Besides these well-documented differences in elasticity between cell types and within a single cell, Mathur et al. (2001) also report variation in elasticity with indentation depth in an endothelial cell (Fig. 2.8).

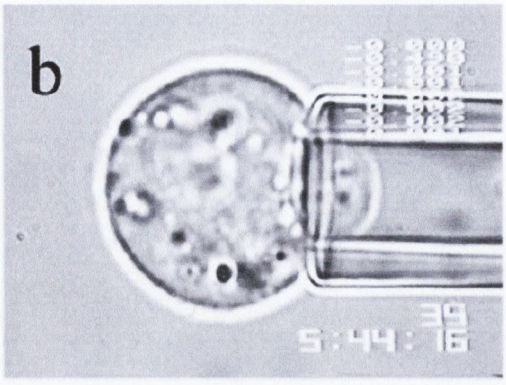

Fig. 2.6 *Micropipette aspiration of a chondrocyte 4 s after application of the aspiration pressure. Adapted from Trickey et al. (2004).*

Magnetic twisting cytometry involves measuring the rotation of a ferromagnetic bead attached to the cell membrane under application of a magnetic torque. Wang and Ingber (1994) used magnetic twisting cytometry to measure the stiffness of both round and spread endothelial cells. Stiffness ranged from 3 to 9 Pa in spread cells, but was 50% lower in round cells. Since then Stamenovic and Wang (2000) have attributed these low stiffness values to free rotation of the bead. Such errors associated with the magnetic twisting technique have now been addressed and higher stiffness values (up to 0.1 kPa) have been obtained for smooth muscle cells using a similar method (Maksym et al., 1999), which is in closer agreement with data obtained by other experimental methods.

Other novel experimental methods have been developed to measure cell elasticity. These include a piezo-controlled micromanipulation system developed by Thoumine and Ott (1997) to impose dynamic deformation on individual chick fibroblasts. By fitting their results to a three-element Kelvin model, an elastic modulus in the range of 0.6 kPa to 1 kPa was calculated – this value increased by 40% for more highly spread fibroblasts. Using magnetic beads, Lo and Ferrier (1999) applied forces to layers of osteosarcoma cells adherent on gold electrodes. The cells were cultured on an electrode, and electrical cell-substrate impedance sensing was used to measure the continuous stress-induced mechanical strain of the cells. An elastic modulus of ~1 kPa was determined for these osteosarcoma cells.

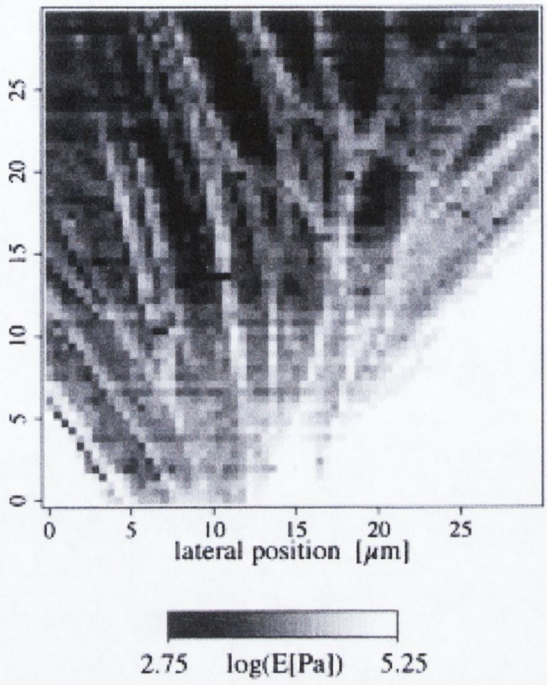

Fig. 2.7 *Elasticity map of a region of an osteoblast. Elasticity (E) was calculated from the force-deflection characteristics determined at numerous points using atomic force microscopy. Adapted from Domke et al. (2000).*

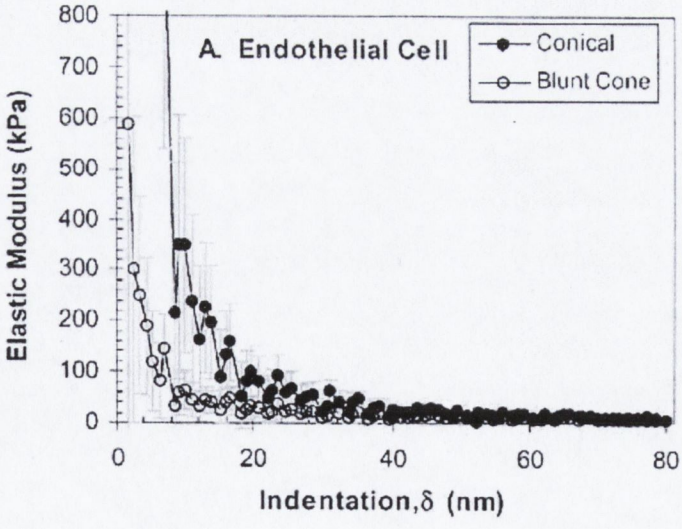

Fig. 2.8 *Variation in elastic modulus with indentation for an endothelial cell. Note the decreasing stiffness with indentation depth and the dependence of elastic modulus on probe geometry, which becomes less significant at higher indentation depths.*

Table 2.1 *Summary table of overall elastic modulus for various cell types. Abbreviations: AFM, atomic force microscopy; MTC, magnetic twisting cytometry; MA, micropipette aspiration; MM, microplate manipulation; EC, endothelial cell; SMC, smooth muscle cell.*

Authors	Year	Method	Cell type	Elasticity (kPa)
Charras	2001	AFM	Osteoblast	> 2.1
Domke et al.	2000	AFM	Osteoblast	2.1 – 8.8
Shin et al.	1999	-	Osteoblast	2.05
Lo et al.	1999	-	Osteosarcoma	1
Guilak et al.	1999	MA	Chondrocyte	0.7
Hochmuth	2000	MA	EC/Chondrocyte	0.5
Trickey et al.	2000	MA	Chondrocyte	0.24
Maksym et al.	1999	MTC	Muscle cell	0.1
Peterson et al.	1982	-	Fibroblast	1.6
Thoumine et al.	1997	MM	Fibroblast	0.6 – 1
Sato et al.	1990	MA	Endothelial	0.075 – 0.16
Mathur	2001	AFM	SMC	24.7

2.2.2.2 Cell compressibility

The degree of compressibility of an adherent cell is influenced by the content of the cytoplasm and intracellular fluid. In biomechanical models of chondrocytes (Trickey et al., 2000; Guilak and Mow, 2002), it is often assumed that chondrocytes are incompressible due to the high liquid content of the cytoplasm – estimated to be ~70 % (Alberts et al., 1989). In a linear elastic model of cell material behaviour this assumption corresponds to a Poisson's ratio (the ratio of lateral to axial strain) of 0.5. However, a more extensive review of experimental data in the literature reveals that this assumption of incompressibility may not be entirely valid. For example, Freeman et al. (1994), using a finite element model, determined the parameters that fit experimentally-measured area changes of chondrosarcoma cells under compression, and determined a Poisson's ratio of 0.4. Jones et al. (1999) describe how their measurements of chondrocyte volume changes during micropipette aspiration corresponds to a similar degree of

compressibility to that reported by Freeman et al. (1994). Furthermore, it has been reported that a decrease in chondrocyte volume occurs in compression *in situ* (Guilak, 1995), which is consistent with a degree of compressibility, although it was proposed that this may be explained by loss of water content through the permeable chondrocyte membrane during compression (Gray et al., 1988; Lai et al., 1991). Shin and Athanasiou (1999) used a biphasic model to interpret their measurements of osteoblast deformation under applied forces – it was concluded that a Poisson's ratio value of 0.37 captured osteoblast change in shape. In a biomechanical model by Wu et al. (1999), a compressibility of Poisson's ratio of 0.4 was used, based on the data of both Shin and Athanasiou (1997) and Jones et al. (1997). Also it is worth noting that in their biphasic finite element model of a chondrocyte surrounded by pericellular and extracellular matrix (Guilak and Mow, 2000), the chondrocyte Poisson's ratio was varied parametrically from 0.1 to 0.5. Based on these various studies, it is appropriate to consider 'rigid' eukaryotic cells (such as bone cells) as being compressible to a degree, which should be accounted for in any theoretical model of cell structure.

2.2.2.3 Elastic properties of cell organelles

Several studies in the literature, both theoretical and experimental, that report material properties for specific cell components are now discussed. An overview of this experimental data is provided in Table 2.2.

Caille et al. (2002) devised a method with which whole cells could be deformed under uni-axial compressive displacements applied using a flexible flat plate (termed a microplate). It was reported that suspended (unattached) endothelial cells deformed at lower forces than either adherent endothelial cells or isolated endothelial nuclei. By fitting biomechanical model parameters to the force-deflection response data, a cytoplasm elasticity of 0.5 kPa, nucleus elasticity of ~5 kPa, and isolated nucleus elasticity of ~7 kPa were calculated.

Guilak et al. (2000) report quantitative measurement of the material properties of isolated chondrocyte nuclei determined using micropipette aspiration and theoretical modelling.

It was found that nucleus and cytoplasm both exhibited viscoelastic behaviour, but the nucleus was 3-4 times stiffer and twice as viscous as the cytoplasm.

Kamm et al. (2000) developed a continuum mechanics model of the effects of mechanical stress applied to layers of epithelial cells using a magnetic bead. The material parameters in this model include a linear elastic cytoplasm of 100 Pa, a nucleus with an elasticity of 1 kPa, a membrane assigned a higher elasticity of 100 MPa. Model results indicated that membrane properties determine, to a large extent, how external forces are transmitted into the epithelial cells. However, limitations to this conclusion include the fact that the bead was modelled as attached to the membrane only, and not to the sub-membranous actin network.

By analysing thermally-driven fluctuations in microtubule shape Gittes et al. (1993) estimated the mean flexural rigidity (or bending stiffness) values of microtubules and actin filaments. By assuming that microtubules and actin filaments are isotropic it was determined from flexural rigidity values that microtubules have an elasticity of ~1.2 GPa with a cross-sectional area of 190 nm^2, whereas actin filaments exhibited a slightly higher elasticity of ~2.6 GPa, but were ~10-fold thinner with a cross-sectional area of 18 nm^2. Gittes et al. (1993) also speculated that microtubules are almost inextensible, and that the compliance of cells is due primarily to filament bending or sliding between actin filaments.

Satcher et al. (1997) modelled the microscopic structure of structural actin as a foam cell. Estimates of the shear and elastic material properties of structural actin were determined to be on the order of 10 kPa. It was also reported that stress fibres can potentially increase the elasticity 2 to 10-fold depending on their orientation.

2.3 Computational models of adherent cells

Alterations in cell shape and structure caused by mechanical loads are known to influence several cell functions including growth, motility, differentiation, and proliferation (Chen et al., 1997; Chicurel et al., 1998; Janmey, 1998; Carter and Beaupré, 2003). An imposed mechanical load can elicit functional changes in cell behaviour presumably by the distribution of forces

Table 2.2 *Summary table of elasticity of specific cell components. Note that cytoskeletal components are several orders of magnitude stiffer than the nucleus, cytoplasm or membrane. Abbreviations: microplate manipulation (MM); thermal fluctuations (TF).*

Author	Year	Method	Cell type	Component	Elasticity
Caille	2002	MM	Endothelial	Cytoplasm	0.5 kPa
			Endothelial	Nucleus	5 kPa
Gittes	1993	TF	-	Microtubules	1.2 GPa
			-	Actin filaments	2.6 GPa
Satcher	1996	Model	-	Actin network	10 kPa
Kamm	2000	Model	Epithelial	Membrane	10^7 Pa
			Epithelial	Cytoplasm	0.1 kPa
			Epithelial	Nucleus	1 kPa
Guilak	2000	Model	Chondrocyte	Nucleus	3-4 times cytoplasm

throughout the cell structure (Ingber, 1993; Davies and Tripathi, 1993; Maniotis et al., 1997). According to Stamenovic and Wang (2000) '*..the central question of cellular mechanics is: By what mechanisms do cells resist shape distortion and maintain their structural stability?*'. Addressing this question and determining the consequences of applied forces on bone cell mechanotransduction would be greatly aided by the development of biomechanical models of cells. Such a model could be used to explore several experimentally-observed aspects of cell structural behaviour, the origins of which are not yet understood. These include observations of: (i) non-linear cell stiffening under increasing applied force (Wang et al., 2001), (ii) large variations in compliance along the cell surface (Domke et al., 2000; Mathur et al., 2001), (iii) the influence of contractile tension in the actin filament network (Wang and Ingber, 1994; Pourati et al., 1998; Wang et al., 2002), and (iv) alteration in cell stiffness as a cell becomes more spread (Thoumine and Ott, 1997).

In the literature there have been several different approaches to modelling the complexity of living cells. The first category of models, discussed in Section 2.3.1, generally

adopt a continuum approach, whereby the structural contribution of cell components is modelled as a continuum for simplicity. The second category of models includes those models where the structural contribution of specific organelles is explicitly modelled, such as components of the cytoskeleton that are known to influence cell behaviour and shape. Among this latter category of models, dealt with in Section 2.3.2, are the open-cell foam model, the percolation model of the cytoskeleton, and the tensegrity stress-supported approach.

2.3.1 The continuum approach

A continuum approach to cell mechanics was first used by Evans and Yeung (1989) to model blood cells (non-adherent) with a cortical membrane and viscous cytoplasm as blood cells do not have nuclei. This model had limited success in describing the structure of adherent cells such as bone cells. Kamm et al. (2000) developed a biomechanical model to investigate the effects of pressure applied to the apical surface of an adherent epithelial cell, to determine if the cell would deform and slip into an underlying porous substrate. The model follows closely after a previous study of Dembo et al. (1988), and consists of a membrane, nucleus, the cytoplasm and cytoskeleton combined as a continuum for simplicity all modelled as linear elastic materials. The cytoplasm and nucleus were both treated as incompressible (with a Poisson's ratio of ~0.49) due to the liquid cytosol. The model deformations suggested that membrane elasticity would largely determines how forces are transmitted to the cytoskeleton. However, this conclusion is hampered by the limitation that the bead is modelled as attached to the membrane only and does not address attachment to the sub-membrane actin network via integrins and adhesion plaques. A more recent advance on this model, but with a similar continuum approach, was published by Karcher et al. (2003). A model was constructed of a cell region to which a magnetic bead was attached (Fig. 2.9). The membrane/cortex and cytoskeleton were both modelled as continuum viscoelastic materials. Other models adopting similar continuum approaches include a biomechanical model by Guilak and Mow (2000) of the deformation of a chondrocyte within its extracellular matrix.

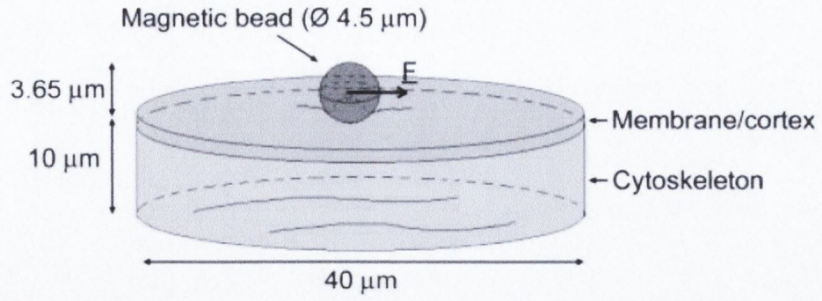

Fig. 2.9 *A three-dimensional model of cell manipulation by magnetocytometry, comprising a membrane/cortex and cytoskeleton both modelled as viscoelastic materials. Source: Karcher et al. (2003).*

A shortcoming of the continuum approach is that the role of individual cytoskeletal components (such as microtubules and actin filaments) in maintaining cell structure and stiffness under external mechanical forces is not accounted for (as discussed in Section 2.2.1.1). In fact, in a recent paper, Hochmuth (2000) suggests 'the modelling of cellular deformation in the future may combine elements of both continuum models and tensegrity models. This may be especially important for cells attached to surfaces at points of focal adhesion where molecular cross bridging occurs'.

2.3.2 Discrete models incorporating cell organelles

A growing number of studies highlight the importance of the cytoskeleton in providing structural stability in adherent cells, in transmitting mechanical loads from the cell surface (Wang and Ingber, 1994; Pourati et al., 1998), in intracellular communication (Janmey, 1998; Juliano and Haskill, 2004) and in mechanotransduction and anchorage of key molecules and enzymes involved in mechanotransduction (Ingber, 1993; Janmey, 1998; Janmey and Weitz, 2004). Several biomechanical models in the literature have attempted to explicitly address the importance of the cytoskeleton, which has been modelled as an open-cell foam model (Satcher and Dewey, 1996), as a percolation network of fibres in a viscous cytoplasm (Shafrir and Forgacs, 2002), and as a stress-supported tensegrity structure (Wang et al., 1993; Stamenovic et al., 1996; Stamenovic and Coughlin, 2000). Each model will be discussed in turn below.

2.3.2.1 Open-cell foam model

Open-cell foam models consist of a unit of interconnected struts (Fig. 2.10). Satcher and Dewey (1996) devised this model by assuming that bending and twisting of actin filaments is the main mechanism by which the actin network responds to loading.

Using this model the shear modulus for the structural unit of actin filaments was obtained using the following expression:

$$G \propto E_F . \varphi^2 ,$$

where E_F is elastic modulus of individual struts and φ is the relative foam density (volume fraction of the struts relative to the volume of the foam). Taking φ to be on the order of 10^{-3} Pa and E_F as on the order of 10^9 Pa from experimental data (Satcher et al., 1997), it followed that the shear modulus of the actin network is estimated to be on the order of 10^3 Pa. Relative to more recent experimental work (Section 2.2.2), this value is now considered excessive for adherent cells. The model does, however, predict a strain hardening that arises due to bending and twisting of the actin filaments during compression, which is consistent with observations obtained by indentation of cultured adherent cells (Peterson and McConnaughey, 1982; Shroff et al., 1995; Radmacher, 2002). The open-cell foam model does not attempt to model neither the contractile forces in the actin cytoskeleton nor the rotation, re-positioning, or length changes of actin filaments as they equilibrate with imposed mechanical forces.

2.3.2.2 Percolation models

The third category of discrete models that have been developed are known as percolation models (Shafrir and Forgacs, 2002; Head et al., 2003). In these models, actin cytoskeleton filaments in a viscous cytoplasm are free to form network pathways by attaching to other filaments via cross-linking molecules (Fig. 2.11). Because filaments are free to reposition, rotate, attach and detach to other filaments, several uninterrupted pathways can dynamically form to ensure percolation of a force applied at the membrane to within the cell. Shafrir and Forgacs (2002) report that, even with a density of filaments and cross-linking molecules below

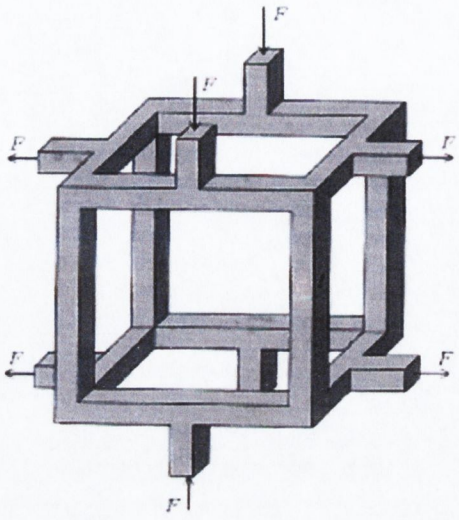

Fig. 2.10 *Representative structural unit of the open-cell foam network devised by Satcher and Dewey (1996).*

physiological concentrations, there is a reliable transfer of mechanical forces from the membrane to the nucleus. By incorporating the dynamic organisation of the cytoskeleton in response to external forces, percolation models illustrate the force-transmission capacity of the cytoskeleton and a possible mechanism for cytoskeleton-mediated intracellular signal transduction. Due to the requirement for simplicity of geometry in implementing percolation theory, the development of a whole-cell model to which various loading conditions could be applied was not feasible.

2.3.2.3 Tensegrity

In the tensegrity (tensional integrity) approach the cytoskeleton is modelled as a interconnected network of cables and struts (Ingber, 1997; Stamenovic and Coughlin, 1999), as illustrated in the six-strut, 24 cable model in Fig. 2.12. Stability of the network is achieved by a balance of tension transmitted by cables (i.e. actin filaments) and compression in struts (microtubules). A certain degree of pre-tension or prestress is therefore required to maintain cell shape. The approach has been used to model many experimentally- observed aspects of cellular structural behaviour (Wang et al., 2001), such as prestress-induced stiffening and strain hardening (Coughlin and Stamenovic, 1998; Wendling et al., 1999), and to demonstrate upper and lower

Fig. 2.11 *Schematic representation of the percolation model of the cell cytoskeleton. Filaments that form an uninterrupted path from the membrane (outer box) to the nucleus (inner box) are denoted by heavy lines. Shaded circles represent elastic cross-linkers. Adapted from Shafrir and Forgacs (2002).*

bounds for the elastic modulus of an adherent cell (Stamenovic and Coughlin, 2000). This range was determined using estimates of the yield force of actin, and the buckling force of microtubules, as measured by Gittes et al. (1993) and by Tsuda et al. (1996), respectively. A finite element implementation of a tensegrity structure has also been used to describe cell migration (Moretti, 2001). Wendling and Canadas (2002) found that increasing the number of cortical actin components in the tensegrity structure did not increase stiffness, suggesting that prestress within the actin components of the cytoskeleton, and not the number of individual actin components, dictates cell rigidity.

The experimental basis of tensegrity has been subject to controversy. Its main proponents argue that microtubules balance (along with the extracellular matrix) contractile forces, thereby preventing cell retraction or rounding (Wang, 2000; Stamenovic and Coughlin, 1999). For example, it has been reported that microtubule buckling increases when cytoskeleton contractility is increased by addition of thrombin to cells cultured on flexible surfaces (Stamenovic et al., 2002). Other key experimental observations that support tensegrity include observations of the 'action at a distance' phenomenon, whereby cell probing causes movement

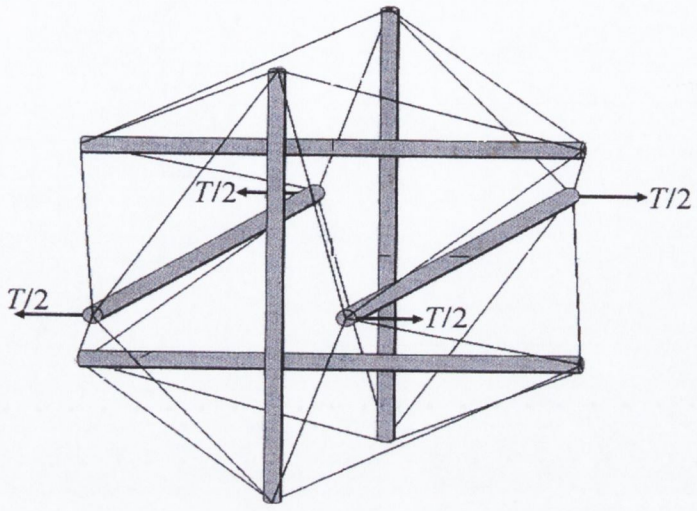

Fig. 2.12 *A stress-supported tensegrity structure as a representative unit of the cytoskeleton. The grey struts in three orthogonal pairs represent microtubules, while the thinner lines represent actin filaments. Adapted from Stamenovic et al. (1996).*

of cytoskeletal components away from the site of manipulation as reported by Ingber et al. (2000) in several publications. Pourati et al. (1998) observed coordinated movement of mitochondria when microtubules were disrupted. These results lend support to the tensegrity hypothesis that cell structure is greatly influenced by contractile forces carried by the actin cytoskeleton, which forms an interconnected network with other cytoskeletal components.

Other researchers argue that forces applied to cells only result in local deformations, with any displaced microtubules or actin filaments being those already attached to the micro-needles – both sides of this discussion are published in Ingber et al. (2000). An explanation offered for why the 'action at a distance' phenomenon is not always observed is that if the force is applied to a compliant area of the cell membrane away from any underlying cytoskeleton, the resulting stress will dissipate locally, and cytoskeletal restructuring and force transmission to other parts of the cell will not occur. The opponents of tensegrity do agree that acto-myosin contractile forces are probably transmitted by actin, and balanced by the microtubule-rich central cytoplasm, they insist that 'action at a distance' will only occur when molecular couplings are formed.

2.4 Biochemical responses in mechanically-induced bone formation

2.4.1 Introduction

The biochemical responses of interest in bone formation are reviewed in this Section. Section 2.4.2 focuses on nitric oxide and prostaglandin E_2, both signalling molecules found in bone, that are the focus of this thesis.

Bone cell response to mechanical loading occurs over a range of timescales (from seconds to days), and includes changes in gene expression, proteins, enzymes and signalling molecules associated with osteoblast or osteocyte functions. Osteoblasts produce all the constituents of the bone matrix. Responses to mechanical stimuli that are characteristic of osteoblastic function include the expression of proteins such as osteocalcin, osteonectin, alkaline phosphatase, bone sialoprotein and osteopontin (all non-collagenous proteins, NCPs), and secretion of collagen type I, the predominant bone matrix protein (Cowin, 2001). The role of NCPs is unclear although it is probable that they play a role in the calcification and fixation of hydroxyapatite crystals to the collagen. Bone cell production of alkaline phosphotase and osteocalcin synthesis are often taken as evidence of osteoblastic maturation towards the mineralisation phase (Kaspar et al., 2000; Afzal et al., 2004). Up-regulation of proteins such as *c-fos* are also important and may form part of a larger cascade of transcriptional responses in bone matrix remodelling (Kawata and Mikuni-Takagaki, 1998; KleinNulend et al., 1998). Osteocytes are also involved in regulation of bone mineral and architecture by maintaining appropriate levels of ions and by coordination of adaptive bone cell responses to mechanical stimuli by cell-cell interaction.

Several enzymes and kinases are involved in various stages of bone cell signal transduction of mechanical forces. It is known, for example, that inhibiting protein kinase C, phospholipase C, or cyclooxygenase-2 (COX-2) (the inducible form of cyclooxygenase enzymes) all inhibit mechanically-induced prostaglandin E_2 response (Ajubi et al., 1999; Bakker et al., 2003). Two hours of fluid flow stimulation results in an increase in mitogen-activated protein kinase (MAPK), the inhibition of which prevents increases in osteopontin mRNA levels

(You et al., 2001). The constitutive endothelial nitric oxide synthase (eNOS) is required for the synthesis of nitric oxide, an important signalling molecule discussed in Section 2.4.2. Estrogen stimulates eNOS activity in bone cells (Armour and Ralston, 1998), which may partly explain the importance of estrogen in the prevention of osteoporosis.

There are several important bone cell signalling responses to mechanical forces in both osteoblasts and osteocytes. Increases in intracellular calcium (Ca^{2+}) concentration are early bone cell responses to receptor-mediated extracellular signals and to mechanical forces, and may also regulate signal transduction of other bone cell activities (Hung et al., 1996; Ajubi et al., 1999). Early expression of the gene heme-oxygenase-1 catalyses the carbon monoxide (CO) signalling molecule (Shivaram et al., 2004). Further discussion of the well-established role for both nitric oxide and prostaglandin as mediators of bone metabolism follows in Section 2.4.2.

2.4.2 Nitric oxide and prostaglandin E_2

Nitric oxide (NO) is a short-lived diffusible chemical messenger. It is involved in diverse physiological functions including vasodilation, cell apoptosis, and cell differentiation in the cardiovascular, lymphatic, and neural systems. There is now substantial evidence that NO has an essential role in bone metabolism (Evans and Ralston, 1996; Afzal et al., 2004). Fox et al. (1996) report that NO plays a crucial role in mechanically-induced bone formation. This is supported by Turner et al. (1996) who confirmed that suppression of nitric oxide synthase (an enzyme involved in NO synthesis) prevents loading-induced bone formation in rats. NO is also required for bone growth and remodelling during fracture repair (Diwan et al., 2000), and in modulating remodelling imbalances during ovariectomy-induced bone loss (Wimalawansa et al., 1997). It has been shown that activation of NO involves conversion of L-arginine to NO via the endothelial isoform of nitric oxide synthase (eNOS) in bone cells (Klein-Nulend et al., 1998; Helfrich et al., 1997) in endothelial cells (Busse and Fleming, 1995) and in osteocytes (Zaman et al., 1999; Klein-Nulend et al., 1995). Bone metabolism is regulated via eNOS-mediated NO control of expression of genes involved in specific phases of osteoblast differentiation and bone formation (Afzal et al., 2004). Indeed, the importance of NO in bone growth is evident from the

marked bone abnormalities that arise in mice lacking eNOS genes (Aguirre et al., 2001; Armour et al., 2001).

Prostaglandins are eicosanoid lipid derivatives, and are important paracrine factors that coordinate cellular activity in almost every tissue in the body (Martini, 2004). They are generated by the release of arachidonic acids in the phospholipids in the cell membrane. It has been reported that administering prostaglandin E_2 prevents bone loss, and adds bone mass in immobilised femurs of female rats (Akamine et al., 1992). Prostaglandin E_2 also has a role in mechanically-induced bone formation; loading of canine cancellous bone explants induces prostaglandin release (Rawlinson et al., 1991), while indomethacin (which blocks PGE_2 activity) administered prior to mechanical loading has been shown to prevent any osteogenic response (Pead and Lanyon, 1989). Cellular PGE_2 release involves cyclooxygenase-2 (COX-2: an enzyme required for prostaglandin synthesis) mediated conversion of arachadonic acid to PGE_2 (Ajubi et al., 1996). It has been shown that osteoyctes are more responsive to fluid flow stimulation than other osteogenic cells, with respect to prostaglandin G/H synthase-2 (the enzyme responsible for conversion of arachidonic acid to prostaglandins), NO, and PGE_2 (KleinNulend et al., 1995; Westbroek et al., 2000).

It has been well established in several *in vitro* experiments that mechanical stimulation induces both NO and PGE_2 release in osteogenic cells over a range of time points from 15 mins to 2 hrs (Klein-Nulend et al., 1995; Johnson et al., 1996; Klein-Nulend et al., 1998; Bakker et al., 2001; Smalt et al., 1997; Ajubi et al., 1996; Bacabac et al., 2004; McAllister and Frangos, 1999). However, how *mechanical forces* can influence both NO and PGE_2 signalling pathways in osteogenic bone cells remains unclear. In the literature, a role for the cytoskeleton in the transduction of mechanical signals has been established in: (i) fluid shear-induced COX-2 expression in bone cells (Pavalko et al., 1998); (ii) in chicken calvarial osteocyte PGE_2 response (Ajubi et al., 1996); and (iii) in nitric oxide response in endothelial cells (Knudsen and Frangos, 1997). It is also possible that other cellular mechanisms are involved in mechanoreception and subsequent transduction of mechanical signals to a NO or PGE_2 response, and may be modulated by cytoskeleton activity – for example, integrin-cytoskeletal coupling (Wang et al.,

1993; Janmey, 1998), mechanosensitive cation channels (Ajubi et al., 1999; Rawlinson et al., 1996), and gap junctions (Saunders et al., 2003).

NO has widespread downstream actions on cells within the bone environment, i.e. in bone, vascular endothelial, bone marrow stromal, and immune system cells. NO exerts its multiple actions via effects on intermediary metabolism, DNA synthesis, ion transport, ADP deamination, nitrosylation of proteins, regulation of gene expression and transcription, chemical reactions with reactive oxygen species, and in particular via cyclic guanosine monophosphate (cGMP) (Collin-Osdoby et al., 1995). It is well-established that NO is the endogenous activator of soluble guanylyl cyclase (which contains a heme group for which NO has high affinity), leading to formation of cGMP and a cascade of phosphorylation events. In bone physiology, both NO and PGE_2 are among an assortment of regulators of osteoblast and osteoclast activity and therefore bone remodelling. These include systemic regulators (such as parathyroid hormone, vitamin D_3, and estrogen), cytokines (such as interleukins and TNF), arachidonic acid metabolites (such as the prostaglandins), and free radicals (including NO and superoxide). It appears that NO has opposite effects on osteoblasts and osteoclasts: for example, Kasten et al. (2004) report that NO inhibits osteoclast function and therefore bone resorption via cGMP as second messenger, whereas Mancini et al. (2000) report that a slow moderate release of nitric oxide stimulates proliferation of primary rat osteoblasts and alkaline phosphatase activity, while a rapid release and high concentrations of NO inhibit proliferation and induce apoptosis. Prostaglandins have been implicated as mediators of inflammation for many years. In bone, PGE_2 is also reported as a stimulator of cytokine-induced bone resorption (Vane et al., 1994) most likely via a cAMP pathway (Klein and Raisz, 1970). Inhibitors of prostaglandin synthesis prevent inflammation-related bone loss, as occurs in rheumatoid arthritis (Williams et al., 1992). It has been suggested by Ralston and Grabowski (1996) that the effect of cytokines on bone resorption is determined by the balance of NO and PGE_2 levels – high NO concentrations inhibit bone resorption and antagonize the effects of PGE_2, whereas lower concentrations of NO act with prostaglandins to enhance bone resorption.

2.5 *In vitro* mechanical stimulation of bone cells

2.5.1 Introduction

Several researchers have attempted to understand how bone cells respond to mechanical loading by application of mechanical stimuli to *in vitro* cell cultures and measuring alterations in biochemical responses. It is generally accepted that the candidate mechanical stimuli to which bone cells are subjected during physiological loading are both strain as a result of deformation in the load-bearing matrix (Duncan and Turner, 1995) and strain-induced fluid flow through the lacunar-canalicular network (Hillsley and Frangos, 1994; Weinbaum et al., 1994; Burger and KleinNulend, 1999). Several laboratories attempting to replicate the *in vivo* bone cell mechanical environment have developed a variety of apparatus to apply physiological magnitudes and frequencies of either strain and fluid flow, see Brown (2000) for a review. In Section 2.5.2 substrate strain experiments are discussed and in Section 2.5.3 fluid flow experiments are discussed. In Section 2.5.4, experiments comparing the response of cells to both strain and fluid flow stimulation simultaneously are discussed. Finally, an experiment reporting mechanical stimulation of intracellular calcium response in single bone cells is described in Section 2.5.5.

2.5.2 Strains applied to substrate to which cells adhere

Brown (2000) describes various apparatus for application of mechanical strain to cells adherent to a substrate *in vitro*. These apparatus are designed to maintain normal culturing conditions as for control cells, but with strain of the cell substrate as a controllable parameter (for two examples see Fig. 2.13). Several studies report various cell responses to a range of magnitudes of strain stimuli, generally <3,000 με, which is within the physiological range proposed by Burr et al. (1996).

Jones et al. (1991) used a four-point bending apparatus to apply mechanical strain of ~2,000 με to osteoblast-like cells. Periosteal osteoblasts only responded with enhanced collagen type I production, relative to controls. Interestingly, application of hyper-physiological strains up to

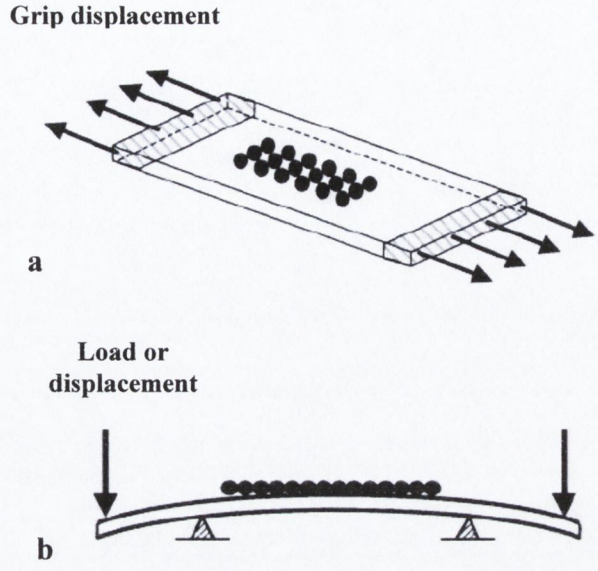

Fig. 2.13 *Apparatus designed to apply longitudinal strains through the substrate to which cells adhere, by (a) uniaxial distension (b) four point bending apparatus. Adapted from Brown (2000).*

10,000 με resulted in a de-differentiation of the osteoblasts to a more fibroblast-like morphology. Meyer and Terrodde (2001) subjected bovine periosteal bone cells to uniaxial strains of ~2,000 με. This caused an increase in bone-specific expression of extracellular matrix proteins including collagen type I, while hyper-physiological loads of 10,000 με caused a synthesis of proteoglycans. Yang et al. (2002) also used a four-point apparatus to apply strains to osteoblast-seeded scaffolds. The applied strain of 1,000 με caused elevated collagen type I and alkaline phosphatase expression, which was further enhanced by incorporating calcium channel agonists within the mechanically loaded scaffolds. Each of these results suggests that applied strains in the region of those proposed by Burr et al. (1996) enhances the bone-forming capacity of osteoblast-like cells by stimulating collagen matrix production.

2.5.3 Fluid flow applied to monolayers of cultured cells

The parallel plate chamber was developed to subject monolayers of adherent cells to fluid shear stress (Fig. 2.14). These experiments are generally designed to maintain normal culturing conditions, but with fluid shear stress as a controllable parameter. During an experiment the

fluid flow rate is generated by a roller pump and the shear stress (τ) inside the chamber can be calculated using the following equation:

$$\tau = \frac{6Q\mu}{bh^2},$$

where Q is the flow rate, μ is the fluid viscosity, and h and b are parallel plate chamber height and width respectively.

Using the parallel plate chamber, endothelial cells were first found to respond to shear stress with enhanced prostacyclin production (Frangos et al., 1985). In later years this apparatus was used to stimulate bone cells. It was reported that osteocytes in particular are most responsive to shear stresses (Klein-Nulend et al., 1996) in the range of those estimated to occur in the lacunar-canalicular network, i.e. from 0.6 Pa to 3 Pa, as reported by Weinbaum et al. (1994).

Other bone cells, such as osteoblastic cell lines and primary cells (Bakker et al., 2001) were also found to be responsive to fluid flow stimulation, particularly with respect to nitric oxide and prostaglandin signalling molecules (Klein-Nulend et al., 1995; Johnson et al., 1996). Bone cells have also been found to respond to steady fluid shear stress with increases in intracellular calcium concentration (Hung et al., 1996). Importantly, it has been convincingly argued that bone cell responses to fluid flow are caused by the magnitude and rate of the applied fluid shear stress, and not due to the consequences of simultaneous effects such as changes in electrical streaming potential or increased nutrient diffusion (McAllister and Frangos, 1999; Bakker et al., 2001; Bacabac et al., 2004).

A device has also been devised with which cells can be subjected to an oscillating shear stress, which the authors contend is more representative of the type of fluid movement to which bone cells would be subject within the bone porosity (Jacobs et al., 1998). Using this device it was reported that oscillatory fluid flow was less potent than either steady or pulsating fluid flow in stimulating calcium response (Jacobs et al., 1998). A more recent study using this device found that oscillating fluid flow stimulated gap junction-mediated PGE_2 response independent of Ca^{2+} levels in rat osteosarcoma cells expressing phenotypic characteristics of

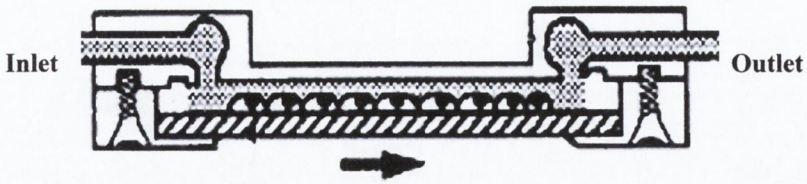

Fig. 2.14 *Schematic of the parallel plate flow chamber. Adapted from Burger et al. (1998).*

differentiated osteoblasts (Saunders et al., 2003). Oscillatory fluid flow also activates osteopontin mRNA, and mitogen-activated protein kinases (MAPKs) within two hours (You et al., 2001). Another study used cDNA microarray approach to identify novel response genes that may regulate mechanoresponsiveness in bone cells subjected to oscillatory fluid flow. Increased expression of cyclooxygenase-2 (COX-2), the enzyme catalysing PGE_2, is consistent with the work of Saunders et al. (2003) and Bakker et al. (2003). Heme-oxygenase 1 the inducible isoform of an enzyme that catalyses the carbon monoxide (CO) signalling molecule was up-regulated 33-fold within 30 mins of oscillatory fluid flow (Shivaram et al., 2004), signifying a dramatic early signalling response.

2.5.4 Differences in bone cell response to fluid flow and strain stimuli

Studies in which bone cell responses to both fluid shear stress and straining treatments have been directly compared report large differences in responsiveness to both stimuli. Owan et al. (1997) found that osteoblasts were more responsive to fluid flow than to applied strain. Fluid flow stimulation increased osteopontin expression (indicates the anabolic response of the cells) regardless of the strain magnitude. Smalt et al. (1997) report that both nitric oxide and prostaglandin E_2 response was induced in osteoblastic cells by 14.8 kPa fluid shear stress, but not by any magnitude of strain from 500 to 5,000 με strain in 1 hr of stimulation.

Mullender et al. (2004) describe the response of human-derived primary osteoblasts to both pulsatile fluid flow and cyclic mechanical strain using identical culturing protocols in each experiment, to allow comparison of bone cell production of collagen type I matrix and the

release of both nitric oxide and prostaglandin E_2 signalling molecules. In the strain experiment, cells were seeded to confluence on glass substrates. Using a four-point bending apparatus these substrates were subjected to tensile strains of ~1,000 με and a cycling frequency of 1 Hz for 1 hr. It was found that collagen type I expression in osteoblasts was significantly elevated, but the nitric oxide and prostaglandin E_2 response was largely unchanged from control levels. Using a parallel plate chamber (Fig. 2.14) the primary osteoblasts were also subjected to a pulsating fluid shear stress of magnitude 0.6 ± 0.3 Pa and frequency 3 Hz for one hour. This fluid flow stimulation resulted in enhanced NO and PGE_2 release (2 to 9-fold increase, respectively) (Fig. 2.15), and a down-regulation of collagen type I matrix production relative to controls. It was concluded that bone cells could distinguish between, and respond differently to, strain and fluid flow stimulation, perhaps via activation of different signal transduction pathways. It was noted that it was not necessarily valid to directly compare the consequences of two differing stimulation regimes, as the degree to which they deform the cell could be entirely different.

2.5.5 Application of mechanical stimuli to single cells

Atomic force microscopy (AFM) was developed by Binnig et al. in 1986, and has since become an invaluable tool in cell biology. The principle of AFM involves measuring the deflection of an AFM cantilever by detecting the position of a laser beam reflected off the cantilever to a position-sensitive photodiode (Fig. 2.16). Cantilever deflection is governed by nanoscale surface interactions between a tip on the end of the cantilever and a sample or underlying substrate. Cantilevers are barely visible to the naked eye, while the dimensions of a conical tip, for example, are typically 20 to 25 μm in length with an end-radius of ~10 nm. A piezo driver controls the position of the base of the cantilever in the z-direction, and a piezoelectric scanner allows sample movement in the x- and y-directions (Fig. 2.16) – the high sensitivity with which the cantilever tip position can be controlled in a feedback loop makes possible precise measurement of various physical properties of surfaces and samples on the nanoscale.

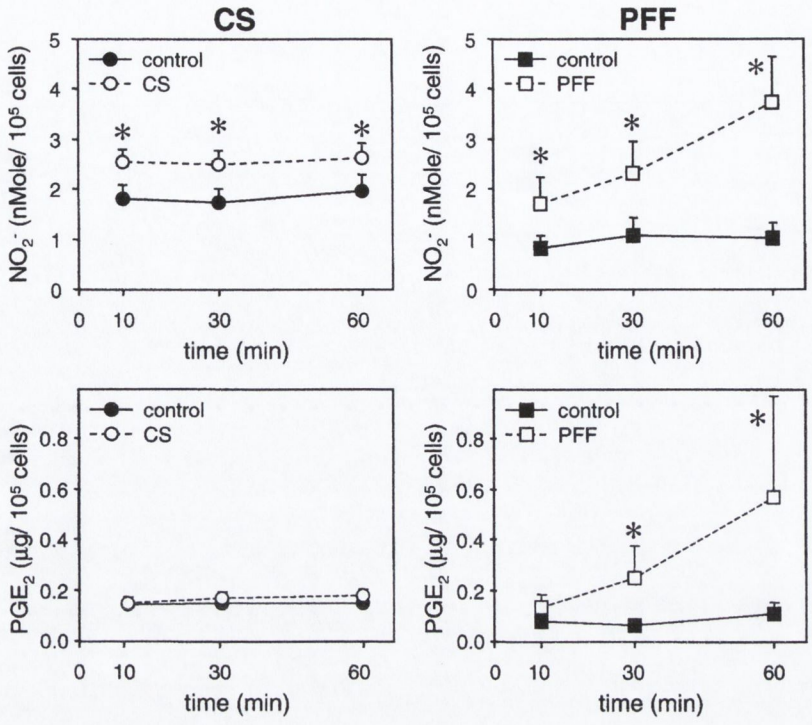

Fig. 2.15 *Effect of cyclic strain (CS) and pulsatile fluid flow (PFF) on prostaglandin E_2 (PGE_2) and nitric oxide (NO) release by human bone cells in vitro. Both NO and PGE_2 were significantly increased relative to controls after 60 minutes PFF. Also, collagen type I was increased ~1.6-fold in the CS group, but decreased ~0.6-fold by PFF, as measured after 24 hours of post-incubation (result not shown). Adapted from Mullender et al. (2004).*

In recent years, the AFM has been adapted for use in liquid environments, and has since become a valuable tool for studying biological materials (Weisenhorn et al., 1993). This has enabled imaging and probing of the material behaviour of adherent cells (Henderson et al., 1992; Radmacher et al., 1996), measurement of the forces required to unfold molecules such as DNA (Rief et al., 1999), of hydrogen bond energy of a single peptide molecule (Lantz et al., 1999), and application of low magnitude forces that elicit a calcium response in primary bone cells (Charras and Horton, 2002a). In that study it was found that cyclic indentation (~1 Hz) into the cell membrane with a force of ~30 nN increased intracellular calcium concentration. Cell elasticity was determined using a Hertz contact theory (Charras et al., 2001b) and the radial strain caused by the indentation was calculated using a theoretical expression first derived by

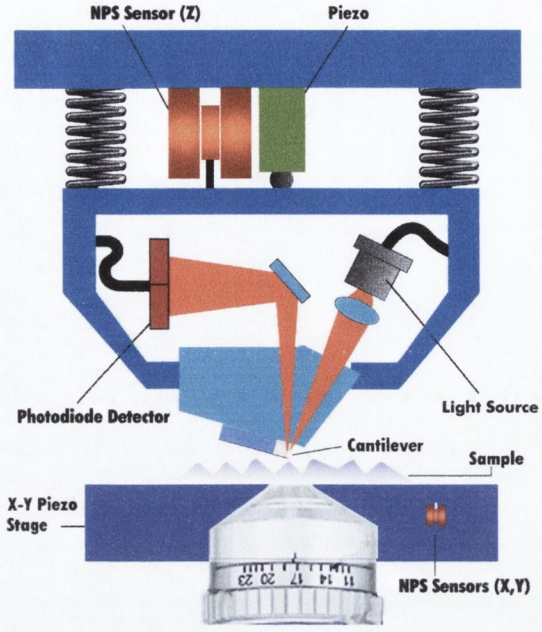

Fig. 2.16 *Schematic illustration of the principal and components of an atomic force microscope (AFM). The deflection of the AFM cantilever tip (as measured by photodiode detection of laser position) on contact with a sample (such as an adherent cell) is controlled with sub-micron precision by movement of the z-direction piezo. Sample position can be controlled by precise movement of the x-y piezo stage. Adapted from www.asylumresearch.com/Applications/AfmFluo/AfmFluo.pdf*

Johnson (1985) that relates the radial strain to the cell elasticity, tip radius, radius of contact, pressure at the centre of indentation, Poisson's ratio, and the force applied. The absolute value of radial strain that elicited an intracellular calcium response was calculated to be >40,000 με. It appears that these local strain values greatly exceed those substrate strains that have been shown to cause calcium response in monolayer experiments (Section 2.5.1).

In another study, Yellowley et al. (2000) report a calcium response in a single osteoblast subjected to an unquantified mechanical force using a glass patch pipette. The osteoblasts responded with an increase in intracellular calcium that appeared to propagate to other osteoblasts via gap-junction communication, as suggested by the passage of calcein dye between cells.

2.6 Conclusion

An examination of the structural contribution of the various organelles shows that the cytoskeletal components, in particular actin filaments and microtubules, influence cell shape and the positioning of other organelles. It is evident from several experimental studies that actin-transmitted contractile forces dictate cell shape, stiffness and degree of adhesion via coupling of actin to the extracellular matrix at focal adhesion complexes. In order to understand how mechanical forces impact on bone cells, it is thus important to recognise this contribution of the cytoskeleton independently of other organelles in the cytosol. Other structurally significant cell components include the cytoplasm, nucleus and membrane. In the literature it is evident that there has also been considerable interest in developing theoretical models of cell structure. The assumption adopted in several continuum models that the cytoskeleton can be accounted for in a continuum representation of the cytosol is not justified if one wants to model cell mechanosensitivity. Discrete models, on the other hand, adopt the opposite extreme as they focus on the contribution of cytoskeletal components alone in maintaining cell structure and in force transmission. It is thus apparent from the literature that a whole-cell model attempting to incorporate all significant organelles, including cytoskeletal components, has not been achieved to the extent that would allow testing of the hypotheses of this thesis.

Evidently a large number of researchers have investigated cell response to mechanical stimuli, providing strong evidence that bone cells do indeed respond to mechanical forces *in vitro* with a variety of responses, ranging from matrix protein production (such as collagen or osteopontin), to early signalling responses (such as calcium, nitric oxide, and prostaglandins). Many different mechanical stimulation regimes have been applied meaning that comparison of experiments is difficult. However, it is now recognised that bone cells are more responsive to fluid shear stress than to strain, particularly with respect to NO and PGE_2 release. This result has led researchers to hypothesise that fluid flow is the more likely mechanism of transmitting mechanical loading within bone. Such interpretation of bone cell responses, and the relevance of these results to *in vivo* mechanobiology, is not a simple matter and is hindered by the fact that

the physical consequences of applied mechanical stimuli on the cellular level could vary considerably. In fact, very few researchers in the literature have attempted to address this fundamental issue, presumably due to the difficulty in performing measurements at the cellular level. Clearly there is a requirement for new computational and experimental approaches that address the gap in knowledge concerning processes underlying the conversion of an applied mechanical stimulus to a biochemical response.

It is evident from the literature that there are several other issues that remain to be substantiated in uncovering how osteocytes and osteoblasts respond to mechanical forces. For example, it is not known whether the cytoskeleton modulates (either directly or indirectly via ion channels, focal adhesions or other mechanosensors) the signalling pathways that transduce mechanical signals to important signalling responses, such as nitric oxide or prostaglandin E_2. The magnitude of force required for, and the dynamics of, nitric oxide response in a single bone cell are also of particular interest in establishing mechanisms of bone cell mechanotransduction. While there is a considerable foundation of experimental results in the literature that have led to the questions of this thesis, new experimental approaches will be required to address the main hypothesis, i.e. that signalling responses in bone cells are dependent on the magnitude of mechanical stimuli and are mediated by cytoskeleton components.

Chapter 3

Methods

3.1 Introduction

3.2 Development of a computational model of an adherent cell

3.2.1 Cell model description

3.2.1.1 Model Geometry

3.2.1.2 Constitutive modelling of cellular components

3.2.1.3 Initial conditions

3.2.2 Quantitative corroboration of the cell model

3.2.2.1 Boundary conditions for corroboration of the model

3.2.2.2 Theoretical analysis of AFM probe indentation

3.3 Application of the computational cell model

3.3.1 Probing the structural characteristics of adherent cells

3.3.1.1 Spreading effects

3.3.1.2 Variable compliance of the cell

3.3.1.3 Prestress and strain hardening

3.3.1.4 Parametric variation of material properties

3.3.2 Determining the consequences of fluid flow and strain stimuli on bone cells

3.3.2.1. Initial conditions

3.3.2.2 Loading conditions to model substrate strain

3.3.2.3 Loading conditions to model fluid shear stress

3.4 In vitro mechanical stimulation of osteoblasts and osteocytes using fluid flow

3.4.1 Pulsatile fluid shear stress stimulation of bone cells in monolayers

3.4.1.1 Cell culture

3.4.1.2 Pulsatile fluid flow stimulation

3.4.2 Determining cell response: nitric oxide and prostaglandin E_2 release

3.4.3 Investigating cytoskeletal involvement in bone cell responses

3.4.3.1 Disruption of the actin and microtubule cytoskeleton

3.4.3.2 Cytoskeletal staining

3.5 Using atomic force microscopy to mechanically stimulate single osteoblasts

3.5.1 Synchronised cell indentation and nitric oxide response measurement

3.5.1.1 Cell culture and intracellular nitric oxide monitoring

3.5.1.2 Cell indentation procedure

3.5.1.3 Quantifying the applied indentation force

3.5.1.4 Calculating membrane surface strain due to indentation

3.5.1.5 Control experiments

3.6 Using the methods to investigate the thesis

3.1 Introduction

In this Chapter the approaches taken in arguing that magnitude-dependent cytoskeleton-mediated transduction of a mechanical force by mechanosensitive bone cells elicits rapid synthesis and release of signalling molecules are introduced. Both computational and experimental methodologies are devised to explore four related facets of this primary research question: (i) An investigation of what cell organelles maintain cell structure under applied forces and are therefore involved in intracellular force transmission and mechanotransduction – for this purpose a computational model of an adherent cell is developed, as described in Section 3.2. It is intended that upon corroboration of the model it will be justifiable to utilise the model as a mechanobiological tool. (ii) Attempting to understand how the physical consequences of a mechanical stimulus on the cellular level may be involved in the mechanisms underlying mechanotransduction of signalling responses measured in several *in vitro* experiments – for this purpose the computational cell model developed is used to examine the consequences of fluid flow and strain stimuli on adherent bone cells, as described in Section 3.3. (iii) An investigation of osteoblast and osteocyte response to mechanical stimuli, in particular which organelles are involved in mechanotransduction of signalling responses – this is achieved experimentally by application of a fluid flow shear stress to cultured bone cells, as described in Section 3.4. (iv) The focus of the thesis then converges to the single cell level in order to determine the magnitude of force required for, and the dynamics of, nitric oxide (NO) mechanotransduction – for this purpose atomic force microscopy is used to apply quantifiable indentation forces to single osteoblasts, while simultaneously monitoring intracellular nitric oxide intensity, as described in Section 3.5.

3.2 Development of a computational model of an adherent cell

3.2.1 Cell model description

The finite element method is a mathematical tool that can be used to calculate the deformation of three-dimensional shapes divided into a finite number of elements and nodes under any desired loading conditions. The method has proven a useful tool for insight into mechanobiology at the microscopic level where experimental measurements are often difficult (Prendergast, 1997). In the present study the finite element method was used to develop a computational model of an adherent cell and to model the deformation of a bone cell due to commonly-applied magnitudes of fluid shear stress and strain mechanical stimuli.

3.2.1.1 Model Geometry

Based on images of a spreading cell (Fig. 3.1), a finite element model was developed to represent a spread bone cell adherent on a flat substrate (Fig. 3.2). This idealised biomechanical model comprises a nucleus, an internal cytoskeleton of tensile actin and compressive microtubule elements, together with cytoplasm, and membrane components (Fig. 3.2). The nucleus was formed from an ellipse with a major axis of 8 μm, minor axis of 5 μm, and a distance of 2 μm from the lower flat surface of the model representing the cell-substrate interface. The cytoplasm and nucleus components are meshed with 8-node lower-order hexahedral elements, and the membrane is meshed with 4-node shell elements (Fig. 3.2).

The internal cytoskeleton in the model was formed by repositioning an originally rounded tensegrity structure (Fig. 3.3). In this structure the end of each microtubule strut connects with four actin filament cables at 12 common nodes, which are also coincident with membrane and underlying cytoplasm nodes and are therefore analogous to focal adhesion complexes. Re-positioning of the internal cytoskeletal network to comply with the more spread shape of the model (Fig. 3.2) was achieved by establishing new positions for nine cytoskeletal 'focal adhesion' nodes (nodes 4 to 12 in Fig. 3.3) on the membrane surface of the model. To determine the exact new focal adhesion positions, radial planes defined by the central axis of the

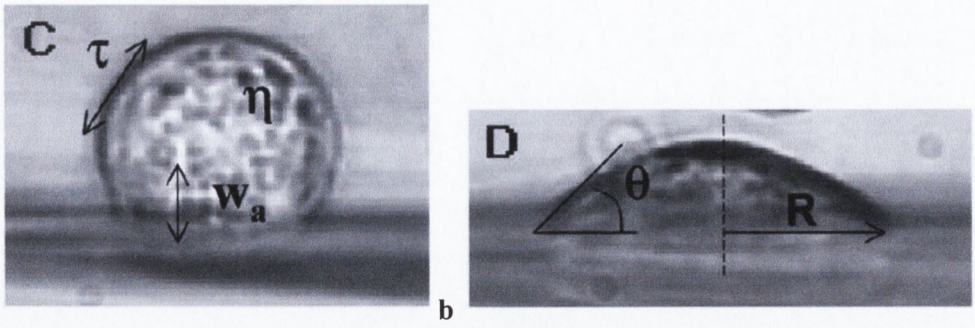

Fig. 3.1 *Images of a spreading chick embryo fibroblast adherent on a glass microplate for (a) 5 minutes, and (b) after 3 hours. The dimensions of the finite element models developed (Table 1) correspond to contact angles (θ) and contact radii (R) highlighted in (b). Adapted from Frisch and Thoumine (2002).*

model and the original positions of the focal adhesion nodes in Fig. 3.2 were established. The intersection of these radial planes with the model surface yielded lines along which the new nodal positions must lie. Points of intersection of these surface lines with horizontal planes that maintain the vertical proportions of the original tensegrity structure, i.e. the planes defined by focal adhesion nodes 4, 5, 6, nodes 7, 8, 9 and nodes 10, 11, 12 (Fig. 3.3), yielded nine new positions for cytoskeletal focal adhesion nodes on the membrane surface (Fig. 3.2). The original lengths and positioning of microtubule and microfilament elements are altered to comply with these new positions to yield the configuration for the internal cytoskeleton in the biomechanical model (Fig. 3.3).

The cell-substrate interface of the model includes three end-nodes (nodes 1, 2, 3 in Fig. 3.3) of microtubule struts, one from each orthogonal direction. Microtubule struts and microfilament cables are meshed with single link elements (2-node three-dimensional spar elements with a bilinear stiffness matrix), supporting compression-only and tension-only respectively. This coincidence of nodes is achieved through either re-sizing of the solid cytoplasm (and membrane shell) elements, or by slight re-positioning of nodes of the cytoskeletal elements.

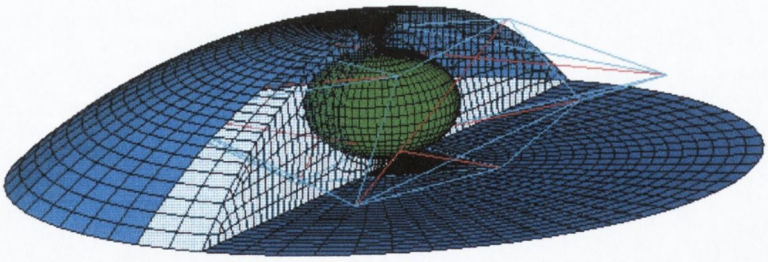

Fig. 3.2 *Three-dimensional computational biomechanical model of an adherent cell. The cell model comprises nucleus (in green), microfilament (blue lines), microtubule (red lines), cytoplasm (internal transparent elements) and membrane (dark blue) components. Half of the cytoplasm and membrane components are omitted for clarity. Cell model dimensions (contact radius, 19.2 μm; height, 7.6 μm) are based on the radius (R) and contact angle (θ) highlighted in Fig. 3.1 and model volume is ~3,000 μm³.*

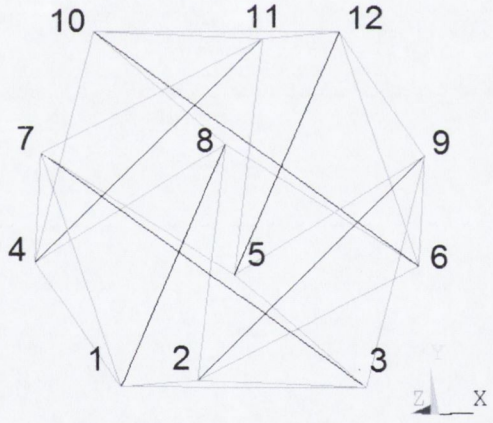

Fig. 3.3 *A three-dimensional tensegrity network of six compression-bearing struts (two in each orthogonal direction) representing the aggregate behaviour of microtubules (dark lines), surrounded by and connected with 24 tensional cables representing actin filaments (light lines). The internal cytoskeleton in the cell model (Fig. 3.3) is arrived at by altering the lengths and positioning of the microtubule and actin filament components in order to fit the cytoskeletal network to a more spread configuration (Fig. 3.2). See Section 3.1.1.1 for further explanation.*

Table 3.1 *Elastic properties assigned to the components in the model.*

Cell component	Elastic modulus (Pa)	Poisson's ratio (v)
Cytoplasm	100 *	0.37
Nucleus[¶]	400	0.37
Membrane†	10^3	0.3
Microtubules[§]	1.2×10^9	0.3
Microfilaments[§]	2.6×10^9	0.3

[¶] Guilak et al. (2000); † Kamm et al. (2000); [§] Gittes et al. (1993)

3.2.1.2 Constitutive modelling of cellular components

Material properties for cellular components of bone cells are currently unknown and were therefore estimated from published data for various cell types (Table 2.2, Section 2.2.2.3). The cytoplasm and nucleus were treated as linear elastic and isotropic continua. Following Kamm et al. (2000), the elastic modulus of the cytoplasm is chosen as 100 Pa. The nucleus has been reported as four times stiffer than the cytoplasm (Guilak et al. 2000) and is therefore taken as 400 Pa. Poisson's ratio (v) for both nucleus and cytoplasm is taken to be 0.37 (Shin and Athanasiou, 1999). In a model developed by Kamm et al. (2000), in which epithelial cell membrane elasticity was specified as 10^7 Pa with a thickness of 6 nm, it was concluded that membrane elasticity was likely over-estimated. In the model a lower value of 10^3 Pa was therefore taken (with $\nu = 0.3$) while maintaining the same membrane thickness. The elastic properties applied to the cytoskeletal components in the model are based on the elasticity values determined by Gittes et al. (1993), who measured the flexural rigidity (bending stiffness) of microtubules and microfilaments when subjected to thermal fluctuations. In the model the microtubules were assigned cross-sectional areas of 190 nm^2, while the microfilaments are thinner with an area of 18 nm^2. These values were also taken from the study by Gittes et al. (1993).

3.2.1.3 Initial conditions

In the modelling approach, it was assumed that each cell was attached only to the underlying substrate. Cytoskeleton nodes 1, 2, 3 and membrane nodes on the lower surface (cell-substrate interface) of the model are constrained in all degrees of freedom and are therefore analogous to focal adhesion sites in adherent cells. An arbitrary initial strain (or prestress) can be applied as a tensile strain to actin cytoskeleton components, to account for contractile forces in the sub-membranous actin network.

3.2.2 Quantitative corroboration of the cell model

Regarding model confirmation, it was necessary to mesh the model with hexahedral elements that use linear shape functions since it was found that displacement boundary conditions applied to nodes of tetrahedral elements resulted in significant warping of those elements. Sweep meshing with hexahedral elements resulted in a nodal density on the top surface that was sufficiently refined for application of constraints that reflect the probe geometry at each indentation depth. Further refinement would lead to a greater number of nodes and hence increased accuracy, but was avoided due to technical difficulty and computational expense.

3.2.2.1 Boundary conditions for corroboration of the model

Quantitative corroboration of the model is addressed by subjecting the model to loading conditions that replicate indentation by atomic force microscopy (AFM). Two approaches are adopted to simulate the indentation of an AFM probe into the surface of the model:

(i) application of a point load on a node to investigate differences between the point load and probe modelling methods (see (ii) below). Indentation depths resulting from a point load of 1 pN (applied to node A in Fig. 3.4) are compared to the reaction forces that resist applied displacements on nodes (60 nm) in the same region of the mesh. Variations in compliance along the model surface are assessed by applying a larger indentation force of 50 pN to nodes at three points along the model surface (B, C and D in Fig. 3.4).

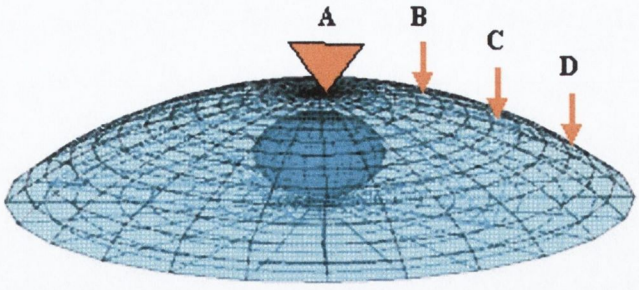

Fig. 3.4 *Loading conditions used for model confirmation: prescribed displacements and a point load are both applied at location A in a refined area of the surface mesh, to allow comparisons between both methods (see (i) and (ii) in the text). Point loads are also applied at locations B - D along the model surface (B and D are ~6 and 4 μm respectively from focal adhesion node C).*

(ii) application of displacement boundary conditions to a number of nodes to better simulate how an indenting tip indents and displaces the cell membrane surface. This allows comparisons with force-indentation curves obtained experimentally. Vertical displacement boundary conditions are chosen to reflect the actual geometry of a conical probe with a contact angle of 50^0 as it indents the cell surface. The prescribed displacements applied in modelling the probe, ranging from 50 nm to 100 nm, are applied to nodes in an area of the mesh that has been refined for that purpose (in the region of node A in Fig. 3.4). The reaction forces resisting these indentation constraints will yield force-deflection curves that can be used in determining local elasticity values through use of an appropriate theoretical relation.

3.2.2.2 Theoretical analysis of AFM probe indentation

The problem of contact between isotropic elastic bodies was first addressed by Hertz (1881), and later by Boussinesq (1885). Sneddon (1965) followed Boussinesq's classical elasticity approach and developed expressions for the relation between load and infinitesimal indentation of a semi-infinite elastic material for several axisymmetric rigid indenter geometries. As derived

by Sneddon (1965), the total load F required for normal penetration δ of a cone of semi-vertical angle α is given by:

$$F = \frac{\pi \mu r^2}{(1-\upsilon)} \tan\alpha \qquad (3.1)$$

where $\mu = \frac{E}{2(1+\upsilon)}$ is the rigidity modulus, ν is Poisson's ratio, and the contact radius r is related to indentation depth δ by:

$$r = \frac{4\,\delta^2}{\pi^2 \tan^2\alpha}$$

Substituting for μ, and r gives the relation between force and indentation depth:

$$F = \frac{2E}{\pi \tan\alpha (1-\upsilon^2)} \delta^2 \qquad (3.2)$$

In the model developed in this thesis, the axial component of the total reaction force at all nodes to which displacement constraints are applied is taken as equivalent to F (cell-substrate reaction forces are considered negligible in accordance with the assumption of infinite sample thickness used in the derivation of equations (3.1) and (3.2): see Sneddon (1965)), δ is the applied indentation, and α is taken as 50^0. The expression cannot yield both the elastic modulus E and Poisson's ratio ν from the force-deflection (F vs. δ) curves; ν is therefore chosen to have a value of 0.37, identical to the underlying cytoplasm. Using eqn. (3.2), the reaction force versus applied indentation depths can then be used to determine E (elasticity) values, which can then be compared to those experimentally-derived estimates (Section 2.2.2.1).

3.3 Application of the computational cell model

3.3.1 Probing the structural characteristics of adherent cells

To investigate the structural behaviour of adherent cells, the biomechanical model was recreated in six increasingly spread configurations, the geometries of which were based on images of spreading fibroblasts (Table 3.2), with the cell immediately post attachment having its most rounded configuration (Fig. 3.1a). The cytoskeleton was formed in each model in a similar manner to that described for the spread configuration in Section 3.2.1.1, with microtubule and

Table 3.2 *Dimensions of each finite element model A to F in Fig. 3.5.*

Model	Contact radius (μm)	Cell model height (μm)
a	6	14
b	8.5	12.8
c	11.2	10.6
d	14.3	10.1
e	17.5	8.5
f	19.2	7.6

microfilament elements altering in length and position from the original tensegrity structure (Fig. 3.3) in finding the nine new nodal positions for each new model. Contact radii and heights of each of the finite element models are provided in Table 3.2. The corresponding cell volumes are ~3,000 μm^3 and the nucleus in each model was formed as described for the spread model in Section 3.2.1.1. The cytoplasm and nucleus elements in each model were meshed with 4-node lower-order tetrahedral elements. The membrane is meshed with 3-node shell elements.

In all models with the various degrees of spreading (Fig. 3.5a to 3.5f), nodes at the cell-substrate interface are constrained in all three translational degrees of freedom. These constrained points are analogous to focal adhesion sites in adherent cells. Initial constraints for each of the six models also involve application of a prestress (initial strain) in the first loadstep of each analysis, as described below. This prestress is a tension applied to the microfilament elements, effectively accounting for the contractile effect of acto-myosin sliding mechanisms in the membrane/cortex region.

3.3.1.1 Spreading effects

All six models were used to investigate alterations in stiffness as contact radius increases. A force of 100 pN is applied horizontally (load vectors denoted by 'A' in Fig. 3.5a), but in both x and z horizontal directions. Averages of displacements in each direction yield stiffness estimates for each model. Prestress values applied to microfilaments are kept constant in each model, which is in accordance with observations of constant cortical membrane tension in spreading cells (Thoumine et al., 1999).

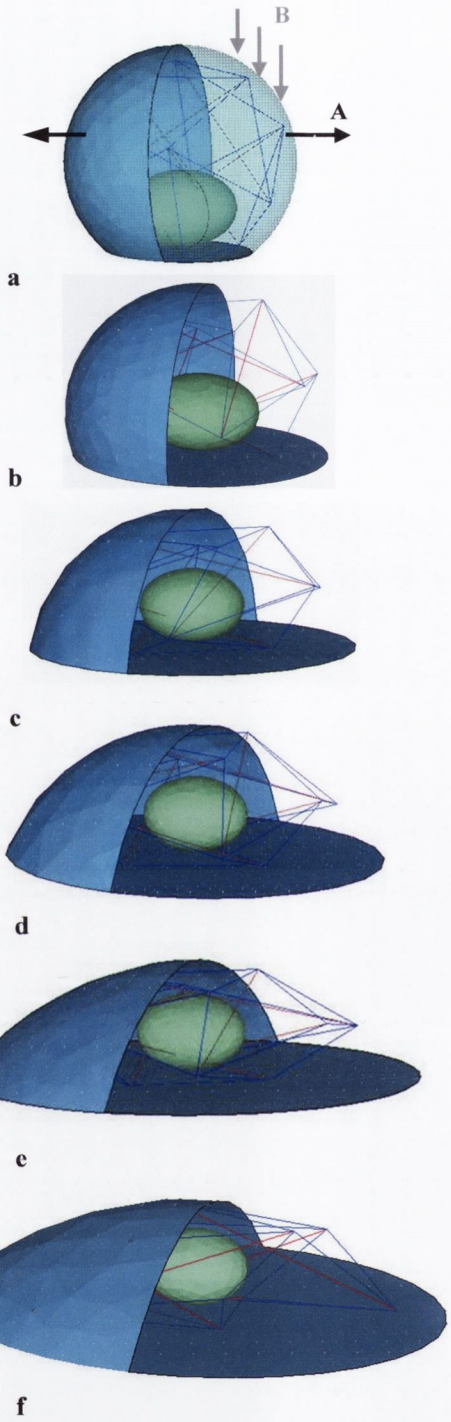

Fig. 3.5 *Three-dimensional finite element models (a) to (f) of adherent cells at increasingly spread shapes to the final configuration in Fig 3.1b. Each model comprises membrane, nucleus, cytoplasm, and cytoskeleton components. The cytoplasm is omitted for clarity in all models.*

3.3.1.2 Variable compliance of the cell

All six degrees of spread cell configurations in Fig. 3.5 are used to investigate differences in rigidity along the model membrane surface. Again, prestress is maintained at a constant value (2%) in each model. In each model, vertical forces (50 pN) are applied to a focal adhesion node, and at various distances (<5 μm) from the node (load vectors denoted by 'B' in Fig. 3.5a).

3.3.1.3 Prestress and strain hardening

All other analyses of cell structural behaviour are investigated using the post-attachment cell model only, i.e. Fig. 3.5a. The loads applied involve application of either (i) horizontal forces (50 pN) applied to two surface nodes in opposite directions, or (ii) the application of vertical indentation forces (50 pN) to membrane surface nodes.

Prestress values assigned to microfilament elements of model (a) are varied from 0 to 10% in the first loadstep of each analysis, while subsequent loadsteps involve application of a 100 pN force (50 pN applied to two membrane surface nodes as illustrated in Fig. 3.5a, load vectors denoted by 'A'). The displacement of nodes in each direction due to the applied force are used to calculate cell model stiffness (nN/μm). To investigate strain hardening, the force applied in the second loadstep is increased from 25 to 150 pN while maintaining constant prestress values in the first loadstep.

3.3.1.4 Parametric variation of material properties

The influence of material properties on stiffness is investigated in the rounded cell configuration (Fig. 3.5a) by modulating the elasticity of each model component by 50% and 200% of the original values, and computing displacements in response to 100 pN. Poisson's ratio value for the cytoplasm is also altered from 0.37 to 0.25 and 0.49 in order to determine the effect, if any, of the degree of cytoplasm incompressibility. Constant prestress values are maintained during the parameter study.

3.3.2 Determining the consequences of fluid flow and strain stimuli on bone cells

3.3.2.1. Initial conditions

In experimental stimulation of bone cells, substrate strain and fluid shear stress treatment are generally applied to monolayers of sub-confluent cells. In the modelling approach adopted, it was therefore assumed that each cell was attached only to the underlying substrate and not to neighbouring cells. This assumption allowed application of the original cell model (Fig. 3.2) to determine the deforming effect of 0.6 Pa fluid shear stress and 1,000 με substrate strain on adherent bone cells – these are the magnitudes of mechanical stimuli used by Mullender et al. (2004), as described in Section 2.5.4. Cellular deformation was expressed as the displacement (μm) of the cell model, or as the von Mises stress induced in the various model components, relative to original material properties (% deformation). Von Mises stress (σ_e, N.μm^{-2}) combines the stress values in each direction:

$$\sigma_e = \left\{ \frac{1}{2} \left[(\sigma_{xx} - \sigma_{yy})^2 + (\sigma_{xx} - \sigma_{zz})^2 + (\sigma_{yy} - \sigma_{zz})^2 + 6(\sigma^2{}_{xx} + \sigma^2{}_{xz} + \sigma^2{}_{yz})^2 \right] \right\}^{1/2}$$

Cytoskeleton nodes 1, 2, 3 and membrane nodes on the lower surface (cell-substrate interface) of the model were constrained in all degrees of freedom and are therefore analogous to focal adhesion sites in adherent cells. No initial strain (prestress) was applied to either microfilaments or microtubules, although microfilament prestress was subsequently varied to determine its impact on model results. As the material properties assigned to cell model components are linear elastic and geometric non-linearity can be neglected (given the very small displacements occurring), by computing the deforming effect of one magnitude of fluid shear stress or strain, the deformations that would occur at various magnitudes of fluid shear stress or strain (used in other published studies) can be directly inferred.

3.3.2.2 Loading conditions to model substrate strain

In the four-point bending apparatus used by Mullender et al. (2004), because the height of the adherent bone cells (< 7 μm) is small relative to the thickness of the bending substrate (200 μm), bone cells are subjected to axial strain only and not to bending moments. To model the

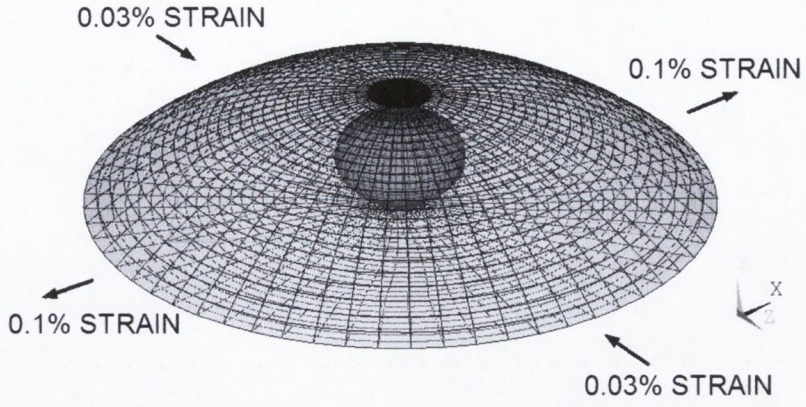

Fig. 3.6 *Loading conditions applied to the cell model in order to model the effect of substrate strain on a single adherent bone cell. Nodes at the at the cell-substrate interface (see text) are constrained in the y (vertical) direction, and displaced by 0.1% and 0.03% strain in the x and z directions respectively.*

effect of substrate strain on an adherent bone cell, each node at the cell-substrate interface of the cell model was displaced axially by 0.1% (1,000 με) strain (Fig. 3.6). As Poisson's ratio (υ) for the glass substrate equals 0.3 the corresponding displacement of nodes in the lateral direction was taken as 0.03% strain (Fig. 3.6).

3.3.2.3 Loading conditions to model fluid shear stress

As the fluid flow in the parallel plate chamber used by Mullender et al. (2004) was laminar, it was assumed that the shear stress to which the bone cells were subjected was equal to the theoretical shear stress at the wall (calculated as 0.6 Pa). Recognizing that cellular dimensions (< 7 μm) are small relative to the distance between the plates (~300 μm), it was assumed that this shear stress acts tangentially along the cell surface in the direction of flow. The forces applied to the cell model (see Fig. 3.7) were found from the shear stress, denoted τ, distributed over the surface area exposed to fluid flow (A_S):

$$F = \tau \times A_S \tag{3.3}$$

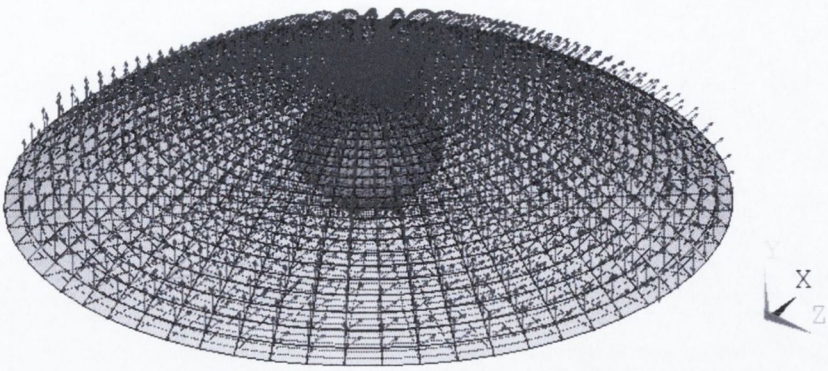

Fig. 3.7 *Loading conditions applied to the cell model in order to model the effect of fluid shear stress on a single adherent bone cell. Tangential forces (resolved to x and y components) are applied to each membrane surface node (arrows), based on the area of each surrounding membrane elements.*

From the model (Fig. 3.2) it is determined that $A_S = 1329\ \mu m^2$. Using Eqn. 3.3, total force is:

$$F = 0.6\ pN/\mu m^2 \times 1329\ \mu m^2$$
$$= 797.4\ pN$$

This force was assumed to be distributed evenly over the membrane surface area. The force applied to each node is the sum of one quarter of the force assigned to each of its surrounding elements. As it is assumed that shear stress acts tangentially, nodal forces are then resolved to horizontal and vertical components based on the contact angle between each node and the cell-substrate horizontal plane (Fig. 3.7).

3.4 In vitro mechanical stimulation of osteoblasts and osteocytes using fluid flow

3.4.1 Pulsatile fluid shear stress stimulation of bone cells in monolayers

3.4.1.1 Cell culture

Osteoblastic MC3T3-E1 cells (OB) were cultured in alpha minimum essential medium (α-MEM; Gibco, Paisley, UK), supplemented with 10% fetal bovine serum (FBS; Gibco), 1% β-glycerophosphate, 1% L-glutamin (Sigma-Aldrich, St. Louis, MO, USA), 1% ascorbic acid (Merck, Darmstadt, Germany), and 0.5% fungizone and gentamicin antibiotics (Gibco).

Osteocytic MLO-Y4 cells (OCY: Kato et al., 1997) were cultured in α-MEM, supplemented with 5% FBS, 5% calf serum (Gibco), 0.1% penicillin and streptomycin (Sigma-Aldrich), and 0.5% fungizone and gentamicin. The day preceding an experiment, 5 x 10^5 of either OB or OCY cells were plated on polylysine-coated (50 μg/ml; poly-L-lysine hydrobromide, mol. wt. 15-30 x 10^4; Sigma-Aldrich) glass slides such that the cells could be subjected to pulsatile fluid flow (PFF) stimulation in a parallel plate chamber, as was used by Klein-Nulend et al. (1995) (Fig. 2.10). Cells were cultured in Petri dishes for 24 hrs in the appropriate medium (as described above) and were maintained at 37°C in a 95% air and 5% CO_2 environment throughout the experiment (Fig. 3.8).

3.4.1.2 Pulsatile fluid flow stimulation

Cells were then selected at random from the three groups, i.e. untreated, actin-disrupted, or microtubule-disrupted (see Section 3.4.3.1). After the 1 hr pre-incubation the 13 ml experimental medium was refreshed, i.e. replaced with the appropriate medium for that group. Cells were either (i) cultured under static conditions in Petri dishes containing 13 ml experimental medium for 10 mins, or (ii) subjected to pulsatile fluid flow (PFF)-derived shear stress of magnitude 0.39 Pa (3 Hz) or 0.64 Pa (5 Hz) for 10 mins (Table 3.3). The glass slides to which cells were attached served as the base of the parallel plate chamber. The PFF was generated by pumping 13 ml of the experimental medium for each group through a parallel plate chamber using a roller pump in an incubator, also at 37°C with the cycling medium in the presence of a steady flow of CO_2 (Fig. 3.8). In both static and pulsatile fluid flow cultures, a 1 ml sample of medium was taken from the flow loop after 10 mins for biochemical analysis. The rate of flow was confirmed using a small animal blood flow meter (T206, Transonic Systems Inc.) included in the flow loop to confirm the accuracy of the flow characteristics above.

3.4.2 Determining cell response: nitric oxide and prostaglandin E_2 release

Nitric oxide was measured as nitrate (NO_2^-) accumulated in the experimental medium using Greiss reagent, consisting of 0.1% napthylethylene-diamine-dihydrochloride, 1% sulfanilamide,

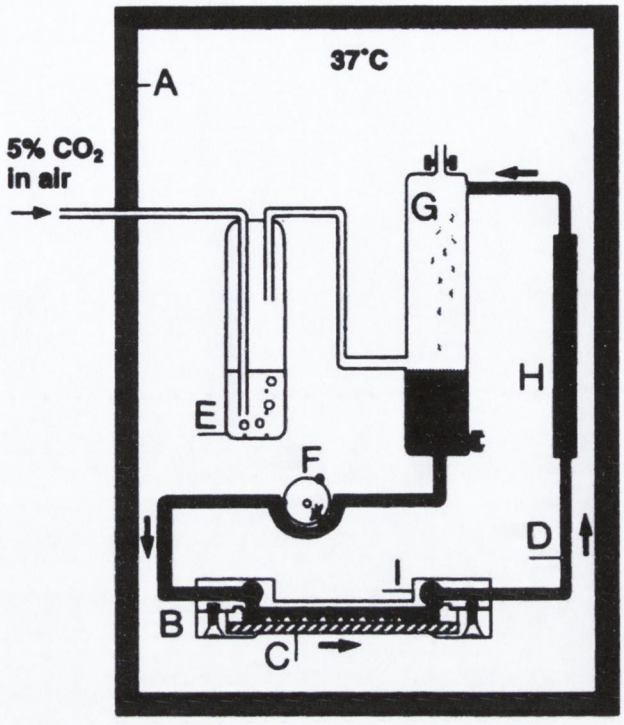

Fig. 3.8 *Schematic illustration of the apparatus used to apply pulsatile fluid shear stress to osteocytes or osteoblasts by pumping experimental medium through a parallel plate chamber. 37° incubator (A); parallel plate chamber (B); polylysine-coated glass slide containing cells (C); experimental medium (D); H_2O (E); revolving pump (F); 5% CO_2-air mixture (G); flow probe (H); plate with two openings through which experimental medium enters and exits chamber (I). Adapted from Klein-Nulend et al. (1995).*

and 2.5M H_3PO_4. Serial dilutions of $NaNO_2$ in medium were used to obtain a standard curve for each measurement. The absorbance was measured at 550 nm. The detection threshold of Griess reagent assay is 0.1 μM (Kleinhenz et al., 2003), which was confirmed with $NaNO_2$ standards. PGE_2 release in the conditioned medium was measured by an enzyme immunoassay (EIA) system (Amersham, Buckinghamshire, UK) using an anti-body raised against mouse PGE_2. The detection limit was 16 pg/ml. Absorbance was measured at 450 nm.

Data obtained from separate experiments were pooled and expressed as mean values ± SEM. Comparisons between groups were made using the Mann-Whitney U test. Differences were considered significant if $p < 0.05$.

Table 3.3 *Flow characteristics of the applied pulsatile fluid flow regimes.*

	Low PFF	Medium PFF
Frequency (Hz)	3	5
Flow rate (cm^3/s)	0.2	0.33
Shear stress (Pa)	0.4	0.64

3.4.3 Investigating cytoskeletal involvement in bone cell responses

3.4.3.1 Disruption of the actin and microtubule cytoskeleton

Prior to fluid flow stimulation, plated cells were incubated for 1 hr in 13ml of the appropriate medium with the total serum content reduced to 2% (referred to as experimental medium). Cells were then divided at random into three groups:

(i) untreated control medium;

(ii) actin-disrupted: medium supplemented with 1 μM of cytochalasin B (Sigma-Aldrich), a toxin that prevents actin polymerisation (Theodoropoulos, 1994), and consequently blocks formation of contractile microfilaments (Carter, 1967; Krishan, 1972). The concentration of cytochalasin B used was based on a previous study in which it was shown that PFF-induced PGE_2 release in embryonic chicken calvarial osteocytes was dependent on the actin cytoskeleton (Ajubi et al., 1996);

(iii) microtubule-disrupted: medium supplemented with 1 μM of colchicine (Sigma-Aldrich), a toxin that prevents microtubule polymerisation (Wilson and Friedkin, 1966; Farrell and Wilson, 1980; Andreu et al., 1991; Luduena et al., 1992). 1 μM of colchicine was used as that concentration was considered a medium concentration in a previous study (Trickey et al., 2004) .

It was observed that these concentrations of both cytoskeleton-disrupting agents had a significant non-toxic effect on cell morphology within 1 hr.

3.4.3.2 Cytoskeletal staining

Immediately after 10 mins of pulsatile fluid flow (or static controls), the glass slides containing either OBs or OCYs were removed from the parallel plate chamber and, along with static controls, were washed twice in phosphate buffered saline (PBS) in Petri dishes. The cells were then fixed using 4% formaldehyde in PBS for 15 mins, washed in PBS and permeabilised using 0.1% Triton in PBS for 10 mins, followed by two washes in PBS. To reduce non-specific binding, cells were then incubated in PBS containing 1% bovine serum albumin for 15 mins. To fluorescently label actin, cells were incubated in ~80 µl of FITC-phalloidin (Molecular Probes, Leiden, The Netherlands) for 45 mins in a covered container, and were then washed twice in PBS. Hence, changes in the actin cytoskeleton due to pulsatile fluid flow and due to both actin and microtubule disruption could be visualised. The percentage of cells in which alignment of stress fibers occurred in each of the images obtained from 4 separate experiments was calculated as mean values ± SEM. Fluorescent images were obtained at 488 nm using a fluorescent microscope.

3.5 Using atomic force microscopy to mechanically stimulate single osteoblasts

This section describes the experimental apparatus and procedure used to apply quantified mechanical forces to single bone cells, while simultaneously measuring resultant changes in osteoblastic nitric oxide release. Of particular interest is the magnitude of the force required to elicit a response, the delay in and duration of nitric oxide release after mechanical stimulation, and whether any response is transmitted to neighbouring cells.

3.5.1 Synchronised osteoblast indentation and nitric oxide response measurement

An Asylum Research (CA, USA) MFP-3D atomic force microscope (AFM) is combined with an Olympus Cell^{R} Imaging Station (Olympus Biosystems, GmbH, Germany). In this system the AFM scanner and head are positioned above the stage of the fluorescent microscope. Hence, movement of the sample and AFM tip relative to the objective lens of the inverted microscope

is made possible. An advantage of the combined system is that real-time measurement of the fluorescence within the field of view of the objective lens can be obtained simultaneously during operation of the AFM.

Specifically, in this experiment, the combined AFM and fluorescent microscope system is used to apply quantified mechanical forces to single MC3T3-E1 osteoblasts, while measuring real-time NO response as indicated by the intensity of an intracellular fluorescent dye activated by intracellular nitric oxide or by nitric oxide in the extracellular medium.

3.5.1.1 Cell culture and intracellular nitric oxide monitoring

MC3T3-E1 osteoblasts were cultured in alpha minimum essential medium (α-MEM: Sigma-Aldrich, Dorset, UK) containing 10% foetal bovine serum (FBS: Gibco, Paisley, UK), 1% penicillin-streptomycin solution 1000 IU (Gibco), 2mM L-glutamine (Gibco) and 0.5% 100 mM Sodium Pyruvate (Sigma-Aldrich). The osteoblasts were kept an incubator at 37°C in a 95% air 5% CO_2 environment. Subculture was routinely performed at ~80% confluence, using 0.25% trypsin.

The day preceding each experiment, osteoblasts were plated at low density on 40 mm diameter glass coverslips, and incubated in culture medium in Petri dishes until the osteoblasts had attached. The osteoblasts were incubated overnight in 5 ml of the experimental culture medium described above. Prior to each experiment, the culture medium was removed and the osteoblasts were washed with a Mg^{2+}/Ca^{2+} buffer solution, containing 130 mM NaCl, 5 mM KCl, 1mM Na_2HP0_4, 1mM $MgCl_2$, and 1mM $CaCl_2$. The osteoblasts were then incubated for 40 mins in buffer solution containing 5μM DAF-FM (Molecular Probes, The Netherlands). DAF-FM (4-amino-5-methylamino- 2′,7′ -difluorofluorescein diacetate) is a fluorescent dye with a fluorescent emission wavelength of 520 nm that is cell-permeant. It is non-fluorescent until it reacts with NO to form a fluorescent benzotriazole. The NO concentration limit for detection is ~3 nM (Kojima et al., 1999). The DAF-FM solution is then removed, the osteoblasts are washed twice, and incubated for a further 15 mins with the Mg^{2+}/Ca^{2+}buffer buffer to remove any cell debris. The glass coverslips to which the osteoblasts are attached to an annulus of plastic

machined from the bottom of a Petri dish, such that the cell surface positioning allowed for simultaneous use of the combined microscope and AFM system. The Petri dish is positioned above the objective lens of the inverted microscope and below the AFM head and cantilever tip. The osteoblasts and AFM tip are constantly immersed in buffer solution for the duration of the experiment. Using the Olympus inverted microscope software platform (Cell R^{TM}) the osteoblasts were exposed at intervals to excitation light of wavelength 488 nm during the course of the indentation experiment. Nitric oxide levels during the experiment are measured by drawing boundaries around 'regions of interest' within which the intensity of fluorescence can be automatically quantified over the course of the experiment (Fig. 3.9).

3.5.1.2 Cell indentation procedure

The glass slide to which the osteoblasts are attached, which must remain immersed in cell medium, is placed on the AFM scanner directly above the objective lens of the inverted microscope. The AFM head and cantilever tip is positioned above this cell surface. The cantilevers used are rectangular NSC36 cantilevers, with a stiffness range from 0.5 to 2.5 N/m (Mikromasch, Germany). The stiffness and sensitivity of the cantilever are then calibrated (see Section 3.4.3), both in air and when completely immersed in the PBS solution. The level of the AFM head is lowered such that the tip lies slightly above the surface (on the order of mm's). In this position, the AFM cantilever tip can now be visualised through the objective lens and a droplet of liquid medium can be formed between the cell surface and the AFM holder, completely immersing the cantilever (Fig. 3.10).

An osteoblast with a well-spread morphology is chosen, ensuring that a clear fluorescent image of the osteoblast can be obtained without excessive background staining – this means the fluorescent dye has successfully internalised within the osteoblasts, and has been sufficiently washed. The cantilever is brought to the substrate by engaging in contact mode, meaning that any cantilever deflection during advancement towards the cell surface is controlled in a feedback loop that maintains deflection at a predetermined 'setpoint' value via appropriate movement of the piezo driver. This ensures a 'soft landing' and minimises risk of tip damage.

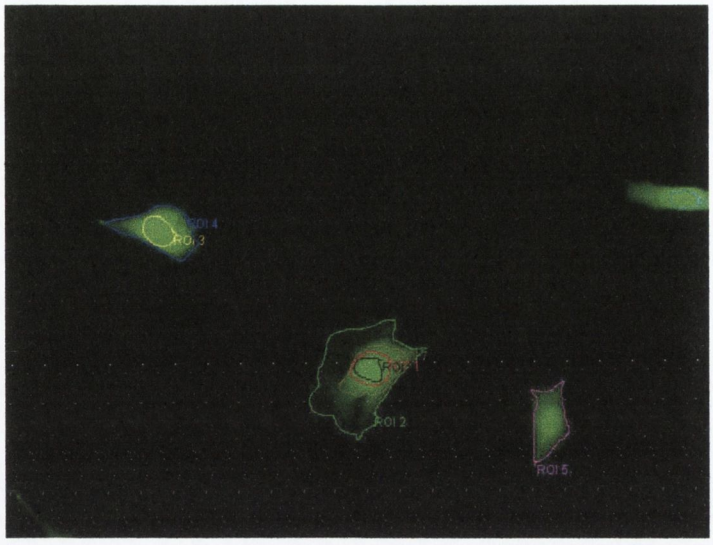

Fig. 3.9 *Fluorescent image of intracellular nitric oxide in MC3T3-E1 osteoblasts, incubated in DAF-FM fluorescent sensor and buffer solution for 35 mins. Also shown are regions of interest drawn around whole osteoblasts of an internal region of an osteoblast, such that changes in nitric oxide levels within these regions can be precisely quantified.*

The height of the tip is then adjusted to > 5 μm above the cell surface ensuring that the tip is at least 2 μm above any adherent osteoblasts. The final part of experimental setup is to position the point of the conical tip above a region of the osteoblast cytoplasm.

At time 0 of each experiment the tip is stationary for 30 s. This is to establish the baseline level of osteoblast nitric oxide fluorescence before indentation. At 30 s, the AFM tip is actuated downwards at a velocity of < 1 μm/s by an estimated travel distance such that the tip will contact with, and indent, the osteoblast membrane. The estimated travel distance is equal to the tip height above the cell surface minus the estimated osteoblast height, and is typically 1 to 2 μm. Once the distance that results in a tip deflection that corresponds to a specified trigger force is established (between 15 and 50 nN), those parameters are maintained for continuous indentation for a further 60 s. The rate of force application is dictated by the actuation time, i.e. the time required for the piezo to extend and retract between successive indents, and is typically ~3 Hz. The microscope shutter is triggered to open every 3 s for the entire experiment (from 0 to 300 s) to capture the fluorescence intensity within the regions of interest for each successive time point. This shutter speed yielded the optimal balance between resolution required to

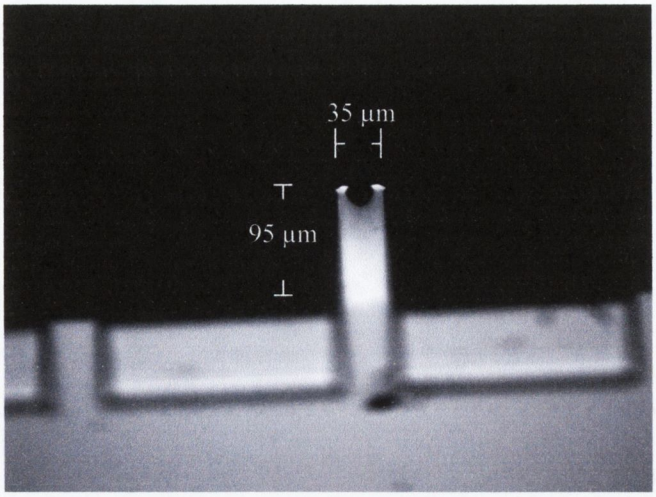

Fig. 3.10 *Image of a typical cantilever used in each indentation experiment. Prior to each experiment a new cantilever is chosen from three rectangular NSC36 Mikromasch cantilevers and the remaining two (in this case the left and right) cantilevers are removed to prevent uncontrolled contact with other osteoblasts or with the substrate during indentation. This image is taken from below using a 20x objective lens of the inverted fluorescent microscope. The conical tip extends a height of ~20 µm (out from the page) and has a curvature end-radius of ~14 nm (tip dimensions courtesy of Dr. M. Polcik, SFI Nanoscience Laboratory, TCD).*

capture transient changes in short-lived nitric oxide levels, while avoiding excessive sample bleaching through over exposure. A force versus travel distance graph (force curve) is obtained for each successive indent; 60 s of indentation yields ~20 force curves.

3.5.1.3 Quantifying the applied indentation force

To determine the magnitude of force applied to the osteoblast membrane by deflection of the AFM tip, it is necessary to determine the stiffness and sensitivity of the cantilever. Once the stiffness, i.e. spring constant (N/m) of the cantilever is known, it is then possible to determine the force that corresponds to a certain cantilever deflection (Fig. 3.11). As cantilever deflection is measured by the photodiode as a voltage, the sensitivity (nm/V) of the cantilever must be known to determine the deflection that corresponds to a certain voltage. Here, the method used in calibrating the sensitivity and spring constant of the rectangular AFM cantilevers used in all

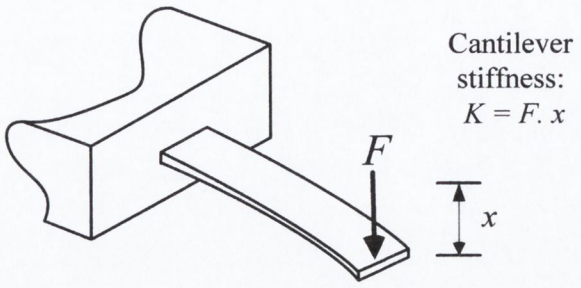

Fig. 3.11 *Schematic illustration of Hooke's Law - the spring constant (K) of the cantilever must be known to relate the measured deflection (x) to an applied force (F).*

experiments is briefly outlined.

The method used to determine the spring constant is based on an expression derived by Sader (1998) given in Eqn. 3.3 below, which relates the spring constant (K) to the rectangular dimensions of the cantilever (L and b), the density of the fluid (ρ), the resonant frequency of oscillation (ω_f) of the cantilever, and the quality factor (Q_f) of the resonant peak. Γ_i^f is a function of the fluid hydrodynamics:

$$K = 0.1906\,\rho b^2 L Q_f \omega_f^2 \Gamma_i^f\left(\omega_f\right) \tag{3.3}$$

The hydrodynamic function Γ_i^f was first derived by Green and Sader (2002) by solving Fourier-transformed equations of motion (based on the velocity field, the hydrodynamic pressure, the fluid density and viscosity) for an infinitely long rigid beam with a cross-section identical to that of the cantilever of interest. By interpolating to asymptotic limits the numerical expression was made valid for all Reynolds numbers (Green and Sader, 2002). The plan view dimensions of the rectangular cantilever are taken from the manufacturers specification. The resonant frequency and quality factor are obtained by measuring the cantilever thermal noise spectra – essentially cantilever oscillations due to thermal noise (a typical spectrum is given in Fig. 3.12). The blue line in Fig. 3.12a and 3.12b is the theoretical fit used to determine the parameters required for Eqn. 3.3. The sensitivity of the cantilever, i.e. deflection corresponding to the measured photodiode voltage, is also determined from this spectrum.

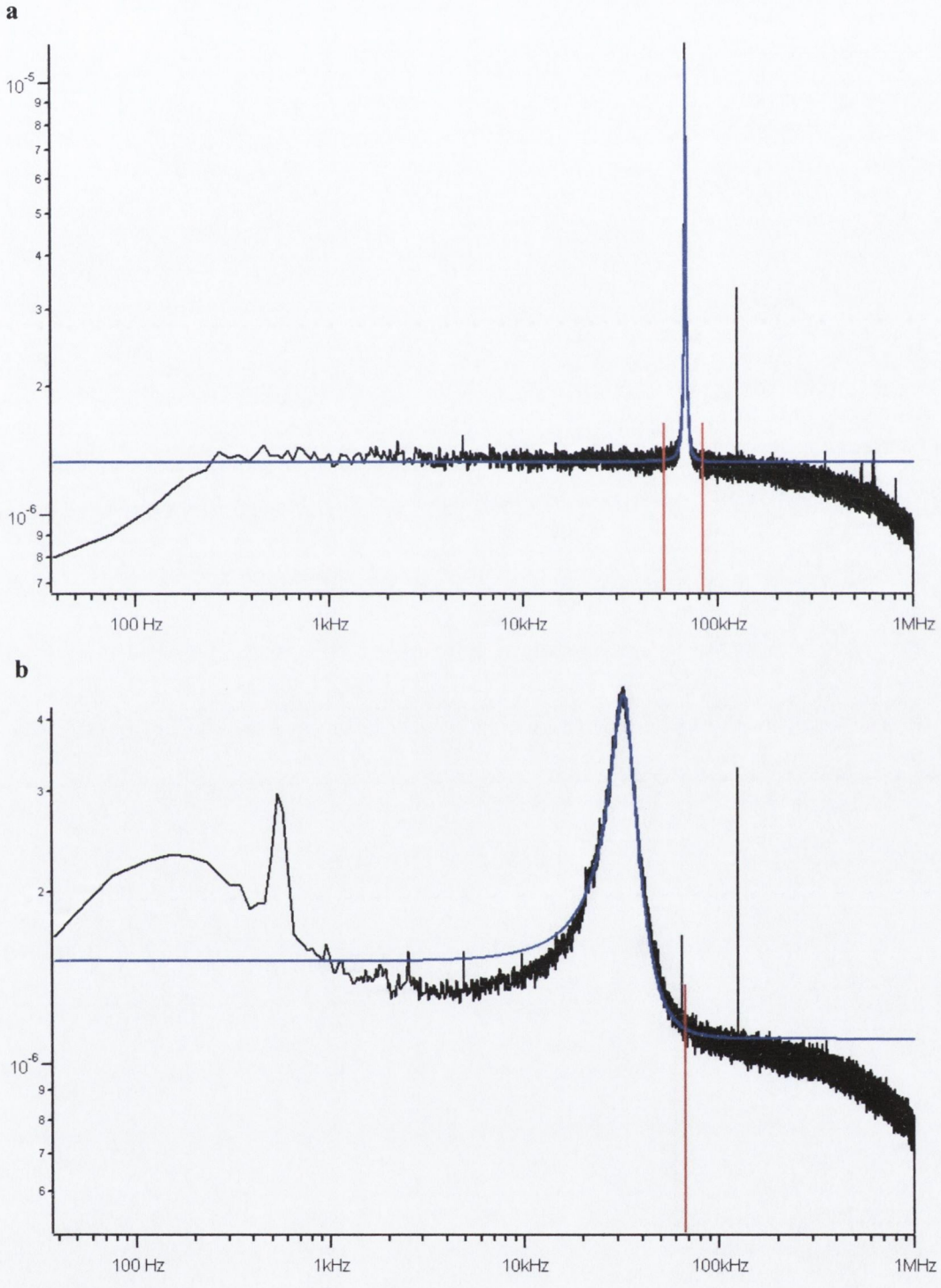

Fig. 3.12 *Thermal noise power spectrum – frequency (x-axis: Hz) versus cantilever amplitude (y-axis: metres) of a NSC36 Mikromasch cantilever oscillating in air (a) and in liquid medium (b). The characteristic resonant frequency (in kHz), the stiffness (in N/m) and sensitivity (in nm/V) of each cantilever are determined by fitting the various parameters required for implementation of the 'Sader' method to these thermal spectra.*

Prior to each experiment, the stiffness and sensitivity are immediately calculated using the above method, firstly in air and again once the cantilever is immersed in liquid medium, which introduces damping to cantilever movement. Two thermal spectra are therefore obtained and both should yield similar stiffness values, as the hydrodynamic properties of each medium are accounted for (Fig. 3.12b). The 'Sader' method has been experimentally validated (Chon et al., 2000), and is accurate provided that the length of the cantilever greatly exceeds its width, which in turn must greatly exceed its thickness, and that the quality factor significantly exceeds unity. It is therefore less accurate in liquid as the resonant peak is less pronounced and the quality factor is lower than in air. However, it is ensured that the cantilever used provides good agreement between stiffness values obtained in air and liquid before proceeding with each experiment. After each experiment the tip is re-positioned above the glass substrate (away from any osteoblasts) and the piezo is actuated downwards to indent the glass surface, yielding a voltage-deflection curve. Assuming zero deformation of the tip or sample, the slope of the linear contact region of this curve yields the correct sensitivity value in nm/V, which should be within 5% of the estimated sensitivity using the method described above. The force-indentation data from each successful indentation can be used to calculate elasticity values using the Hertz method, as described in Section 3.2.2.2. Hence comparisons of elasticity values from each experiment are possible and will illustrate how elasticity varies with depth of indentation into the membrane.

3.5.1.4 Calculating membrane surface strain due to indentation

The force-indentation characteristics obtained during tip indentation into an osteoblast membrane can be used to calculate the surface strains using theory describing the normal contact of elastic bodies. Johnson (1985) reports that during contact between a cone (in this case a conical AFM tip) of semi-vertical angle α and a deformable flat surface, the pressure on the face of the indenting cone is:

$$p(r) = \frac{E\cot(\alpha)\cosh^{-1}\left(a/r\right)}{2\left(1-\upsilon^2\right)} \tag{3.4}$$

and the total force (F) applied by conical tip is:

$$F = \frac{\pi a^2 E \cot(\alpha)}{2(1-\upsilon^2)} \quad , \tag{3.5}$$

where E is the elasticity, a is the contact radius, and r is the distance from the centre of indentation (note that in Eqn. 3.4, when $r = 0$ at the centre of indentation the pressure is infinite, whereas when $r = a$ where tip-membrane contact ends the pressure is zero). The contact radius is determined from the experimentally-derived indentation depth (determined from a force curve) using the following expression, as reported by Sneddon (1965):

$$a = \frac{2\delta}{\pi \tan(\alpha)} \tag{3.6}$$

The relationship between the applied force and the pressure distribution can be written as (combining Eqns. 3.4 and 3.5):

$$p(r) = \frac{F \cosh^{-1}\left(a/r\right)}{\pi a^2} \tag{3.7}$$

The radial (tangential) stress in the surface, which also rises to an infinite value at the apex, is related to the pressure distribution in the following expression (Johnson, 1965):

$$\sigma_r(r) = -\frac{1}{2}(1+2\upsilon)\, p(r) \tag{3.8}$$

The radial stress can be related to the strain by:

$$\varepsilon_r = \frac{\sigma_r}{E} \quad , \tag{3.9}$$

where E is the elasticity value calculated from force-indentation values using the Hertz method, as described in Section 3.2.2.2. Hence, combining Eqns. 3.7 to 3.9 yields an expression for the radial membrane strain ε_r arising from indentation to a depth of indentation δ of a conical tip with an applied force F:

$$\varepsilon_r = -\frac{(1+2\upsilon)\, F \cosh^{-1}\left(a/r\right)}{2E\pi a^2}, \tag{3.10}$$

where α is the semi-vertical angle of the AFM tip, ν is Poisson's ratio (specified as 0.37 based on experimental data in Section 2.2.2.2), E is the elasticity, and a is the tip-membrane contact

radius (resulting from indentation depth δ using Eqn. 3.6 above). Once F and δ are known, membrane radial strain can be calculated using Eqn. 3.10 for any value of r within the tip-membrane circle of contact, i.e. for any value of $r < a$.

3.5.1.5 Control experiments

Each set of osteoblast indentation experiments is accompanied by a control experiment using osteoblasts from the same cell passage. In this control the tip is positioned adjacent to an osteoblast but without any tip-membrane contact or tip movement during the experiment. The purpose of these controls is to establish any alteration in osteoblast NO fluorescence that will occur due to exposure to excitation light regardless of application of mechanical stimuli.

Additional control experiments were performed to address the possibility that:

(i) Fluid flow movement during cantilever actuation (and not the force applied via the tip) is responsible for activation of NO in the osteoblasts. To examine this possibility, standard experimental procedure was followed in 10 experiments (Sections 3.5.1.3 and 3.5.1.4), but the tip was actuated above the osteoblast approximately 2-3 μm above the osteoblast membrane without contacting.

(ii) Alteration in NO fluorescence levels during an indentation experiment may be due to interference of the cantilever with the fluorescence within an osteoblast, or to reflection of fluorescent light from the cantilever during indentation. To examine this possibility, in 15 experiments osteoblasts were incubated in a mitochondrial-selective fluorescent label, Mitotracker Green™. This dye accumulates in the mitochondrial matrix where it covalently binds to mitochondrial proteins. Standard experimental protocol was followed but with the osteoblasts in 5 μM of Mitotracker Green in place of DAF-FM (the NO fluorescent label). Changes in mitochondrial protein content or mitochondrial proliferation occur over a much larger time-scale (18 hrs) than used in the present indentation experiment (Maguire et al., 2005); any changes in mitochondrial fluorescence during this control experiment would

therefore be due to experimental artefacts such as tip interference with fluorescence, and not to osteoblast mechanotransduction.

(iii) It is possible that tip indentation may also result in non-viable osteoblasts by necrosis or apoptosis due to damage to the osteoblast membrane. This is examined in a number of controls using propidium iodide (PI: Sigma-Aldrich), a reagent that is impermeable to the membrane and binds to double-stranded nucleic acid. The standard indentation protocol is followed with osteoblasts incubated in NO indentation, rinsed in PBS buffer, and immersed in buffer containing 1 μl/ml of PI fluorescent dye immediately prior to and during osteoblast indentation. The wavelength of light for PI excitation and emission (580 nm and 630 nm, respectively) differs to that for NO. As PI is membrane impermeable, a positive PI fluorescent staining suggests that the membrane has been damaged or ruptured and that the osteoblast may be non-viable.

3.6 Using the methods to investigate the thesis

The experimental and computational methods presented in this Chapter will be used to obtain evidence in support of the thesis that transduction of nitric oxide and prostaglandin E_2 signalling responses in bone cells subjected to mechanical stimuli is magnitude-dependent and mediated by the cytoskeleton. Computational methods involve the development of a cell model comprising cytoplasm, cytoskeleton, membrane and nucleus components. Previous finite element modelling approaches would have been too rudimentary to give useful data for this thesis, so a cell model based on experimentally-derived evidence of structural involvement of the various organelles was developed and used to examine the origins of qualitative aspects of cell structural behaviour.

The experimental methods allow for several other important aspects of both osteoblast and osteocyte mechanotransduction of signalling responses to be studied. In particular, the experiments involve: (i) application of a pulsating fluid flow to monolayers of cultured bone

cells with visualisation of the involvement of actin and microtubule cytoskeleton components in mechanotransduction of signalling responses, and (ii) application of indenting forces to single osteoblasts with real-time monitoring of dynamic changes in intracellular nitric oxide intensity. Hence, these methods can address the primary question of the thesis by integrating new experimental techniques with computational modelling approaches.

Chapter 4

Results

4.1 Description and structural characteristics of the computational cell model

4.1.1 Structural contribution of the cytoskeleton and other organelles

4.1.2 Corroboration of the cell model by analysis of AFM tip indentation

4.2 Application of computational cell model to *in vitro* experiments

4.2.1 Comparison of cell deformation due to both fluid flow and strain stimuli

4.3 Osteoblast and osteocyte response to fluid flow *in vitro*

4.3.1 The effects of fluid flow and cytoskeletal disruption on the actin cytoskeleton

4.3.2 The effects of fluid flow and cytoskeleton disruption on NO and PGE_2 response

4.4 Osteoblast response to continuous indentation using atomic force microscopy

4.4.1 Dynamic osteoblast response to indentation

4.4.1.1 Control experiments

4.4.1.2 Indentation increases NO in osteoblast perinuclear region

4.4.1.3 Indentation causes diffusion of nitric oxide from localised pools

4.4.1.4 Increased intracellular NO diffuses to the extracellular medium

4.4.1.5 Indentation causes retraction of osteoblast spread morphology

4.4.2 Variation in osteoblast elasticity and membrane radial strain due to indentation

4.1 Description and structural characteristics of the computational cell model

4.1.1 Structural contribution of the cytoskeleton and other organelles

When forces in the picoNewton (pN) range are applied to the computational cell model, the displacements computed are on the order of nanometres (nm). The stiffness values obtained range from 0.5 – 3 nN/μm whether the model is subjected to horizontal or vertical applied forces. As prestress in the actin components of the cell model is increased linearly, a non-linear increase in stiffness arises (Fig. 4.1). This non-linear increase in stiffness arises particularly when the force is applied to a focal adhesion site (where the cytoskeleton is tied to the membrane and cytoplasm), but is also observed when the force is applied at distances from a focal adhesion site (Fig. 4.1). As the force applied to the cell model is increased, the stiffness also increases, indicating a non-linear strain hardening effect. The effect disappears when the contribution of the actin cytoskeleton-transmitted prestress is omitted from the model by assigning a 0 % prestress (Fig. 4.2).

To examine the effect of treating bone cells with microtubule inhibitors such as colchicine, the microtubule components in the cell model were omitted. It was found that, using an arbitrary prestress value of 1%, the cell stiffness was ~77% lower than when microtubules are included. This effect is illustrated in Fig. 4.3 along with the contribution of other cell organelles to overall cell stiffness. The cytoplasm has a more significant influence on stiffness than the nucleus or membrane, and that decreasing actin elasticity to 50% of original values has a much greater influence on cell stiffness than does an increase to 200% (Fig. 4.3).

The degree of cytoplasm compressibility, i.e. the Poisson's ratio, has a significant effect on the cell model stiffness. Increasing the Poisson's ratio (υ) from the original value of 0.37 to 0.49 increases cell stiffness by 45 %, whereas decreasing υ to 0.25 decreases stiffness by ~4 %. The properties of the membrane and nucleus components were found to have an almost inappreciable effect on cell stiffness relative to other components (Fig. 4.3).

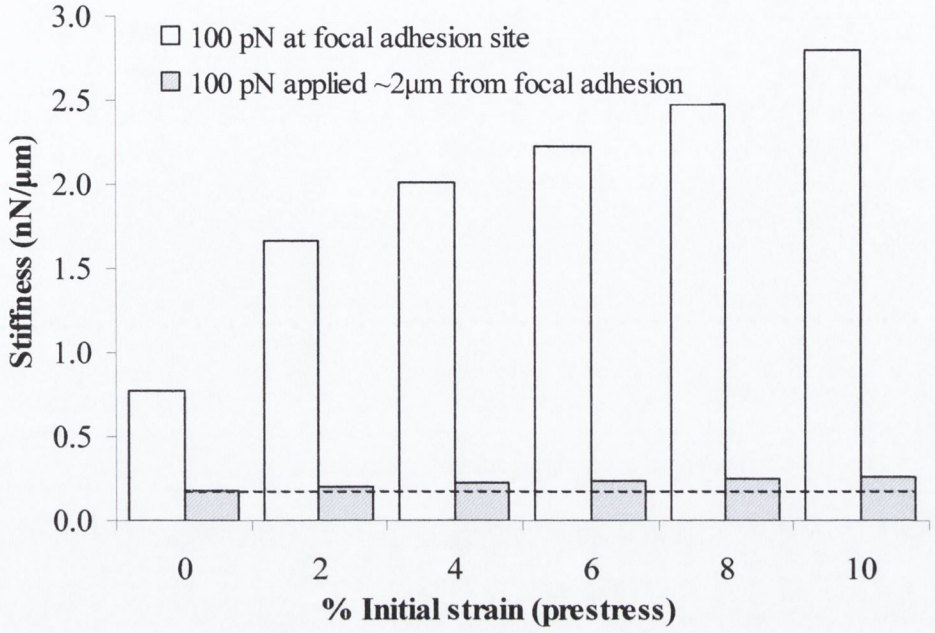

Fig. 4.1 *The effect of prestress on cell model stiffness. The dotted line (stiffness at 0% prestress) illustrates the small increases in stiffness that can also occur when the force is not applied directly to a focal adhesion site.*

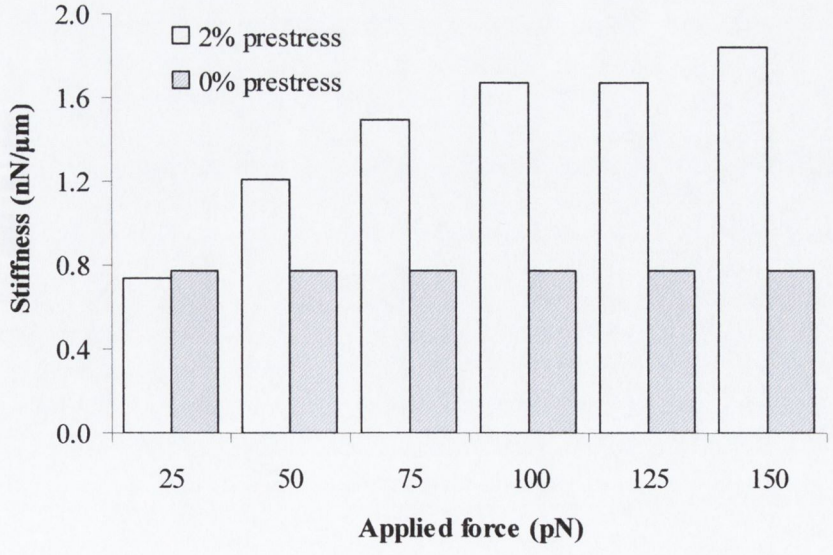

Fig. 4.2 *Stiffness versus applied force. Note that at 0% prestress in the cytoskeleton there is no strain hardening effect.*

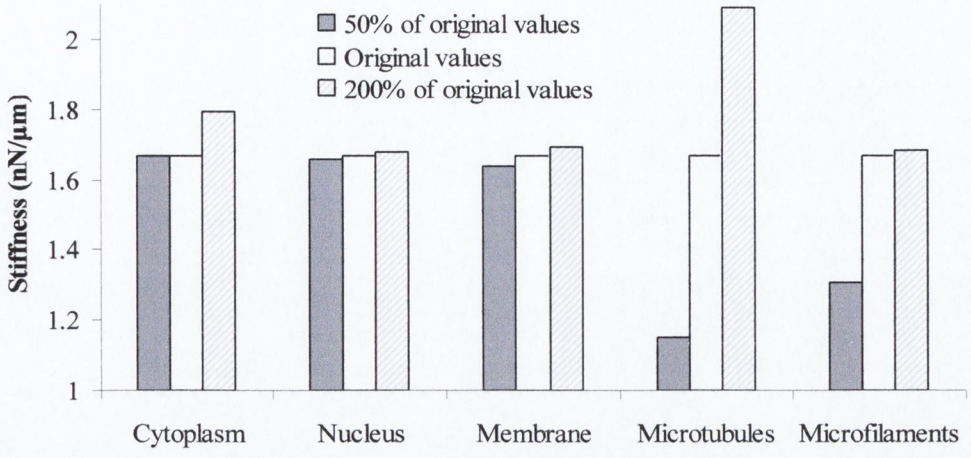

Fig. 4.3 *The effect on cell model stiffness of altering the material properties of each cell component from the original values in Table 3.1.*

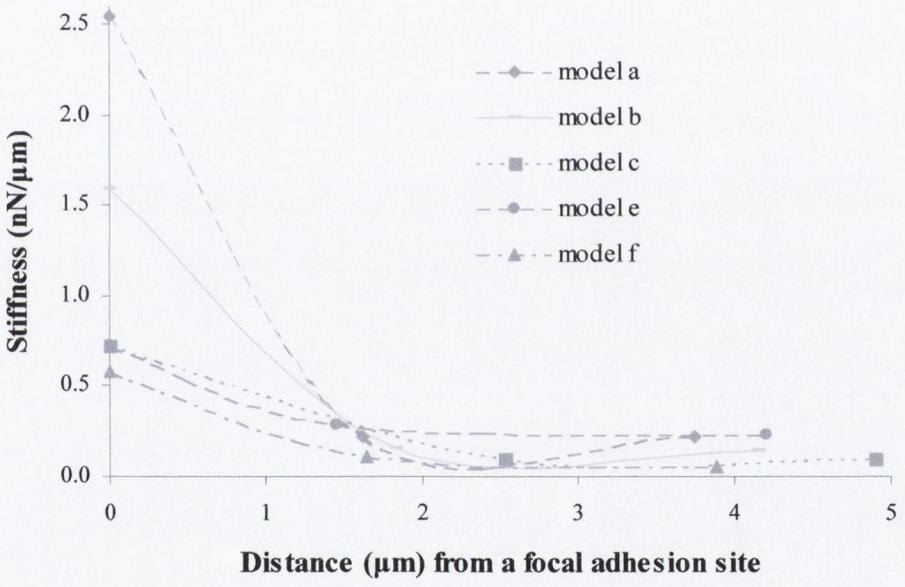

Fig. 4.4 *Variable stiffness on application of vertical indentations of 50 pN along the surface of increasingly spread models A to F (model d is not included as it did not support 50 pN at a distance from a focal adhesion). The dimensions of models A to F are provided in Table 3.2.*

Application of vertical indenting forces to the increasingly spread models illustrates significant variation in compliance of each model (Fig. 4.4). Despite their having material properties in common, each of the models have differing maximum stiffness values, which is explored in more detail in Fig. 4.5. In each model resistance to applied force increases with proximity to focal adhesion sites due to the more rigid underlying cytoskeleton components.

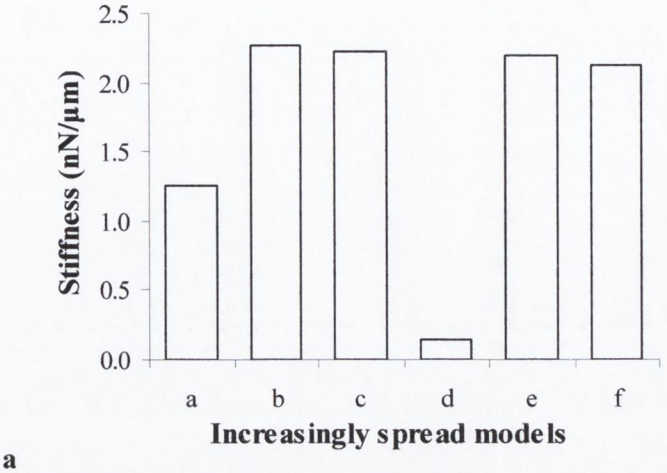

a

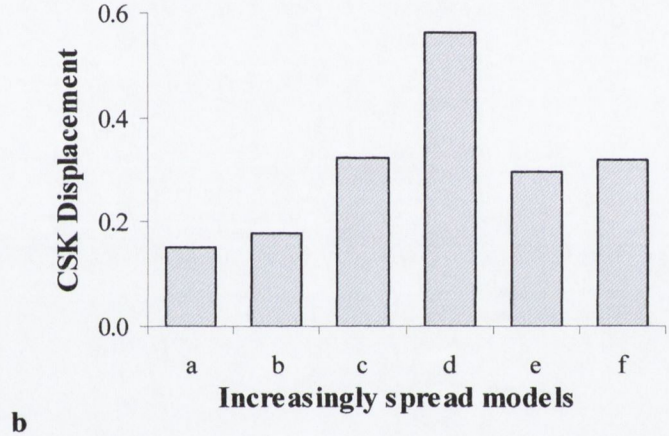

b

Fig. 4.5 *(a) Cell stiffness for increasingly spread configurations from models A to F. Graph (b) shows the corresponding cytoskeleton (CSK) displacements (µm) due to prestress prior to application of horizontal forces that yield stiffness values.*

Mechanical properties vary and do not change systematically in increasingly spread configurations of the cell model. Cell stiffness increases initially from models a to c, model d is the most compliant configuration, and the stiffness increases from models e to f (Fig. 4.5a). Examining the cytoskeleton displacement as each model equilibrates to the prestress applied in the first loadstep (prior to application of the 50 pN force, as described in Section 3.3.1), provides some explanation for these differences in stiffness. Cytoskeleton displacement increases in increasingly spread models but with a maximum in model d (the model with the greatest compliance) (Fig. 4.5b). These displacements due to the initial prestress may reflect the

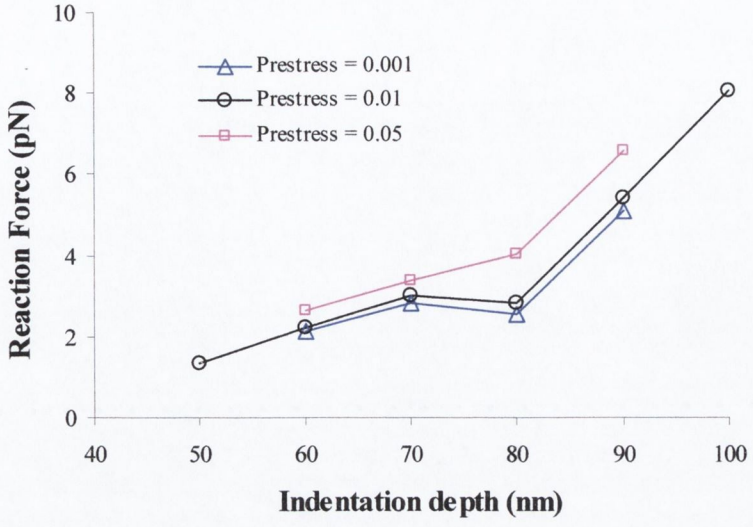

Fig. 4.6 *Reaction force versus indentation displacements for nodes resisting indentation displacements at the apical surface of the computational cell model, for three arbitrary prestress values.*

trend in how cell stiffness values change for each increasingly spread configuration (Figs. 4.4 and 4.5a), i.e. cell stiffness is determined by the prestressed cytoskeleton.

4.1.2 Corroboration of the cell model by analysis of AFM tip indentation

Two methods were used to model the indentation of a conical AFM tip into the cell model membrane. The point load indentation method [part (i) in Section 3.2.2.1] computes elasticity values lower than those obtained by modelling the actual probe geometry [part (ii) in Section 3.2.2.1]. An applied point load of 1 pN penetrates to a depth of 51.5 nm, whereas a reaction force of ~2 pN resists indentation constraints of 60 nm (Fig. 4.7).

Proceeding with the probe geometry modelling method (see Discussion) it was computed that, using arbitrary prestress values of 0.1, 1 and 5%, application of indentation depths ranging from 50 - 100 nm to the cell membrane are resisted by reaction forces ranging from 1 - 8 pN (Fig. 4.6).

The Hertz contact theory method (Eqn. 3.2 in Section 3.2.2.2) is used to relate force-indentation characteristics to local elasticity values E. It is found that E values range from 0.6 to 1.4 kPa, with resistance to indentation increasing with depth of indentation (Fig. 4.8) (these

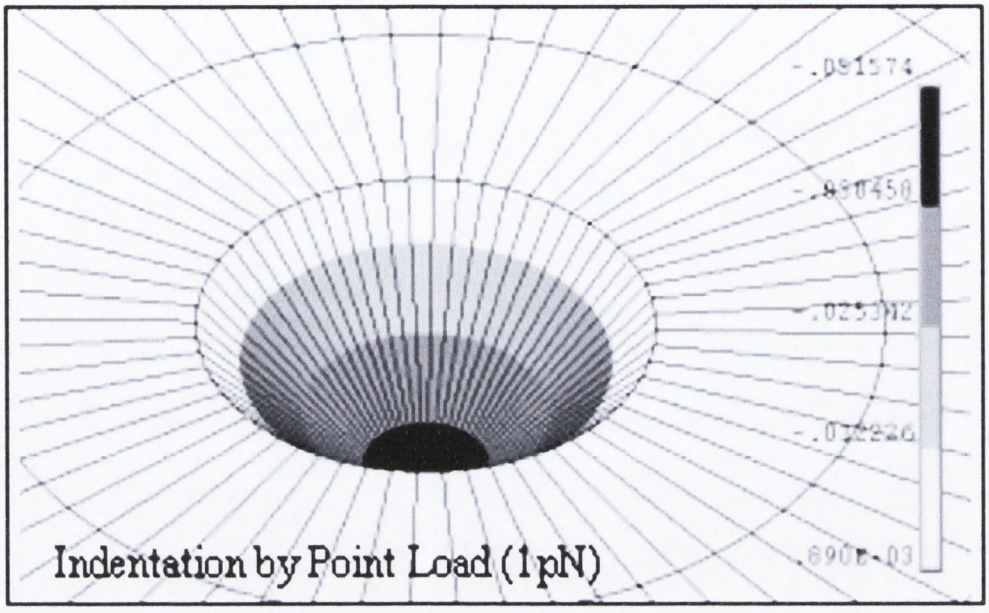

a

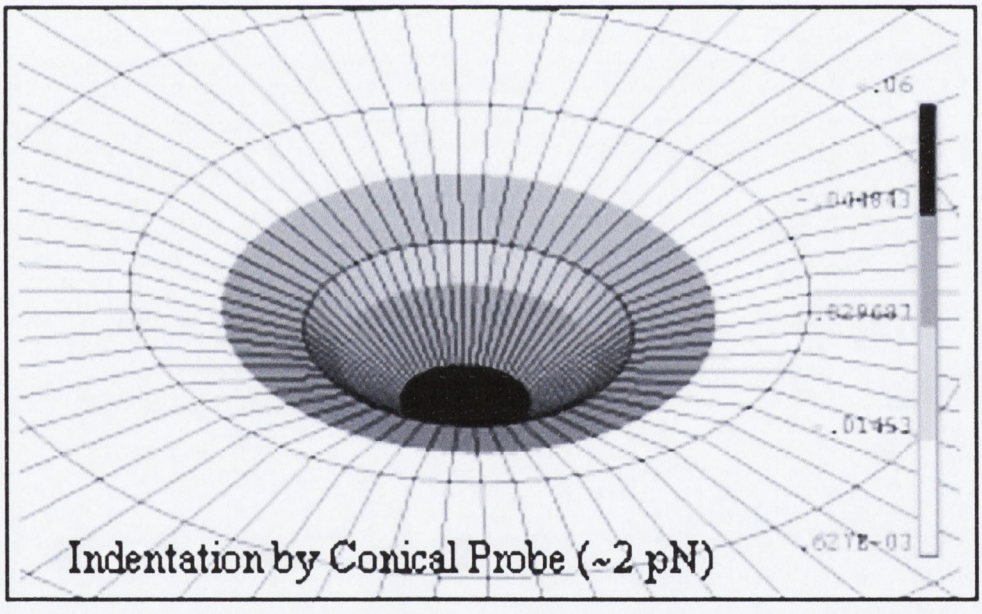

b

Fig. 4.7 *Illustration of differences in computed cell stiffness due to the point load and probe modelling methods: (a) a point load of 1 pN indents the membrane to ~51.5 nm (0.0515 μm); (b) applied indentation displacement constraints of 60 nm (0.06 μm) is resisted by a reaction force of ~2 pN.*

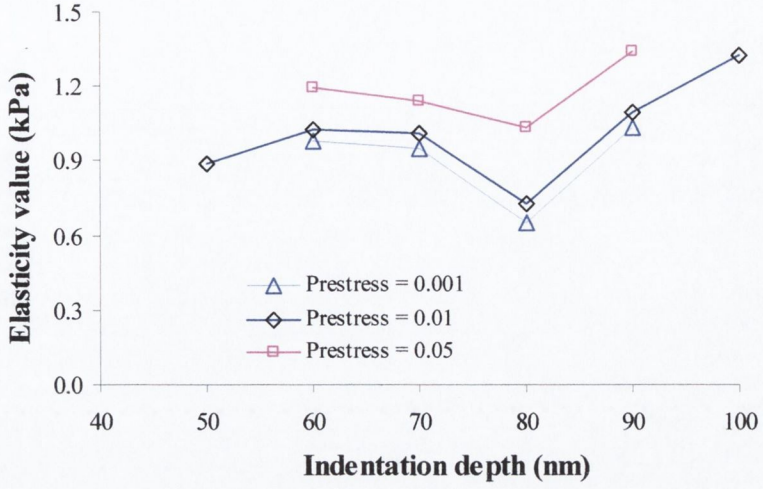

Fig. 4.8 *Elastic modulus versus indentation depth applied to the apical surface of the computational cell model, for three arbitrary prestress values.*

values can be compared to the elasticity values obtained in Section 4.4.2). Increases in the arbitrary prestress values also result in slight increases in elasticity, even though the region of indentation is ~5 μm from a focal adhesion site. The change in slope at ~80 nm is an artefact, due to a change in the number of nodes to which the indentation displacements are applied.

4.2 Application of the computational cell model to *in vitro* experiments

4.2.1 Comparison of cell stress and deformation due to both fluid flow and strain stimuli

In the experiments by Mullender et al. (2004), large differences were found in bone cell responses to 0.6 Pa pulsatile fluid shear stress at ~3 Hz compared to 1,000 με cyclic substrate strain at ~1 Hz – see Section 2.4.3 where it was described that the application of fluid shear stress caused a more than 7-fold increase in NO release and 3-fold increase in PGE_2 release, whereas substrate strain caused only 1.65-fold and 1.3-fold increases in NO and PGE_2 release, respectively (Fig. 2.15). On the other hand, collagen I production was increased 1.6-fold by substrate strain but decreased 0.6-fold by fluid shear stress.

When the computational cell model was used to determine the physical consequences of these stimuli on a cellular level large differences were also found. The contour plots of

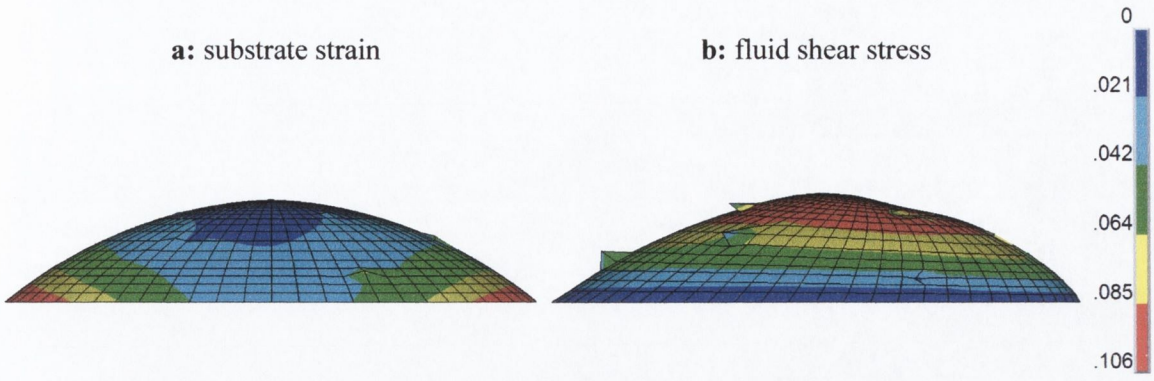

Fig. 4.9 *Comparison of displacements in the cell model due to both (a) substrate strain and (b) fluid shear stress loading conditions. The contour legend indicates the magnitude of displacement (μm). The image is exaggerated 30-fold to illustrate the differences in deformation. Note also the increased resistance to displacement at focal adhesion sites, where the cytoskeleton merges with the membrane.*

predicted displacements due to both fluid shear stress and strain loading conditions illustrate that there are fundamental qualitative differences in the cellular deformation caused by both types of mechanical stimuli (Fig. 4.9). Fluid shear stress has a larger overturning effect on the adherent bone cells, while the displacing effect of substrate strain is largest at cell-substrate attachments. These qualitative differences would be predicted no matter what magnitude of stimulation was used. Maximum displacement due to 1,000 με substrate strain was computed as 19 nm, occurring at the cell-substrate interface, whereas 0.6 Pa fluid shear stress caused a much larger displacement of 106 nm along the apex of the cell membrane where resistance to deformation is minimal (Fig. 4.9).

The stresses induced reflect the stimulation that is likely caused by both fluid shear stress and strain. The deformation computed in all cell model components is given in Fig. 4.10. For example, the maximum stress induced in the *membrane* is ~7.5-fold higher in fluid shear stress than in strain (Fig. 4.10). These maximum stress values occur at focal adhesion sites due to the more rigid underlying cytoskeleton. Although deformation is smaller in magnitude in the more internal parts of the model, i.e. the nucleus and cytoplasm-nucleus region, it is noteworthy that the differences in deformation between both methods of mechanical stimulation are greater

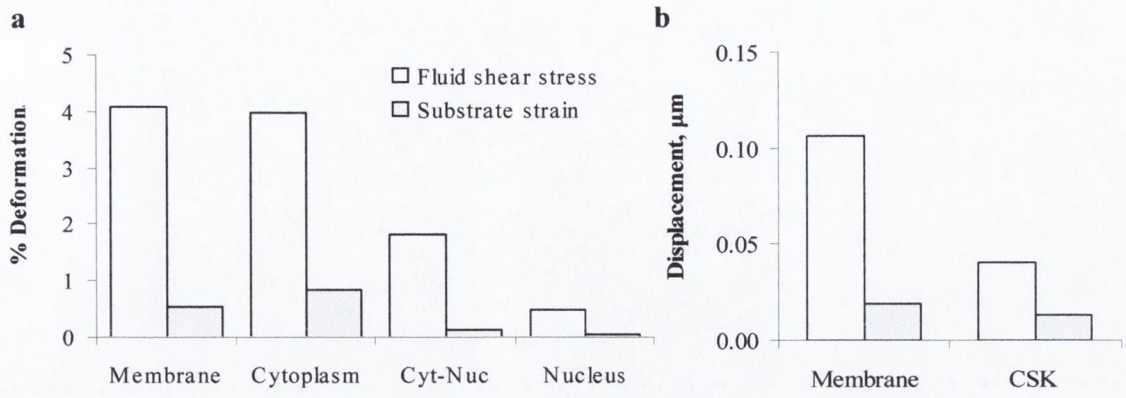

Fig. 4.10 *Overview of the differences in (a) deformation and (b) displacement of cell model components caused by both fluid flow and substrate strain loading conditions. % deformation is the maximum von Mises stress as a percentage of original elastic properties for each cell model component. Membrane and cytoskeleton displacement (µm) are maximum values. Abbreviations: Cyt-Nuc, the region of the cytoplasm immediately surrounding the nucleus; CSK, cytoskeleton.*

in this region (Fig. 4.10a). This suggests that, in addition to causing higher deformation of all cellular components, fluid shear stress transmits deformation more effectively to internal cellular regions than does substrate strain.

The cellular deformation as a result of both mechanical stimuli can be used to interpret several experimentally-determined bone cell responses to both fluid shear stress and substrate strain stimulation. This involves correlating the results in Figs. 4.9 and 4.10 with those results of Mullender et al. (2004) described in Section 2.5.5 (Fig. 2.15). How these cell model results may explain the differences in bone cell NO and PGE_2 response to mechanical loading – the quantitatively larger deformation caused by 0.6 Pa fluid shear stress relative to 1,000 µε strain appear to be directly related to whether a bone cell will respond with release of signalling molecules such as NO and PGE_2 or not collagen matrix production (see Discussion, Sections 5.3.2 to 5.3.4). To investigate the stimuli under higher levels of substrate strain, the strain that would yield a maximum membrane displacement equivalent to that caused by 0.6 Pa fluid shear stress was computed. This substrate strain value was found to be 5,531 µε. The strain values

required to induce equal stress in the nucleus were even higher (~8,200 με) since deformation is not distributed uniformly throughout the cell model components.

By varying the material properties of the various components of the cell model, it was found that cytoplasm elasticity in particular has a large influence on cellular deformation. For example, increasing cytoplasm elasticity by a factor of 2 (to 200 Pa) reduces nucleus deformation due to fluid shear stress from the original 0.48% to 0.34%. Decreasing cytoplasm elasticity by a factor of 2 (to 50 Pa) increases nucleus deformation from 0.48% to 0.6%. Variations in cytoplasm elasticity have less of an influence on cellular deformation under substrate strain loading conditions, again indicating more effective cell deformation in fluid shear stress. Increases in microtubule elasticity, or introducing a prestress (i.e. initial strain values > 0) to the microtubule or microfilament elements results in increased membrane and cytoplasm stresses in the region of focal adhesion sites, but does not alter the overall differences in deformation between fluid shear stress and strain loading conditions found in the model. This is because maximum displacements occur at points of least resistance at a distance from the cytoskeleton. Variation in the density of the model mesh (i.e. the number of elements) results in slight variation in the results reported, although the overall differences in deformation due to both fluid shear stress and strain methods remain consistent.

4.3 Osteoblast and osteocyte response to fluid flow *in vitro*

4.3.1 The effects of pulsatile fluid flow and cytoskeletal disruption on the actin cytoskeleton

Application of pulsatile fluid flow increased the number of osteoblasts (OBs) in which formation and parallel alignment of stress fibres (actin filaments bundled into long fibres) occurred, from 6.6 ± 2.6% to 73 ± 7% of OBs (mean ± SEM), comparing for example Fig. 4.11 A, B. Treatment of OB cultures with actin or microtubule disrupting agents significantly reduced the number of OBs with parallel alignment of stress fibres when subjected to pulsatile fluid flow (to 12 ± 4 % and 11 ± 5 %, respectively) (Fig. 4.11 C–F). In OBs, both actin and

microtubule disrupting treatments caused spots of fluorescent intensity, presumably clustering at focal adhesion sites, in both static and pulsatile fluid flow treated OB cultures (Fig. 4.11 C–F).

Applying pulsatile fluid flow to untreated osteocytes (OCYs) slightly increased formation and parallel alignment of stress fibres, comparing for example Fig. 4.12 A, B); the percentage of OCYs with this 'combed' appearance increased from 22.6 ± 3.6 % to 36 ± 11 % of OCYs (mean ± SEM, n=4). Several OCYs treated with actin-disruptors had reduced cell body size, with rounded stellate morphologies extending thinner processes (e.g. Fig. 4.12 C, D). Microtubule disruption had a less severe effect on morphology than actin disruption but did cause ruffling of actin boundaries/outer edges (Fig. 4.12 E, F). The number of OCYs with parallel alignment of stress fibres due to pulsatile fluid flow treatment was significantly reduced (to 10±0.3 % of OCYs) when treated with actin disrupting agents (e.g. Fig 4.12 C-D).

4.3.2 The effects of pulsatile fluid flow and cytoskeleton disruption on NO and PGE_2 response

Neither the NO nor PGE_2 response in osteoblasts (OBs) or osteocytes (OCYs) when subjected to 3 Hz (0.39 Pa) was statistically different to those responses induced by 5 Hz (0.64 Pa) pulsatile fluid flow (PFF); results were therefore combined and expressed as PFF-treated relative to static controls. In OBs, a PFF-induced increase in NO release was inhibited by disrupting actin alone (Fig. 4.13 a). A PFF-induced increase in PGE_2 release could be observed only when either the actin or microtubule cytoskeleton was disrupted (Fig. 4.13 b).

In OCYs, there was a significant pulsatile fluid flow-induced increase in NO release, which did not require an intact actin cytoskeleton but was enhanced with microtubule disruption (Fig. 4.14 a). A large PFF-induced increase in PGE_2 release in OCYs required both an intact actin and microtubule cytoskeleton (Fig. 4.14 b), i.e. it was inhibited if either cytoskeletal element was disrupted.

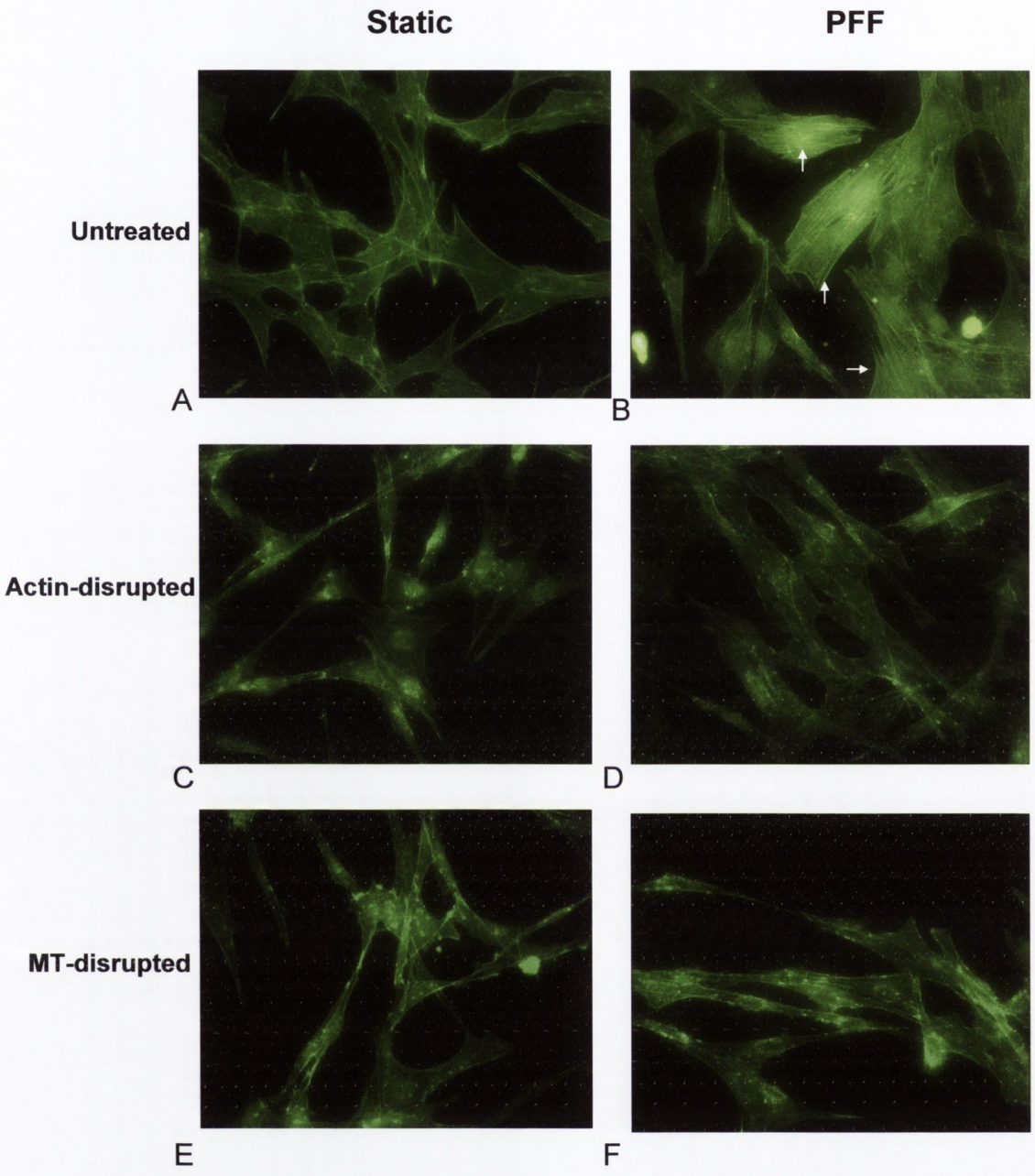

Fig. 4.11 *Fluorescent staining of the actin cytoskeleton of osteoblastic (MC3T3-E1) cells illustrating the effect of pulsatile fluid flow (PFF) and disruptors of both actin and microtubule (MT) polymerization (400x magnification). The white arrows indicate examples of cells with parallel alignment of stress fibres.*

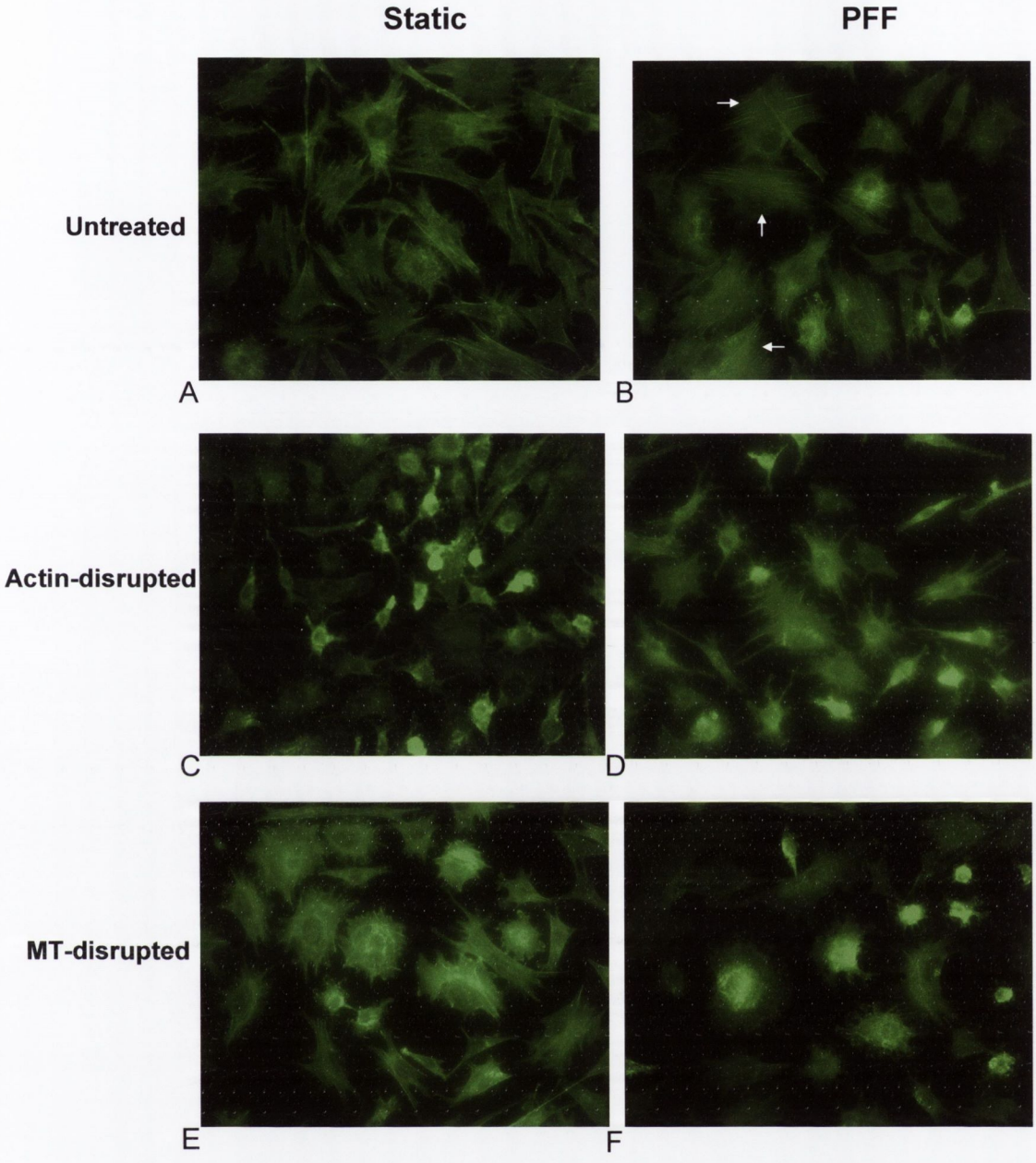

Fig. 4.12 *Fluorescent staining of the actin cytoskeleton of osteocytic (MLO-Y4) cells illustrating the effect of pulsatile fluid flow (PFF) and disruptors of both actin and microtubule (MT) polymerization. The white arrows indicate examples of cells with parallel alignment of stress fibres.*

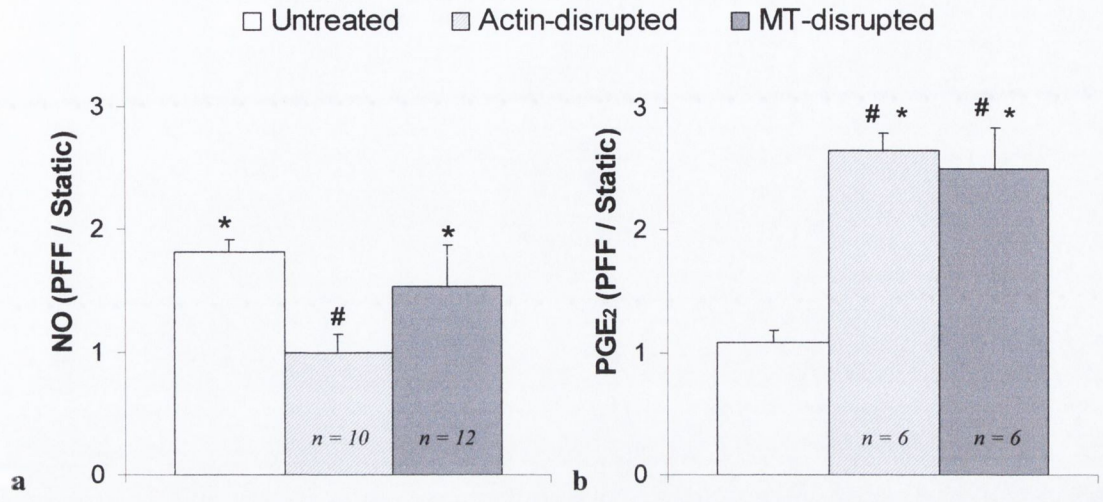

Fig. 4.13 *The effect of actin and microtubule (MT) cytoskeleton disruption on pulsatile fluid flow-induced (a) NO and (b) PGE_2 release in osteoblastic cells. * Significantly different from 1; # significantly different from untreated. Values are mean ± SEM, $p < 0.05$.*

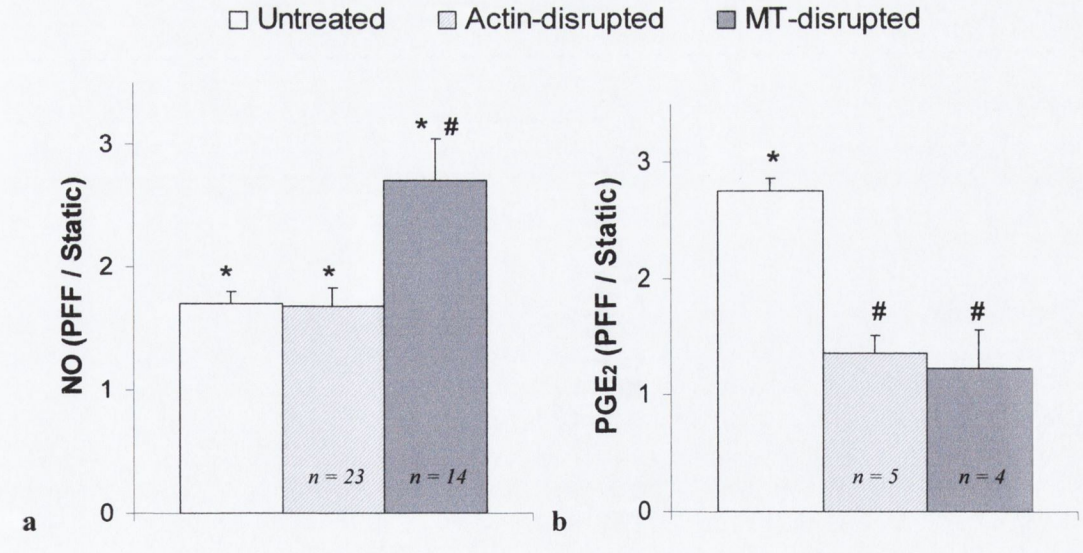

Fig. 4.14 *The effect of actin and microtubule (MT) cytoskeleton disruption on pulsatile fluid flow-induced (A) NO and (B) PGE_2 release in osteocytic cells. * Significantly different from 1; # significantly different from untreated. Values are mean ± SEM, $p < 0.05$.*

4.4 Osteoblast response to continuous indentation using atomic force microscopy

4.4.1 Dynamic osteoblast response to indentation

133 single osteoblasts were successfully indented in a total of 180 experiments. The results of the various control experiments performed are described in Section 4.4.1.1. In each indentation experiment both real-time fluorescent data and force-indentation characteristics (force curves) are obtained. In sections 4.4.1.2 to 4.4.1.5, results from those experiments in which osteoblasts respond to the applied indentation force are illustrated in fluorescent images at various time intervals. An example of a typical force curve (Fig. 4.15) illustrates extension of the AFM tip into the osteoblast membrane, followed by retraction once a specified force is reached. In describing specific indentation experiments, the large number of force curves (or successive extension-retraction cycles) generated by continuous indentation are not illustrated; instead the duration of the continuous indentation and the maximum tip force are provided. The membrane radial strain and osteoblast elasticity are calculated for various force curves in Section 4.4.2.

4.4.1.1 Control experiments

In each day of experiments, a standard control experiment was performed in which the tip was positioned in the vicinity of an osteoblast but without any contact. In each of these controls, there was no change in nitric oxide (NO) fluorescence intensity but for a gradual decrease in fluorescence due to photobleaching over the duration of the experiment. In 10 control experiments in which the tip was positioned above the osteoblast and actuated vertically without contacting the osteoblast membrane no response was observed, suggesting that fluid movement alone does not activate NO response in these osteoblasts. In 12 control experiments in which osteoblasts were stained with Mitotracker Green, indentation into the osteoblast membrane did not result in any alteration in fluorescence (Fig. 4.16 is an example of this control) but for slight fluorescence interference over the indented osteoblast exclusively due to tip reflection. This interference was quantified (by drawing regions of interest around the indented osteoblast) and the percentage change in normalised fluorescence was determined to be < 1 %. In the control

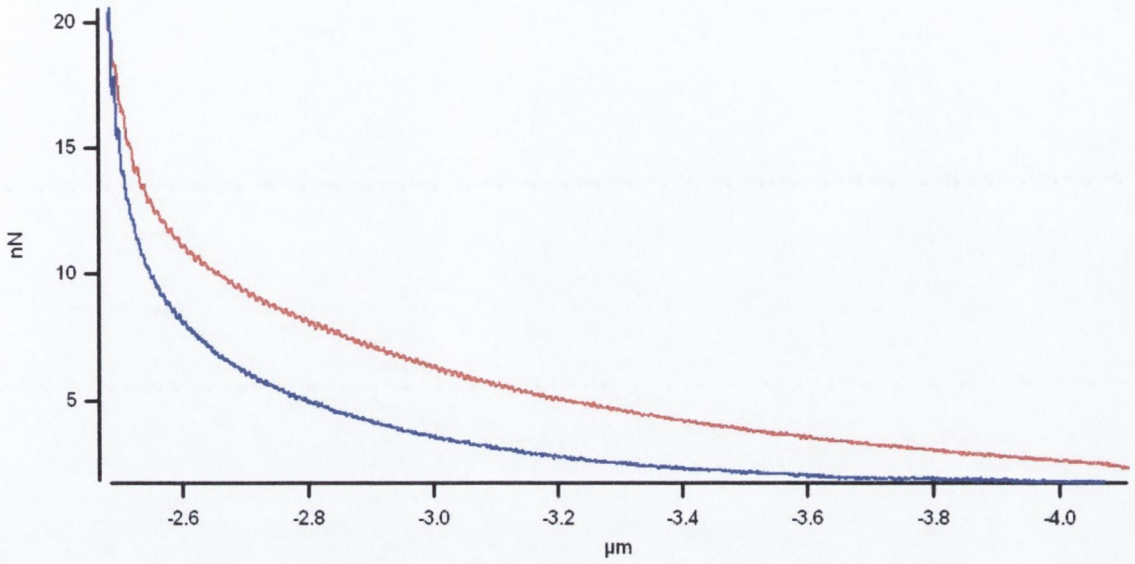

Fig. 4.15 *Graph of tip indentation force versus piezo movement. The red curve illustrates how the force increases to reach a maximum cantilever deflection corresponding to 20 nN, as the piezo extends the tip into the osteoblast membrane. The blue curve illustrates the force on the tip during piezo retraction.*

experiments in which osteoblasts were indented while immersed in buffer containing propidium iodide (PI), with a range of applied forces (from 5 to 70 nN) no positive fluorescent staining at the PI emission wavelength was observed. This indicates that the magnitude of indenting force applied to osteoblasts in these experiments does not rupture the osteoblast membrane within the time-scale (6 to 10 mins) of a typical indentation experiment.

4.4.1.2 Indentation increases NO in osteoblast perinuclear region

In four experiments, continuous indentation with forces ranging from ~17 to 25 nN results in increased fluorescence intensity in the perinuclear region of the indented osteoblast, shortly (within < 15 s) after the first successful indent. Nitric oxide (NO) fluorescent images are provided at various times intervals for one example of the 4 experiments in which this response was observed (Fig. 4.17). It is evident from these fluorescent images that an increase in intracellular nitric oxide fluorescence occurs in the indented osteoblast only. To quantify this response, the normalised NO fluorescence intensity in specified 'regions of interest' around the

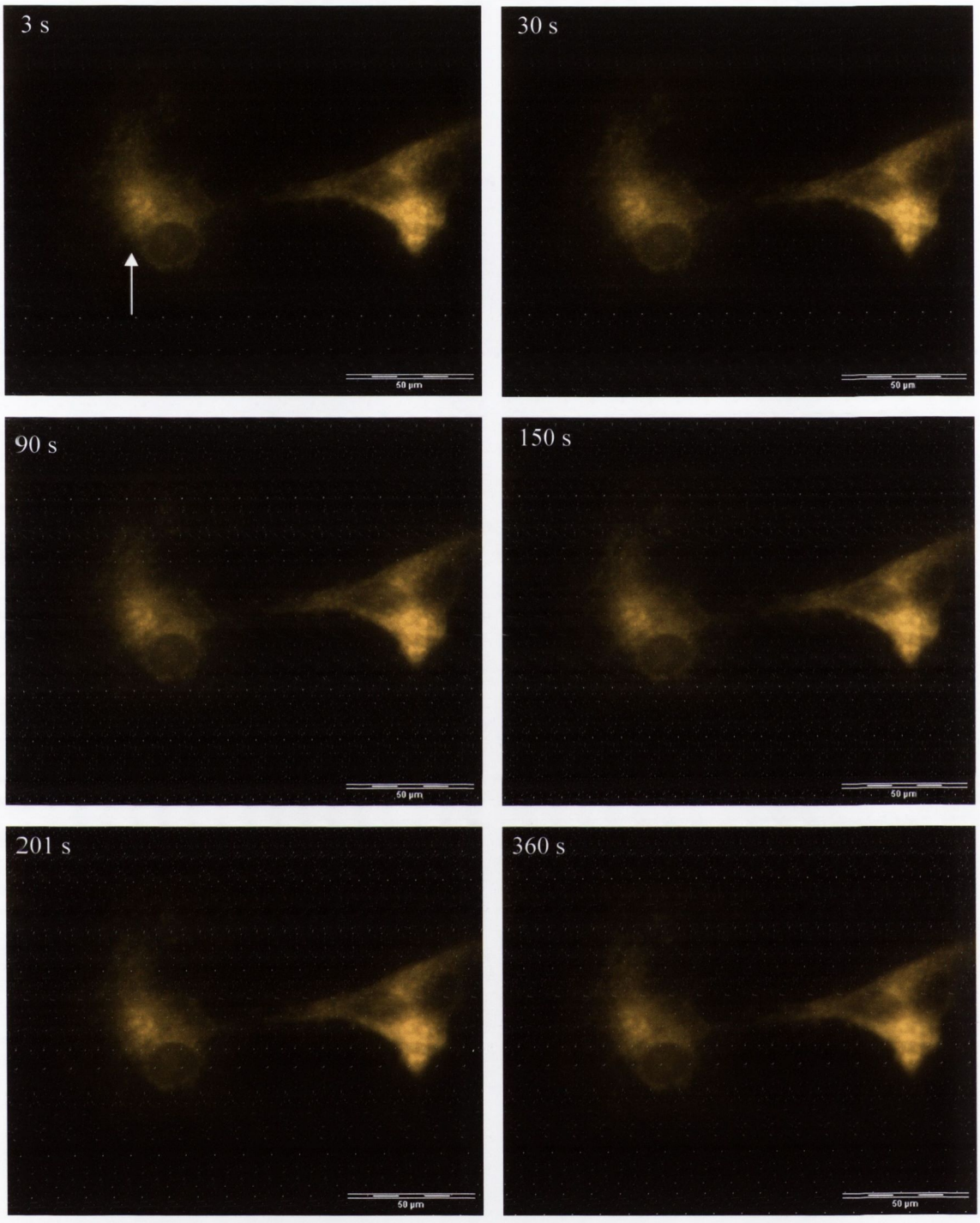

Fig. 4.16 *Fluorescent images of mitochondrial protein intensity at various time intervals. The point of indentation is indicated by the white arrow. An indentation force ranging from 20 to 25 nN is applied continuously from 31 s until 93 s.*

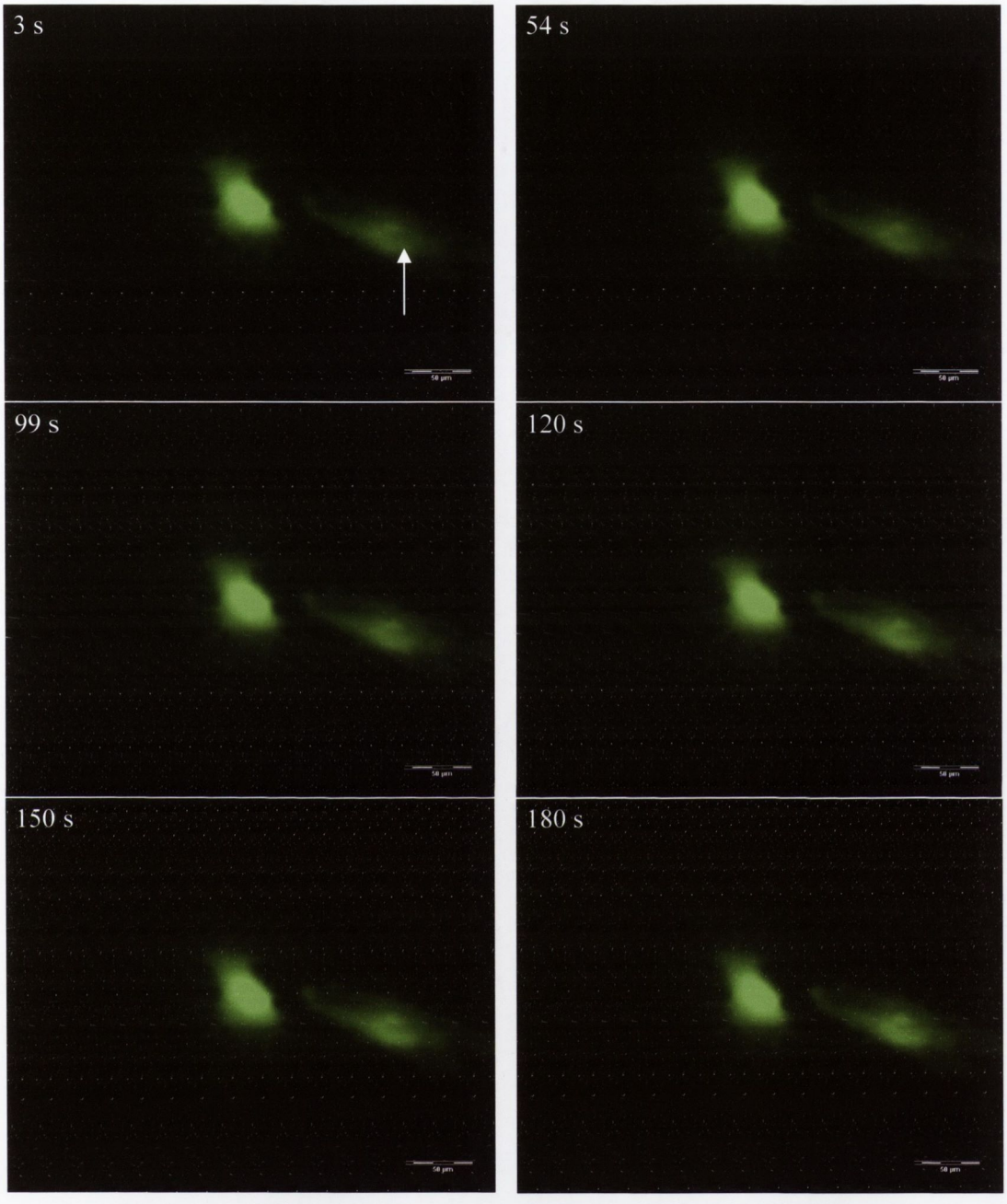

Fig. 4.17 *Images of nitric oxide fluorescence at various time intervals. The point of indentation is indicated by the white arrow. An indentation force of ~20 nN is applied continuously from 57 s until 117 s.*

indented osteoblast and its perinuclear region, is calculated for each time point (i.e. at 3 s intervals). The resulting graph is provided in Fig. 4.18. These data points indicate that increased nitric oxide intensity begins within 10 s of the first successful indentation at 57 s. The rate of increase of NO intensity is higher in the perinuclear region (than in the whole osteoblast)

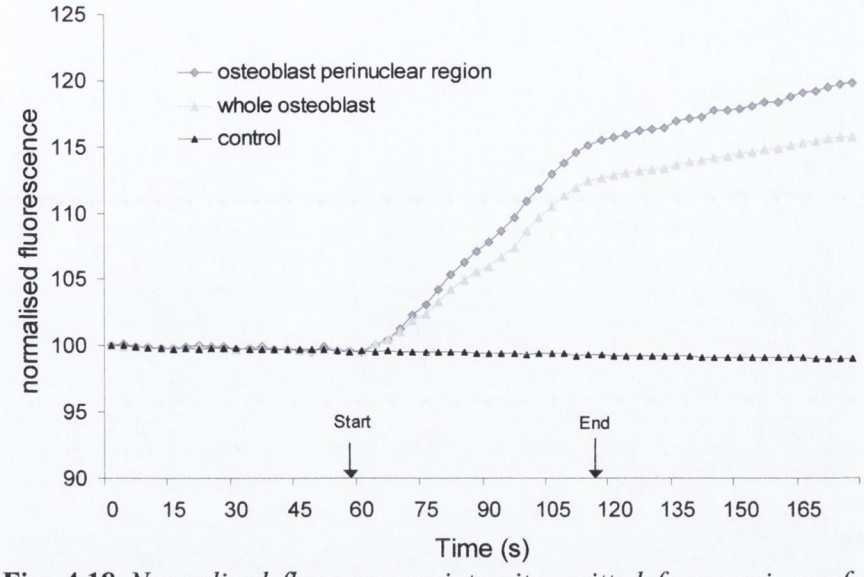

Fig. 4.18 *Normalised fluorescence intensity emitted from regions of interest drawn around the indented osteoblast, and its peri-nuclear region. First successful indentation occurs at 57 s and is continuous until 117 s (as indicated by arrows) after which time the tip is withdrawn. The control values obtained from an accompanying experiment on the same day exhibit a steady decrease in fluorescence due to photobleaching.*

indicating that nitric oxide diffuses from the perinuclear region (Fig. 4.18). Continuous indentation evidently has an ongoing influence on NO synthesis and diffusion, as the rate of increase in NO intensity decreases slightly after the tip is withdrawn at 117 s (Fig. 4.18).

4.4.1.3 Indentation causes diffusion of nitric oxide from localised pools

In four experiments, continuous indentation into the osteoblast membrane with forces ranging from 15 to 30 nN results in increased intracellular NO fluorescence intensity in localised pools throughout the osteoblast. Fluorescent images are provided at various times intervals for two experiments in which this response was observed (Figs. 4.19 and 4.20). In the first of these examples, the spots of nitric oxide fluorescent intensity are visible within 270 s and continue to grow in size beyond the duration of the experiment (the images taken after 270 s are snapshots at later times) (Fig. 4.19). In the second example of this response, similar localised pools of NO intensity are visible prior to indentation (Fig. 4.20). At 120 s however, they grow in size and do

so beyond the duration of the experiment (to at least 460 s). In both these examples (Figs. 4.19 and 4.20), that the NO intensity in these pools does not decrease as they increase in size, which suggests that NO is being synthesised continuously in these localised pools in the osteoblast. Unlike the response in which NO increased in intensity in the perinuclear region, the NO response in localised pools is more delayed as any change in NO intensity does not occur until ~100 to 300 s after the initial indent.

4.4.1.4 Increased intracellular NO and diffusion to the extracellular medium

In two experiments indentation results in increased intracellular nitric oxide (NO) fluorescence intensity within ~60 s. Nitric oxide fluorescent images are provided at various times intervals for both experiments in which this response was observed (Figs. 4.21 and 4.22). In the first example (Fig. 4.21), the initial increase in NO intensity is followed by an outward diffusion of pools of NO that increase in size together with a simultaneous gradual decrease in intracellular NO intensity. In Fig. 4.22 the indented osteoblast appears to lose all intracellular NO as it effectively disappears from the fluorescent image.

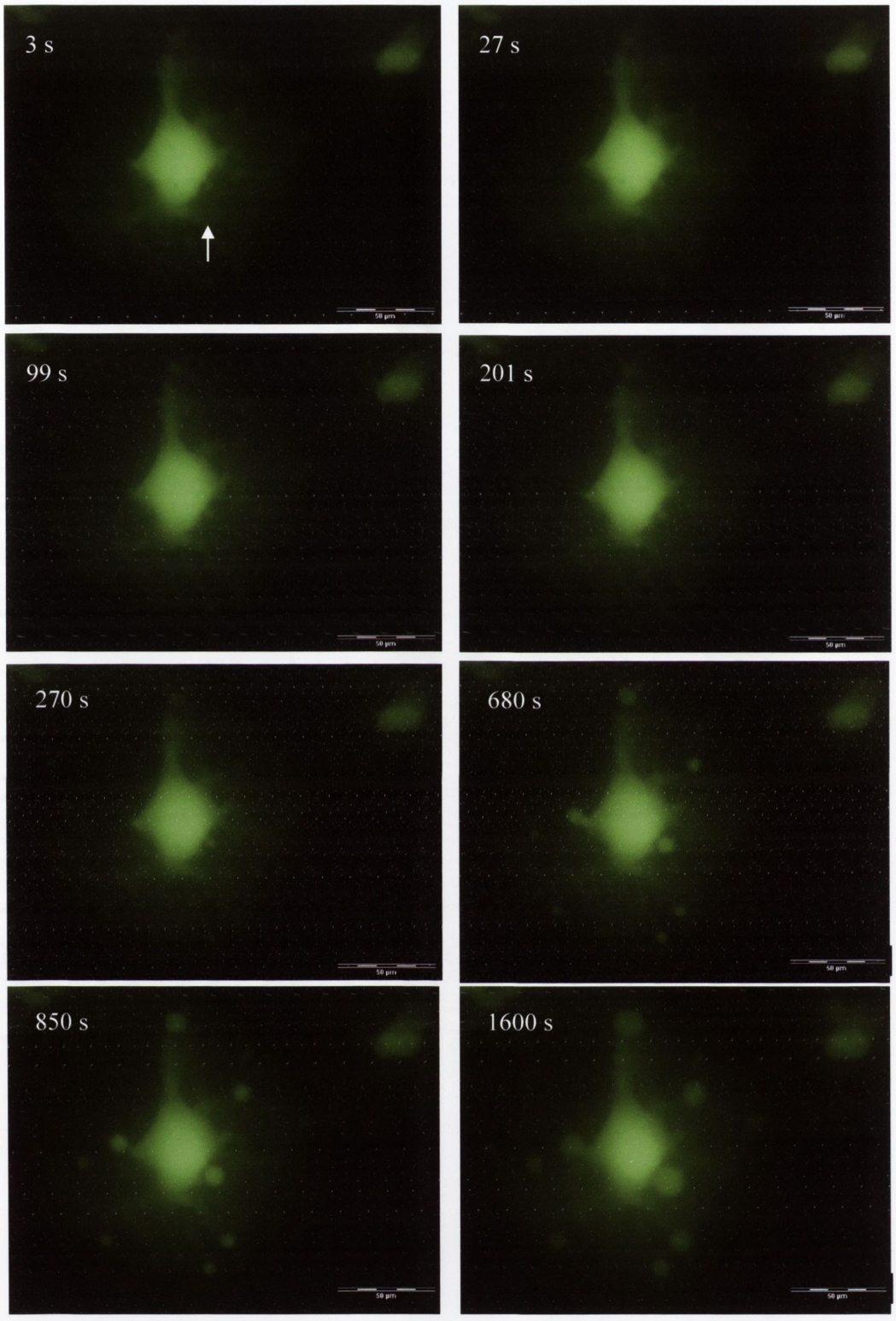

Fig. 4.19 *Images of nitric oxide fluorescence at various time intervals. The point of indentation is indicated by the white arrow. An indentation force of ~22 nN is applied continuously from 30 s until 60 s.*

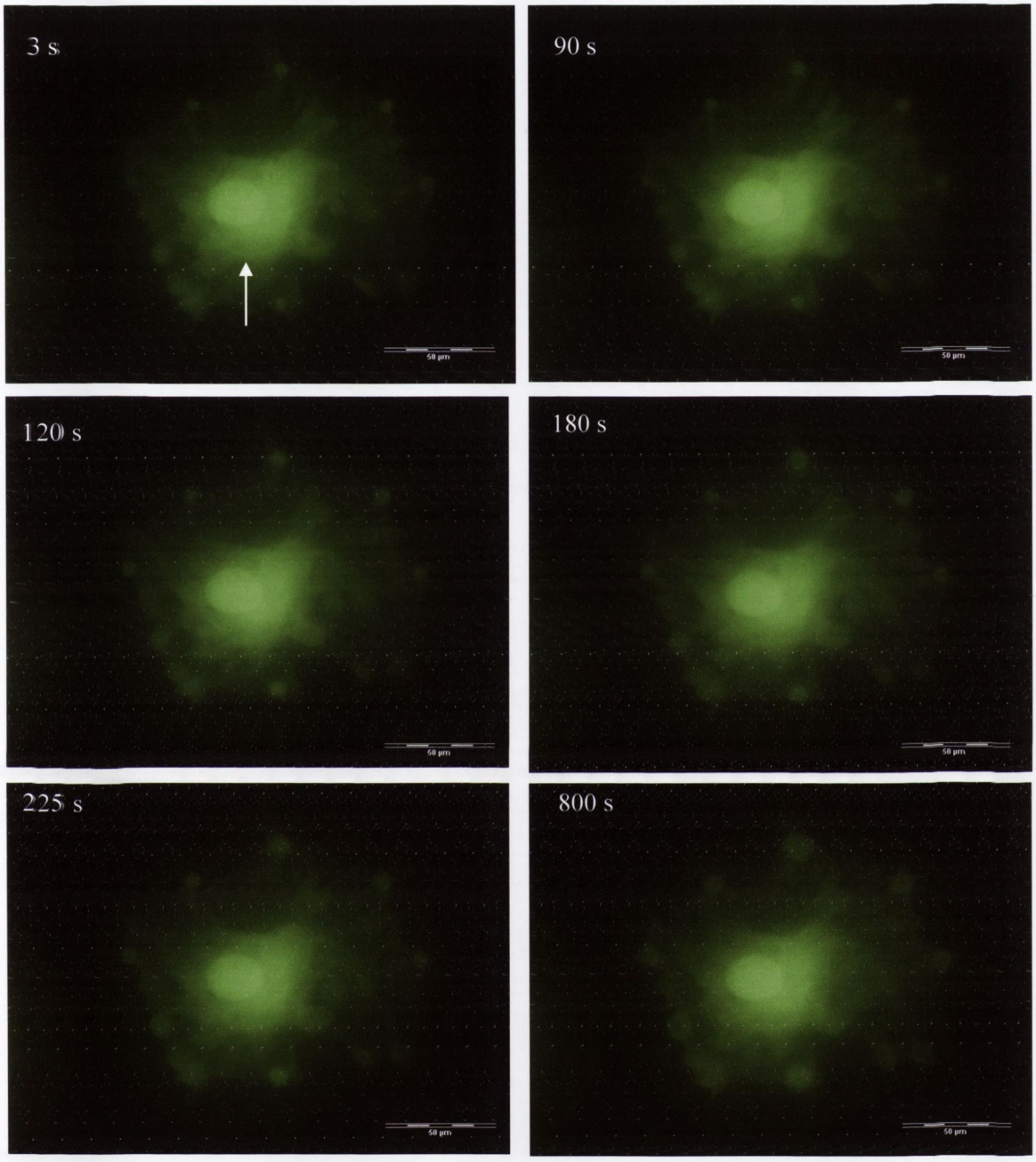

Fig. 4.20 *Images of nitric oxide fluorescence at various time intervals. The point of indentation is indicated by the white arrow. An indentation force of ~24 nN is applied continuously from 52 s until 112 s.*

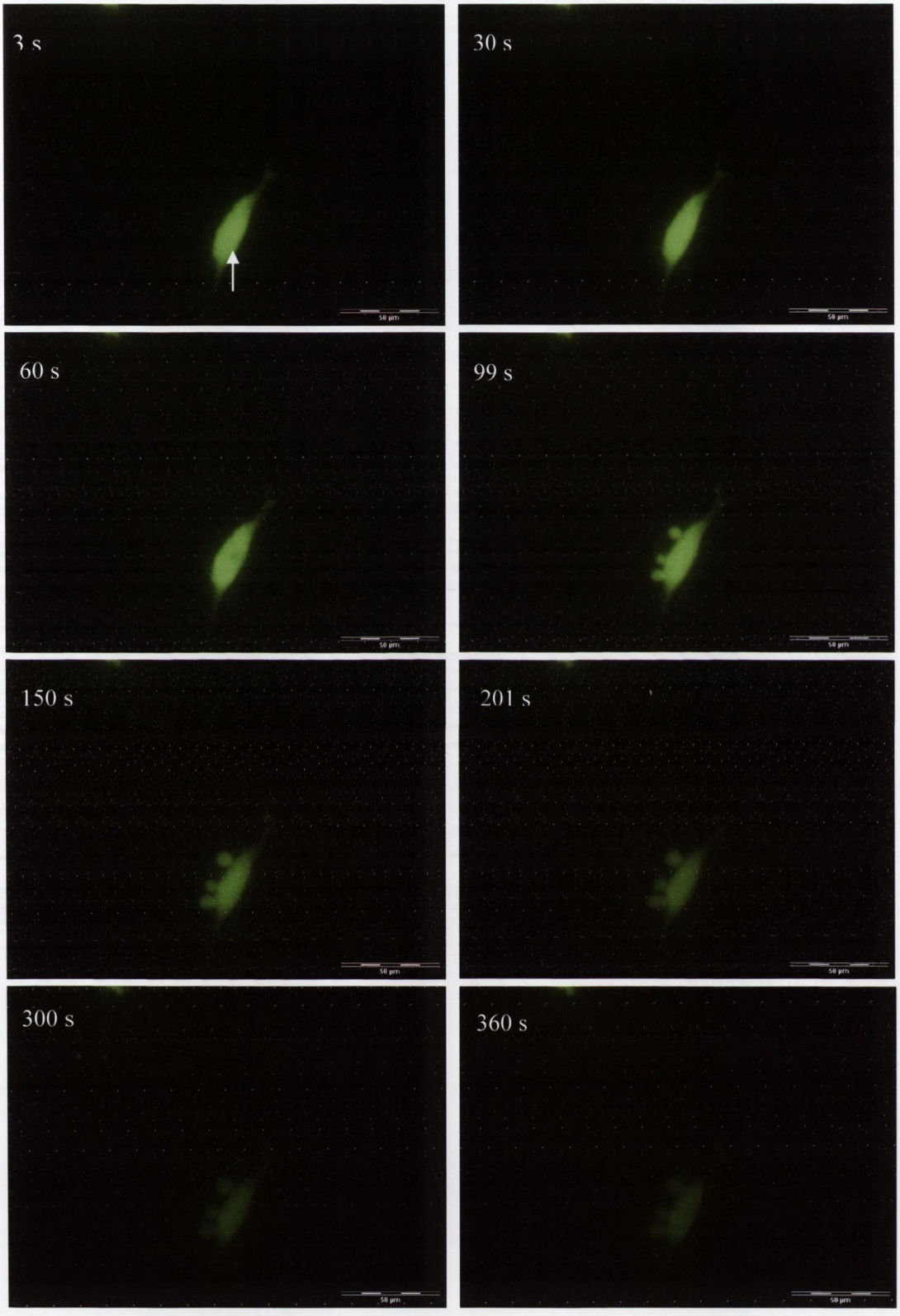

Fig. 4.21 *Images of nitric oxide fluorescence at various time intervals. Site of indentation is indicated by the white arrow. The first indentation with a force ranging ~47 nN is applied continuously from 32 s until 93 s.*

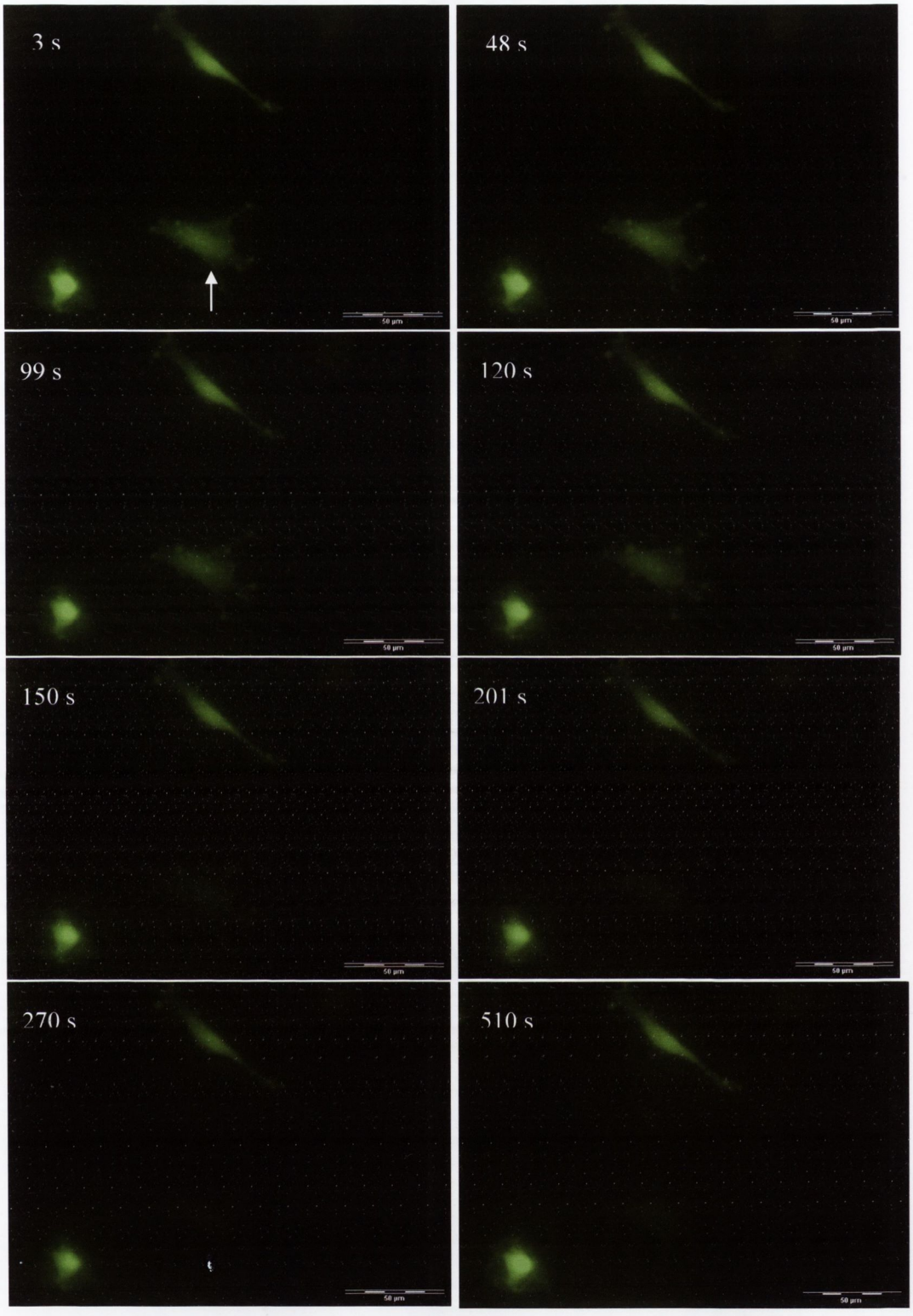

Fig. 4.22 *Images of nitric oxide fluorescence at various time intervals. Site of indentation is indicated by the white arrow. The first indentation with a force of ~25 nN is applied continuously from 52 s until 112 s.*

4.4.1.5 Indentation causes retraction of osteoblast spread morphology

In three experiments, indentation results in a retraction of the indented osteoblast spread morphology. This occurs in response to a force of ~20 nN in two of these experiments, and in response to a force of > 60 nN in the third. Nitric oxide (NO) fluorescent images at various time-intervals for two examples of this response are provided in Figs. 4.23 and 4.24. In the first example, a dramatic retraction of osteoblast morphology when indented with a force of 60 nN is observed over the duration of the experiment (Fig. 4.23). This response is not accompanied by any alteration in NO fluorescence. In the second example, in addition to a retraction of the indented osteoblast morphology, there is also evidence that the indenting force of 20 nN results in increased NO intensity at localised spots in the perinuclear region, and at the edges of the osteoblast membrane (Fig. 4.24). These spots of fluorescent intensity continue to grow beyond the duration of the indentation experiment, as is the case for the NO response in localised pools described in Section 4.4.1.3. The retraction of the indented osteoblast morphology is not due to excessive cell exposure to excitation light as it occurs only in the indented osteoblast. The osteoblasts do not become rounded or non-viable within 10 mins beyond the duration of the experiment.

4.4.2 Variation in osteoblast elasticity and membrane radial strain due to indentation

In this section, results illustrating the variables that may influence osteoblast mechanotransduction of nitric oxide response are reported. It is evident from the various force-indentation curves (in Figs. 4.15, 4.25 or 4.26) that the depth to which the tip must indent to reach a specified indentation force varies considerably. Elasticity values corresponding to the these force-indentation characteristics were calculated using the Hertz contact theory method (as described in Section 3.2.2.2), i.e.:

$$F = \frac{2E}{\pi(1-\upsilon^2)\tan\alpha}\delta^2$$

Once the applied force (F), the depth of indentation (δ), the semi-vertical contact angle of the tip (α: 15^0), and the Poisson's ratio (v, assumed 0.37 based on Section 2.2.2.2) are known,

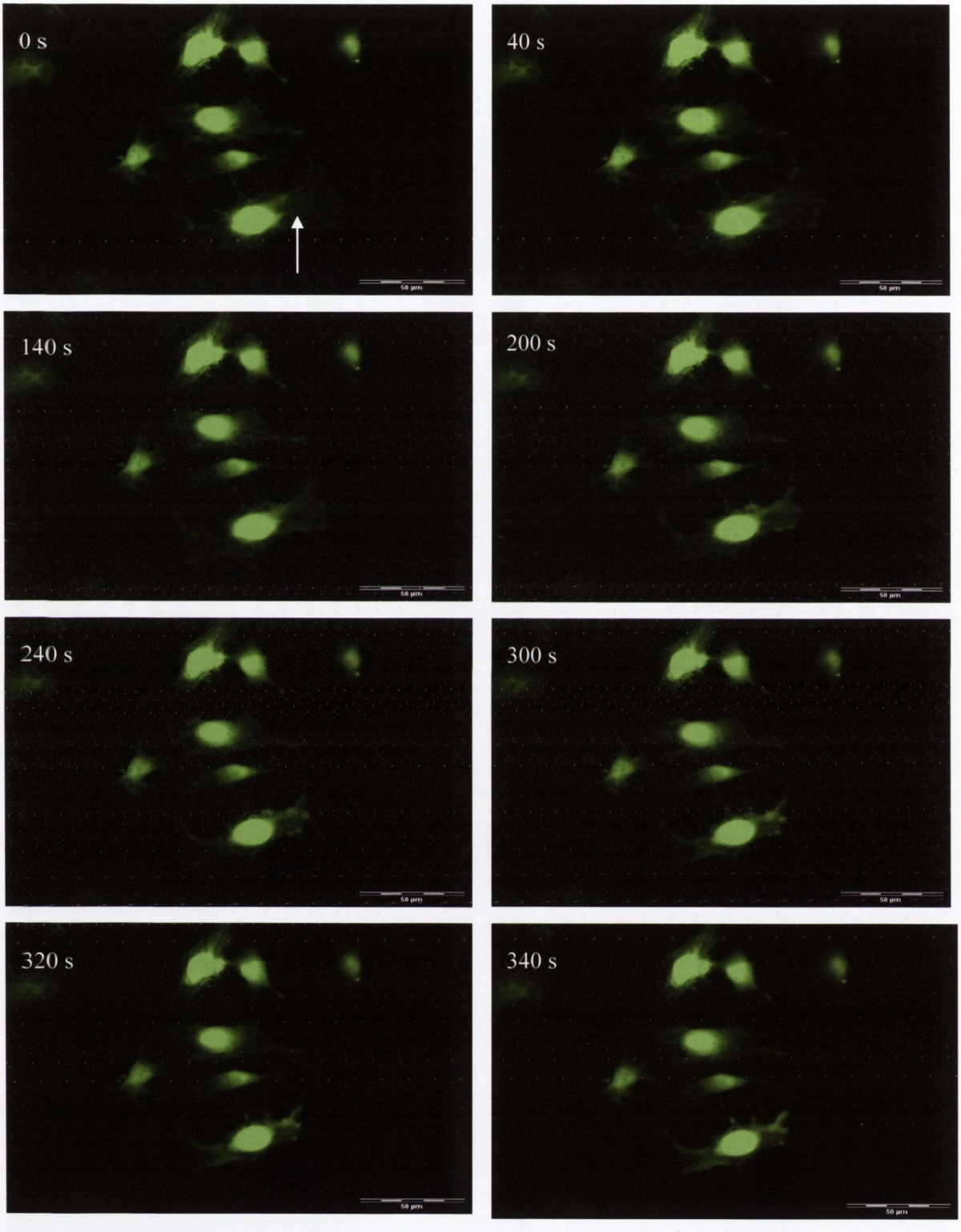

Fig. 4.23 *Images of nitric oxide fluorescence at various time intervals. Site of indentation is indicated by the white arrow. The first indentation with a force of >60 nN is applied continuously from 140 s until 200 s.*

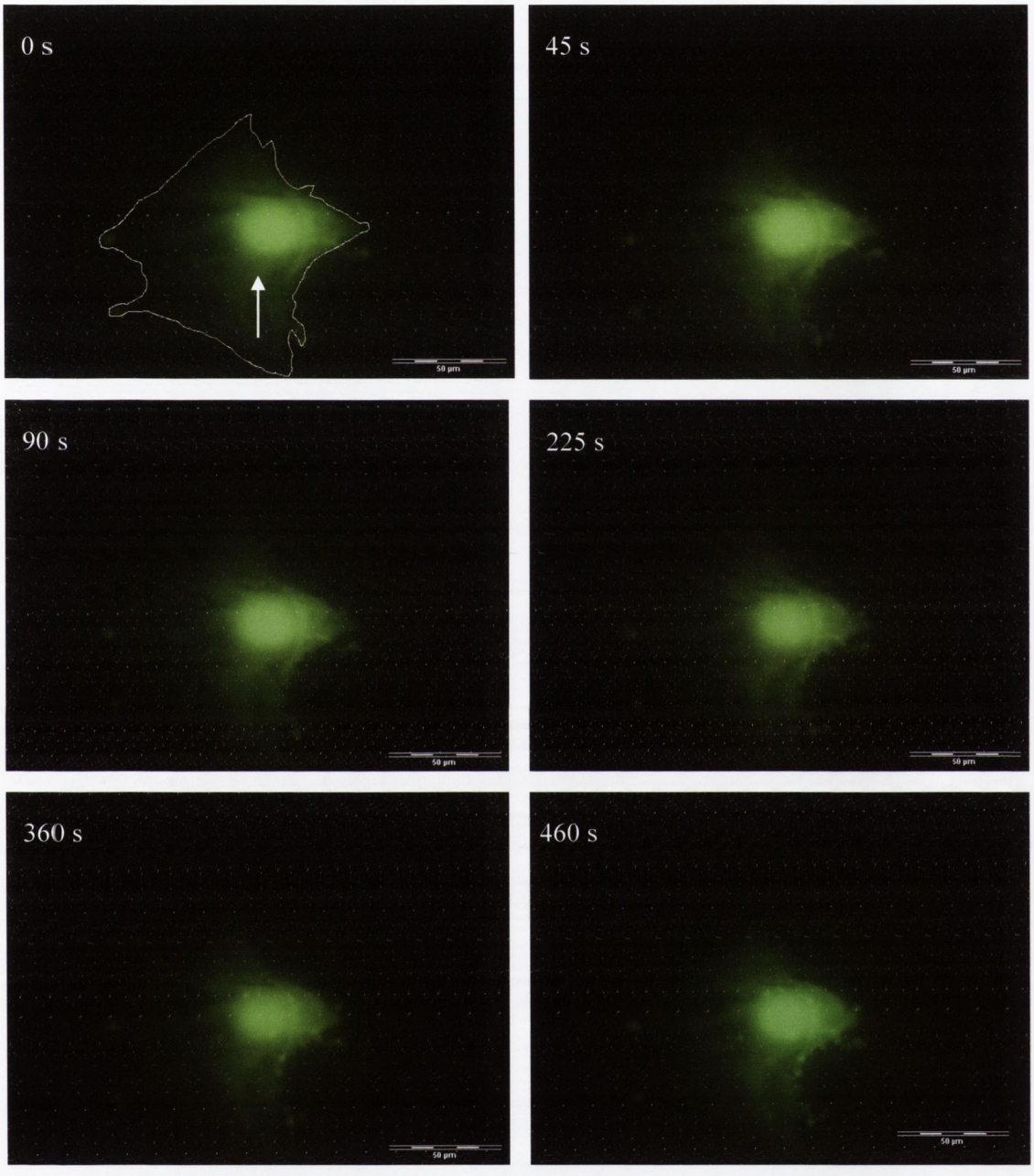

Fig. 4.24 *Images of nitric oxide fluorescence at various time intervals. Site of indentation is indicated by the white arrow. Indentation with a force of ~17 nN is applied continuously from 51 s until 110 s.*

the elasticity at the location of indentation can be calculated. For example, elasticity values were calculated for the force curve in Fig. 4.25, in which a force of 10 nN was applied to the osteoblast membrane by indenting to a depth of ~700 nm (3.2 – 2.5 μm), yielding an elasticity of ~7.4 kPa. Elasticity values ranging from 45.4 kPa to 315.1 kPa were also calculated for each force curve in Fig. 4.26a to 4.26d. Hence there is significant inter-cellular variation in osteoblast elasticity.

It is also evident from the force curves in Fig. 4.25 that increases in the indentation force applied to a particular location on the osteoblast membrane result in non-linear increases in osteoblast resistance to indentation. For example, to apply a force of 5 nN to the osteoblast membrane the tip indents to ~500 nm (3.1 – 2.6 μm), whereas to apply 10 nN the tip must indent to only ~700 nm (3.2 – 2.5 μm), and for a force of 50 nN the tip must indent to ~1.4 μm (2.8 – 1.6 μm). This 'strain hardening' effect was also captured in the cell model and was attributed to the contribution of cytoskeleton components (in Section 4.1.1).

Osteoblast membrane radial strains were calculated for examples of each NO response reported in this thesis. The validity of these values is discussed in Section 5.5.4 of the Discussion. The tip-membrane contact radius for each curve on this graph corresponds to the zero radial strain point on the x-axis. Force curve (a), or the 'localised pool' response, has the largest contact radius and the highest strains. This is because the force was applied at a location where elasticity is 45.4 kPa, significantly lower than for the other force curves. The tip must therefore indent further into the osteoblast (up to 400 nm) to reach the specified force of 20 nN, which results in higher radial strain and a larger contact area.

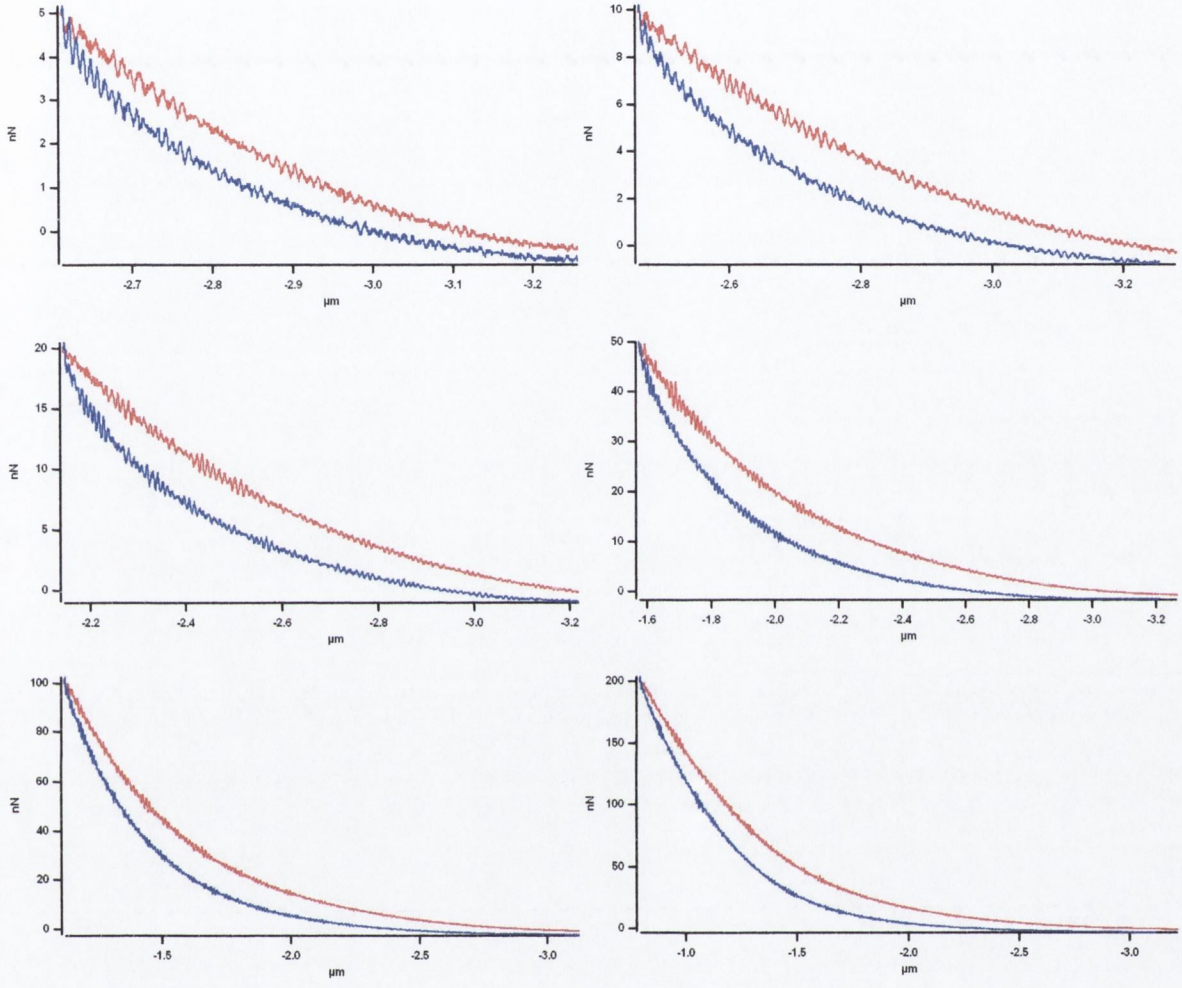

Fig. 4.25 *The effect of increasing force (nN), from 1 nN to 400 nN, on cell indentation characteristics. Velocity of indentation is ~ 1.86 µm.s^{-1} (0.4 Hz).*

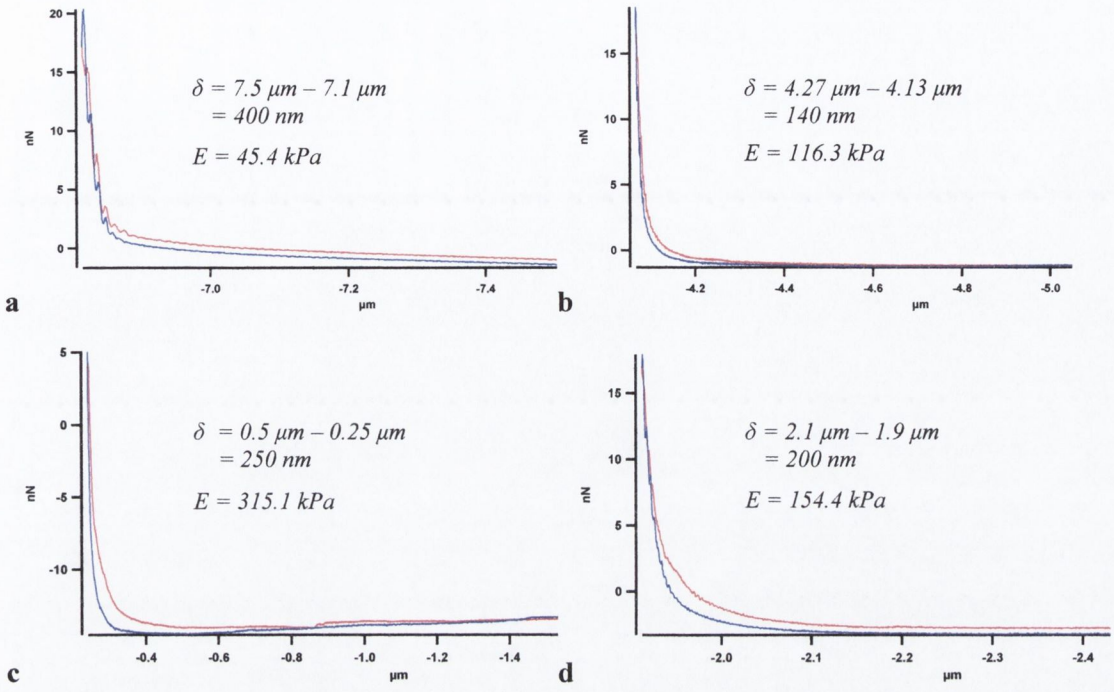

Fig. 4.26 *Force curves associated with each osteoblast response to indentation: (a) NO diffusion from localised pools; (b) Increases in NO in the perinuclear region; (c) Increases in intracellular NO then diffusion into extracellular medium; (d) Osteoblast retraction and diffusion of NO from localised pools. Indentation depth (δ) and elasticity (E) and radial strains (in Fig. 4.27) are calculated for each response.*

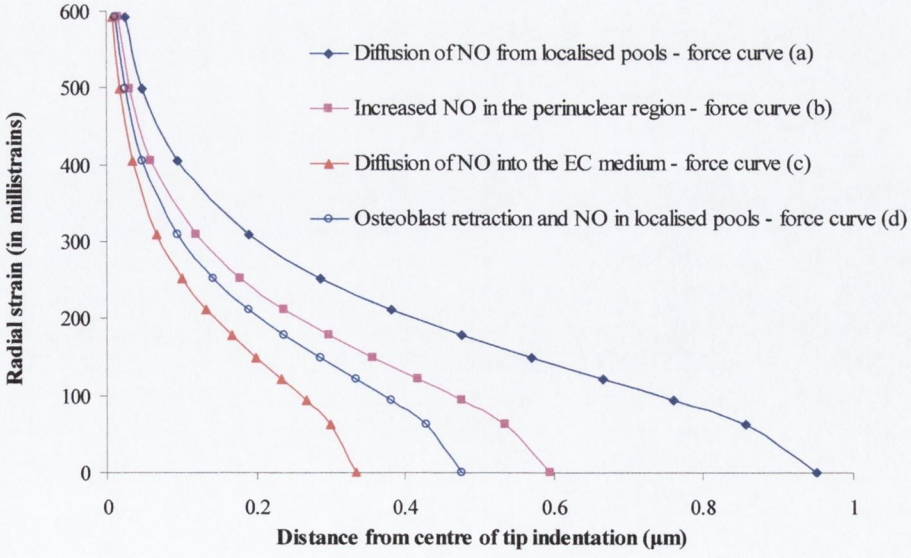

Fig. 4.27 *Comparison of osteoblast membrane radial strains associated with each response to indentation. The force curves referred to for each response are given in Fig. 4.26.*

Chapter 5

Discussion

5.1 Overview of results

5.2 Computational cell model

5.2.1 Tension in the actin cytoskeleton influences cell structural behaviour

5.2.2 The cytoskeleton and cytoplasm largely dictate cell stiffness

5.2.3 Predicted elasticity is in the range of experimentally-derived measurements

5.2.4 Cell model limitations

5.2.5 Application of the cell model to mechanotransduction

5.3 The physical consequences of fluid flow and strain stimulation on bone cells

5.3.1 Cell deformation due to 0.6 Pa fluid shear stress and 1,000 με strain is not equivalent

5.3.2 Bone cell NO and PGE_2 release is related to cell deformation

5.3.3 Strain may be related bone cell intracellular calcium and matrix production

5.3.4 Implications of deformation-dependent cell response for bone mechanobiology

5.4 Osteoblast and osteocyte NO and PGE_2 to fluid flow differs and is modulated by the cytoskeleton

5.4.1 Introduction

5.4.2 Osteoblast cytoskeleton involvement in fluid flow-stimulated NO and PGE_2

5.4.3 Osteocyte cytoskeleton involvement in fluid flow-stimulated NO and PGE_2

5.4.4 Differences in osteocyte and osteoblast mechanotransduction

5.5 Nitric oxide mechanotransduction in a single osteoblast

5.5.1 Introduction

5.5.2 Increased intracellular nitric oxide diffuses to the extracellular medium

5.5.3 Mechanotransduction of nitric oxide involves activation of localised eNOS

5.5.4 Membrane strains associated with osteoblast NO mechanotransduction

5.1 Overview of results

The cell model exhibits non-linear structural behaviour due to the contribution of the cytoskeleton prestress. Of all organelles, microtubules yield the most resistance to mechanical forces applied to the cell model, followed by actin and the cytoplasm. Elasticity of the cell model ranges from 0.6 to 1.4 kPa with highest values at focal adhesion sites. Cell model displacement due to 1,000 με strain is computed as 19 nm at the cell-substrate interface, whereas 0.6 Pa fluid shear stress causes a larger displacement of 106 nm along the apex of the cell membrane. The magnitude of strain required to yield membrane displacement equivalent to that caused by 0.6 Pa fluid shear stress is ~5,500 με. Experimentally, the involvement of the cytoskeleton in mechanotransduction of nitric oxide (NO) and prostaglandin E_2 (PGE_2) response is determined – in osteoblasts, a pulsatile fluid flow (PFF)-induced increase in nitric oxide (NO) release is inhibited by disrupting actin, whereas PFF-induced prostaglandin E_2 (PGE_2) release is observed only when either the actin or microtubule cytoskeleton is disrupted. In osteocytes, PFF-induced NO is enhanced with microtubule disruption, whereas increased PGE_2 release in osteocytes is inhibited by disruption of actin or microtubules. Mechanotransduction of NO in a single osteoblast subjected to indentation forces is also reported – forces ranging from ~17 to 50 nN cause rapid and sustained diffusion of nitric oxide from the osteoblast perinuclear region, and from localised pools throughout the osteoblast. Osteoblast force versus indentation characteristics illustrate considerable variation in elasticity between osteoblasts, and the membrane radial strains associated with indentation-induced NO response are in the range of 50 to 200,000 με. To argue the hypotheses of the thesis, these computational and experimental results are interpreted alongside relevant studies in the literature, to illustrate both the importance of the magnitude of deformation in bone cell NO and PGE_2 release, and the mechanisms by which the cytoskeleton mediates mechanotransduction of these important signalling responses.

5.2 Computational cell model

5.2.1 Tension in the actin cytoskeleton influences cell structural behaviour

Many researchers have speculated that the cytoskeleton largely dictates overall cell structural properties (for a review see Stamenovic and Coughlin, 2000). In the cell model, cytoskeleton stiffness is dependent on the relative positioning of the cytoskeleton components, which can vary in proportion to the magnitude of external force applied. Although all components are linear elastic, this 'structural non-linearity' occurs because the degree of repositioning of cytoskeleton components due to, and in achieving structural equilibrium with, each applied force dictates the stiffness of the overall structure – it is not due to position-dependent alterations of material properties of individual components (as in large displacement analyses). For example, in the cell model, stiffness increases as a result of increasing prestress values. Experimental observations of the influence of such a contractile force or prestress in the sub-membranous actin network have also been reported by several authors for endothelial cells (Wang and Ingber, 1994; Pourati et al., 1998) and for airway smooth muscle cells (Wang et al., 2001). In the absence of prestress (analogous to actin disruption), this structural non-linearity does not occur as a balance of tension and compression is required to maintain structural stiffness.

The second non-linear effect computed by the model is that increasing magnitudes of applied force results in increased resistance to deformation. Similar 'strain-hardening' effects have also been reported in experiments in which cell stiffness increases in response to increasing loads, observed in endothelial cells by Sato et al. (1990) and Wang et al. (1993), in myocytes by Shroff et al. (1995), and in fibroblasts by Peterson et al. (1982). This stiffening effect is observed to a lesser extent when forces are applied to the membrane at a distance from the underlying cytoskeleton, but does not occur in the absence of prestress. This again suggests that cytoskeleton components in bone cells provide stability to cell structure via prestress, and by dynamic changes in orientation of cytoskeletal components in equilibrating to imposed loads. That the cell cytoskeleton rapidly adapts its geometry to maintain cell structure is a more

plausible mechanism for strain-hardening behaviour than, for example, alterations in the material rigidity or viscosity of other organelles.

5.2.2 The cytoskeleton and cytoplasm largely dictate cell stiffness

It is evident that the cytoskeleton also contributes largely to overall cell stiffness, which agrees with several experimental results (Smith et al., 2003; Domke et al., 2000; Mathur et al., 2001). Besides the cytoskeleton, it is evident from cell model results that the cytoplasm has the most significant influence on the overall resistance to deformation, even though its elasticity is significantly less than that of the nucleus and membrane (this is illustrated in Fig. 4.3). This, of course, may be attributed to the large volume occupied by the cytoplasm relative to other components, and reflects the importance of determining correctly the incompressibility of the cytoplasm in developing biomechanical models of the cell, particularly since a wide range of values have been reported from experimental studies (see Section 2.2.2.2). Interestingly, the membrane, despite its small thickness is predicted to have a larger influence on cell stiffness than does the nucleus.

The cell model also predicts that, of all cell organelles, microtubule properties have the largest influence on the structural stiffness of the cell. This is attributed to their larger cross-sectional area, and their role as compression-bearing elements in the model. This result agrees with experimental observations of significant losses of structural stiffness upon disruption of microtubules (Stamenovic et al., 2002). That microtubules buckle in response to increased cell contraction (Wang et al., 2001) supports this crucial role for microtubules in maintaining cell stability. Increases in the elasticity of the actin filament components have a small effect relative to that of prestress. The decrease in elasticity of actin components is more significant since this also compromises the structural contribution of microtubules. However, altering material properties of actin components has a less significant effect on cell stiffness than the prestress transmitted by actin filaments. This reiterates that actin-transmitted contractile forces have a crucial role in maintaining adherent cell stiffness, as well as in non-linear structural behaviour.

It has been observed that adherent cells increase their resistance to deformation, i.e. their stiffness, as they become more spread with time on a substrate (Thoumine and Ott, 1999). The models developed in the thesis to represent increasing degrees of cell spreading do not conclusively reflect these findings. The lack of such stiffening in the cell model may reflect the overly simplified representation of how the cytoskeleton is re-arranged as the cell spreads (see Section 5.2.4 for model limitations). However it is evident that there may be a relation between stiffness and the cytoskeleton in each model – the movement of the cytoskeleton in response to arbitrary prestress value appears to be related to the final stiffness value. For example, high initial cytoskeleton displacement results in low stiffness (as in model d) and vice versa (model b) (Fig. 4.5). These results do not capture the mechanism of cytoskeleton involvement in cell spreading, but do reiterate the influence of the cytoskeleton rearrangement on cell structure and stiffness during cell spreading.

5.2.3 Predicted elasticity is in the range of experimentally-derived measurements

In the cell model, forces in the range of pico-Newtons result in displacements of nanometres, which is consistent with the experimental force-indentation characteristics obtained using AFM tip indentation into the osteoblast membrane, as reported in Section 4.4.2. To achieve further corroboration of the cell model, indentation of an AFM tip was modelled. Of the two methods used, the point load method is least valid, as the angle of tip contact with the cell membrane is infinitesimally small when a force is applied to a single node, and does not accurately reflect the geometry of the probe that transmits the indenting force. The point load assumption consequently yields lower values of cell model elasticity than obtained using the probe modelling method (Fig. 4.7). Using the more justifiable probe modelling method, the elasticity values calculated from the indentation versus reaction force data (Fig. 4.6) are in the range of those determined experimentally for fibroblasts using micromanipulation (0.6 – 1 kPa) (Thoumine and Ott, 1997), using micropipette aspiration of chondrocytes (0.6 kPa) (Guilak et al., 1999), and lower than those reported by Domke et al. (2000) (2.1 – 8.8 kPa), and are significantly lower than those values reported in Section 4.4.2 for indentation of osteoblasts.

Other papers (Radmacher et al., 1996; A-Hassan et al., 1998; Domke et al., 2000; Charras and Horton, 2002; Mathur et al. 2001) have reported large differences in elasticity when probing cells at various locations along the membrane using atomic force microscopy. For example, Charras and Horton (2002a) report average values of ~1kPa for osteoblast elasticity while reporting peak values of up to ~100 kPa due to underlying cytoskeletal stress fibres. Similarly, in the cell model compliance varies considerably, with the highest resistance to indentation at focal adhesion sites due to the positioning of the underlying cytoskeleton. This may explain the inter-cellular variation in force-indentation characteristics reported in Section 4.4.2. Stiffness decreases considerably at short distances from focal adhesion sites, although not as dramatically as reported experimentally (Charras and Horton, 2002) and converges to differing stiffness values in each spread model, despite their common material properties (Fig. 4.4). This suggests that cell geometry must also, to a small extent, impact on cell stiffness. At an indentation location nearer to a focal adhesion site, prestress effects also have an increasingly noticeable influence, although the proximity of indentation to the cytoskeleton, and not the prestress within the cytoskeleton, has the larger bearing on elasticity values determined.

5.2.4 Cell model limitations

By accounting for the role of all structurally relevant components in maintaining a cell's stability, the models developed in this thesis can be viewed as a hybrid approach that fuses features of contrasting previous approaches, the stress-supported tensegrity approach (Ingber, 1997) and the continuum approach (Kamm et al., 2000). Repositioning of the tensegrity-based cytoskeleton to increasingly spread shapes is justified by the fact that orientation, positioning and length of internal cytoskeleton components is altered by polymerisation, and by clustering of actin filaments during spreading as adhesion bonds form between intra- and extra-cellular structural proteins such as vinculin, talin, and fibronectin (Alberts et al., 1989; Janmey, 1998). In fact, Thoumine and Ott (1999) also correlate spreading-induced stiffening with cytoskeletal reorganisation, and it has been suggested by Gittes et al. (1993) that to account for the seemingly excessively rigid mechanical properties measured, sliding and movement may occur

between filaments and tubules. The approach to spreading-induced cytoskeletal changes in the cell model might be considered as taking a "snapshot" of the cytoskeletal network in increasingly spread configurations without incorporating the mechanisms that drive these changes. For example, in a spreading cell the number and strength of integrins and ligands present modulates the binding of structural proteins at focal adhesion complexes and therefore alters the distribution, length and orientation of the cytoskeleton, and in turn, cell structural properties. In the cell model the distribution of integrin-ligand binding sites is approximated as a continuum and the number of focal adhesion complexes attaching the cytoskeleton to the substrate does not increase in more spread configurations. By manually repositioning the cytoskeleton our approach does not model the dynamics of cell spreading, but rather the consequences of it in terms of the cellular biomechanical properties.

The material properties chosen to represent the cytoskeleton have been used in previous models (Stamenovic and Coughlin, 2000), while similar values for flexural rigidity have been estimated theoretically by Ben-Avraham and Tirion (1995), and are in agreement with other experimental work (Tsuda et al., 1996). However, any interpretation of cytoskeletal contribution to cell structure must not ignore that the approach taken in the cell model approach focuses on incorporating specific tensile or compressive roles for actin and microtubules in an idealised interconnected network, rather than attempting to model physiological amounts of either cytoskeletal component. In the cell model, a specific tensile or compression-bearing role was not assigned to intermediate filaments since, according to Janmey (2001) and Wang and Stamenovic (2000), their contribution to cellular rigidity only becomes significant above 20% strain; their properties were therefore assumed incorporated in those of the cytoplasm. As linear elastic material properties are used for each of the cell model components, time-dependent deformation due to viscoelastic material behaviour under continuous mechanical stimulation, (such as pulsatile fluid shear stress or cyclic strain) is not accounted for.

Regarding model corroboration by simulation of AFM tip indentation, the validity of applying the expressions derived by Sneddon (1965) to determine localised elasticity values has been discussed by other authors (Costa and Yin, 1999). The expressions are based on the

assumption of infinite sample thickness. As the indentation depths (<100 nm) are significantly less than the height of the cell model (~7000 nm), this condition is considered adequately satisfied. The load-indentation relation used here (Eqn 3.2 in Section 3.2.2.2) is in agreement with that used by both Weisenhorn et al. (1993) and Charras and Horton (2002), but it seems that it has been reported erroneously in recent AFM publications (Radmacher et al., 1996; Mathur et al., 2002). The contact angle chosen in simulating AFM tip indentation into the cell model has a significant influence on elasticity, but is in the range of angles (35^0 - 50^0) used in those experimental measurements to which comparisons are made in Section 5.2.3. However, it has been suggested by Costa and Yin (1999) that the assumption that strains are infinitesimal is not valid when applied via a conical or pyramidal tip with a contact angle of < 45^0, suggesting that finite strains most likely occur in the contact region. Hence a large displacement contact analysis would perhaps more accurately reflect material behaviour during probe indentation.

5.2.5 Application of the cell model to mechanotransduction

While the need to incorporate mechanisms of polymerisation and focal adhesion formation in physiological concentrations of cytoskeletal components within more morphologically accurate model geometries with time-dependent material properties is recognised, the model of a single cell developed here is proposed as one that is sufficiently complex to capture the structural behaviours of cells in response to mechanical forces, whilst not being so complex that the parameters cannot be specified. Because the cell model yields quantitative data in the range of experimentally-derived values, and facilitates modelling of whole-cell mechanical stimuli, its use as a predictive tool in mechanobiology is justifiable – for example, in computing the consequences of various mechanical stimuli *in vitro*, such as fluid flow, substrate strain, or microgravity conditions, in order to understand the biomechanical origins of differences in observed cell response.

5.3 The physical consequences of fluid flow and strain stimulation on bone cells

5.3.1 Cell deformation due to 0.6 Pa fluid shear stress and 1,000 με strain is not equivalent

When the experimental stimulation of primary bone cells with 0.6 Pa fluid shear stress and 1,000 με substrate strain (Mullender et al., 2004) is modelled using the computational cell model it is revealed that fluid flow and strain are quite different in terms of the pattern of cellular deformation caused. Fluid shear stress causes significantly higher displacement and stressing of all cell model components (i.e. cytoplasm, cytoskeleton, nucleus and membrane) relative to strain.

When adherent bone cells are subjected to substrate strain, as the frequency of applied strains (1 Hz) exceeds the rate at which new adhesion bonds can be formed, the assumption that the cell must deform with the substrate is justifiable. It is contended that because strain-induced deformations have a basis, the fact that 0.6 Pa fluid shear stress causes even greater cellular deformation than 1,000 με substrate strain means that fluid shear stress deformations must also have a basis. Although this remains to be confirmed for bone cells, images of rolling leukocytes deforming (decreased cell height and increased cell-substrate contact length) under fluid shear stresses ranging from 0.2 to 1.5 Pa (Dong and Lei, 2000) support the contention that bone cells deform under fluid shear stress also.

5.3.2 Bone cell NO and PGE_2 release is related to cell deformation

The differences in displacement and stress predicted as a result of 0.6 Pa fluid shear stress and 1,000 με strain are important in investigating the origins of the differences in bone cell responses reported in the experiments of Mullender et al. (2004) (Fig. 2.15), but it also explains the results of other studies in which cellular responses to similar magnitudes of fluid shear stress and strain were also compared (Smalt et al., 1997; You et al., 2000). For example, this result shows that fluid shear stress but not mechanical strain induces increased PGE_2 release [reported by Mullender et al. (2004) and Smalt et al. (1997)] because it causes higher displacement and stressing of the membrane and cytoskeleton. It has been shown previously that: (i) flow-induced

PGE_2 release by bone cells is dependent on the cytoskeleton (Ajubi et al., 1996); and (ii) fluid-shear induced increases in COX-2 expression (COX-2 is a key enzyme for PGE_2 production) involve reorganization of the actin cytoskeleton (Pavalko et al., 1998) – therefore it is likely that increased PGE_2 activity may be related to higher displacement of the cytoskeleton in fluid shear stress as compared to strain. Similarly, the higher NO response due to fluid shear stress could be due to higher membrane stressing because it has been suggested that mechanically-induced formation of NO results from activation of endothelial nitric oxide synthase (eNOS) in bone cells (Klein-Nulend et al., 1998; Helfrich et al., 1997). eNOS is an enzyme located in pools in the region of the plasma and Golgi membrane that may be rendered susceptible to activation by increased stressing of the cell (Helfrich et al., 1997; Fulton et al., 2002). A schematic diagram outlining how the bone cell deformation caused by fluid flow or substrate strain is related to nitric oxide and PGE_2 response is provided in Fig. 5.1.

Since deformation of the cell model will vary linearly (it being a linear elastic model), the model results can be extended to interpreting cell responses to both fluid shear stress and strain stimuli of varying magnitudes. For example, increasing the magnitude of strain in the computational model to ~5,500 με yields deformations in the range of those caused by fluid shear stress of magnitude 0.6 Pa. If, as the model results suggest, the release of NO and PGE_2 signalling molecules is deformation-dependent, then such an increased magnitude of strain should result in equivalent cellular responses. In fact this hypothesis is confirmed by several experimental findings; namely higher NO release by bone cells has been reported at 3,400 με (Zaman et al., 1999), and 3,800 με (Pitsillides et al., 1995), and significant increases in PGE_2 release by primary human osteoblasts at 4,000 με (Fermor et al., 1998). Essentially, this further strengthens the explanation that the preferential *in vitro* stimulation of NO and PGE_2 release by fluid shear stress of magnitude ~0.6 Pa is as a result of the higher cell deformation, in particular the membrane and cytoskeleton.

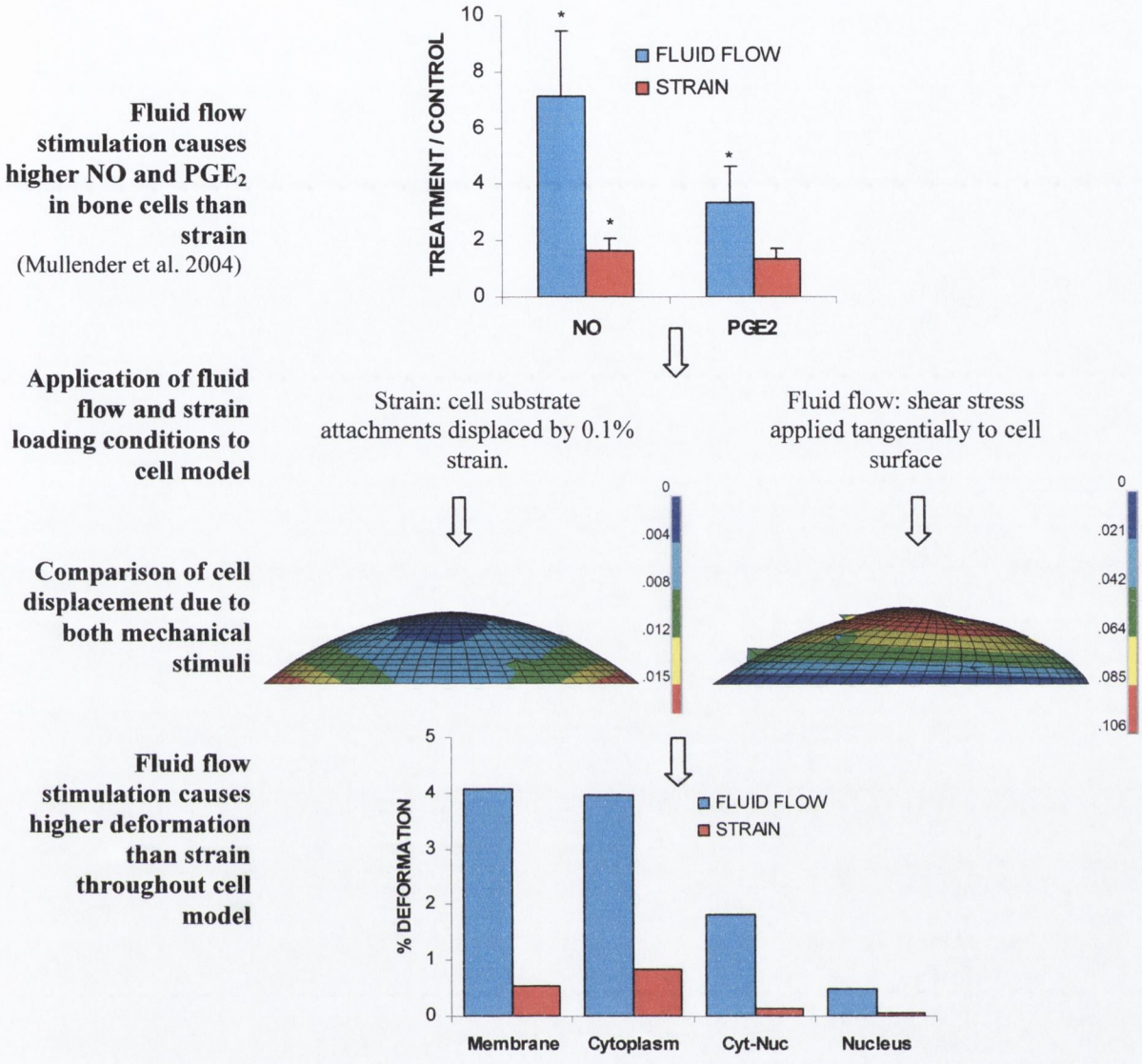

Fig. 5.1 *Schematic diagram illustrating how the cell model explains differences in cell response to fluid flow and strain in terms of cellular deformation.*

5.3.3 Strain may be related bone cell intracellular calcium and matrix production

Increased cellular deformation in fluid shear stress can also shed some light on experimental reports by You et al. (2000) of significant increases in intracellular calcium (Ca^{2+}) due to oscillatory fluid flow and not to physiological magnitudes of strain. These increases in Ca^{2+} may be caused by higher membrane stress in fluid flow, particularly since it is known that stimulation of the membrane influences ion channel activity that can elicit rapid intracellular Ca^{2+} responses (Janmey, 1998). Finally, regarding the opposite effects of commonly applied

magnitudes of fluid shear stress and strain on collagen type I matrix production, as reported by Mullender et al. (2004) (Fig. 2.15), although overall deformation due to strain is relatively low compared to fluid shear stress, increased collagen type I production in strain may be related to the higher stresses occurring at cell-substrate attachments. This possible mechanism of stimulating collagen type I production in bone cells could equally apply to the other studies that report increased activity related to matrix production in response to strain magnitudes (Walker et al., 2000; Jones et al., 1991) also in the physiological range measured by Burr et al. (1996).

5.3.4 Implications of deformation-dependent cell response for bone mechanobiology

As described above, many *in vitro* studies report that bone cells respond to strain with increased collagen or matrix production (Walker et al., 2000; Jones et al., 1991), or with increased proliferation (Kaspar et al., 2000). Such cell behaviour is associated with the osteoblastic phenotype. This makes sense when it is considered that the magnitude of strains applied are generally within the range of the magnitude of strain measured on the surface of long bones, i.e. <2,000 με (Burr et al., 1996), where osteoblasts are located (McCreadie and Hollister, 1997). On the other hand, bone cell responses to commonly applied magnitudes of fluid shear stress *in vitro* do not appear to cause bone cell responses associated with osteoblast *in vivo* function. Instead, these studies report increases in bone cell NO and PGE_2 signalling molecule release, both of which are involved in mechanically-induced bone adaptation possibly by mediating signal transduction or cGMP activity in target cells – for example, it has been hypothesised that osteocyte-sensing of fluid flow may use these messengers in modulating osteoblastic bone formation (Burger and Klein-Nulend, 1999; Klein-Nulend et al., 1995). The shear stresses that induce these responses are in the range of those estimated to occur in the canalicular network where osteocytes are embedded [0.8 - 3 Pa (Weinbaum et al., 1994)]. Hence, it appears that *if* the stimuli applied to bone cells *in vitro* are representative of the *in vivo* mechanical environment associated with the anatomical location of either an osteoblast or osteocyte, the responses induced are characteristic of, or associated with, the osteoblastic or osteocytic phenotype. Of course this conclusion is contingent on whether the accepted estimates of strain

(Burr et al., 1996) and shear stress are indeed close to the actual *in vivo* values (Weinbaum et al., 1994). Also, if the mechanical environment of osteocytes also includes high strains around lacunae (strains up to ~27,000 με have been predicted (McCreadie and Hollister, 1997), the experimental reports of increased NO and PGE_2 release at higher applied strain as described in Section 5.3.2 (Zaman et al., 1999; Pitsillides et al., 1995; Fermor et al., 1998) also support this possibility.

In this study a static analysis was considered sufficient to compute the instantaneous structural response of bone cells under imposed mechanical loads. Recognizing that certain experimental studies suggest the importance of strain rate (and not merely strain magnitude) in determining cell response (Bacabac et al., 2004; Turner et al., 1995; Mosley and Lanyon, 1998), and that several experimental studies (see Section 2.5) involve application of pulsating and cycling shear stress and strain to bone cells, a transient viscoelastic analysis is required to investigate time-dependent changes in the cellular deformations reported here.

5.4 Osteoblast and osteocyte NO and PGE_2 to fluid flow differs and is modulated by the cytoskeleton

5.4.1 Introduction

Several of the early nitric oxide (NO) and prostaglandin E_2 (PGE_2) responses to pulsatile fluid flow stimulation reported in this thesis (in the absence of cytoskeletal disruption) confirm previous results (Klein-Nulend et al., 1995; Johnson et al., 1996; Mullender et al., 2004; Helfrich et al., 1997; Ajubi et al., 1996). By visualizing the changes in the actin cytoskeleton that accompany PFF-induced NO and PGE_2 response, the following insights were also obtained:

- there are considerable differences in actin and microtubule cytoskeleton involvement between both osteoblastic and osteocytic cell mechanotransduction of NO and PGE_2 release;
- cytoskeletal disruption has opposite effects on osteoblast and osteocyte prostaglandin E_2 response.

5.4.2 Osteoblast cytoskeleton involvement in fluid flow-stimulated NO and PGE_2

(i) In osteoblastic cells (OBs), complete inhibition of PFF-induced nitric oxide (NO) response by actin cytoskeleton disruption (Fig. 4.13 A) is accompanied by significantly reduced parallel alignment of actin bundles/stress fibres (Fig. 4.11). This suggests that the mechanism of PFF-induced NO response is mediated by the actin cytoskeleton – this has not been previously observed in OBs, but has been reported for fluid flow-induced NO response in endothelial cells (Su et al., 2003; Zharikov et al., 2001). This similar result in endothelial cells is of interest here because it has been shown that shear stress-induced NO production in primary OBs proceeds via activation of endothelial nitric oxide synthase (eNOS) (Klein-Nulend et al., 1998) as it does in endothelial cells (Busse and Fleming, 1995). Hence, the actin cytoskeleton (but not the microtubule cytoskeleton) may similarly regulate PFF-induced NO response via eNOS conversion of L-arginine pathway (this is discussed in further detail in Section 5.5.3).

(ii) In OBs, disruption of the actin and microtubule cytoskeleton results in decreased stress fibre formation and alignment (Fig. 4.11), but simultaneously activates PFF-induced PGE_2 response (Fig. 4.13). This indicates that (unlike NO response as discussed in (i) above) PFF-induced PGE_2 response is independent of actin cytoskeleton reorganization. In both static and PFF-stimulated OBs, a PGE_2 response occurred only in those OBs in which cytoskeletal disruption causes actin clustering at focal adhesions. Interestingly, Ponik and Pavalko (2004) reported that increased focal adhesion formation in OBs promotes fluid shear stress-induced PGE_2 release and COX-2 production (a key enzyme for PGE_2 response). In this thesis, that increased PGE_2 response occurs only when actin clusters at focal adhesions as a result of cytoskeletal disruption, suggests that increased stimulation of mechanosensitive focal adhesions when subjected to pulsatile fluid flow leads to increased PGE_2 response in OBs via COX-2 activation (see also Fig. 5.2). This does not, however, agree with Norvell et al. (2004) in which higher concentrations of cytoskeleton disrupting agents than used in these experiments do not alter OB PGE_2 response to 90 mins steady fluid shear stress. A key difference is that in their study the

OBs were subjected to steady fluid flow – the *pulsatile* fluid flow is used in the present study is more physiologically relevant and likely more stimulatory, which may explain why increased PGE_2 response is detected over a much shorter time-scale.

5.4.3 Osteocyte cytoskeleton involvement in fluid flow-stimulated NO and PGE_2

(i) Few studies have investigated the effects of mechanical stimulation on osteocytes or osteocytic cells (OCYs), as in this thesis. It was anticipated that the actin cytoskeleton would be involved in mechanically-stimulated nitric oxide (NO) response as in endothelial cells and osteoblasts – Zaman et al. (1999) report that mechanical strain-induced NO production in OCYs also proceeds via activation of eNOS activity, which in endothelial cells is mediated by the actin cytoskeleton (Su et al., 2003; Zharikov et al., 2001). Possible explanations for why this is the case for osteoblasts and not for osteocytes are discussed in Section 5.4.4 below. Additionally, PFF-induced increase in OCY nitric oxide response is not dependent on microtubules, and is in fact further enhanced by microtubule disruption. This effect has not been observed previously for OCYs, although once again a parallel result has been reported for endothelial cells in which microtubule disruption has been shown to enhance fluid shear stress-induced eNOS response (Knudsen and Frangos, 1997). Hence, this supports the possibility that mechanically-induced OCY bone cell responses to mechanical loading also involve the same eNOS mediated mechanisms as in endothelial cells.

(ii) The present results indicate that both an intact actin and microtubule cytoskeleton are required for PFF-induced PGE_2 response in OCYs. Although Ajubi et al. (1996) also report that an intact actin cytoskeleton is required for PGE_2 response (in embryonic chicken calvarial osteocytes), no previous studies to date report microtubule involvement in OCY responses to mechanical stimulation. Since it has been reported that cytoskeletal disruption modulates PGE_2 response via passage of calcium ions (Ajubi et al., 1999), it is therefore possible that the PFF-induced PGE_2 responses observed here arise because cytoskeletal disruption alters mechanosensitive ion channel activity in OCYs (Fig. 5.2).

5.4.4 Differences in osteocyte and osteoblast mechanotransduction

A higher osteocyte (OCY) PFF-induced NO responsiveness relative to osteoblasts (OBs) was anticipated, as osteocytes have been previously shown to be more mechanosensitive (Klein-Nulend et al., 1995; Westbroek et al., 2000). Although this was not the case with the OCY cell lines in these experiments, comparisons of OB and OCY results do uncover interesting differences in cytoskeletal involvement in NO and PGE_2 response to pulsatile fluid flow. For example, unlike PFF-induced NO response in OBs, it cannot be concluded that stress fibre alignment or actin cytoskeleton reorganization is related to PFF-induced OCY NO response (Figs. 4.12 and 4.14). Also, there are opposite effects of cytoskeletal disruption on OCY and OB PFF-induced PGE_2 response (Figs. 4.11 and 4.13). Both these differences in NO and PGE_2 response in OCYs and OBs may be related to differences in cytoskeleton composition between both cell types. In addition to inhibiting direct cytoskeletal involvement in mechanotransduction, disrupting cytoskeleton components also alters mechanical connections between integrins, cytoskeletal filaments and the nucleus (Janmey, 1998; Maniotis et al., 1994; Wang et al., 1993). Cytoskeleton disruption can therefore also alters bone cell mechanical properties and mechanosensitivity as has been demonstrated experimentally (Trickey et al., 2004; Duncan and Hruska, 1994). As the consequences of cytoskeleton disruption are dependent on cell characteristics such as relative amounts and distribution of cytoskeleton components, the effect of disrupting the osteocyte and osteoblast cytoskeleton cannot be assumed equivalent. Indeed, the more significant effect of actin disruption (than microtubule disruption) on OCY morphology indicates that OCY structure is largely dependent on actin. This has also been observed by Tanaka-Kamioka et al. (1995). It is possible that such differences in actin composition are involved in the differences in PFF-induced NO response. In Section 5.5.3, a mechanism by which actin components may mediate endothelial nitric oxide synthase (eNOS) conversion of L-arginine to NO in osteoblasts and osteocytes when subjected to fluid shear stress (as described in this Section) or to an indentation force (as in Section 5.5) is proposed.

In this thesis inhibition of PGE_2 is observed in OCYs treated with cytoskeleton disrupting agents, but not OBs. It is interesting to compare these results to those of Rawlinson et al. (1996), in which it was found that blocking shear/stretch sensitive ion channels abolishes glucose-6-phosphate dehydrogenase (G6PD) activity, for which PGE_2 response is required in OCYs (El Haj et al., 1996). The importance of stretch-sensitive ion channels in OCY PGE_2 response has also been confirmed by Ajubi et al. (1996). In OBs, however, voltage-dependent calcium channels have the dominant influence on mechanically-induced G6PD response, and blocking stretch-sensitive ion channels only slightly reduces PGE_2 release (Rawlinson et al., 1996). That cytoskeletal disruption abolishes PFF-induced PGE_2 response in OCYs, but not in OBs, may be because of this greater dominance of stretch-sensitive ion channels in OCY response to mechanical loading, i.e. the cytoskeleton modulates PGE_2 response in OCYs via these mechanosensitive ion channels.

A mechanism by which the cytoskeleton influences the PGE_2 signalling pathway in both OBs and OCYs is illustrated in Fig. 5.2. In this proposal, disruption of actin or microtubules modulates ion channel activity (either by direct cytoskeleton connection or via altered membrane tension) leading to an influx of calcium ions. Calcium entry through single ion channels has been observed for smooth muscle cells (Zou et al., 2002), is regulated by actin filaments in human fibroblasts (Wu et al., 1999), and high calcium levels are associated with COX-2 and PGE_2 response (Choudhary et al., 2003). Calcium modulates the functions of various enzymes linked to the prostaglandin signalling pathway, including phospholipase C (PLC). PLC, which may be regulated by the actin-filament linked protein profilin, breaks down into diacylglycerol (DAG). DAG and Ca^{2+} are activators of protein kinase C (PKC) (Nishizuka, 1992), which in turn enhances cytosolic phospholipase A_2 (PLA_2) (Ajubi et al., 1996) from which arachidonic acid is generated. An increase in arachidonic acid, together with activation of COX-2 leads to prostaglandin synthesis, including PGE_2 (Ajubi et al., 1996; Bakker et al. 2003) (see Fig. 5.2). In this thesis, when the actin cytoskeleton is disrupted in OCYs, the resultant disruption of ion channel activity would inhibit the influx of calcium ions that initiates the signalling pathway that leads to PGE_2 response. The fact that these stretch-sensitive ion

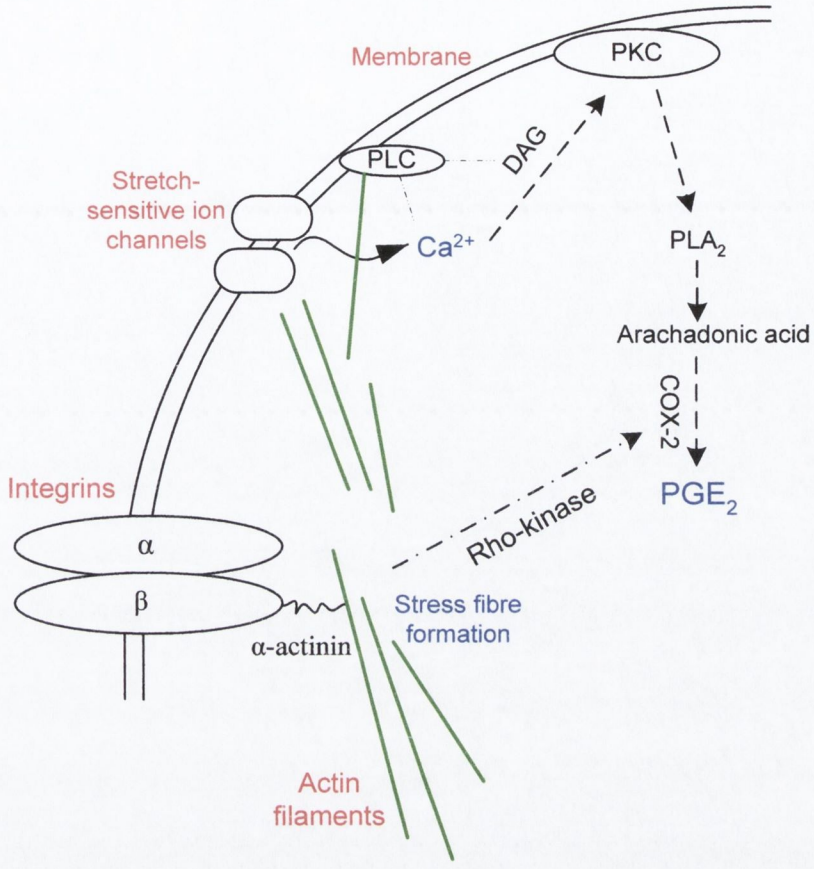

Fig. 5.2 *Schematic representation of cytoskeleton involvement in signal transduction of mechanical stimulation-induced prostaglandin E_2 release in osteoblasts or osteocytes (see text for full explanation). Abbreviations: PKC, protein kinase C; PLA_2, cytosolic phospholipase A_2; COX-2, cyclooxygenase-2; DAG, diacylglycerol; PLC, phospholipase C; PGE_2, prostaglandin E_2.*

channels are more dominant in OCYs than in OBs would explain inhibition of PGE_2 response by cytoskeleton disruption in OCYs only. This proposed mechanism does not rule out involvement of other mechanosensors that have been implicated in PGE_2 response, such as G-protein-coupled receptors (Gudi et al., 1996), gap-junctions (Saunders et al., 2001; Cherian et al., 2005) the glycocalyx (Mochizuki et al., 2003; Reilly et al., 2003), or focal adhesions. In fact in OBs, PGE_2 response is evidently related to α-actinin-mediated recruitment of actin filaments to focal adhesions, that then leads to Rho kinase-mediated COX-2 activity and enhanced PGE_2 response (Ponik and Pavalko, 2003) (Fig. 5.2). This may well explain why

clustering of actin at focal adhesions after disruption of actin and microtubules corresponds with enhanced PGE_2 response in fluid flow stimulated OBs.

5.5 Nitric oxide mechanotransduction in a single osteoblast

5.5.1 Introduction

In the following Sections the significance of the results reporting mechanotransduction of intracellular nitric oxide response in single osteoblasts *in vitro* is discussed. The various control experiments performed in verifying that nitric oxide response is due to mechanotransduction are discussed here in Section 5.5.1. The implications of the various osteoblast responses to indentation are discussed in Sections 5.5.2 and 5.5.3. In Section 5.5.4 the estimated membrane strains associated with mechanotransduction of NO response are discussed.

Nitric oxide (NO) is not stored within a cell as it is toxic in high concentrations (Evans and Ralston, 1996). The rapid responses occurring over the time-scale of the indentation experiments in this thesis indicate that synthesis and diffusion of NO occurs within a short time (ranging from <10 s to 2 mins) after receiving the mechanical signal. Such a rapid response indicates that bone cell NO response is independent of longer-term changes in cell activity that result from transcription in the nucleus. The reason that only ~10 % of indented osteoblasts respond to the indenting mechanical force at any one time is unknown, but it may be that the osteoblasts respond only in one phase of the cell cycle. The varied mechanoresponsiveness may also be related to the osteoblast passage number, proximity of indentation to mechanosensory components of the cell (for example, cytoskeletal proteins, ion channels or integrins), and to variation in osteoblast strain due to variables such as osteoblast elasticity and depth of indentation, as discussed in Section 5.5.4.

It is clear from each of the control experiments that none of the responses are artefacts of the methods used during osteoblast indentation. In the 'mitotracker' controls, for example, there was no alteration in fluorescence over the time-scale of the experiment, besides photobleaching and slight increases in fluorescent intensity due to tip reflection during

indentation only. This artefact due to tip reflection was also observed during nitric oxide indentation experiment – when quantified it was found that normalised fluorescent intensity increased by ~1 % and coincided exactly with tip actuation times. This small percentage increase is insignificant relative to the magnitude of any response reported in Section 4.4.1. Another concern addressed was that indentation would result in non-viable or apoptotic osteoblasts by puncture of the indented membrane. Such non-viable cells would stain positive for the propidium iodide dye. Relative to the positive control, this was not recorded in any of these controls experiments, indicating that the osteoblasts remain viable and are not irreversibly damaged during mechanotransduction of the various nitric oxide (NO) responses. In the control experiments in which the tip was actuated above, or stationary in the proximity of, an osteoblast no change in fluorescence besides photobleaching was observed. This confirms that the force applied via tip-membrane contact initiates mechanotransduction of any NO response. It is therefore clear that any response recorded arises due to altered osteoblast behaviour (and not from fluorescent artefacts), does not result in apoptotic or non-viable osteoblasts within the tim-scale of the indentation experiment, and is due to application of a force via contact of the AFM tip with the osteoblast membrane.

5.5.2 Increased intracellular nitric oxide diffuses to the extracellular medium

In the response reported in Section 4.4.1.4, indentation results in increased intracellular NO within 60 s, which begins to decline rapidly within 300 s. While it is possible that the rapid decrease in intracellular NO concentration is due to a mechanism that inactivates the NO within the cell, there is evidence to support the possibility that NO is gradually diffusing into the extracellular medium – the fact that the initial increase in NO intensity is accompanied by the emergence of pools of NO that diffuse outwards from the membrane in tandem with a drop in intracellular NO intensity indicates that the NO is diffusing through the membrane. If so, this response is most likely the mechanism by which pulsatile fluid flow results in increased nitrate in the experimental medium, as discussed for the fluid flow experiments in this thesis (Section

5.3) and in several other studies also reporting increased nitrate levels after mechanical stimulation of bone cells (discussed in Section 2.5.3).

Nitrate forms immediately when short-lived NO molecules are mixed with oxygen in the extracellular medium, where it accumulates over the duration of an experiment. However, to relate NO concentration produced by a single osteoblast to the concentration of nitrate after 10 mins would be difficult because: (i) all osteoblasts in a monolayer population are unlikely to respond to a mechanical stimulus (the differences in osteoblast mechanoresponsiveness reported in Section 5.5 would also arise in fluid flow stimulation), and (ii) it is not known whether all of the short-lived NO will be converted to nitrate or diffuse into the medium.

5.5.3 Mechanotransduction of nitric oxide involves activation of localised eNOS

Osteoblast response to indentation forces ranging from 17 to 50 nN causes synthesis and diffusion of NO to occur from both localised pools throughout the osteoblast and from the perinuclear region (see Sections 4.4.1.2 and 4.4.1.3). This NO synthesis appears to be sustained beyond the duration of the indentation experiment as the localised pools of NO fluorescence do not decrease in intensity as they diffuse outwards. Similarities in the dynamics of the perinuclear and localised pools response (i.e. the time-scale, magnitude of increase, and the fact that it is sustained) indicate that both responses may involve similar mechanisms. The response to indentation described in Section 4.4.1.5 shows that indentation can lead to rapid alteration in osteoblast morphology. In one such response, this retraction accompanied by increased NO intensity also at localised pools. Considering the crucial role for the cytoskeleton in maintaining cell structure and shape (as discussed in Section 2.2.1.1 and predicted in the cell model), it is likely that osteoblast retraction is due to cytoskeleton movement – if so, this provides convincing evidence for cytoskeleton involvement in the transduction of a mechanical stimulus to a diffusion of NO from localised pools.

To explain both these single osteoblast NO responses to indentation, and also the differences in cytoskeletal involvement in osteocyte and osteoblast response to fluid flow stimulation (Section 5.4), these results are discussed in the context of what is known in the

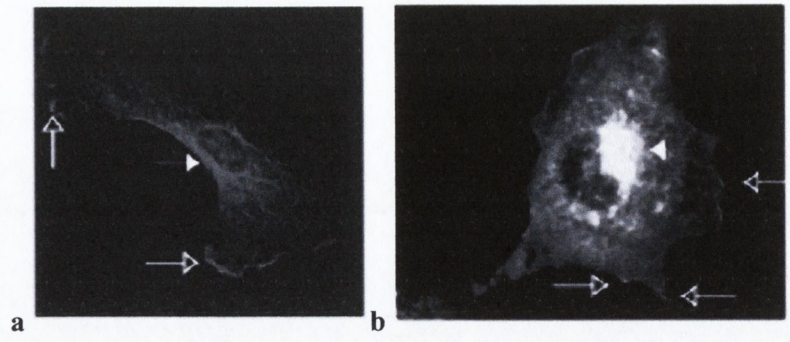

Fig. 5.3 *Fluorescent image of cells immuno-labelled with antibodies to total eNOS. (a) bovine aortic endothelial cells after stimulation with vascular endothelial growth factor, and (b) COS-7 cells transfected with eNOS. In both cells total eNOS is localised to the plasma membrane (open arrows) and perinuclear region (arrow heads). Adapted from Fulton et al. (2002).*

literature of the well-established eNOS-mediated mechanotransduction of NO. It has been shown by Fulton et al. (2002) that eNOS resides in two pools of active enzyme: in the perinuclear region and in the plasma membrane of endothelial cells (Fig. 5.3). It is now known that eNOS is in fact localised to components of the plasma membrane known as caveolae. Caveolae are cholesterol-rich membrane domains in which several proteins involved in signal transduction have been found (Gratton et al., 2004). The eNOS observed in the perinuclear region is in fact localised to the membranes of Golgi – the function of both Golgi and caveolae as sites for eNOS activity is supported by several studies (Shaul et al., 1996; Sessa et al., 1995; Garcia-Cardena et al., 1996). More recently Shaul (2002) suggests that trafficking of eNOS to both Golgi membranes and to plasma membrane caveolae facilitates dynamic protein interactions and calcium- and phosphorylation-dependent signal transduction events that modify NO activity. It is therefore possible that the localised pools of NO (as seen in osteoblasts in this thesis) are emerging from these regions of localised eNOS activity. Cationic amino acid transporter-1 (CAT-1) is a protein that transports L-arginine, and forms a caveolar complex with eNOS in endothelial cells (Su et al., 2003; McDonald et al., 1997). This location for CAT-1 is ideally suited to the provision of L-arginine for eNOS conversion to NO. An explanation for how mechanical forces may influence the activity of either eNOS or CAT-1 lies in the

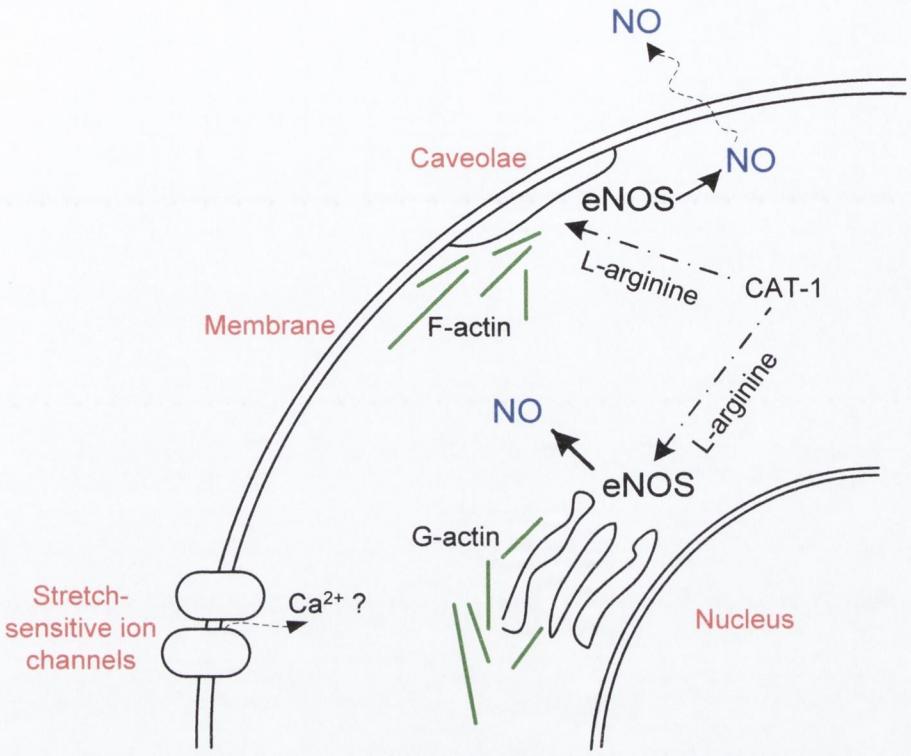

Fig. 5.4 *Schematic representation of cytoskeleton involvement in signal transduction of mechanical stimulation-induced nitric oxide release in osteoblasts or osteocytes, based on results in this thesis and on several results in the literature (see text). Abbreviations: CAT-1, cationic amino acid transporter-1; eNOS, endothelial nitric oxide synthase; NO, nitric oxide.*

documented interaction between both Golgi and caveolae with actin filaments (Conrad et al., 1995; Fujimoto et al., 1995, Lisanti et al., 1994). In fact it has been shown that eNOS in the membrane is colocalised with F-actin, and eNOS in the Golgi within the perinuclear region is colocalised with G-actin (Su et al., 2003). A mechanical stimulus resulting from fluid shear stress or AFM tip indentation may activate eNOS conversion of L-arginine to NO via F- and G-actin regulation of caveolar eNOS activity (see Fig. 5.4). The resultant diffusion of NO from the perinuclear region (the Golgi) and from the plasma membrane (caveolae) would lead to rapid and sustained increases in nitric oxide levels in these cell regions, as observed in this thesis. Hence the reason why actin is crucial for eNOS-mediated NO response in osteoblasts subjected to fluid flow (as discussed in Section 5.4.2) is disruption of actin filaments prevents

eNOS and CAT-1 activity in the caveolae and Golgi membranes. Microtubules do not have a direct role in this mechanism, which may explain why their disruption does not inhibit NO response in either osteoblasts or osteocytes. The fact that microtubule disruption does increase NO in osteocytes may be due to a secondary effect, such as increased movement of actin filaments to which they are networked.

It has been shown by Rawlinson et al. (1996) that osteoblast NO and PGE_2 response to mechanical loading involves an ingress of calcium via both voltage-activated and stretch sensitive ion channels, although the voltage-activated channels appear to dominate in osteoblasts. In endothelial cells, involvement of intracellular calcium in eNOS activation has been determined (Busse and Mulsch, 1990; Busse and Fleming, 1995) although other studies do not agree that high calcium levels are required for nitric oxide response (Ayajiki et al., 1996). In the experiments of Charras and Horton (2002b) application of a 30 nN indentation force to the a primary osteoblast membrane results in increased intracellular calcium intensity. In this thesis application of a similar range of forces and indentation depths increases intracellular nitric oxide (NO) response. That both these response occur over a similar time-scale suggests that calcium-mediated NO response is possible. While a role for calcium in PGE_2 response is highly likely (Fig. 5.2), the possibility that mechanotransduction of NO response is dependent on an influx of calcium via activation of stretch-sensitive ion channel activity may also influence the mechanism proposed in Fig. 5.4.

5.5.4 Membrane strains associated with osteoblast nitric oxide mechanotransduction

The magnitude of indenting forces and corresponding indentation depths used in this thesis to mechanically stimulate single osteoblast nitric oxide responses are in the same range as those reported for indentation-induced calcium response in primary osteoblasts (Charras and Horton, 2002b). Similar theoretical assumptions were adopted in applying contact theory to calculate radial strains in both studies, i.e. the contact assumes linear elastic material behaviour and no adhesion effects. As the theoretical expression used to calculate the membrane radial strains in this thesis is based on a theoretical cone that converges to a point at its apex (Johnson, 1985),

the radial strains for each response in Fig. 4.27 increase to infinity at the apex (or centre of indentation). This does not accurately reflect the geometry of the indenting AFM tip, which has an end-radius of ~14 nm, particularly at low depths of indentation. Hence, the strain values calculated for each osteoblast NO response to indentation are not valid near the centre of indentation. In the absence of a theoretical expression that accounts for actual AFM tip geometry (and large displacements), these radial strain values should be considered as an inconclusive estimates of the range of radial strains (from ~50 to 200 millistrains) associated with osteoblast NO mechanotransduction.

These membrane radial strains associated with NO mechanotransduction may be ~5-fold higher than those associated with indentation-induced calcium response (< 40,000 με). In their experiments, Charras and Horton (2002b) attached a 1 μm diameter glass bead to the cantilever end in order to apply the indentation force over a larger membrane area – the spherical geometry of the glass bead results in lower strain gradients, and the force is distributed over a larger contact area. The range of membrane radial strains estimated to correspond with indentation–induced NO response (Fig. 4.27) are also significantly larger than those determined to cause a nitric oxide or prostaglandin E_2 response in whole-cell stimulation of monolayers of adherent bone cells (as determined by application of the cell model to *in vitro* experiments in Section 5.3.2) – there it was reported that strains in the range of 3,800 με to ~8,000 με applied by either fluid shear stress or substrate strain result in a nitric oxide signalling response. This large difference in strain values associated with NO mechanotransduction may be explained by a fundamental difference between deformation caused by whole-cell stimuli and application of localised indentation forces – whole-cell stimulation results in a more effective straining cell-substrate attachments and transmission of mechanical forces to cytoskeleton-related mechanosensory function that leads to NO response.

There are several sources of inter-experimental variation in the physical consequences of, and the magnitude of strain induced in, the indented osteoblast membrane. The variation in force-indentation characteristics in these force curves is considerable, with elasticity values calculated from the various force curves (Figs. 4.15, 4.25 and 4.26) ranging from 7.4 to 315.1

kPa. Resistance to indentation also increase with distance into the osteoblast, as illustrated in Section 4.4.2). This suggests that osteoblast material rigidity increase with depth, perhaps due to the increasing presence of cytoskeletal structures. Although the possibility that the substrate contributes to resistance to tip indentation cannot be disregarded (Costa and Yin, 1999), it is not likely that the substrate contributes to the strain hardening that is evident on comparison of the indentation depths associated with 5 and 10 nN as these depths are within 10 to 15% of estimated osteoblast height (~4 to 5 μm). These sources of variation in the physical consequences of an indenting force may explain, in part, why the osteoblastic cells do not exhibit uniform mechanosensitivity in terms of mechanotransduction of NO response. It is also worth noting that the elasticity values computed for each NO mechanotransduction response in Fig. 4.27 are mostly at the higher end of elasticity values determined for these osteoblasts (the lowest elasticity is 45.4 kPa and the highest is 315.1 kPa). Although this data is not conclusive, it indicates that successful mechanotransduction of NO may be occurring when indentation forces are applied to more rigid parts of the osteoblast, perhaps in the proximity of cytoskeletal structures.

Chapter 6

Conclusions

6.1 Main results of this thesis

6.2 Future work

6.1 Main results of the thesis

In this thesis the hypothesis that osteoblast and osteocyte response to mechanical stimuli involves magnitude-dependent cytoskeleton-mediated release of nitric oxide and prostaglandin E_2 signalling molecules was investigated. This hypothesis was tested using both computational and experimental methods which yielded the following insights into bone cell mechanotransduction:

- It was concluded from the finite element model of an eukaryotic cell that the actin cytoskeleton and microtubules in particular are the most significant organelles in cell resistance to deformation due to mechanical stimuli. Also, actin-transmitted prestress gives rise to experimentally-observed non-linearity in cell response to applied forces. Such a structural role for the cytoskeleton supports its suitability for both detection and transmission of forces acting on the cell membrane to other organelles that transduce short-term responses such as NO or PGE_2 release.
- By modelling the physical effects of fluid flow and substrate strain on adherent bone cells *in vitro*, it was concluded that NO and PGE_2 signalling response in mechanically-stimulated bone cells is dependent not only on the magnitude of deformation but also the nature of cell deformation caused by the applied stimulus. Furthermore, such is the extent of the qualitative and quantitative differences in cell deformation caused by commonly applied magnitudes of fluid flow and strain stimuli *in vitro*, that inter-experimental comparisons of bone cell response are not justified. Although these conclusions demand further experimental substantiation, the integrated approach adopted does provide insight that would not have been otherwise possible, for example, how magnitude-dependence of bone cell signalling responses can explain bone cell capacity to distinguish between fluid flow or strain stimuli in several experimental studies.
- When this magnitude-dependent response of bone cells *in vitro* is extrapolated to *in vivo* mechanobiology, it appears that mechanical forces have direct control on

osteoblast or osteocyte function simply due to exposure to the mechanical environment characteristic of their anatomical location, i.e. strains of < 3,000με (on bone surface where osteoblasts adhere) cause osteoblastic matrix production, whereas fluid shear stress < 3Pa (estimated to occur in osteocyte lacunae) causes signalling responses associated with osteocyte signalling function, for example NO or PGE_2.

- From experimental results in this thesis it was concluded that dynamic changes in the cytoskeleton occur during mechanotransduction of NO and PGE_2 response. Actin and microtubule cytoskeletal components influence mechanotransduction pathways of both NO and PGE_2 response differently in osteoblasts and osteocytes. For example, fluid flow-induced NO response in osteoblasts involves an actin- (but not microtubule) mediated eNOS pathway, whereas osteocyte nitric oxide response is not dependent on actin but is further enhanced by disruption of microtubules. Both results, however, do agree with previous reports of actin cytoskeleton involvement in eNOS-mediated conversion of L-arginine to NO in endothelial cells, suggesting a similar mechanism occurs in bone cells. Increased osteoblast PGE_2 response may be related to stimulation by fluid flow of actin clustered at focal adhesions, whereas both an intact actin and microtubule cytoskeleton are required for fluid flow-induced PGE_2 response in osteocytes. Differences in osteoblast and osteocyte mechanotransduction of NO response may be related to differences in cytoskeleton composition between both cell types – osteocytes have a more actin-rich cytoskeleton. That cytoskeletal disruption abolishes PGE_2 response in osteocytes, but not in osteoblasts, is probably because of the greater dominance of stretch/shear-sensitive ion channels in osteocyte response to mechanical loading.
- From the single osteoblast indentation experiments it was concluded that osteoblasts respond to localised indenting forces ranging from 17 nN to 50 nN with a rapid synthesis and release of intracellular nitric oxide. Continuous indentation causes sustained diffusion of NO from the perinuclear region of the osteoblast or

from localized pools in the cytoplasm or membrane. It is also observed that diffusion of NO through the membrane into the extracellular medium is the mechanism by which fluid flow stimulation of osteoblasts leads to measurement of increased nitrate levels in the experimental medium. Interpreting the single cell results alongside what has been reported in literature suggests that actin filaments can regulate NO release, as both actin and eNOS are co-localised in Golgi membranes and caveolae, where the eNOS conversion of L-arginine to nitric oxide takes place.

- Membrane strains associated with indentation-induced mechanotransduction of NO significantly exceed those strains associated with NO response due to whole-cell stimulation under fluid flow or substrate strain (as computed in the cell model). That NO activation occurs at lower strain levels in whole-cell stimulation may be due to a more effective transmission of forces throughout the cell than would occur in localised indentation, which reiterates the importance of qualitative and quantitative differences in the physical effects of an applied force in mechanotransduction.

In summary, how macroscale mechanical forces control bone quality is very much based on the physical consequences of that mechanical stimulus on the bone cell level. Mechanotransduction of the received stimulus occurs via cytoskeleton-related subcellular mechansensory mechanisms that influence the signalling pathways that ultimately lead to NO and PGE_2 response, both of which are crucial for bone formation.

6.2 Future work

That cell response is magnitude-dependent suggests that, *if* the estimates of fluid shear stress and strain estimated to occur *in vivo* are correct, there must be independent roles for strain and fluid flow in bone mechanobiology in terms of the bone cell responses they elicit. Besides the fundamental value of this result for understanding bone physiology, it provides new information

that could be used to predicting expected cell behaviour when exposed to various magnitudes of biophysical stimuli and incorporated into improved mechanoregulation algorithms that predict the mechanisms and dynamics of tissue formation in osteochondral defects (Kelly and Prendergast, 2005) or in fracture repair (Lacroix and Prendergast, 2002).

The insights of this thesis are also applicable to tissue engineering – that osteoblasts appear to have the capacity to adapt their function according to the prevailing mechanical stimuli indicates that a focus on replicating the *in vivo* mechanical environment of bone cells may yield most promise in engineering of tissues *in vitro*. The question remains, however, whether responses exhibited by bone cells adherent on 2-dimensional surfaces are representative of those occurring in the more complex 3-dimensional environment of *in vivo* bone architecture or within the pores of a tissue engineering scaffold (McMahon et al., 2005). The influence of qualitative differences in cell deformation on mechanotransduction would suggest that the degree of cell attachment in 3-dimensions, such as for osteocytes embedded in lacunae, must greatly influence mechanotransduction of a cell response. Future work could therefore include: (i) a fundamental comparision of bone cell behaviour in both 2- and 3-dimensional environments, and (ii) attempts to devise methods of mechanical stimulation that better replicate the *in vivo* mechanical environment, for example, the micro-fabrication chamber developed by Jacobs and co-workers (You et al., 2005).

Both computational predictions and experimental results in this thesis point to cytoskeletal involvement in this mechanotransduction mechanism. If this involvement is not direct, perhaps it occurs via cytoskeleton-attached focal adhesions, integrin-cytoskeleton couplings, cytoskeletal modulation of ion channels, gap junctions, cytoskeletal force transmission and cytoskeleton-bound mechanotransducing molecules. The involvement of each of these possible mechanosensory candidates in mechanotransduction of NO or PGE_2 should be explored in future experiments. The possibility that calcium, as a second messenger, mediates transduction of NO or PGE_2 must also be the subject of future work, particularly since mechanical stimulation of calcium in single bone cells occurs over a time-scale similar to that reported for NO in this thesis (Charras and Horton, 2002a). The experimental results obtained,

by indentation of single osteoblasts and fluid flow-stimulated monolayers of bone cells, indicate that the actin cytoskeleton is involved in eNOS-mediated synthesis and diffusion of NO, perhaps from localised sites in the Golgi region and in caveolae in the plasma membrane. Further experimental investigation using immunofluorescent staining of eNOS in mechanosensitive bone cells would yield further insight into this potential site for mechanical and biochemical coupling, that leads to NO response.

REFERENCES

Afzal, F., Polak, J., Buttery, L. (2004) Endothelial nitric oxide synthase in the control of osteoblastic mineralising activity and bone integrity. *J. Pathol.* 202: 503-510.

Aguirre, J., Buttery, L., O'Shaughnessy, M. (2001) Endothelial nitric oxide synthase-deficient mice demonstrate marked retardation in post-natal bone formation, reduced bone volume and defects in osteoblast maturation and activity. *Am. J. Pathol* 158: 247-257.

A-Hassan, E., Heinz, W.F., Antonik, M.D., Costa, D., Nageswaran, S. (1998) Relative microelastic mapping by AFM. *Biophys. J.* 74: 1564-1578.

Ajubi, N.E., Klein-Nulend, J., Alblas, M.J., Burger, E.H., Nijweide, P.J. (1999) Signal transduction pathways involved in fluid flow-induced PGE_2 production by cultured osteocytes, *Am. J. Physiol.* 276: E171-178.

Ajubi, N.E., Klein-Nulend, J., Nijweide, P.J., Vrijheid-Lammers, T., Alblas, M.J., Burger, E.H. (1996) Pulsating fluid flow increases prostaglandin by cultured chicken osteocytes: a cytoskeleton dependent process. *Biochem. Biophys. Res. Commun.* 225: 62-68.

Akamine, T., Jee, W.S.S., Ke, H.Z., Li, J., Lin, B.Y. (1992) Prostaglandin E_2 prevents bone loss and adds extra bone to immobilized distal femoral metaphysic in female rats. *Bone* 13: 11-22.

Alberts, B., Bray, D., Lewis, J., Raff, M., Roberts, K., Watson, J.D. (1989) Molecular Biology of the Cell. *Garland Publishing Inc.* NY & London, 2nd Edition.

Albrecht-Buehler, G. (1987) Role of cortical tension in fibroblast shape and movement. *Cell Motility and the Cytoskeleton* 7: 1, 54-67.

Andreu, J.M., Gorbunoff, M.J., Medrano, F.J., Rossi, M., Timasheff, S.N. (1991) Mechanism of colchicine binding to tubulin. Tolerance of substituents in ring C' of biphenyl analogues. *Biochemistry* 16: 30, 3777-86.

Armour, K.E., Ralston, S.H. (1998) Estrogen upregulates endothelial constitutive nitric oxide synthase expression in human osteoblast-like cells. *Endocrinology* 139: 799-802.

Armour, K.J., Armour, K.E., Gallagher, M.E. (2001) Defective bone formation and anabolic response to exogenous nitric oxide in mice with targeted disruption of endothelial nitric oxide synthase. *Endocrinology* 142: 760-766.

Ayajiki, K., Kindermann, M., Hecker, M., Fleming, I., Busse, R. (1996) Intracellular pH and tyrosine phosphorylation but not calcium determine shear stress-induced nitric oxide production in native endothelial cells. *Circ. Res.* 78:750-8.

Bacabac, R.G., Smit, T.H., Mullender, M.G., Dijcks, S.J., Van Loon, J.J.W.A., Klein-Nulend, J. (2004) Nitric oxide production by bone cells is fluid shear stress rate dependent. *Biochem. Biophys. Res. Commun.* 315: 823-829.

Bakker, A.D., Klein-Nulend, J., Burger, E.H. (2003) Mechanotransduction in bone cells proceeds via activation of COX-2, but not COX-1. *Biochem. Biophys. Res. Commun.* 305 (2003) 677-83.

Bakker, A.D., Soejima, K., Klein-Nulend, J., Burger, E.H. (2001) The production of nitric oxide and Prostaglandin E_2 by primary bone cells is shear stress dependent. *J. Biomech.* 34: 671-677.

Bao, G., Suresh, S. (2003) Cell and molecular mechanics of biological materials. *Nature Materials* 2: 715-726.

Ben-Avraham, D., Tirion, M.M. (1995) Dynamic and elastic properties of F-actin: a normal modes analysis. *Biophys. J.* 68: 1231-1245.

Binnig, G., Quate, C.F., Gerber, C. (1986) Atomic force microscope. *Physical Review Letters* 56: 9, 930-933.

Boussinesq, J. (1885) Applications des potentiels a l'etude de l'equilibre et du mouvement des solides elastiques. *Gauther-Villars*, Paris.

Brown, T.D. (2000) Techniques for Mechanical Stimulation of Cells in vitro: a review. *J. Biomech.* 33: 3-14.

Burger, E. H., Klein-Nulend, J. (1999) Mechanotransduction in bone – role of the lacuno-canalicular network. *FASEB J.* 13: S101-S112.

Burr, D.B., Milgrom, C., Fyhrie, D., Forwood, M., Nyska, M., Finestone, A., Hoshaw, S., Saiag, E., Simkin, A. (1996) In vivo measurement of human tibial strains during vigorous activity. *Bone* 18: 405-410.

Busse, R., Fleming, I. (1995) Regulation and functional consequences of endothelial nitric oxide formation, *Ann. Med.* 27: 331-340.

Busse, R., Mulsch, A. (1990) Calcium-dependent nitric oxide synthesis in endothelial cytosol is mediated by calmodulin. *FEBS Lett.* 4: 265, 133-6.

Caille, N., Thoumine, O., Tardy, Y., Meister, J. J. (2002) Contribution of the nucleus to the mechanical properties of endothelial cells. *J. Biomech.* 35: 177-187.

Carter, D.R., Beaupré, G.S. (2003) Skeletal function and form. *Cambridge University Press*, 1st edition.

Carter, S.B. (1967) Effects of cytochalasin B on mammalian cells. *Nature (Lond.)* 213: 261.

Charras, G.T., Horton, M.A. (2002a) Single cell mechanotransduction and its modulation analyzed by atomic force microscopy indentation. *Biophys. J.* 82: 2970-2981.

Charras, G.T., Horton, M.A. (2002b) Determination of cellular strains by combined atomic force microscopy and finite element modelling. *Biophys. J.* 83: 858-879.

Chen, C.S., Ingber, D.E. (1999) Tensegrity and mechanoregulation: from skeleton to cytoskeleton. *Osteoarthritis and Cartilage* 7: 81-94.

Chen, C.S., Mrksich, M., Huang, S., Whitesides, G.M., Ingber, D.E. (1997) Geometric control of cell life and death. *Science* 276: 1425-1428.

Cherian, P.P., Siller-Jackson, A.J., Gu, S., Wang, X., Bonewald, L.F., Sprague, E., Jiang, J.X. (2005) Mechanical strain opens connexion-43 hemichannels in osteocytes: a novel mechanism for the release of prostaglandin. Mol. Biol. Cell 16: 3100-6.

Chicurel, M.E., Chen, C.S., Ingber, D.E. (1998) Cellular control lies in the balance of forces. *Curr. Opin. Cell Biol.* 10: 232-239.

Chon, J.W.M., Mulvaney, P., Sader J.E. (2000) Experimental validation of theoretical models for the frequency response of atomic force microscope cantilever beams immersed in fluids. *J. Appl. Phys.* 87: 3978-88.

Choudhary, S., Wadhwa, S., Raisz, L.G., Alander, C., Pilbeam, C.C. (2003) Extracellular calcium is a potent inducer of cyclooxygenase-2 in murine osteoblasts through an ERK signalling pathway. *J. Bone Miner. Res.* 18: 1813-24.

Collin-Osdoby, P., Nickols, A., Osdoby, P. (1995) Bone cell function, regulation and communication: a role for nitric oxide. *J. Cell. Biochem.* 57: 399-408.

Conrad, P.A., Smart, E.J., Ying, Y.S., Anderson, R.G., Bloom, G.S. (1995) Caveolin cycles between plasma membrane caveolae and the Golgi complex by microtubule-dependent and microtubule-independent steps. *J. Cell Biol.* 131: 1421-33.

Costa, K.D., Yin, F.C. (1999) Analysis of indentation: implications for measuring mechanical properties with the atomic force microscope. *J. Biomech. Eng.* 121: 462-471.

Coughlin, M.F., Stamenovic, D. (1998) A tensegrity model of the cytoskeleton in spread and round cells. *J. Biomech. Eng.* 120: 770-777.

Cowin, S.C. (editor) (2001) Bone mechanics handbook. *CRC Press*, Boca Raton, FL.

Danowski, B.A. (1989) Fibroblast contractility and actin organisation are stimulated by microtubule inhibitors. *J. Cell Sci.* 93: 2, 255-266.

Davies, P.F., Tripathi, S.C. (1993) Mechanical stress mechanisms and the cell. An endothelial paradigm. *Circ. Res.* 72: 239-45.

Dembo, M., Torney, D., Saxman, K., Hammer, D. (1988) The reaction limited kinetics of membrane-to-surface adhesion and detachment. *Proceedings of the Royal Society London B, Biological Sciences* 234: 55-83.

Diwan, A.D., Wang, M.X., Jand, D., Zhu, W., Murrell, G.A. (2000) Nitric oxide modulates fracture healing. *J. Bone Miner. Res.* 15: 342-351.

Domke, J., Dannohl, S., Parak, W.J., Müller, O., Aicher, W.K., Radmacher, M. (2000) Substrate dependent differences in morphology and elasticity of living osteoblasts investigated by atomic force microscopy. *Colloids Surf. B Biointerfaces* 19: 367-379.

Dong, C., Lei X.X. (2000) Biomechanics of cell rolling: shear flow, cell-surface adhesion, and cell deformability. *J. Biomech.* 33: 1, 35-43.

Duncan, R., Turner, C.H. (1995) Mechanotransduction and the functional response of bone to mechanical strain. *Calcified Tissue International* 57: 344-358.

Duncan, R.L., Hruska, K.A. (1994) Chronic, intermittent loading alters mechanosensitive channel characteristics in osteoblast-like cells. *Am. J. Physiol.* 267: F909-916.

El Haj, A.J., Minter, S.L., Rawlinson, S.C., Suswillo, R., Lanyon, L.E. (1990) Cellular responses to mechanical loading in vitro. *J. Bone Miner. Res.* 5: 923-32.

Evans, D.M., Ralston, S.H. (1996) Nitric oxide and bone. *J. Bone. Miner. Res.* 11: 300-305.

Evans, E., Yeung, A. (1989) Apparent viscosity and cortical tension of blood granulocytes determined by micropipette aspiration. *Biophys. J.* 56: 151-160.

Farrell, K.W., Wilson, L. (1980) Proposed mechanism for colchicine poisoning of microtubules reassembled in vitro from strongylocentrotus purpuratus sperm tail outer doublet tubulin. *Biochemistry* 24: 19, 3048-54.

Fermor, B., Gundle, R., Evans, M., Emerton, M., Pocock, A., Murray, D. (1998) Primary human osteoblast proliferation and prostaglandin release in response to mechanical strain in vitro. *Bone* 22: 637-643.

Fox, S.W., Chambers, T.J., and Chow, J.W. (1996) Nitric oxide is an early mediator of the increase in bone formation by mechanical stimulation. *Am. J. Physiol.* 270: E955-960.

Frangos, J.A., Eskin, S.G., McIntire, L.V., Ives, C.L. (1985) Flow effects on prostacyclin production by cultured human endothelial cells. Science 22: 227, 1477-1479.

Freeman, P.N., Natarhan, R.N., Kimura, J.H., Andriacchi, T.P. (1994) Chondrocyte cells respond mechanically to compressive loads. *J. Orthop. Res.* 12: 311-320.

Frisch, T., Thoumine, O. (2002) Predicting the kinetics of cell spreading. *J. Biomech.* 35: 1137-1141.

Fujimoto, T., Miyawaki, A., Mikoshiba, K. (1995) Inositol 1,4,5-trisphosphate receptor-like protein in plasmalemmal caveolae is linked to actin filaments. *J. Cell Sci.* 108: 7-15.

Fulton, D., Fontana, J., Sowa, G., Gratton, J-P, Lin, M., Li, K-X, Michell, B., Kemp, B.E., Rodman, D., Sessa, W.C. (2002) Localisation of endothelial nitric oxide synthase phosphorylated on serine 1179 and nitric oxide in golgi and plasma membrane defines the existence of two pools of active enzyme. *J. Biol. Chem.* 277: 6, 4277-4284.

Galbraith, C. G., Sheetz, M. P. (1998) Forces on adhesive contacts affect cell function. *Current Opinion in Cell Biology* 10: 566-571.

Garcia-Cardena, G., Oh, P., Liu, J., Schnitzer, J.E., Sessa, W.C. (1996) Targeting of nitric oxide synthase to endothelial cell caveolae via palmitoylation: implications for nitric oxide signaling. *Proc. Natl. Acad. Sci. USA* 25: 6448-53.

Gittes, F., Mickey, B. (1993) Flexural Rigidity of Microtubules and Actin Filaments Measured from Thermal Fluctuations in Shape. *J. Cell Biol.* 120: 4, 923-34.

Gratton, J.P., Bernatchez, P., Sessa, W.C. (2004) Caveolae and caveolins in the cardiovascular system. *Circ. Res.* 11: 94, 1408-1417.

Gray, M.L., Pizzanelli, A.M., Grodzinsky, A.J., Lee, R.C. (1988) Mechanical and physiochemical determinants of the chondrocyte biosynthetic response. *J. Orthop. Res.* 6: 777-792.

Green, C.P., Sader, J.E. (2002) Torsional frequency response of cantilever beams immersed in viscous fluids with applications to the atomic force microscope. *J. Appl. Phys.* 92: 6262-6274.

Gudi, S., Nolan, J.P., Frangos, J.A. (1998) Modulation of GTPase activity of G proteins by fluid shear stress and phospholipid composition. *Proc. Natl. Acad. Sci. USA* 3: 95, 2515-9.

Guilak, F., Jones, W. R., Ting-Beall, H. P., Lee, G. M. (1999) The deformation behaviour and mechanical properties of chondrocytes in articular cartilage. *Osteoarthritis Cartilage* 7: 1, 59-70.

Guilak, F., Mow, C. (2000) The mechanical environment of the chondrocyte: a biphasic finite element model of cell-matrix interactions in articular cartilage. *J. Biomech.* 33: 1663-1673.

Guilak, F., Ratcliffe, A., Mow, V.C. (1995) Chondrocyte deformation and local tissue strain in articular cartilage: a confocal microscopy study. *J. Orthop. Res.* 13: 410-21.

Guilak, F., Tedrow, J.R., Burgkart, R. (2000) Viscoelastic properties of the cell nucleus. *Biochem. Biophys. Res. Commun.* 269: 781-786.

Head, D.A., Levine, A.J., MacKintosh, F.C. (2003) Deformation of cross-linked semi-flexible polymer networks. *Phys. Rev. Lett.* 91: 10, 108102.

Heidemann, S.R., Kaech, S., Buxbaum, R.E., Matus, A. (1999) Direct observations of the Mechanical Behaviors of the Cytoskeleton in Living Fibroblasts. *J. Cell Biol.* 145: 109-122.

Heijnen, H.F.G., Waaijenborg, S., Crapo, J.D., Bowler, R.P., Akkerman, J-W.N., Slot, J.W. (2004) Co-localization of eNOS and the catalytic subunit of PKA in endothelial cell junctions: a clue for regulated NO production. *J. Histochem. Cytochem.* (2004) 52: 1277-1285.

Helfrich, M.H., Evans, D.E., Grabowski, P.S., Pollock, J.S., Ohshima, H., Ralston, M.H. (1997) Expression of nitric oxide synthase isoforms in bone and bone cell cultures. *J. Bone Miner. Res.* 12: 1108-1115.

Henderson, E., Haydon, P.G., Sakaguchi, D.S. (1992) Actin filament dynamics in living glial cells imaged by atomic force microscopy. *Science* 257: 1944-1946.

Hertz, H. (1881) Uber den Kontakt elasticher korper. *Journal für die reine und angewandte Mathematik* 92: 156.

Hillsley, M.V., Frangos, J.A. (1994) Review: Bone tissue engineering: the role of interstitial fluid flow. *Biotech. Bioeng.* 43: 573-581.

Hochmuth, R.M. (2000) Micropipette aspiration of living cells. *J. Biomech.* 33: 15-22.

Hubmayr, R.D., Shore, S.A., Fredberg, J.J. (1996) Pharmacological activation changes stiffness of cultured human airway smooth muscle cells. *Am. J. Physiol.* 271: 5, 1660-1668.

Huiskes, R., Ruimerman, R., van Lenthe, G.H., Janssen, J.D. (2000) Effects of mechanical forces on maintenance and adaptation of form in trabecular bone. *Nature* 405: 704-706.

Hung, C.T., Allen, F.D., Pollack, S.R., Brighton, C.T. (1996) What is the role of the convective current density in the real-time calcium response of cultured bone cells to fluid flow? *J. Biomech.* 29: 1403-1409.

Ingber, D.E. (1993) Cellular Tensegrity: defining new rules of biological design that govern the cytoskeleton. *J. Cell Sci.* 104: 613-627.

Ingber, D.E. (1997) Tensegrity: the architectural basis of cellular mechanotransduction. *Annu. Rev. Physiol.* 59: 575-599.

Ingber, D.E., Heidemann, S.R., Lamoroux, P., Buxbaum, R.E. (2000) Opposing views on tensegrity as a framework for understanding cell mechanics. *J. Appl. Physiol.* 89: 1663-1670.

Jacobs, C.R., Yellowley, C.E., Dvais, B.R., Zhou, Z., Donahue, H.J. (1998) Differential effect of steady versus oscillating flow on bone cells. *J. Biomech.* 31: 969-976.

Janmey, P.A. (1998) The cytoskeleton and cell signaling: component localisation and mechanical coupling. *Physiol. Rev.* 78: 763-781.

Janmey, P.A., Eutenauer, U., Traub, P., Schliwa, M. (1991) Viscoelastic properties of vimentin compared with other filamentous biopolymer networks. *J. Cell Biol.* 113: 155-160.

Janmey, P.A., Weitz, D.A. (2004) Dealing with mechanics: mechanisms of force transduction in cells. *Trends Biochem. Sci.* 29: 364-70.

Johnson, D.L., McAllister, T.N., Frangos, J.A. (1996) Fluid flow stimulates rapid and continuous release of nitric oxide in osteoblasts. *Am. J. Physiol.* 271: E205-208.

Johnson, K.L. (1985) Contact mechanics. *Cambridge University Press*. Cambridge, New York, Melbourne.

Jones W.R., Ting-Beall H.P., Lee G.M., Kelley S.S., Hochmuth R.M., Guilak F. (1997) Mechanical properties of human chondrocytes and chondrons from normal and osteoarthritic cartilage. *Transactions of the Orthopaedic Research Society* 22: 199.

Jones, D.B., Nolte, H., Scholubbers, J.G., Turner, E., Veltel, D. (1991) Biochemical signal transduction of mechanical strain in osteoblast-like cells. *Biomaterials* 12: 101-110.

Jones, W.R., Ting-Beall, H.P., Lee, G.M., Kelley, S.S., Hochmuth, R.M., Guilak, F. (1999) Alterations in the Young's modulus and volumetric properties of chondrocytes isolated from normal and osteoarthritic human cartilage. *J. Biomech.* 32: 119-27.

Juliano, R.L., Haskill, S. (1993) Signal transduction from the extracellular matrix. *J. Cell Biol.* 120: 577-85.

Kamm, R.D., McVittie, A.K., Bathe, M. (2000) On the role of continuum models in mechanobiology. *American Society of Mechanical Engineers (ASME) International Congress - Mechanics in Biology* 242: 1-9.

Karcher, H., Lammerding, J., Huang, H., Lee, R.T., Kamm, R.D., Kaazempur, M.R. (2003) A three-dimensional viscoelastic model for cell deformation with experimental verification. *Biophys. J.* 85: 3336-3349.

Kaspar, D., Seidl, W., Neidlinger-Wilke, C., Ignatius, A., Claes, L. (2000) Dynamic cell stretching increases human osteoblast proliferation but decreases osteocalcin synthesis and alkaline phosphotase activity. *J. Biomech.* 33: 45-51.

Kasten, T., Collin-Osdoby, P., Patel, N., Osdoby, P., Krukowski, M., Misko, T., Settle, S. Currie, M., Nickols, A. 1994) Potentiation of osteoclast resorption activity by inhibition of nitric oxide synthase activity. *Proc. Natl. Acad. Sci. USA 91: 3569-3573.*

Kato, Y., Windle, J.J., Koop, B.A., Mundy, G.R., Bonewald, L.F. (1997) Establishment of an Osteocyte-like Cell Line, MLO-Y4. *J. Bone Miner. Res.* 12: 12, 2014.

Kawata, A., Mikuni-Takagaki, Y. (1998) Mechanotransduction in stretched osteocytes--temporal expression of immediate early and other genes. *Biochem. Biophys. Res. Commun.* 19: 404-8.

Kelly, D.J., Prendergast, P.J. (2005) Mechano-regulation of stem cell differentiation and tissue regeneration in osteochondral defects. *J. Biomech.* 38: 1413-22.

Klein, D., Raisz, L. (1970) Prostaglandins: stimulation of bone resorption in tissue culture. *Endocrinology* 86: 1436-1440.

Kleinhenz, D.J., Fan, X., Rubin, J., Hart, C.M. (2003) Detection of endothelial nitric oxide release with the 2,3-diaminonapthalene assay. *Free Radic. Biol. Med.* 34: 856-61.

Klein-Nulend, J, van der Plas, A., Semiens, C.M., Ajubi, N.E., Frangos, J.A., Nijweide, P.J., Burger, E.H. (1995) Sensitivity of osteocytes to biomechanical stress in vitro. *FASEB J.* 9: 441-445.

Klein-Nulend, J., Helfrich, M.H., Sterck, J.G., MacPherson, H., Joldersma, M., Ralston, M.H., Semiens, C.M., Burger, E.H. (1998) Nitric oxide in response to shear stress by human bone cell cultures is endothelial nitric oxide synthase dependent. *Biochem. Biophys. Res. Comm.* 250: 108-114.

Knothe-Tate, M.L., Steck, R., Forwood, M.R., Niederer, P. (2000) In vivo demonstration of load-induced fluid flow in the rat tibia and its potential implications for processes associated with functional adaptation. *J. Exp. Biol.* 203: 2737-2745.

Knudsen, H.L, J.A. Frangos (1997) Role of cytoskeleton in shear stress-induced endothelial nitric oxide production. *Am. J. Physiol.* 273: H347-55.

Kojima, H., Urano, Y., Kikuchi, K., Higuchi, T., Hirata, Y., Nagano, T. (1999) Fluorescent indicators for imaging nitric oxide production. *Angewandte Chemie International Edition* 2: 38, 3209-3212.

Krishan A. (1972) Cytochalasin-B: time-lapse cinematographic studies on its effects on cytokinesis. *J. Cell Biol.* 54: 657-664.

Lacroix, D., Prendergast, P.J. (2002) A mechano-regulation model for tissue differentiation during fracture healing: analysis of gap size and loading. *J. Biomech.* 35: 1163-71.

Lai, W.M., Hou, J.S., Mow, V.C. (1991) A triphasic theory for the swelling and deformation behaviors of articular cartilage. *J. Biomech. Eng.* 113: 245-258.

Lantz, M.A., Jarvis, S.P., Tokumoto, H., Martynski, T., Kusumi, T., Nakamura, C., Miyake, J. (1999) Stretching the a-helix – a direct measure of the hydrogen bond energy of a single peptide molecule. *Chem. Phys. Lett.* 315: 61.

Lisanti, M.P., Scherer, P.E., Tang, Z., Sargiacomo, M. (1994) Caveolae, caveolin and caveolin-rich membrane domains: a signalling hypothesis. *Trends Cell Biol.* 4: 231-5.

Lo C.M., Ferrier J. (1999) Electrically measuring viscoelastic parameters of adherent cell layers under controlled magnetic forces. *European Biophysics Journal* 28: 2, 112-8.

Luduena, R.F., Banerjee, A., Khan, I.A. (1992) Tubulin structure and biochemistry. *Curr. Opin. Cell Biol.* 4: 53-57.

Maguire, P., Mothersill, C., Seymour, C., Lyng, F.M. (2005) Medium from irradiated cells induced dose-dependent mitochondrial Chnanges and BCL2 responses in unirradiated human keratinocytes. *Radiation Research* 163: 4, 384-390.

Maksym, G.N., Fabry, B., Butler, J.P., Navajas, D., Tschumperlin, D.J., Laporte, J.D., Fredberg, J.J. (2000) Mechanical properties of activated human airway smooth muscle cells from 0.05 to 0.4 Hz. *J. Appl. Physiol.* 89: 4, 1619-1632.

Mancini, L., Moradi-Bidhendi, N., Becherini, L., Martineti, V., MacIntyre, I. (2000) The biphasic effects of nitric oxide in primary rat osteoblasts are cGMP dependent. *Biochem. Biophys. Res. Commun.* 274: 477-481.

Maniotis, A.J., C.S. Chen, Ingber, D.E. (1997) Demonstration of mechanical connections between integrins, cytoskeletal filaments, and nucleoplasm that stabilize nuclear structure, *Proc. Natl. Acad. Sci. USA* 4: 94, 849-54.

Martini, F.H. (2004) Fundamentals of Anatomy and Physiology. *Pearson Education Inc.* San Francisco, 6th Edition..

Mathur, A.B., Collinsworth, A.M., Reichert, W.M., Kraus, W.E., Truskey, G.A. (2001) Endothelial, cardiac muscle and skeletal muscle exhibit different viscous and elastic properties as determined by atomic force microscopy. *J. Biomech.* 34: 1545-1553.

McAllister, T.N., Frangos, J.A. (1999) Steady and transient fluid shear stress stimulate NO release in osteoblasts through distinct biochemical pathways. *J. Bone Miner. Res.* 14: 930.

McCreadie, B.R., Hollister, S.J. (1997) Strain concentrations surrounding an ellipsoid model of lacunae and osteocytes. *Computer Methods in Biomechanics and Biomedical Engineering* 1: 61-68.

McDonald, K.K., Zharikov, S., Block, E.R., Kilberg, M.S. (1997) A caveolar complex between the cationic amino acid transporter 1 and endothelial nitric-oxide synthase may explain the "arginine paradox". *J. Biol. Chem.* 12: 31213-6.

McMahon, L., Farrell, E., O'Brien, F.J., O'Connell, B.C., Campbell, V.A., Prendergast, P.J. (2005) Chondrogenesis of Mesenchymal Stem Cells in Static and Dynamic Cultures. *4th annual meeting of the European Tissue Engineering Society*, Munich, Germany.

Meyer, U., Terodde, M. (2001) Mechanical Stimulation of Osteoblasts in Cell Culture. *Mund-, Kiefer-Und Gesichtschirurgie* 5: 3, 166-172.

Mochizuki, S., Vink, H., Hiramatsu, O., Kajita, T., Shigeto, F., Spaan, J.A., Kajiya, F. (2003) Role of hyaluronic acid glycosaminoglycans in shear-induced endothelium-derived nitric oxide release. *Am. J. Physiol.* 285: H722-6.

Morretti, M. (2001) Endothelial cell alignment on deforming silicone surfaces. *M.Sc. Thesis, University of Dublin, Trinity College.*

Mosley, J.R., Lanyon, L.E. (1998) Strain rate as a controlling influence on adaptive modeling in response to dynamic loading of the ulna in growing male rat. *Bone* 23: 313-318.

Mullender, M.G., El Haj, A.J., Yang, Y., van Duin, M.A., Burger, E.H., Klein-Nulend, J. (2004) Mechanotransduction of bone cells in vitro: mechanobiology of bone tissue. *Med. Biol. Eng. Comput.* 42: 14-21.

Nishizuka, Y. (1992) Intracellular signaling by hydrolysis of phospholipids and activation of protein kinase C. *Science* 23: 258, 607-14.

Norvell, S.M., Ponik, S.M., Bowen, D.K., Gerard, R., Pavalko, F.M. (2004) Fluid shear stress induction of COX-2 protein and prostaglandin release in cultured MC3T3-E1 osteoblasts does not require intact microfilaments or microtubules. *J. Appl. Physiol.* 96: 957-66.

Owan, I., Burr, D.B., Turner, C.H., Qui, J., Tu, Y., Onyia, J.E., Duncan, R. L. (1997) Mechanotransduction in bone: osteoblasts are more responsive to fluid forces than mechanical strain. *Am. J. Physiol.* 273: C810-815.

Pavalko, F.M., Chen, N.X., Turner, C.H., Burr, D.B., Atkinson, S., Hsieh, Y-F., Qui, J., Duncan, R.L. (1998) Fluid shear-induced mechanical signaling in MC3T3-E1 osteoblasts requires cytoskeleton-integrin interactions. *Am. J. Physiol.* 275: C1591-1601.

Pead, M.J., Lanyon, L.E. (1989) Indomethacin modulation of load-related stimulation of new bone formation in vivo. *Calcified Tissue International* 45: 34-40.

Peake, M.A., Cooling, L.M., Magnay, J.L., Thomas, P.B.M., El Haj, A.J. (2000) Cellular responses to mechanical stress. Selected contribution: regulatory pathways involved in mechanical induction of c-fos gene expression in bone cells. *J. Appl. Physiol.* 89: 2498-2507.

Peterson, N.O., McConnaughey, W.B. (1982) Dependence of locally measured cell deformability on position on the cell. *Proc. Natl. Acad. Sci. USA* 79: 5327-5331.

Pitsillides, A.A., Rawlinson, S.C., Suswillo, R.F., Bourrin, S., Zaman, G., Lanyon, L.E. (1995) Mechanical strain-induced NO production by bone cells: a possible role in adaptive bone (re)modeling? *FASEB J.* 9: 1614-1622.

Ponik, S.M., Pavalko, F.M. (2004) Formation of focal adhesions on fibronectin promotes fluid shear stress induction of COX-2 and PGE_2 release in MC3T3-E1 osteoblasts. *J. Appl. Physiol.* 97: 135-42.

Pourati, J., Maniotis, A., Spiegel, D., Schaffer, J.L., Butler, J.P., Fredberg, J.J., Ingber, D.E., Stamenovice, D., Wang, N. (1998) Is cytoskeletal tension a major determinant of cell deformability in adherent endothelial cells? *Am. J. Physiol.* 274: C1283-1289.

Prendergast, P.J. (1997) Finite element analysis in tissue mechanics and orthopaedic implant design. *Clinical Biomechanics* 12: 343-368.

Radmacher, M. (2002) Measuring the elastic properties of living cells by the atomic force microscope. *Methods Cell Biol.* 68: 67-90.

Radmacher, M., Fritz, M., Kacher, C.M., Cleveland, J.P., Hansma, P.K. (1996) Measuring the viscoelastic properties of human platelets with the atomic force microscope. *Biophys. J.* 70: 556-567.

Ralston, S.H., Grabowski, P.S. (1996) Mechanisms of cytokine induced bone resorption: role of nitric oxide, cyclic guanosine monophosphate, and prostaglandins. *Bone* 19: 29-33.

Raucher, D., Sheetz, M.P. (1999) Characteristics of a membrane reservoir buffering membrane tension. *Biophys. J.* 77: 4, 1992-2002.

Rawlinson, S.C., El Haj, A.J., Minter, S.L., Tavares, I.A., Bennett, A., Lanyon, L.E. (1991) Loading related increases in prostaglandin production in cores of adult canine cancellous bone in vitro: a role for prostacyclin in adaptive bone remodeling? *J. Bone Miner. Res.* 6: 1345-1351.

Rawlinson, S.C., Pitsillides, A.A., Lanyon, L.E. (1996) Involvement of different ion channels in osteoblasts' and osteocytes' early responses to mechanical strain. *Bone* 19: 609-614.

Reilly, G.C., Haut, T.R., Yellowley, C.E., Donahue, H.J., Jacobs, C.R. (2003) Fluid flow induced PGE_2 release by bone cells is reduced by glycocalyx degradation whereas calcium signals are not. *Biorheology* 40: 591-603.

Rief, M., Clausen-Schaumann, H., Gaub, H.E. (1999) Sequence-dependent mechanics of single DNA molecules. *Nature Structural Biology* 6: 346-349.

Roux, W. (1881) Der Kampf der Teile im Organismus. *Engelmann* Leipzig.

Sader, J.E. (1998) Frequency response of cantilever beams immersed in viscous fluids with applications to the atomic force microscope. *J. Appl. Phys.* 84: 64.

Satcher, R.L. Jr., Dewey, C.F. Jr. (1996) Theoretical estimates of mechanical properties of the endothelial cell cytoskeleton. *Biophys. J.* 71: 1, 109-118.

Satcher, R.L., Dewey, C. F. Jr., Hartwig, J.H. (1997) Mechanical remodelling of endothelial surface and actin cytoskeleton induced by fluid flow. *Microcirculation* 4: 439-453.

Sato, M., Theret, D.P., Wheelerm, L.T., Ohshima, N., Nerem, R.M. (1990) Application of the micropipette technique to the measurement of cultured porcine aortic endothelial cell viscoelastic properties. *J. Biomech. Eng.* 112: 3, 263-268.

Saunders, M.M., You, J., Zhou, Z., Li, Z., Yellowley, C.E., Kunze, E.L., Jacobs, C.R., Donahue, H.J. (2003) Fluid flow-induced prostaglandin E_2 response of osteoblastic ROS 17/2.8 cells is gap junction-mediated and independent of cytosolic calcium. *Bone* 32: 350-356.

Sessa, W.C., Garcia-Cardena, G., Liu, J., Keh, A., Pollock, J.S., Bradley, J., Thiru, S., Braverman, I.M., Desai, K.M. (1995) The Golgi association of endothelial nitric oxide synthase is necessary for the efficient synthesis of nitric oxide. *J. Biol. Chem.* 28: 17641-4.

Shafrir, Y.G., Forgacs, G. (2002) Mechanotransduction through the cytoskeleton. *Am. J. Physiol.* 282: C479-486.

Shaul, P.W. (2002) Regulation of endothelial nitric oxide synthase: location, location, location. *Annu. Rev. Physiol.* 64: 749-774.

Shaul, P.W., Smart, E.J., Robinson, L.J., German, Z., Yuhanna, I.S., Ying, Y., Anderson, R.G., Michel, T. (1996) 'Acylation targets eNOS to plasmalemmal calveolae' *J. Biol. Chem.* 271: 6518-6522.

Shin, D., Athanasiou, K. (1999) Cytoindentation for obtaining cell biomechanical properties. *J. Orthop. Res.* 17: 6, 880-890.

Shivaram, G.M., Kim, C.H., Batra, N.N., Jacobs, C.R. (2004) Novel early response genes in MC3T3-E1 pre-osteoblasts exposed to oscillatory fluid flow. *Transactions of the 51st Orthopaedic Research Society Conference,* Washington DC, USA.

Shroff, S.G., Saner, D.R., Lal, R. (1995) Dynamic micromechanical properties of cultured arterial myocytes measured by atomic force microscopy. *Am. J. Physiol.* 269: C286-292.

Smalt, R.G., F.T. Mitchell, R.L. Howard, T.J. (1997) Chambers, Induction of NO and prostaglandin E_2 in osteoblasts by wall-shear stress but not mechanical strain. *Am. J. Physiol.* 273: E751-758.

Smith, P.G., Deng, L., Fredberg, J.J., Maksym, G.N. (2003) Mechanical strain increases cell stiffness through cytoskeletal filament reorganisation. *Am. J. Physiol.* 285: L456-463.

Sneddon, I.N. (1965) The relation between load and penetration in the axisymmetric Boussinesq problem for a punch of arbitrary profile. *International Journal of Engineering Science* 3: 47-57.

Stamenovic, D., Coughlin, M. F. (1999) The role of prestress and architecture of the cytoskeleton and deformability of cytoskeletal filaments in mechanics of adherent cells: a quantitative analysis. *J. Theor. Biol.* 201: 1, 63-74.

Stamenovic, D., Coughlin, M.F. (2000) A Quantitative Model of Cellular Elasticity Based on Tensegrity. *J. Biomech. Eng.* 122: 39-43.

Stamenovic, D., Fredberg, J.J., Wang, N., Butler, J., Ingber, D.E. (1996) A microstructural approach to cytoskeletal mechanics based on tensegrity. *J. Theor. Biol.* 181: 2, 125-136.

Stamenovic, D., Wang, N. (2000) Engineering approaches to cytoskeletal mechanics. *J. Appl. Physiol.* 89: 2085-2090.

Stamenovice, D., Mijailovich, S.M., Tolic-Norrelykke, I.M., Chen, J., Wang, N. (2002) Cell prestress. II. contribution of microtubules. *Am. J. Physiol.* 282: 3, C617-624.

Su, Y., S. Edwards-Bennett, M.R. Bubb, E.R. (2003) Block, Regulation of endothelial nitric oxide synthase by the actin cytoskeleton. *Am. J. Physiol.* 284: C1542-9.

Tanaka-Kamioka, K., Kamioka, H., Ris, H., S-S, L.I.M. (1998) Osteocyte shape is dependent on actin filaments and osteocyte processes are unique actin-rich projections. *J. Bone Miner. Res.* 13: 1555.

Theodoropoulos, P.A., Gravanis, A., Tsapara, A., Margioris, A.N., Papadogiorgaki, E., Galanopoulos, V., Stournaras, C. (1994) Cytochalasin B may shorten actin filaments by a mechanism independent of barbed end capping. *Biochem. Pharmacol.* 18: 47, 1875-1881.

Thoumine, O., Cardoso, O., Meister, J-J. (1999) Changes in the mechanical properties of fibroblasts during spreading: a micromanipulation study. *European Biophysical Journal* 28: 3, 222-234.

Thoumine, O., Ott, A. (1997) Time scale viscoelastic and contractile regimes in fibroblasts probed by microplate manipulation. *J. Cell Sci.* 110: 2109-2116.

Trickey, T.R., Lee, M., Guilak, T. (2000) Viscoelastic properties of chondrocytes from normal and osteoarthritic human cartilage. *J. Orthop. Res.* 18: 891-898.

Trickey, W.R., Vail, T.P., Guilak, F. (2004) The role of the cytoskeleton in the viscoelastic properties of human articular chondrocytes. *J. Orthop. Res.* 22: 131-139.

Tsuda, Y., Yasutake, H., Ishijima, A., Yanagida, T. (1996) Torsional rigidity of single actin filaments and actin bond breaking force under torsion measured directly by in vitro micromanipulation. *Proc. Natl. Acad. Sci. USA* 93: 12937-12942.

Turner, C.H., Owan, I., Takano, Y. (1995) Mechanotransduction in bone: role of strain rate. *Am. J. Physiol.* 269: E438-442.

Turner, C.H., Takano, Y., Owan, I., Murrell, G.A. (1996) Nitric oxide inhibitor L-NAME suppresses mechanically induced bone formation in rats. *Am. J. Physiol.* 270: E634-639.

van der Meulen, M.C.H., Huiskes, R. (2002) Why mechanobiology? A survey article. *J. Biomech.* 35: 401-414.

Vane, J.R., Mitchell, J.A., Appleton, I., Tomlinson, A., Bishop-Bailey, Croxtall, J., Willoughby, D.A. (1994) Inducible forms of cyclooxygenase and nitric oxide synthase in inflammation. *Proc. Natl. Acad. Sci. USA 91: 2046-2050.*

Walker, L.M., Publicover, J.M., Preston, M.R., Said Ahmed, M.A.A., El Haj, A.J. (2000) Calcium channel activation and matrix protein upregulation in bone cells in response to mechanical strain. *J. Cell Biochem.* 79: 648-661.

Wang, J.H. (2000) Substrate deformation determines actin cytoskeleton reorganisation: a mathematical modelling and experimental study. *J. Theor. Biol.* 202: 1, 33-41.

Wang, N., Butler, J.P., Ingber, D.E. (1993) Mechanotransduction across the cell surface and through the cytoskeleton. *Science* 260: 5111, 1080-1081.

Wang, N., Ingber, D.E. (1994) Control of cytoskeletal mechanics by extracellular matrix, cell shape, and mechanical tension. *Biophys. J.* 66: 2181-2189.

Wang, N., Naruse, K., Stamenovic, D. (2001) Mechanical behaviour in living cells consistent with the tensegrity model. *Proc. Natl. Acad. Sci. USA* 98: 14, 7765-7770.

Wang, N., Stamenovic, D. (2000) Contribution of intermediate filaments to cell stiffness, stiffening and growth. *Am. J. Physiol.* 279: C188-194.

Wang, N., Tolic-Norrelykke, I.M., Chen, J., Mijailovich, S.M., Butler, J.P., Fredberg, J.J., Stamenovice, D. (2002) Cell prestress I. Stiffness and prestress are closely associated in adherent contractile cells. *Am. J. Physiol.* 282: 3, C606-616.

Weinbaum, S., Cowin, S.C., Zeng, Y. (1994) A model for the excitation of osteocytes by mechanical loading-induced bone fluid shear stresses. *J. Biomech.* 27: 339-360.

Weisenhorn, A.L., Khorsandi, M., Kasas, S., Gotzos, V., Butt, H.J. (1993) Deformation and height anomaly of soft surfaces studied with an AFM. *Nanotechnology* 4: 106-113.

Wendling, S., Canadas, P. (2002) Increasing number of interconnected elements in tensegrity models induces a structural softening consistent with cortical cytoskeletal function. *Proceedings of the 4th World Congress of Biomechanics*, Calgary.

Wendling, S., Oddou, C., Isabey, D. (1999) Stiffening response of a cellular tensegrity Model. *J. Theor. Biol.* 196: 309-325.

Westbroek, I., Ajubi, N.E., Alblas, M.J., Semeins, C.M., Klein-Nulend, J., Burger, E.H., Nijweide, P.J. (2000) Differential stimulation of prostaglandin G/H Synthase-2 in osteocytes and other osteogenic cells by pulsating fluid flow. *Biochem. Biophys. Res. Commun.* 268: 414-419.

Williams, R., Jeffcoat, M., Kaplan, M., Goldhaber, P., Johnson, A., Wechter, W. (1992) Flurbiprofen: a potent inhibitor of alveolar bone resorption in beagles. *Science* 227: 640-642.

Wilson, L., Friedkin, M. (1966) The biochemical events of mitosis. I. Synthesis and properties of colchicine labeled with tritium in its acetyl moiety. *Biochemistry* 5: 2463-68.

Wimalawansa, S.J., De Marco, G., Gangula, P., Yallampali, C., Zhang, R., Simmons, D.J. (1997) Nitric oxide donor alleviates ovariectomy-induced bone loss. *Bone* 18: 301-304.

Wu J.Z., Herzog W., Epstein M. (1999) Modelling of location- and time-dependent deformation of chondrocytes during cartilage loading. *J. Biomech.* 32: 563-572.

Yang, Y., Magnay, J.L., Cooling, L., El Haj, A. (2002) Development of a 'mechano-active' scaffold for tissue engineering. *Biomaterials* 23: 2119-2126.

Yellowley, C.E., LI, Z., Zhou, Z., Jacobs, C.R., Donahue, H.J. (2000) Functional gap junctions between osteocytic and osteoblastic cells. *J. Bone Miner. Res.* 15: 2, 209.

You, J., Reilly, G.C., Zhen, X., Yellowley, C.E., Chen, Q., Donahue, H.J., Jacobs, CR. (2001) Osteopontin gene regulation by oscillatory fluid flow via intracellular calcium mobilization and activation of mitogen-activated protein kinase in MC3T3-E1 osteoblasts. *J. Biol. Chem.* 20: 276, 13365-71.

You, J., Yellowley, C.E., Donahue, H.J., Zhang, Y., Chen, Q., Jacobs, C.R. (2000) Substrate deformation levels associated with routine physical activity are less stimulatory to bone cells relative to loading-induced oscillatory fluid flow. *J. Biomech. Eng.* 122: 387-393.

You, L.D., Batra N.N., Jacobs, C.R. (2005) 3D microfabricated chamber system for in vitro study on bone cells. *Transactions of the 51st Orthopaedic Research Society*, Washington D.C.

Zaman, G., Pitsillides, A.A., Rawlinson, S.C.F., Suswillo, R.F.L., Mosley, J.R., Cheng, M.Z., Platts, L.A.M., Hukkanen, M., Polak, J.M., Lanyon, L.E. (1999) Mechanical strain stimulates nitric oxide production by rapid activation of endothelial nitric oxide synthase in osteocytes. *J. Bone Miner. Res.* 14: 1123-1131.

Zharikov, S.I., Sigova, A.A., Chen, S., Bubb, M.R., Block, E.R. (2001) Cytoskeletal regulation of the L-arginine/NO pathway in pulmonary artery endothelial cells. *Am. J. Physiol.* 280: L465-473.

Zou, H., Lifshitz, L.M., Tuft, R.A., Fogarty, K.E., Singer, J.J. (2002) Visualization of Ca2+ entry through single stretch-activated cation channels. *Proc. Natl. Acad. Sci. USA* 30: 99, 6404-9.

APPENDICES

McGarry, J.G., Klein-Nulend, J., Mullender, M.G., Prendergast, P.J. (2005) A comparison of strain and fluid shear stress in stimulating bone cell responses – a computational and experimental study. *FASEB J.* 19: 3, 482-484.

McGarry, J.G., Klein-Nulend, J., Prendergast, P.J. (2005) The effect of cytoskeletal disruption on pulsatile fluid flow-induced nitric oxide and prostaglandin E2 release in osteocytes and osteoblasts. *Biochem. Biophys. Res. Commun.* 29: 341-348.

McGarry, J.G., Prendergast, P.J. (2004) A three-dimensional finite element model of an adherent eukaryotic cell. *Eur. Cell Mater.* 7: 27-34.

McGarry, J.G., Prendergast, P.J. (2003) A finite element model of an adherent cell: comparison of simulated cell indentation with atomic force microscopy experiments. *Proceedings of the International Congress on Computational Bioengineering* 2: 552-559.

McGarry, J.G., Klein-Nulend, J., Prendergast, P.J. (2005) Cytoskeletal modulation of fluid flow-induced NO and PGE2 release in osteocytes and osteoblasts. *Transactions of the 51st Orthopaedic Research Society*, Washington D.C.

McGarry, J.G., Klein-Nulend, J., Mullender, M.G., Prendergast, P.J. (2005) A Computational cell model reveals significant differences in bone cell deformation in response to flow vs. strain stimuli. *Transactions of the 51st Orthopaedic Research Society*, Washington D.C.

McGarry, J.G., Klein-Nulend, J., Mullender, M.G., Prendergast, P.J. (2004) A biomechanical cell model reveals the importance of deformation in the response of bone cells to mechanical stimuli. *Transactions of the 14th European Orthopaedic Research Society*, 2004, Amsterdam, The Netherlands.

The FASEB Journal • *FJ Express*

A comparison of strain and fluid shear stress in stimulating bone cell responses—a computational and experimental study

James G. McGarry, Jenneke Klein-Nulend,* Margriet G. Mullender,* and Patrick J. Prendergast[1]

Centre for Bioengineering, Department of Mechanical Engineering, Trinity College, Dublin, Ireland; and *Department of Oral Cell Biology, ACTA-Universiteit van Amsterdam and Vrije Universiteit, Amsterdam, The Netherlands

To read the full text of this article, go to http://www.fasebj.org/cgi/doi/10.1096/fj.04-2210fje; doi: 10.1096/fj.04-2210fje

Redacted

0892-6638/05/0019-0482 © FASEB

Redacted

Redacted

©2004 FASEB

The FASEB Journal express article 10.1096/fj.04-2210fje. Published online December 29, 2004.

A comparison of strain and fluid shear stress in stimulating bone cell responses—a computational and experimental study

James G. McGarry,* Jenneke Klein-Nulend,† Margriet G. Mullender,† and Patrick J. Prendergast*

*Centre for Bioengineering, Department of Mechanical Engineering, Trinity College, Dublin, Ireland; †Department of Oral Cell Biology, ACTA-Universiteit van Amsterdam and Vrije Universiteit, Amsterdam, The Netherlands.

Corresponding author: Patrick Prendergast, Centre for Bioengineering, Department of Mechanical Engineering, Trinity College, Dublin 2, Ireland. E-mail: pprender@tcd.ie; www.biomechanics.ie

Redacted

Redacted

Redacted

Redacted

Redacted

Redacted

Redacted

Redacted

Redacted

Redacted

Redacted

Redacted

Redacted

Redacted

Redacted

Redacted

Redacted

Redacted

Redacted

Redacted

Redacted

Redacted

Available online at www.sciencedirect.com
SCIENCE DIRECT®
ELSEVIER
Biochemical and Biophysical Research Communications 330 (2005) 341–348
BBRC
www.elsevier.com/locate/ybbrc

The effect of cytoskeletal disruption on pulsatile fluid flow-induced nitric oxide and prostaglandin E_2 release in osteocytes and osteoblasts

James G. McGarry [a,b], Jenneke Klein-Nulend [b], Patrick J. Prendergast [a,*]

[a] *Centre for Bioengineering, Department of Mechanical Engineering, Trinity College, Dublin, Ireland*
[b] *Department of Oral Cell Biology, ACTA—Universiteit van Amsterdam and Vrije Universiteit, Amsterdam, The Netherlands*

Received 6 February 2005

Abstract

Fluid flowing through the bone porosity might be a primary stimulus for functional adaptation of bone. Osteoblasts, and osteocytes in particular, respond to fluid flow in vitro with enhanced nitric oxide (NO) and prostaglandin E_2 (PGE_2) release; both of these signaling molecules mediate mechanically-induced bone formation. Because the cell cytoskeleton is involved in signal transduction, we hypothesized that the pulsatile fluid flow-induced release of NO and PGE_2 in both osteoblastic and osteocytic cells involves the actin and microtubule cytoskeleton. In testing this hypothesis we found that fluid flow-induced NO response in osteoblasts was accompanied by parallel alignment of stress fibers, whereas PGE_2 response was related to fluid flow stimulation of focal adhesions formed after cytoskeletal disruption. Fluid flow-induced PGE_2 response in osteocytes was inhibited by cytoskeletal disruption, whereas in osteoblasts it was enhanced. These opposite PGE_2 responses are likely related to differences in cytoskeletal composition (osteocyte structure was more dependent on actin), but may occur via cytoskeletal modulation of shear/stretch-sensitive ion channels that are known to be dominant in osteocyte (and not osteoblast) response to mechanical loading.
© 2005 Elsevier Inc. All rights reserved.

Redacted

0006-291X/$ - see front matter © 2005 Elsevier Inc. All rights reserved.
doi:10.1016/j.bbrc.2005.02.175

Redacted

Redacted

Redacted

Redacted

Redacted

Redacted

Redacted

European Cells and Materials Vol. 7. 2004 (pages 27-34) ISSN 1473-2262

A THREE-DIMENSIONAL FINITE ELEMENT MODEL OF AN ADHERENT EUKARYOTIC CELL

J. G. McGarry and P.J. Prendergast*

Centre for Bioengineering, Department of Mechanical Engineering, Trinity College Dublin, Ireland

Abstract

Mechanical stimulation is known to cause alterations in the behaviour of cells adhering to a substrate. The mechanisms by which forces are transduced into biological responses within the cell remain largely unknown. Since cellular deformation is likely involved, further understanding of the biomechanical origins of alterations in cellular response can be aided by the use of computational models in describing cellular structural behaviour and in determining cellular deformation due to imposed loads of various magnitudes. In this paper, a finite element modelling approach that can describe the biomechanical behaviour of adherent eukaryotic cells is presented. It fuses two previous modelling approaches by incorporating, in an idealised geometry, all cellular components considered structurally significant, i.e. prestressed cytoskeleton, cytoplasm, nucleus and membrane components. The aim is to determine if we can use this model to describe the non-linear structural behaviour of an adherent cell and to determine the contribution of the various cellular components to cellular stability. Results obtained by applying forces (in the picoNewton range) to the model membrane nodes suggest a key role for the cytoskeleton in determining cellular stiffness. The model captures non-linear structural behaviours such as strain hardening and prestress effects (in the region of receptor sites), and variable compliance along the cell surface. The role of the cytoskeleton in stiffening a cell during the process of cell spreading is investigated by applying forces to five increasingly spread cell geometries. Parameter studies reveal that material properties of the cytoplasm (elasticity and compressibility) also have a large influence on cellular stiffness. The computational model of a single cell developed here is proposed as one that is sufficiently complex to capture the non-linear behaviours of the cell response to forces whilst not being so complex that the parameters cannot be specified. The model could be very useful in computing cellular structural behaviour in response to various *in vitro* mechanical stimuli (e.g. fluid flow, substrate strain), or for use in algorithms that attempt to simulate mechanobiological processes.

Key words: Cell model, finite elements, tensegrity, microtubules, actin, prestress, cellular deformation, nuclear deformation, mechanobiology, cell biomechanics.

*Address for correspondence:
Patrick Prendergast
Centre for Bioengineering,
Department of Mechanical Engineering,
Parsons Building, Trinity College, Dublin 2, Ireland.
Telephone Number: +353-1-608 1383
FAX Number: +353-1-679 5554.
E-mail: pprender@tcd.ie
Web.: www.biomechanics.ie

Introduction

Alterations in cell shape and structure caused by mechanical loads are critical to cell functions including growth, motility, differentiation, and proliferation (Chen *et al.*, 1997; Chicurel *et al.*, 1998; Janmey, 1998; Carter and Beaupré, 2003). Much current research focuses on investigating the mechanisms by which cells sense and transduce mechanical forces into biochemical signals, and it has emerged that the extent to which an imposed mechanical load can elicit changes in cell behaviour partly depends on the distribution of forces within the structural components of the cell. The mechanisms by which cells resist deformation under imposed mechanical loads, and the contribution of each cellular component to structural stability, are therefore significant questions in cell mechanics.

Mechanical models could give insight into the structural properties of adherent cells. Previous modelling approaches involve either attributing the primary structural role to the cytoskeleton, or treating the cytoplasm as a continuum. The first category of models includes the tensegrity approach, which views the cytoskeleton as a network of microfilaments and microtubules that distribute forces within the cell through a balance of compression and tension (Ingber, 1997; Stamenovic *et al.*, 1996). By attributing a central role to cytoskeleton contractile forces, the tensegrity approach has described many aspects of cell deformability including non-linear features of cellular structural behaviour (Wang *et al.*, 2001). In the second category of models, the continuum approach has been used to model blood cells with a cortical membrane and viscous cytoplasm (Evans and Yeung, 1989), airway epithelial cells in a 2D finite element model (Kamm *et al.* 2000), the deformation of a chondrocyte within its extracellular matrix (Guilak and Mow, 2000), and cell deformation in magnetocytometry with a viscoelastic representation of the membrane/cortex and cytoskeleton (Karcher *et al.*, 2003). The third category includes models of the cytoskeleton as a percolation network of fibres in a viscous cytoplasm, where the fibres recombine via linker molecules to transmit forces across the cytoskeleton (Shafrir and Forgacs, 2002; Head *et al.*, 2003).

Charras and Horton (2001) have suggested a model comprising a cytoskeleton tethered to both membrane and nucleus components to explain their observations of the effects of cytoskeletal disruption. It has also been proposed by Hochmuth (2000) that "the modelling of cellular deformation in the future may combine elements of both continuum models and tensegrity models". The present paper describes the development a model of a eukaryotic cell adherent to a substrate using the finite element method, incorporating those cellular components that are likely to be structurally significant, i.e. nucleus, cytoplasm, membrane components, and a cytoskeleton network of filaments

and tubules. The aim is to determine whether or not we can successfully describe the non-linear structural behaviour of an adherent cell, including non-linear stiffening, variable compliance along the cell surface, the influence of tension (i.e., prestress) in the actin filament network, alterations in stiffness during spreading, and the contribution of each structural component to the cellular stability/stiffness. If this is possible then we would have a *prima facie* case for using such models as predictive tools in mechanobiology.

Methods

Model Geometry

A finite element model was created to represent the shape of a rounded cell adherent to a substrate in various spread configurations. The geometry was based on images of spreading fibroblasts (Fig. 1). The cell immediately post attachment has its most rounded configuration (Fig. 2a) and consists of a cytoskeleton incorporating microfilaments and microtubules, together with cytoplasm, nucleus and membrane components. Similar models were created to represent the adherent cells at increasingly spread shapes (Fig. 2b – 2f). The internal cytoskeleton consists of a tensegrity network of six compression-bearing struts (two in each orthogonal direction) and twenty-four tensional cables representing the aggregate behaviour of microtubules and microfilaments respectively. The end of each strut connects with four cables, creating 12 common nodes representing 'receptor' sites where actin filaments cluster at adhesion complexes in adherent cells. In the increasingly spread models (Fig. 2a – 2f), the microtubule and microfilament elements are altered in length and position as these nodes are re-positioned downwards to comply with the spread shapes. New surface locations for the 'receptor' nodes are established by firstly determining the nodal positions that maintain the original vertical proportions of the internal cytoskeleton structure in the rounded configuration shown in Fig. 2a, i.e. three horizontal planes formed by nodes 4, 5, 6 nearest the substrate, nodes 7, 8, 9 next, and nodes 10, 11, 12 farthest from the substrate (Fig. 2a shows the original positions of these nodes). Radial planes defined by the central axis and the original nodal positions are then established; the intersection of these planes with each new model surface yields surface lines along which the new nodal positions must lie. Points of intersection of these surface lines with each of the three horizontal planes established in each model yield nine new nodal positions of the cytoskeleton nodes when repositioned to conform to the spread shape of each model. The nodes of the membrane are coincident with nodes of the underlying cytoplasm and with nodes of the cytoskeleton at receptor sites. Contact radii and heights of each of the finite element models are provided in Table 1.

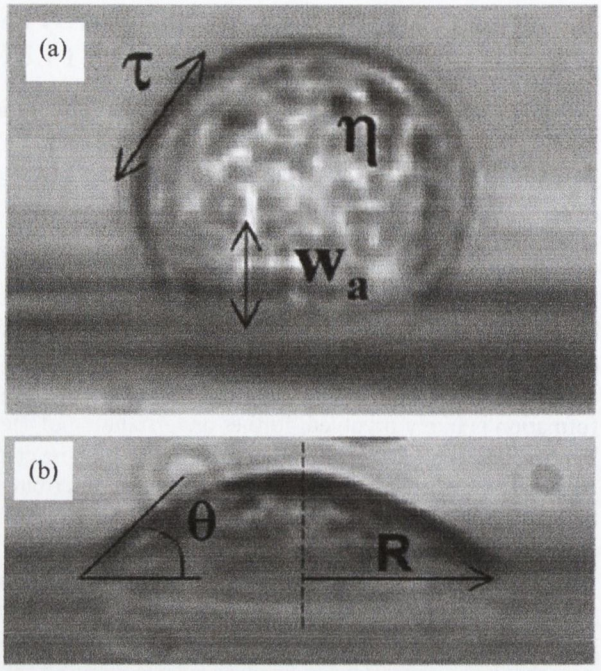

Figure 1. Images of a spreading chick embryo fibroblast adherent on a glass microplate for (a) 5 minutes, and (b) after 3 hours, adapted with permission from Frisch and Thoumine (1999). The dimensions of the finite element models developed (Table 1) correspond to contact angles (θ) and contact radii (R) highlighted in (b).

The corresponding cell volumes are ~3,000 μm^3 and the nucleus in each model formed from an ellipse with a major axis of 8 μm, minor axis of 5 μm, and a distance of 2 μm from the substrate, also based on experimental observations by Thoumine *et al.* (1999).

The model is developed using ANSYS (Palo Alto, CA, USA). The cytoplasm and nucleus elements are meshed with 4-node lower-order tetrahedral elements. The membrane is meshed with 3-node shell elements. Microtubule struts and microfilament cables are meshed with single link elements (a three-dimensional spar element with bilinear stiffness matrix), compression-only and tension-only respectively.

Constitutive modelling of cellular components

Material properties for each of the cell components are not known precisely and can only be estimated from various sources (see Table 2). The cytoplasm and nucleus are here treated as linear elastic and isotropic continua. The elastic modulus of the cytoplasm is chosen as 100 Pa (Kamm *et al.*, 2000), while the nucleus is chosen as 400 Pa, ~four times stiffer than the cytoplasm, as reported by

	Cytoplasm	Nucleus	Membrane¶	Microtubules§	Microfilaments§
Elastic modulus (Pa)	100 *	400†	10^3	1.2×10^9	2.6×10^9
Poisson's ratio (ν)	0.37‡	0.37‡	0.3	0.3	0.3

* 1×10^{-10} N/μm²

‡Shin and Athanasiou, 2001, †Guilak *et al.*, 2000, ¶ Kamm *et al.*, 2000, § Gittes *et al.*, 1993.

Table 2. Material properties assigned to the cellular components in each model.

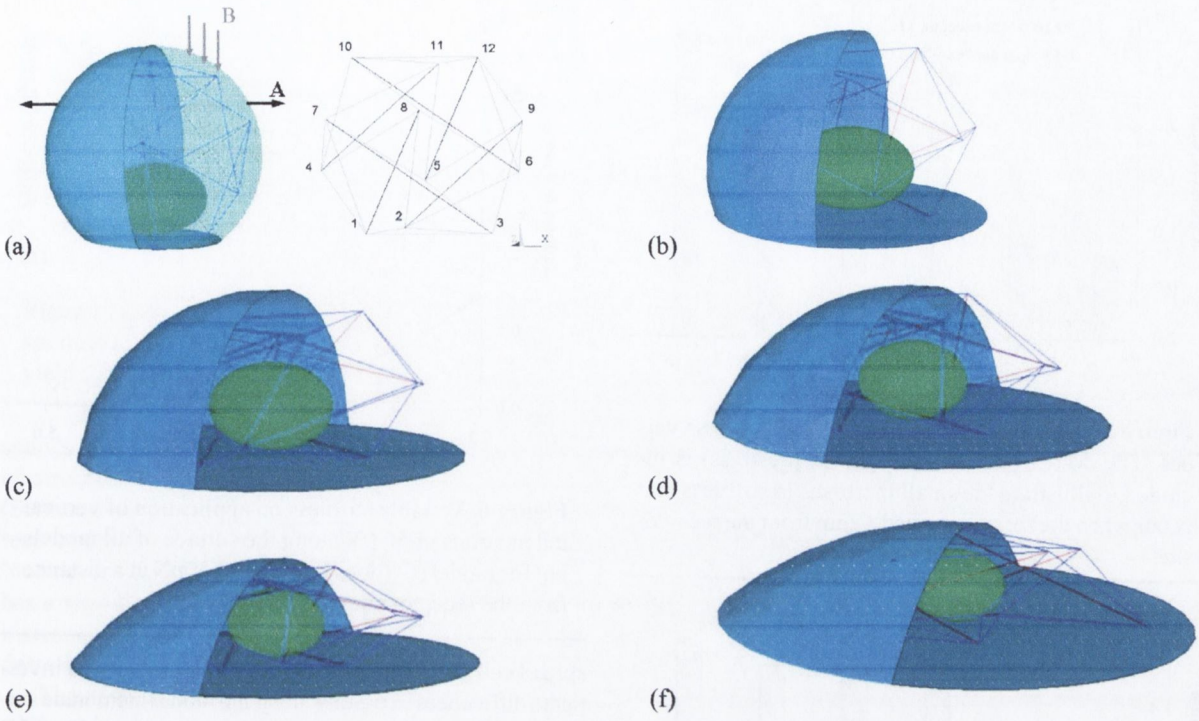

Figure 2. Three-dimensional finite element models (a) to (f) of adherent cells at increasingly spread shapes to the final configuration in Fig 1b. Each model comprises membrane, nucleus, cytoplasm, and cytoskeleton components. The cytoplasm is omitted for clarity in all models except model (a). Also shown is the internal cytoskeleton of model (a) consisting of a 3-dimensional tensegrity network of interconnected microtubule (dark lines) and microfilament elements (light lines). Loading conditions applied to the models involve either (A) horizontal forces (50 pN) applied to two surface nodes in opposite directions, or (B) the application of vertical indentation forces (50 pN) to membrane surface nodes.

Guilak *et al.* (2000). Poisson's ratio value (υ) for both nucleus and cytoplasm is chosen as 0.37 (Shin and Athanasiou, 1999). In the model developed by Kamm *et al.* (2000) epithelial cell membrane elasticity was taken to be 10^7 Pa with a thickness of 6 nm. Since in that study, it was concluded that the membrane elastic properties were over-estimated, a lower value of 10^3 Pa (with $\nu = 0.3$) is selected for the present model, while maintaining the same membrane thickness. Gittes *et al.* (1993) measured the flexural rigidity (bending stiffness) of microtubules and microfilaments subjected to thermal fluctuations. The properties applied to the cytoskeleton components, i.e. the microtubules and microfilaments are based on the elasticity values calculated from these bending stiffness values under the assumption of isotropy and homogeneity; the microtubules are assigned corresponding cross-sectional areas of 190 nm^2, while the microfilaments are thinner with an area of 18 nm^2.

Initial constraints

In all models with the various degrees of spreading (Fig. 2a to 2f), nodes at the cell-substrate interface, including the three receptor nodes that establish a cell-substrate plane in each model (nodes 1, 2, 3 in Fig. 2a), are constrained in all three translational degrees of freedom. Therefore the constrained points are analogous to focal adhesion sites in adherent cells. Initial constraints in each analysis also involve application of a prestress (initial strain) to the microfilament elements in each of the six models. Prestress is an initial tension that effectively accounts for the contractile effect of acto-myosin sliding mechanisms in the membrane/cortex region.

Model	Contact radius (μm)	Cell Height (μm)
a	6	14
b	8.5	12.8
c	11.2	10.6
d	14.3	10.1
e	17.5	8.5
f	19.2	7.6

Table 1. Dimensions of each finite element model (a) to (f) illustrated in Fig. 2.

Prestress and strain hardening. Prestress values assigned to microfilament elements of model (a) are varied from 0 to 10% in the first loadstep of each analysis, while subsequent loadsteps involve application of a 100 pN force (50 pN applied to two membrane surface nodes as illustrated in Fig. 2a, load vectors denoted by 'A'). The displacement of the nodes in each direction due to the applied force yields stiffness (nN/μm) estimates. To investigate strain hardening, the force applied in the second loadstep is increased from 25 to 150 pN while maintaining constant prestress values in the first loadstep.

Parametric variation of material properties. The influence of material properties on stiffness is investi-

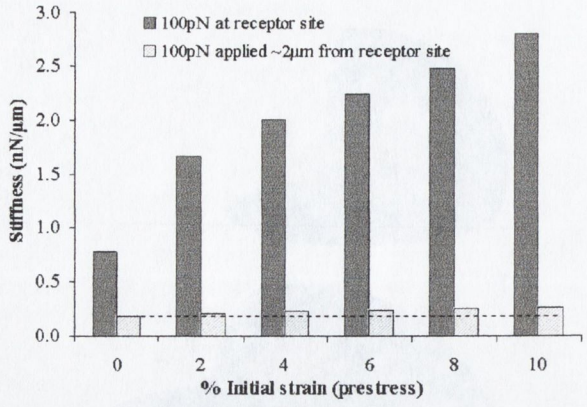

Figure 3. The effect of prestress on cell stiffness values. The dotted line (stiffness at 0% prestress) is included to illustrate the small increases in stiffness that occur when the force is applied ~2μm from the receptor site.

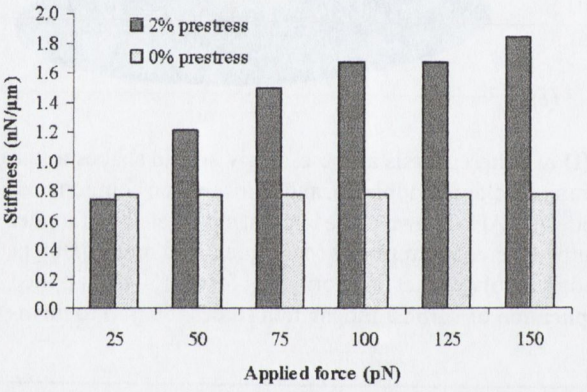

Figure 4. Stiffness versus applied forces. At 0% prestress in the cytoskeleton there is no strain hardening effect.

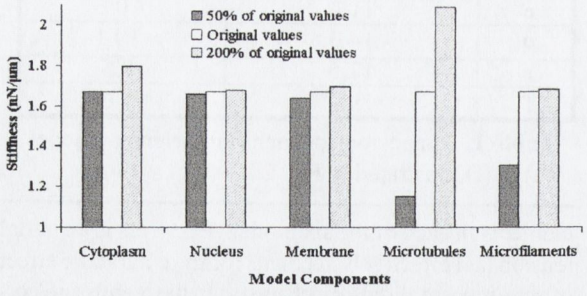

Figure 5. The effect on cell stiffness of altering the Young's modulus of each component from the original values outlined in Table 2.

gated in the unspread cell configuration [Fig. 2a] by modulating the elasticity of each model component by 50% and 200% of the original values, and computing displacements in response to 100 pN. Poisson's ratio value for the cytoplasm is also altered from 0.37 to 0.25 and 0.49 in order to determine the effect, if any, of the degree of cytoplasm incompressibility. Constant prestress values are maintained during the parameter study.

Variable compliance of the cell. All six degrees of

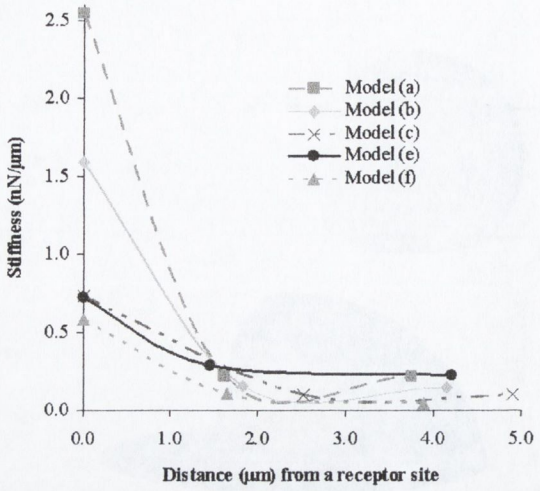

Figure 6. Variable stiffness on application of vertical indentations of 50 pN along the surface of all models but for model (d) (does not support 50pN at a distance from the receptor site).

spread cell configuration [Fig. 2a to 2f] are used to investigate differences in rigidity along the model membrane surface. Again prestress is maintained at a constant value (2%) in each model. In each model vertical forces (50pN) are applied to a receptor node, and at various distances (<5 μm) from the receptor node (as shown in Fig. 2, load vectors denoted by 'B'). This essentially mimics indentation as applied by atomic force microscopy.

Spreading effects. All six models are also used to investigate alterations in stiffness as contact radius increases. A force of 100 pN is applied as in Fig. 2 – vectors 'A', but in both x and z horizontal directions. Averages of displacements in each direction yield stiffness estimates for each model. Prestress values applied to microfilaments are kept constant in each model, which is in accordance with observations of constant cortical membrane tension in spreading cells (Thoumine *et al.*, 1999).

Results

When forces in the pN range are applied to the cell, the model computes small displacements on the order of nanometers. The stiffness values obtained are in a similar range (from 0.5 – 3 nN/μm) whether the model is resisting horizontal forces or vertical indentations. As prestress is increased linearly, a non-linear increase in stiffness arises (Fig. 3). This effect of prestress on cellular stiffness is also seen when the force is applied at a distance from the receptor site.

It is also evident that, as the applied force is increased, the stiffness of the cell increases, and this hardening non-linearity disappears in the absence of a prestress (Fig. 4). Since the amount of compression borne by microtubules has been the subject of debate (Ingber *et al.*, 2000; Heidemann *et al.*, 1999) the microtubule components were deactivated in the model illustrated in Fig. 2(a), effectively modelling the treatment of cells with microtubule inhibitors such as colchicine. It was found that, at 1% prestress, the decrease in stiffness was ~77%. This finding corre-

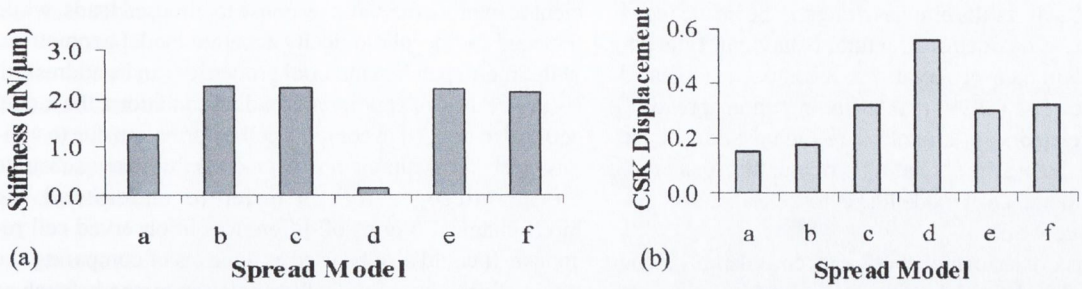

Figure 7. (a) Alterations in stiffness as contact radius increases from models (a) to (f). Graph (b) shows the corresponding cytoskeleton (CSK) displacements (μm) due to prestress prior to application of horizontal forces that yield stiffness values.

sponds to experimental observations of significant losses of structural stiffness upon disruption of microtubules (Stamenovic *et al.*, 2002) and of microtubule buckling in response to increased cell contraction (Wang *et al.*, 2001). Incompressibility of the cytoplasm (i.e. Poisson's ratio, υ) has a significant effect in the model; increasing to 0.49 increases stiffness by 45%, whereas decreasing to 0.25 decreases stiffness by only ~4%.

The cell stiffness changed greatly with changes in the stiffness of certain cell components. Microtubule components have the largest influence on structural stiffness, followed by microfilaments and cytoplasm properties (Fig. 5). The properties of the membrane and nucleus components have a small influence on structural stiffness relative to other components.

In each increasingly spread model applying vertical forces yields differences in compliance along the model surface, i.e. compliance increases with distance from receptor sites (Fig. 6).

As contact radius increases in models (a) to (f) stiffness increases initially, followed by a drop in stiffness in model (d) and a final increase in model (f), as shown in Fig. 7a. Therefore the stiffness is not predicted to change systematically with cell spreading. The corresponding cytoskeleton displacements due to prestress in the first loadstep in each model (Fig. 7b) illustrate slight increases in displacement to a maximum in model (d), which may be related to the trend in stiffness values in Fig. 7a.

Discussion

The non-linear increases in cell stiffness as a result of increasing prestress exhibited by the model is attributed to the internal cytoskeleton – the effect is also seen when forces are applied at a distance from the underlying cytoskeleton, although the effect is less pronounced. Experimental observations of such an effect in adherent cells have been reported by Pourati *et al.* (1998) and Wang *et al.*, (2002). The strain hardening effect captured by the model is also due to the cytoskeleton and corresponds to experimental observations of increases in cell stiffness in response to increasing loads applied using micropipette techniques (Sato *et al.*, 1990) and a magnetic twisting device (Wang *et al.*, 2001). Therefore the results of our finite element model concur qualitatively with the experimental findings that the internal cytoskeleton plays a key role in determining the structural properties of the model.

With the exception of the cytoskeleton, the cytoplasm has the largest influence on the overall resistance to deformation even though its elasticity is significantly less than that of the nucleus and membrane (Fig. 5). This, of course, may be attributed to the large volume occupied by the cytoplasm relative to other components. This indicates the importance of determining correctly the incompressibility of the cytoplasm, particularly since a wide range of values have been reported from experimental studies: Shin and Athanasiou (1999) have reported a value of 0.37 for osteoblasts using a cytoindentation method and linear biphasic finite element analysis; Mathur *et al.* (2001) and Kamm *et al.* (2000) use values of up to 0.49 to describe cytoplasm incompressibility. The membrane, despite its small thickness has a larger influence on stiffness than does the nucleus. Increases in the elasticity of the microfilament components have a small effect, while a decrease is more notable since this compromises the greater structural contribution of the microtubules. This influence of microfilament properties on structural stiffness further confirms the view that the contractile force transmitted by actin filaments in adherent cells has a large effect on cellular structural behaviour. Other recent publications have also suggested the importance of prestress in giving the cell the structural stability to resist cellular deformation (Wang *et al.*, 2002). Changes in microtubule properties have the largest influence on the structural stiffness of the cell – this is attributed to their larger cross-sectional area, their positioning, and their role as compression bearing elements in the model.

It has been observed that adherent cells increase their resistance to deformation (or stiffness) as they become more spread on a substrate (Thoumine *et al.*, 1999). The models developed here do not conclusively reflect these findings (Fig. 7). The lack of such stiffening in our model may reflect the simplistic nature of how we have modelled the rearrangement of the cytoskeleton as the cell spreads. In this respect, the percolation network models mentioned in the Introduction (Shafrir and Forgacs, 2002; Head et al., 2003) may prove superior. However it is evident that there may be a relation between stiffness and the cytoskeleton in each model, i.e. it may be said that the movement of the cytoskeleton in response to arbitrary prestress value is related to the final stiffness value (Fig. 7), e.g. high CSK displacement results in low stiffness (as in model (d)) and vice versa

(model (b)). Such results emphasise again the influence of the cytoskeleton on overall structural behaviour. Interestingly, to explain their observations, it has been suggested by Thoumine *et al.* (1999) that stiffening upon spreading may be correlated with structural re-organisation of the cytoskeleton during the spreading process; this further indicates the importance of modelling cytoskeletal re-arrangements in future work.

We also report that compliance varies considerably along the surface of each model, with the highest resistance to indentation at receptor sites due to the underlying cytoskeleton. The stiffness values decrease considerably at short distances from receptor sites and converge to a range of lower stiffness values in each spread model (Fig. 6). This corresponds to variations in elasticity values determined when indenting into the surface of adherent cells using atomic force microscopy; e.g. local elasticity values vary from ~0.5 kPa to 170 kPa if indentation is applied in the region of stress fibres or actin filaments (Mathur *et al.* 2001; Domke *et al.* 1996). Quantitative confirmation of the present model has been addressed in McGarry and Prendergast (2003). In that work, we applied displacement boundary conditions that reflect the geometry of an indenting AFM probe and, together with the use of an appropriate theoretical relation (Hertz, 1881; Sneddon, 1965), we were able to determine elasticity values in the range of those reported from experiments.

By accounting for the role of all structurally relevant components in maintaining a cell's stability, while incorporating non-linear aspects of adherent cell behaviour that are due to an interconnected cytoskeleton, the models developed in this paper can be viewed as a fusion of two contrasting previous approaches, the stress-supported tensegrity approach (Ingber, 1997) and the continuum approach (Kamm *et al.*, 2000). A benefit of the approach to repositioning the tensegrity-based cytoskeleton to increasingly spread shapes is related to the fact that the orientation, positioning and length of internal cytoskeleton components is altered by polymerisation, and by clustering of actin filaments during spreading as adhesion bonds form between intra- and extra-cellular structural proteins such as vinculin, talin, and fibronectin (Alberts *et al.*, 1989). It has also been suggested by Gittes *et al.* (1993) that to account for the seemingly excessively rigid mechanical properties measured, sliding and movement may occur between filaments and tubules. The material properties chosen to represent the cytoskeleton have been used in previous models (Stamenovic and Coughlin, 2000), while similar values for flexural rigidity have been estimated theoretically by Ben-Avraham and Tirion (1995), and are in agreement with other experimental work (Tsuda *et al.*, 1996). The role of intermediate filaments was not included since their contribution to cellular rigidity only becomes significant above 20% strain (Janmey et al., 1991; Wang and Stamenovic, 2000).

We set out to develop a computational model to provide quantitative predictions of the non-linear structural behaviours that are attributed to the cytoskeleton components, and the relative importance of various cellular components in resisting imposed mechanical loads. The idealised geometry and linear elastic properties used are sufficient to explore the static response to imposed loads, while the need for morphologically accurate model geometries, with time-dependent material properties can be addressed. By application of appropriate loading conditions, the model could also be used to compute cell deformation due to various mechanical stimuli *in vitro* (such as fluid flow, substrate strain, microgravity) in order to understand the biomechanical origins of differences in observed cell response. It could also be used as a means of comparing the effect of various single-cell stimulation methods (such as optical tweezers, atomic force microscopy, or microplate manipulation).

Acknowledgements

Funding provided by the Programme for Research in Third Level Institutions (PRTLI), administered by the Higher Education Authority, and by the BITES (Biomechanical Interactions in Tissue Engineering and Surgical Repair) project funded under the 5th Framework programme of the European Commission.

References

Alberts B, Bray D, Lewis J, Raff M, Roberts K, Watson JD (1989) Molecular Biology of the Cell. Garland Publishing, New York and London, 2nd Edition.

Ben-Avraham D, Tirion MM (1995) Dynamic and elastic properties of F-actin: a normal modes analysis. Biophys J **68**: 1231-1245.

Carter DR, Beaupré GS (2003) Skeletal Function and Form. Cambridge University Press.

Charras GT, Horton MA (2002) Single cell mechanotransduction and its modulation analyzed by atomic force microscopy indentation. Biophys J **82**: 2970-2981.

Chen CS, Mrksich M, Huang S, Whitesides GM, Ingber DE (1997) Geometric control of cell life and death. Science **276:** 1425-1428.

Chicurel ME, Chen CS, Ingber DE (1998) Cellular control lies in the balance of forces. Curr Biol **10**: 232-239.

Domke J, Dannohl S, Parak WJ, Müller O, Aicher WK, Radmacher M (2000) Substrate dependent differences in morphology and elasticity of living osteoblasts investigated by atomic force microscopy. Coll Surf B: Biointerfaces **19:** 367-379.

Evans E, Yeung A (1989) Apparent viscosity and cortical tension of blood granulocytes determined by micropipette aspiration. Biophys J **56**: 151-160.

Frisch T, Thoumine O (2002) Predicting the kinetics of cell spreading. J Biomech **35**: 1137-1141.

Gittes F, Mickey B, Nettleton J, Howard J (1993) Flexural rigidity of microtubules and actin filaments measured from thermal fluctuations in shape. J Cell Biol **120**: 923-934.

Guilak F, Mow C (2000) The mechanical environment of the chondrocyte: a biphasic finite element model of cell-matrix interactions in articular cartilage. J Biomech **33**: 1663-1673.

Guilak F, Tedrow JR, Burgkart R (2000) Viscoelastic properties of the cell nucleus. Biochem Biophys Res

Commun **269**: 781-786.

Head DA, Levine AJ, MacKintosh FC (2003) Deformation of cross-linked semi-flexible polymer networks. Phys Rev Lett **91**: 108102-1.

Heidemann SR, Kaech S, Buxbaum RE, Matus A (1999) Direct observations of the mechanical behaviours of the cytoskeleton in living fibroblasts. J Cell Biol **145:** 109-122.

Hertz H (1881) Über den Kontakt elastischer Körper. Journal für die reine und angewandte Mathematik **92:** 156.

Hochmuth RM (2000) Micropipette aspiration of living cells. J Biomech **33**: 15-22.

Ingber DE (1997) Tensegrity: the architectural basis of cellular mechanotransduction. Annu Rev Physiol **59**: 575-599.

Ingber DE, Heidemann SR, Lamoroux P, Buxbaum RE (2000) Opposing views on tensegrity as a framework for understanding cell mechanics. J Appl Physiol **89**: 1663-1670.

Janmey PA (1998), The cytoskeleton and cell signaling: component localization and mechanical coupling. Physiol Rev **78**: 763-781

Janmey PA, Eutenauer U, Traub P, Schliwa M (1991) Viscoelastic properties of vimentin compared with other filamentous biopolymer networks. J Cell Biol **113:** 155-160.

Kamm RD, McVittie AK, Bathe M (2000) On the Role of Continuum Models in Mechanobiology. ASME International Congress - Mechanics in Biology **242:** 1-9.

Karcher H, Lammerding J, Huang H, Lee RT, Kamm RD, Kaazempur MR (2003) A three-dimensional viscoelastic model for cell deformation with experimental verification. Biophys J **85:** 3336-3349.

Mathur AB, Collinsworth AM, Reichert WM, Kraus WE, Truskey GA (2001) Endothelial, cardiac muscle and skeletal muscle exhibit different viscous and elastic properties as determined by atomic force microscopy. J Biomech **34:** 1545-1553.

McGarry JG, Prendergast PJ (2003) A finite element model of an adherent cell: comparison of simulated cell indentation with atomic force microscopy experiments. Proceedings of the International Congress on Computational Bioengineering (Eds.: M. Doblaré, M. Cerrolaza, and H. Rodrigues), pp. 552-559, University of Zaragoza, Spain, 2003

Pourati J, Maniotis A, Spiegel D, Schaffer JL, Butler JP, Fredberg JJ, Ingber DE, Stamenovice D, Wang N (1998) Is cytoskeletal tension a major determinant of cell deformability in adherent endothelial cells? Am J Physiol Cell Physiol **274:** C1283-1289.

Sato M, Theret DP, Wheelerm LT, Ohshima N, Nerem RM (1990) Application of the micropipette technique to the measurement of cultured porcine aortic endothelial cell viscoelastic properties. J Biomech Eng **112:** 263-268.

Shafrir YG, Forgacs G (2002) Mechanotransduction through the cytoskeleton. Am J Physiol Cell Physiol **282:** C479-486.

Shin D, Athanasiou K (1999) Cytoindentation for obtaining cell biomechanical properties. J Orthop Res **17:** 880-890.

Sneddon IN (1965) The relation between load and penetration in the axisymmetric Boussinesq problem for a punch of arbitrary profile. Int J Eng Sci **3:** 47-57.

Stamenovic D, Coughlin MF (2000) A Quantitative Model of Cellular Elasticity Based on Tensegrity. J Biomech Eng, ASME Transactions **122**: 39-43.

Stamenovic D, Fredberg JJ, Wang N, Butler J, Ingber DE (1996) A microstructural approach to cytoskeletal mechanics based on tensegrity J Theor Biol **181**: 125-136.

Stamenovice D, Mijailovich SM, Tolic-Norrelykke IM, Chen J, Wang N (2002) Cell prestress. II. Contribution of microtubules. Am J Physiol Cell Physiol **282:** C617-624.

Thoumine O, Cardoso O, Meister J-J (1999) Changes in the mechanical properties of fibroblasts during spreading: a micromanipulation study. Eur Biophys J **28:** 222-234.

Tsuda Y, Yasutake H, Ishijima A, Yanagida T (1996) Torsional rigidity of single actin filaments and actin bond breaking force under torsion measured directly by in vitro micromanipulation. Proc Natl Acad Sci USA **93**: 12937-12942.

Wang N, Stamenovic D (2000) Contribution of intermediate filaments to cell stiffness, stiffening and growth. Am J Physiol Cell Physiol **279:** C199-194.

Wang N, Naruse K, Stamenovic D (2001) Mechanical behaviour in living cells consistent with the tensegrity model. Proc Natl Acad Sci USA **98:** 7765-7770.

Wang N, Tolic-Norrelykke IM, Chen J, Mijailovich SM, Butler JP, Fredberg JJ, Stamenovice D (2002) Cell prestress I. Stiffness and prestress are closely associated in adherent contractile cells. Am J Physiol Cell Physiol **282:** C606-616.

Discussion with Reviewers

B. Ashton: When a cell attaches to a substrate integrins in the membrane become linked externally to their ligand on the substrate and to the cytoskeleton internally. Is it legitimate to continue to model the biomechanical properties of this complex as the sum of the individual components – membrane, microfilaments?

Authors: The modelling approach we have taken is legitimate in so far as it approximates the distribution of integrin-ligand links as a continuum. However, the number and strength of integrin-ligand links influences the clustering of actin filaments at focal adhesion complexes which in turn effects the distribution, length, and orientation of the cytoskeletal elements which, we assume, dictate cell biomechanical properties. Therefore, modelling the "individual components" as a continuum is a simplification which would have considerable influence on modelling the dynamic process of cell spreading rather more so than on determining the biomechanical properties of an adherent cell.

Essentially what we have done in our model might be considered as taking a "snapshot" of the cytoskeletal network in increasingly spread configurations without incorporating the mechanisms (such as integrin-ligand links and associated biophysical pathways) that drive these changes. In summary, by manually repositioning the cytoskeleton our

approach does not model the dynamics of cell spreading but rather the consequences of it in terms of the cellular biomechanical properties.

J. Klein-Nulend: How do the forces applied in your model compare quantitatively to the shear stress applied to cells in fluid flow experiments, or to the forces applied in experiments in which cell response has been manipulated with optical tweezers or atomic force microscopy techniques?
Authors: From literature it seems that the localised forces required to elicit biological responses in single adherent cells are higher in magnitude (on the order of nN's) than the forces we have applied to our model (on the order of pN's). For example, pulling magnetically on microbeads adherent to cell receptors with a force of 4.4 pN does not alter calcium response (Wu *et al.*, 1999), whereas higher forces of 10 nN applied by atomic force microscopy indentations can modulate intracellular calcium response (Charras and Horton, 2002). However, we have computed that displacements of our model due to physiological levels of shear stress known to cause alterations in cellular function (e.g. Mullender *et al.*, 2004) are of the same magnitude as those displacements caused by the forces applied to our model here (on the order of nm's). This difference in magnitude suggests that adherent cells may distinguish between and respond differently to whole-cell (e.g. fluid flow) and localised methods of cell stimulation (e.g. AFM, optical tweezers).

J. Klein-Nulend: In your model, material properties are estimated from various sources for different cell types. Can you comment on this variation in properties of different cell types and how such variation would impact on the structural behaviour of the model?
Authors: Differences in material properties have been reported for various cell types – Mathur *et al.* (2001) have reported elastic moduli of 1.4 kPa for endothelial cells, 24.7 kPa for skeletal muscle cells and 100 kPa for cardiac muscle cells. The properties of our model components can be altered accordingly to describe the structural behaviour of these different cell types, and provided that the relative differences in material properties assigned to each component remain consistent, the structural behaviours reported here will remain valid. Perhaps what is more important is to determine why there is such variation in mechanical properties between cell types? Our findings suggest not only that many aspects of cellular structural behaviour seen in our model depend on the cytoskeleton, but also indicate that such large variations in properties between cell types (as in Mathur *et al.* (2001) for example) can only (and most likely) arise from differences in the distribution, lengths and orientations of the more rigid cytoskeleton components. This again emphasises the importance of understanding the mechanisms of adhesion bond formation that control the distribution, positioning and polymerisation of cytoskeletal components, and of developing experimental techniques to determine cytoskeletal properties.
J. Klein-Nulend: Could the authors elaborate on why intermediate filaments were not included in the model?
Authors: Our approach to modelling the cytoskeleton focuses on a specific role for microfilaments in transmitting a tension or prestress which is resisted by interconnected microtubules that are in compression. Although intermediate filaments are thought to contribute largely to the mechanical support of the cell (Alberts *et al.*, 1989), particularly at higher strains (Janmey *et al.*, 1991; Wang and Stamenovic, 2000), we are not aware of a specific tensile or compressive role for intermediate filaments or whether they form an interconnected network for force transmission with the other cytoskeletal components. For this reason, we did not explicitly model intermediate filaments, and their contribution to cellular stiffness was simply assumed to be incorporated in the material properties of the cytoplasm.

Additional References

Mullender MG, El Haj AJ, Yang AJ, van Duin MA, Burger EH, Klein-Nulend J (2004) Mechanotransduction of bone cells in vitro – mechanobiology of bone tissue. Med Biol Eng Comp **42:** 14-21.

Wu Z, Wong K, Glogauer M, Ellen RP, McCulloch CA (1999) Regulation of stretch activated intracellular calcium transients by actin filaments. Biochem Biophys Res Commun **186:** 1212-1219.

INTERNATIONAL CONGRESS ON COMPUTATIONAL BIOENGINEERING
M. Doblaré, M., Cerrolaza and H. Rodrigues (Eds.)
© 13A, España, 2003

A FINITE ELEMENT MODEL OF AN ADHERENT CELL: COMPARISON OF SIMULATED CELL INDENTATION WITH ATOMIC FORCE MICROSCOPY EXPERIMENTS

James G. McGarry and Patrick J. Prendergast

Centre for Bioengineering, Department of Mechanical Engineering, Trinity College, Dublin, Ireland.

SUMMARY

In our opinion the challenge of developing a model for the biomechanical behaviour of a single cell has not yet been met. This research fuses two techniques of mechanics – continuum modelling and tensegrity modelling – to create a finite element model of a cell adherent to a substrate. Details of the modelling procedure are given, including geometric modelling of each of the various cell components. The purpose of this paper is to report on an attempt to confirm the finite element model of an adherent cell by comparing its predictions of force/displacement behaviour with those obtained experimentally by indentation of a cell using the tip of an atomic force microscope. A point load indentation method was found to under-estimate local elasticity values, while a method involving application of prescribed nodal displacements to reflect the geometry of a conical probe yields local elasticity values from 0.6 to 1.4 kPa (on use of an appropriate theoretical relation), in the range of those reported from experimental measurements. In the model, elasticity values can also increase considerably depending on the proximity of the indentation site to the underlying prestressed cytoskeleton. By application of appropriate loading conditions, the model presented in this paper could be used to compute cell deformation due to various mechanical stimuli *in vitro* in order to gain insight into the biomechanical origins of differences in observed cell response.

1. INTRODUCTION

Biomechanical models of adherent cells have generally taken two different approaches:

(i) attributing the primary structural role to the cytoskeleton, and thereby assuming a minimal role for other aspects of cellular composition [1,2,3].

(ii) treating the internal cytoplasm as a continuum and thereby assuming no role for the cytoskeleton in resisting deformation [4, 5].

Structural models of the cytoskeleton include open-cell foam models and stress-supported tensegrity (tensional-integrity) approaches. The tensegrity approach in particular has had considerable success in describing certain features of a cell's structural behaviour, such as the increase in stiffness with increasing applied forces [6], the non-linear effects of prestress on cell stiffness [7, 8], experimental observations of reorientation of the cytoskeleton and nucleus when integrin receptors on the cell surface are pulled [9]. Such observations support the view that rigid cytoskeletal networks distribute forces within the cell, possibly through a balance of compression in microtubules and tension in microfilaments. The alternative continuum approach has been used to model airway epithelial cells in a 2D finite element model [4], blood cells with a cortical membrane and viscous cytoplasm [5], and the deformation of a chondrocyte within its extracellular matrix [10].

Although some advances have been made in modelling the mechanical behaviour of adherent cells, we believe that models incorporating the main structurally-significant components of adherent cells would prove useful in exploring the biomechanical response of cells. Indeed, it has been suggested by Hochmuth [11] that "the modelling of cellular deformation in the future may combine elements of both continuum models and tensegrity models. This may be especially important for cells attached to surfaces at points of focal adhesion where molecular cross bridging occurs".

Atomic force microscopy (AFM; [12]) has become a valuable tool for studying biological materials [13]. It can be used to investigate the mechanical properties of adherent cells [14, 15, 16]. For example, indenting the cell surface with the AFM tip to measure the force required for a certain depth of indentation. Despite technical difficulties of such measurements [17, 18] replicating the indentation of the AFM probe in a structural model could, in principle, be used to confirm a biomechanical model of a cell. The primary objective of this study is to develop a finite element model of an adherent cell that includes all components likely to be of structural relevance, to develop a method that replicates cell indentation by a conical probe, and to quantitatively

confirm the model against experimental measurements of cellular elasticity measured using AFM.

2. METHODS

2.1 Model Geometry

A finite element model is developed to represent a spreading fibroblast adherent on a flat substrate, based on images of a spreading cell (Fig. 1).

Based on experimental observations [19], the volume of the cell is approximately 3,000 μm^3. The nucleus is formed from an ellipse with a major axis of 8 μm, minor axis of 5 μm, and a distance of 2 μm from the cell-substrate interface (Fig. 2a). Next the model comprises an internal cytoskeleton of tensile actin elements (Fig. 2b), and compressive microtubule elements (Fig. 2c), together with cytoplasm (Fig. 2d), and membrane (Fig. 2e) components. The cytoskeleton consists of a network of six compression-bearing struts (two in each orthogonal direction) and 24 tensional cables. These represent the aggregate behaviour of microtubules and microfilaments respectively. The end of each strut connects with four cables at 12 common nodes, which are also coincident with membrane and underlying cytoplasm nodes, and are therefore analogous to 'receptor' sites or adhesion complexes in adherent cells. The microtubule and microfilament elements are altered in length and position from what was an originally rounded tensegrity structure (Fig. 3) to fit the more spread cell shape (Fig. 2). New surface locations for the 'cytoskeleton' nodes are established by firstly determining the nodal positions that maintain the original vertical proportions of the internal structure in a rounded model, i.e. three horizontal planes (Fig. 4). Radial planes defined by the central axis and the original nodal positions are then established; the intersection of these planes with the surface of the new spread model yields lines along which the new nodal positions must lie. Points of intersection of these surface lines with the three horizontal planes established yield nine new nodal positions of the cytoskeleton when repositioned to conform to the spread shape.

The cytoplasm and nucleus elements are meshed with 8-node lower-order hexahedral elements. The membrane is meshed with 4-node shell elements. Microtubule struts (Fig. 2c) and microfilament cables (Fig. 2b) are meshed with single link elements (a three-dimensional spar element with bilinear stiffness matrix), compression-only and tension-only respectively.

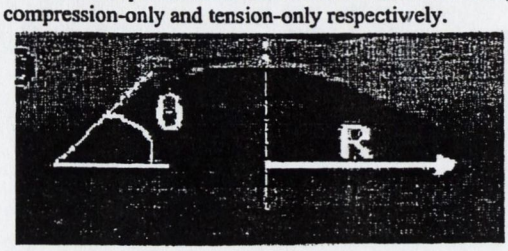

Figure 1. *Image of a spreading chick embryo fibroblast on a glass microplate for 3 hours. Adapted from [20].*

Figure 2. *Illustrating the development of the 3D finite element model of an adherent cell, incorporating a nucleus (a), network of microfilaments (b), microtubules (c), cytoplasm (d), and membrane (e). The dimensions of the model correspond to contact angle and radius highlighted in Fig. 1, i.e. contact radius (19.2 μm) and height (7.6 μm).*

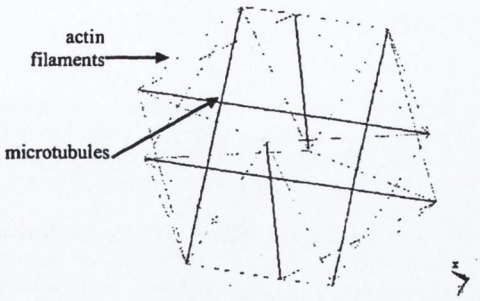

Figure 3. *3-dimensional tensegrity network of microtubules and microfilaments, representing the internal cytoskeleton.*

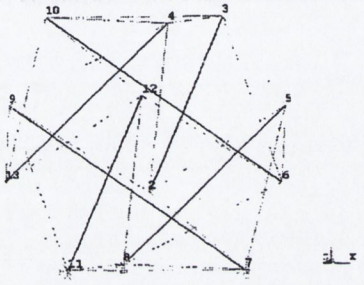

Figure 4. *A plane representing the cell-substrate interface is established by applying constraints to end nodes (7, 8 and 11 in this diagram) of three microtubule struts, one strut from each orthogonal direction. The nine unconstrained nodes lie on unconstrained horizontal planes; nodes 2, 6, 13 nearest the substrate, nodes 5, 9, 12 next, and nodes 3, 4, 10 farthest from the substrate. These nodes are re-positioned downwards to comply with the imposed spread shape to give the final configuration for a spread cell.*

Coincidence of nodes of the membrane, cytoplasm and cytoskeleton components is achieved through either re-sizing of the solid (and shell) elements or by slight re-positioning of the end-nodes of the cytoskeleton elements.

2.2 Constitutive modelling of cell elements

Material properties for each of the cell components are not known precisely and can only be estimated from various sources (Table 1). While generally accepted as being viscoelastic [6, 21], the cytoplasm and nucleus are treated here as linear elastic and isotropic continua. Although this is a simplification of the complex material behaviour of both components, it is considered sufficient for describing static mechanical response and avoids incorporation of unknown non-linear material behaviour. The elastic modulus is chosen as 100 Pa in accordance with values used in [4]. The nucleus has been reported as four times stiffer than the cytoplasm [21], and is therefore given a value of 400 Pa. The Poisson's ratio (v) for both nucleus and cytoplasm is

Component	Elastic modulus (Pa)	Poisson's ratio (ν)
Cytoplasm	100 *	0.37
Nucleus¶	400	0.37
Membrane†	10^3	0.3
Microtubules§	1.2×10^9	0.3
Microfilaments§	2.6×10^9	0.3

* 1×10^{-10} N/μm^2
¶ taken from [21]
†taken from [4]
§ taken from [23]

Table 1. *Elastic properties assigned to the components in the model.*

chosen initially as 0.37 [22]. In the model developed in [4], epithelial cell membrane elasticity was specified as 10^7 Pa, with a thickness of 6 nm. Since in that study it was concluded that the membrane elastic properties were over-estimated, a lower value of 10^3 Pa (with ν = 0.3) is chosen in the present model, while maintaining the same membrane thickness. The properties applied to the cytoskeleton components (Table 1) are based on elasticity values extracted from the flexural rigidity of microtubules and microfilaments subjected to thermal fluctuations [23]. On assumption of isotropy and homogeneity, microtubules and microfilaments are assigned cross-sectional areas (190 nm^2 and 18 nm^2 respectively) that correspond to the elasticity values in Table 1 [23].

2.3 Boundary conditions

2.3.1 Initial constraints

All nodes (shell and solid), at the cell-substrate interface, including the three nodes that establish the cell-substrate plane in each model (Fig. 4), are constrained in all three translational degrees of freedom, and are therefore analogous to focal adhesion sites in adherent cells. Initial constraints in each analysis involve application of a prestress (an initial strain to account for the contractile effect of acto-myosin sliding mechanisms) to the microfilament elements. This initial strain exerts tension on the other components of the model resulting in a prestressed structural stability. A baseline value of 1% strain is used, with 0.1% and 5% used also to investigate the effect of prestress.

2.3.2 Boundary conditions for confirmation of the model

Quantitative confirmation of the model is addressed by subjecting the model to loading conditions that replicate indentation by atomic force microscopy. Two approaches are adopted to simulate the indentation of an atomic force microscope probe into the surface of the model:

(i) application of a point load on a node to investigate differences between the point load and probe modelling methods (see (ii) below). Indentation depths resulting from a point load of 1 pN (applied to node A in Fig. 5) are compared

to the reaction forces that resist applied displacements on nodes (60 nm) in the same region of the mesh. Variations in compliance along the model surface are assessed by applying a larger indentation force of 50 pN to nodes at three points along the model surface (B - D in Fig. 5).

(ii) application of displacement boundary conditions to a number of nodes to better simulate the effect of an indenter. This allows comparisons with force-indentation curves obtained experimentally. Vertical displacement boundary conditions are chosen to reflect the actual geometry of a conical probe with a contact angle of 50^0 as it indents the cell surface. The prescribed displacement applied in modelling the probe, ranging from 50 – 100 nm, are applied to nodes in an area of the mesh that has been refined for that purpose (in the region of node A in Fig. 5). The reaction forces resisting these indentation constraints will yield force-deflection curves that can be used in determining local elasticity values through use of an appropriate theoretical relation.

2.4 Theoretical analysis of indentation

The problem of contact between isotropic elastic bodies was first addressed by Hertz [24], and later by Boussinesq [25]. Sneddon [26] followed Boussinesq's classical elasticity approach and developed expressions for the relation between load and infinitesimal indentation of a semi-infinite elastic material for several axisymmetric rigid indenter geometries. As derived by Sneddon [26], the total load F required for normal penetration δ of a cone of semi-vertical angle α is given by:

$$F=\frac{\pi \mu r^2}{(1-\upsilon)}\tan\alpha \qquad (1)$$

where $\mu=\frac{E}{2(1+\upsilon)}$ is the rigidity modulus, v is Poisson's ratio, and the contact radius r is related to indentation depth δ by:

$$r^2=\frac{4\,\delta^2}{\pi^2\tan^2\alpha}$$

Substituting for μ, and r gives the relation between force and indentation depth:

$$F=\frac{2E}{\pi(1-\upsilon^2)\tan\alpha}\delta^2 \qquad (2)$$

In the model developed in this paper, the axial component of the total reaction force at all nodes to which displacement constraints are applied is taken as equivalent to F (cell-substrate reaction forces are considered negligible in accordance with the assumption of infinite sample thickness used in the derivation of equations (1) and (2): see Sneddon [26]), δ is the applied indentation, and α is taken as 50^0. The expression cannot yield both the elastic modulus E and Poisson's ratio v from the force-deflection (F vs. δ) curves; v is therefore chosen to have a value of 0.37, identical to the underlying cytoplasm. Using eqn. (2), the reaction force versus applied indentation depths can then be used to determine E values.

3. RESULTS

Point load indentation [(i) above] computes elasticity values lower than those obtained by modelling the actual probe geometry [(ii) above]. An applied point load of 1 pN penetrates to a depth of 51.5 nm, whereas a reaction force of ~2 pN resists indentation constraints of 60 nm (Fig. 6). Proceeding with the (more realistic) probe modelling method it was found that applied indentations ranging from 50 - 100 nm are resisted by reaction forces ranging from 1 - 8 pN when a prestress value of 1% is used (see Fig. 7).

On relating these results to local elasticity estimates (eqn. 2) for three prestress values it is found that E values range from 0.6 to 1.4 kPa, with increases in elastic resistance as indentation depth increases (Fig. 8). Increases in the arbitrary prestress values also result in a tendency towards increases in elasticity at the point of indentation.

Point load application at locations B, C, and D (see Fig. 5) yield significant differences, there is a significant increase in rigidity if indentation occurs near to or at a receptor site. For example, in Fig. 9, node C is a receptor site and the indentation for 50 pN is ~34 μm, node B is ~6 μm from this receptor site and indentation is 116 μm with the same applied force.

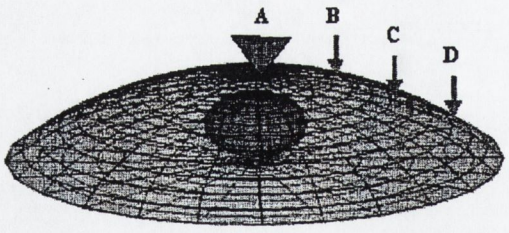

Figure 5. *Loading conditions used for model confirmation: prescribed displacements and a point load are both applied at location A in a refined area of the surface mesh, to allow comparisons between both methods. Point loads are also applied at locations B - D along the model surface (B and D are ~6 and 4 μm respectively from receptor node C).*

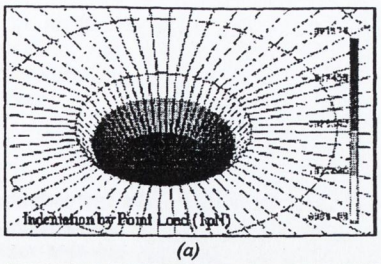

(a)

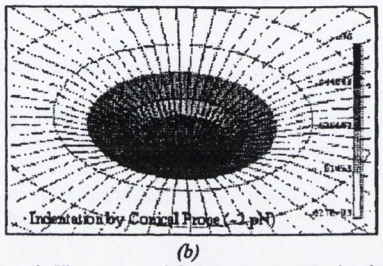

(b)

Figure 6. *Illustration of differences in point load and probe modelling methods: (a) a point load of 1 pN causes indentation depth of ~52 nm (0.0515 μm), and (b) applied indentation of 60 nm (0.06 μm) is resisted by a reaction force of ~2 pN, at the same location (node A).*

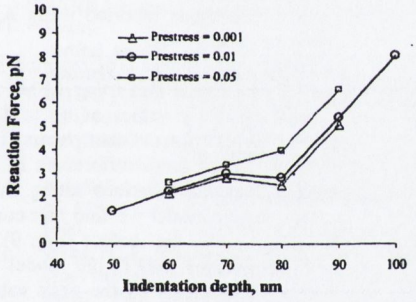

Figure 7. *Graph of indentation depth versus reaction force along the surface of the model for three arbitrary prestress values.*

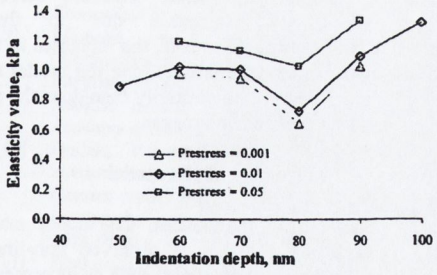

Figure 8. *Graphs of indentation depth versus local elasticity values along the surface of the model for three arbitrary prestress values.*

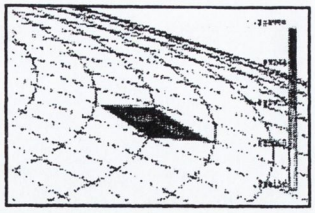

Node B: max. indentation = 116 μm

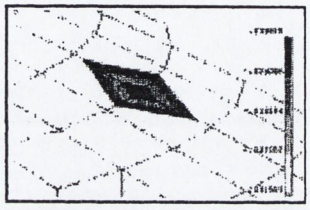

Node C: max. indentation = 34 μm

Node D: max. indentation = 55.5 μm

Figure 9. *Contour plots of displacements caused by application of a point load of 50 pN at nodes (B - D) along the model surface as illustrated in figure 6. Prestress value is 0.01 (1%).*

4. DISCUSSION

The finite element models developed in this paper can be viewed as a fusion of two previous approaches, the stress-supported tensegrity approach [2, 3] and the continuum approach [4, 5]. We attempt to account for the role of all structurally relevant components, while incorporating non-linear aspects of adherent cell behaviour that are due to the interconnected actin and microtubules in the cytoskeleton.

The material properties chosen to represent the cytoskeleton have been used in previous models [2], while similar values for flexural rigidity have been estimated theoretically [27], and are in agreement with other experimental work [28]. Also, Shin and Athanasiou [22] have reported a value of 0.37 for Poisson's ratio of an anchored osteoblast using a linear biphasic finite element analysis to curve-fit experimental data obtained by a cytoindentation method, while other experimental studies [29] and theoretical models [4] use values of up to >0.49 to describe cytoplasm incompressibility (it is considered composed of 70% water). Future parameter studies will suggest the influence of this value on cell structural behaviour.

A benefit of the modelling approach used in this paper is that the rearrangement performed on the tensegrity-based cytoskeleton reflects structural changes that occur within the cell during spreading. In living cells, the orientation, positioning and length of internal cytoskeletal components is altered by polymerisation, and by clustering of actin filaments [30]. During spreading adhesion bonds are formed between internal structural proteins (e.g. vinculin and talin) and extra-cellular proteins (e.g. fibronectin) that influence positioning of the internal components [31]. It has been suggested by Gittes [23] that to account for the seemingly excessively rigid mechanical properties measured, sliding and movement may occur between filaments and tubules. An additional justification for attributing a dominant role to the cytoskeleton is based on the hypothesis that many enzymes and molecules, which physically associate with the insoluble components of the cytoskeleton and the extracellular matrix, mediate cell function such as DNA or RNA synthesis, and signal transduction [31,32].

Regarding model confirmation, it was necessary to mesh the model with hexahedral elements that use linear shape functions since it was found that displacement boundary conditions applied to nodes of tetrahedral elements resulted in significant warping of those elements. Sweep meshing with hexahedral elements resulted in a nodal density on the top surface that was sufficiently refined for application of constraints that reflect the probe geometry at each indentation depth. Further refinement would lead to a greater number of nodes and hence increased accuracy, but was avoided due to technical difficulty and computational expense.

The validity of applying the expressions derived by Sneddon has been discussed by other authors [17]. The expressions are based on the assumption of infinite sample thickness. Since the indentation depths (<100 nm) are significantly less than the height of the cell model (~7000 nm), this condition is considered adequately satisfied. The load-indentation relation used here (eqn. 2) is in agreement with that used by both [13] and [16], but it seems to us that it has been reported erroneously in recent AFM publications [15, 29, 33]. It has, however, been suggested by Costa and Yin [17] that the assumption that strains are infinitesimal is not valid when applied via a conical or pyramidal tip with a contact angle of $<45^0$, suggesting that finite strains most likely occur in the contact region. Hence a large displacement contact analysis would perhaps more accurately reflect material behaviour on probe indentation. Considering Eqn. (2), the probe contact angle chosen for the analysis presented in this paper will have a significant bearing on elasticity results, but is in the range of angles (35^0 - 50^0) used in those experimental measurements to which comparisons are made in Section 4.1 below. The indentation depths applied via displacement constraints are also in the range of those applied experimentally, i.e. (from 10 – 100 nm in [29]), but the upper limit is restricted as the hexahedral elements begin to warp for $\delta > 110$ nm. Other limitations of the approach are related to the fact that elasticity under an indenting probe may be constantly changing, and that material behaviour is viscoelastic [6].

4.1 Comparisons with experimental AFM results

The point load modelling method yields lower values of elasticity than probe modelling (Fig. 6). It is therefore assumed that the point method is not satisfactory since the angle of contact is infinitesimally small when a point load is applied on a single node, and does not accurately reflect the geometry of the probe that transmits the indenting force.

Regarding the probe modelling method, the elasticity values obtained (Fig. 8; 0.6 - 1.4 kPa) from the indentation versus reaction force data (Fig. 7) are in the range of those determined experimentally for fibroblasts using micromanipulation (0.6 – 1 kPa) [34], using micropipette aspiration of chondrocytes (0.6 kPa) [35], and lower than those reported using AFM (2.1 – 8.8 kPa) on osteoblasts [33].

Charras and Horton [16] reported similar average values for osteoblasts also using AFM, while recording peak local elasticity values of up to 100 kPa due to presence of stress fibres. Other papers [15, 18, 33] have also reported such large differences in elasticity when probing at various locations along the cell surface. Similarly, in our model we find that compliance varies considerably along the surface (Fig. 9). Indentation at more rigid receptor sites in our model would result in elasticity values closer to the peak values reported in [16]. Increases in the prestress value applied to the microfilament elements in our model also result in significant increases in elasticity values (Fig. 8; it should be noted that, at an indentation location nearer to a receptor site, these prestress effects would be increasingly noticeable due to the underlying cytoskeleton). However, the increases in rigidity due to position of indentation along the model surface have a larger bearing on elasticity than does the prestress value within the microfilaments.

4.2 Future uses of the model

By altering parameters, the model may be used to explore the origin of observed non-linear aspects of adherent cell behaviour, such as increases in stiffness in spreading fibroblasts [19], contentious issues such as the proportion of compression borne by microtubules in adherent cells [36, 37], and the importance of cytoplasm incompressibility.

The response of adherent cells to mechanical stimuli of various kinds (substrate strain, fluid flow) in culture has been the subject of many studies, e.g. [38, 39]. It has never been possible to fully characterise the effect of various stimuli on cell deformation. Given that the present model has been confirmed against AFM experiments, loading conditions that reflect the mechanical strains imposed on adherent cells *in vitro*

may be applied to it, allowing computation of cell deformation and possible suggestions as to the biomechanical origins of differences in observed cell behaviour.

5. ACKNOWLEDGEMENTS

This work has been financed by BITES project (Biomechanical Interactions in Tissue Engineering and Surgical Repair) under the 5th EU framework, contract no. QLK3-1999-00559, and by the Programme for Research in Third Level Institutes, administered by the HEA.

6. BIBLIOGRAPHY

[1] Ingber, D.E., "Cellular Tensegrity: defining new rules of biological design that govern the cytoskeleton," *Journal of Cell Science*, 104, pp. 613-627, 1993.

[2] Stamenovic, D., and M.F. Coughlin, "A Quantitative Model of Cellular Elasticity Based on Tensegrity," *Journal of Biomechanical Engineering*, 122, pp. 39–43, 2000.

[3] Wendling, S., C. Oddou, and D. Isabey, "Stiffening Response of a Cellular Tensegrity Model," *Journal of Theoretical Biology*, 196, pp. 309–325, 1999.

[4] Kamm, R.D., A.K. McVittie, and M. Bathe, "On the Role of Continuum Models in Mechanobiology," *ASME Mechanics in Biology*, 242, pp. 1-11, 2000.

[5] Evans, E., and A. Yeung, "Apparent viscosity and cortical tension of blood granulocytes determined by micropipette aspiration," *Biophysical Journal*, 56, pp. 151-160, 1989.

[6] Sato, M., D.P. Theret, L.T. Wheelerm, N. Ohshima, and R.M. Nerem, "Application of the micropipette technique to the measurement of cultured porcine aortic endothelial cell viscoelastic properties," *ASME Journal of Biomechanical Engineering*, 112, pp. 263–268, 1990.

[7] Wang, N., K. Naruse, and D. Stamenovic, "Mechanical behaviour in living cells consistent with the tensegrity model," *Proc. of the National Academy of Sciences of the USA*, 98, 14, pp. 7765–7770, 2001.

[8] Stamenovic, D., and M.F. Coughlin, "The Role of Prestress and Architecture of the Cytoskeleton and Deformability of Cytoskeletal Filaments in Mechanics of Adherent Cells: a Quantitative Analysis," *Journal of Theoretical Biology*, 201, pp. 63–74, 1999.

[9] Maniotis, A., C. Chen, and D.E. Ingber, "Demonstration of mechanical connections between integrins, cytoskeletal filaments, and nucleoplasm that stabilise nuclear structure," *Proc. of the National Academy of Sciences of the USA*, pp. 849-854, 1994.

[10] Guilak, F., and V.C. Mow, "The mechanical environment of the chondrocyte: a biphasic finite element model of cell-matrix interactions in articular cartilage," *Journal of Biomechanics*, 33, 12, pp. 1663–1673, 2000.

[11] Hochmuth, R.M., "Micropipette aspiration of living cells," *Journal of Biomechanics*, 33, 1, pp. 15–22, 2000.

[12] Binnig, G., C.F. Quate, and C. Gerber, "Atomic Force Microscope," *Physical Review Letters*, 56, 9, pp. 930-933, 1986.

[13] Weisenhorn, A.L., M. Khorsandi, S. Kasias, V. Gotzos, and H. Butt, "Deformation and height anomaly of soft surfaces studied with an AFM," *Nanotechnology*, 4, pp. 106-113, 1993.

[14] Henderson, E., P.G. Haydon, and D.S. Sakaguchi, "Actin filament dynamics in living glial cells imaged by atomic force microscopy," *Science*, 257, pp. 1944-1946, 1992.

[15] Radmacher, M., M. Fritz, C. Racher, J.P. Cleveland, and P.K. Hansma, "Measuring the viscoelastic properties of human platelets with the atomic force microscope," *Biophysical Journal*, 70, pp. 556-567, 1996.

[16] Charras, G.T., and M.A. Horton, "Determination of cellular strains by combined atomic force microscopy and finite element modelling," *Biophysical Journal*, 83, pp. 858-79, 2002.

[17] Costa, K.D., and F.C. Yin, "Analysis of indentation: implications for measuring mechanical properties with the atomic force microscope," *ASME Journal of Biomechanical Engineering*," 121, pp. 462-471, 1999.

[18] A-Hassan, E., W.F. Heinz, M.D. Antonik, N.P. D'Costa, and S. Nageswaran, "Relative microelastic mapping by AFM," *Biophysical Journal*, 74, pp. 1564-1578, 1998.

[19] Thoumine, O., O. Cardoso, and J.J. Meister, "Changes in the mechanical properties of fibroblasts during spreading: a micromanipulation study," *European Biophysical Journal, EBJ*, 28, 3, pp. 222–234, 1999.

[20] Frisch, T., and O. Thoumine, "Predicting the Kinetics of Cell Spreading," *Journal of Biomechanics*, 35, pp. 1137 – 1141, 2002.

[21] Guilak, F., J.R. Tedrow, and R. Burgkart, "Viscoelastic properties of the cell nucleus," *Biochemical and Biophysical Research Communications* 269, 3, pp. 781-786, 2000.

[22] Shin, D., and K. Athanasiou. "Cytoindentation for obtaining cell biomechanical properties," *Journal of Orthopaedic Research*, 17, 6, pp. 880–890, 1999.

[23] Gittes, F., B. Mickey, J. Nettleton, and J. Howard, "Flexural Rigidity of Microtubules and Actin Filaments Measured from Thermal Fluctuations in Shape," *Journal of Cell Biology*," 120, 4, pp. 923–934, 1993.

[24] Hertz, H., "Uber den Kontakt elasticher korper," *Journal für die reine und angewandte Mathematik*, 92, pp. 156, 1881.

[25] Boussinesq, J., *Applications des Potentiels a l'Etude de l'Equilibre et du mouvement des Solides Elastiques*. Gauther-Villars, Paris, 1885.

[26] Sneddon, I.N., "The relation between load and penetration in the axisymmetric Boussinesq problem for a punch of arbitrary profile," *International Journal of Engineering Science*, 3, pp. 47-57, 1965.

[27] Ben-Avraham, D., and M.M. Tirion, "Dynamic and Elastic Properties of F-actin: a normal modes analysis," *Biophysical Journal*, 68, pp. 1231–1245, 1995.

[28] Tsuda, Y., H. Yasutake, A. Ishijima, and T. Yanagida, "Torsional rigidity of single actin filaments and actin bond breaking force under torsion measured directly by *in vitro* micromanipulation," *Proc. of the National Academy of Sciences of the USA*, 93, pp. 12937–12942, 1996.

[29] Mathur, A.B., A.M. Collinsworth, W.M. Reichert, W.E. Kraus, and G.A. Truskey, "Endothelial, cardiac muscle and skeletal muscle exhibit different viscous and elastic properties as determined by atomic force

microscopy," *Journal of Biomechanics*, 34, pp. 1545–1553, 2001.

[30] Mooney, D., L. Hansen, D.E. Ingber, "Cytoskeletal filament assembly and the control of cell shape and cell function by extracellular matrix," *Journal of Cell Science*, 108, pp. 2311-2320, 1995.

[31] Alberts, B., D. Bray, and J. Lewis. *Molecular biology of the Cell*. 2nd Edition, Garland publishing Inc., NY & London, 1989.

[32] Chen, C.S., and D.E. Ingber, "Tensegrity and mechanoregulation: from skeleton to cytoskeleton," *Osteoarthritis and Cartilage*, 7, pp. 81-94, 1999.

[33] Domke, J., S. Dannohl, W.J. Parak, O. Müller, W.K. Aicher, and M. Radmacher, "Substrate dependent differences in morphology and elasticity of living osteoblasts investigated by atomic force microscopy," *Colloids and Surfaces B: Biointerfaces*, 19, pp. 367–379, 2000.

[34] Thoumine, O., and A. Ott, "Time scale viscoelastic and contractile regimes in fibroblasts probed by microplate manipulation," *Journal of Cell Science*, 110, pp. 2109–2116, 1997.

[35] Guilak, F., W.R. Jones, H.P. Ting-Beall, and G. Lee, "The deformation behaviour and mechanical properties of chondrocytes in articular cartilage," *OARS, Osteoarthritis Research Society*, 7, 1, pp. 59–70, 1999.

[36] Heidemann, S.R., S. Kaech, R.E. Buxbaum, and A. Matus, "Direct observations of the Mechanical Behaviours of the Cytoskeleton in Living Fibroblasts," *Journal of Cell Biology*, 145, 1, pp. 109–122, 1999.

[37] Stamenovice, D., S.M. Mijailovich, I. Tolic-Norrelykke, J. Chen, and N. Wang, "Cell prestress. II. Contribution of microtubules," *American Journal of Physiology, Cell Physiology*, 282, 3, pp. C617–C624, 2002.

[38] Bakker, A.D., K. Soejima, J. Klein-Nulend, and E. Burger, "The production of nitric oxide and prostaglandin E_2 by primary bone cells is shear stress dependent," *Journal of Biomechanics*, 34, pp. 671–677, 2001.

[39] Owan, I., D. Burr, "Mechanotransduction in bone: osteoblasts are more responsive to fluid forces than mechanical strain," *American Journal of Physiology, Cell Physiology*, 273, 42, pp. 810 – 815, 1997.

A COMPUTATIONAL CELL MODEL REVEALS SIGNIFICANT DIFFERENCES IN BONE CELL DEFORMATION IN RESPONSE TO FLOW VS. STRAIN STIMULI

*McGarry, J G; **Klein-Nulend, J; **Mullender, M G; +*Prendergast P J,
+*Centre for Bioengineering, Department of Mechanical Engineering, Trinity College, Dublin, Ireland
pprender@tcd.ie

INTRODUCTION:

Differences in the response of bone cells to fluid shear stress and substrate strain stimulation applied *in vitro* have not been explained, and present a significant challenge to our understanding of how bone cells sense and respond to mechanical stimuli. In particular, human bone cells respond with increased prostaglandin E_2 (PGE_2) and nitric oxide (NO) release to fluid shear stress of magnitude equal to 0.6 Pa, but not to cyclic strain of magnitude 1000 με [1]. Explanation of the origins of these differences is hampered by the fact that the mechanical consequences of both stimuli on a cellular level remain unknown. We tested the hypothesis that these differences in cellular response to both stimuli are related to the amount of cellular deformation caused. For this purpose, we developed a computational cell model in order to compute the deformation of cells under fluid flow and strain loading conditions. By correlating the results to experimental findings, we can explore a basis for the origin of differences in cellular responses and show that the differences have a plausible mechanical origin.

METHODS:

Our approach to modeling sub-confluent monolayers of cells involves the assumption that individual cells were not constrained by neighboring cells. The volume and contact radius of the single-cell model developed are 3,000 μm^3 and 19.2 μm respectively (Fig. 1). The cytoskeleton is modelled as an interconnected network of 6 compressive struts and 24 tensile cables, representing the aggregate behaviour of microtubules and microfilaments respectively. These cytoskeletal elements alter in position and length from a rounded tensegrity structure to merge with nodes of the membrane and underlying cytoplasm (Fig. 1).

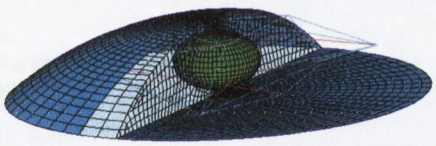

Figure 1: *Finite element model of an adherent cell comprising nucleus, microfilament, microtubule, cytoplasm and membrane components. Properties given in table 1 below.*

Component	Elasticity (Pa)	Poisson ratio
Cytoplasm [2]	100	0.37
Nucleus [3]	400	0.37
Membrane [2]	10^3	0.3
Microtubules [4]	1.2×10^9	0.3
Microfilaments [4]	2.6×10^9	0.3

Table 1: *Material properties of cell model components.*

Assuming rigid cellular attachments at the cell-substrate interface, boundary conditions to model the effect of substrate strain involved displacing each node at the lower membrane surface axially by 0.1%, and laterally by 0.03% (due to the Poisson effect). To model fluid flow effects it was assumed that the flow was laminar and streamlined along the cell surface. Total shear stress (0.6 $pN/\mu m^2$) was therefore distributed by applying tangential forces to surface nodes based on the surface area of each membrane element.

RESULTS:

The displacements in our model due to both fluid flow and strain loading conditions illustrate fundamental differences in the cellular deformation caused by both stimuli (Fig. 2). Maximum displacement due to strain is 19 nm at the cell-substrate interface, while fluid flow has a larger overturning effect on the bone cells (106 nm along the apical surface, Fig 2).

Fluid flow loading conditions also cause higher stress (expressed as % deformation; Fig. 3) in all cellular components, as compared to strain. Similarly, displacement of the membrane and cytoskeleton components is also higher in fluid flow (Fig. 3).

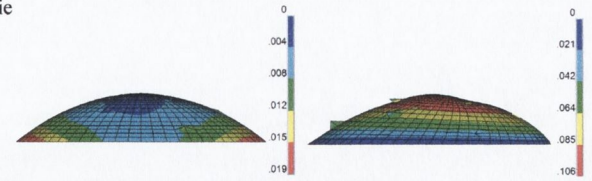

Figure 2: *Comparison of displacements (μm) in the cell due to 1000 με (left) and 0.6 Pa (right). Note the different scales.*

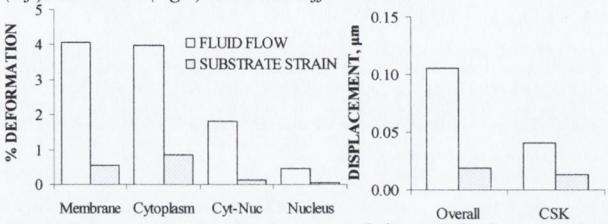

Figure 3: *Comparisons of deformation (left), and displacement (right) due to strain and fluid flow.*

DISCUSSION:

Our computational model is a fusion of complementary approaches: the tensegrity model and continuum model [5]. Our model results reveal that cellular deformation caused by fluid shear stress and strain *in vitro* are quite different – for the experimental magnitudes applied, fluid flow causes higher displacement and stressing of cellular components than strain. It seems that this is the first study to show just how different these stimulation magnitudes might be.

Since fluid flow causes increases in PGE_2 and NO release [1,6,7], it strongly suggests that release of these signaling molecules is likely caused by higher cellular deformation (and hence stimulation) in fluid flow. If (as this finding suggests) NO and PGE_2 release is deformation-dependent, then magnitudes of strain greater than 1000 με could elicit equivalent responses to those caused by the fluid flow. Indeed, this hypothesis has been confirmed in several studies; bone cells have been shown to respond with significant increases in NO release at 3,800 με, and in PGE_2 release at 4,000 με.

If higher deformation is directly related to NO and PGE_2 response, what then are the possible mechanisms involved? Considering each signaling molecule separately: (i) larger displacement of the cytoskeleton in fluid flow may be involved in increased PGE_2 release, as it has been shown that fluid-shear induced increases in COX-2 expression involve actin cytoskeleton reorganization [8] (COX-2 is a key enzyme for PGE_2 release); (ii) Higher NO response in fluid flow may be due to membrane stress – mechanically-induced NO results from ecNOS activity in bone cells [9]. ecNOS, an enzyme bound to the plasma membrane [10], may be stimulated by membrane deformation.

Our findings have implications for understanding bone remodeling: if the physiological estimates of fluid shear stress reported by others are correct (0.5-3 Pa, [11] and strain < 2,000 με, [12]), then the fact that strain values beyond physiological estimates are required to cause equivalent cellular deformations to those caused by fluid flow, provides a physical basis for fluid flow as a more effective means of stimulating bone cell activation, i.e. NO and PGE_2 signaling molecule release as these molecules have been shown to mediate adaptive bone formation *in vivo*. Our findings therefore support the hypothesis that fluid flow through the lacuno-canalicular porosity is a more potent stimulus for mechano-sensory function in bone tissue.

REFERENCES:

[1] Mullender et al. *Med Biol Eng Comp* 42,'04; [2] Kamm et al. *ASME Mech Biol* '00; [3] Guilak et al. *BBRC* 269,'00 ; [4] Gittes et al. *J Cell Biol* 120,'93; [5] Heidemann et al. *J Cell Biol* 145,'99; [6] Smalt et al. *AJP* 273,'97; [7] You et al. *J Biomech Eng* 122,'00; [8] Pavalko et al. *AJP* 275,'98; [9] Zaman et al. *JBMR* 14,'99; [10] Helfrich *JBMR* 12,'97; [11] Weinbaum et al. *J Biomech* 27,'94; [12] Burr et al. *Bone* 18,'96.

**ACTA-Vrije Universiteit, Amsterdam, The Netherlands.

CYTOSKELETAL MODULATION OF FLUID FLOW-INDUCED NO AND PGE_2 RELEASE IN OSTEOCYTES AND OSTEOBLASTS

*McGarry, J G; **Klein-Nulend, J; +*Prendergast P J
+*Center for Bioengineering, Trinity College, Dublin, Ireland.
pprender@tcd.ie

INTRODUCTION:

Fluid flowing through the lacuno-canalicular network is a likely stimulus for bone cell adaptive responses in bone remodeling. Nitric oxide (NO) and prostaglandin E_2 (PGE_2) are both essential mediators of mechanically induced bone adaptation [1,2]. Although it is clear that both osteoblasts and osteocytes respond to fluid shear stress with increased NO and PGE_2 release the mechanisms involved need further investigation. As the cytoskeleton (CSK) is likely involved in the transduction of external mechanical forces to biochemical response, in the present study, we tested the hypothesis that both the actin and microtubule CSK are involved in pulsatile fluid flow (PFF) induced NO and PGE_2 release by both osteoblastic and osteocytic cells.

METHODS:

Osteocytic MLO-Y4 (OCY) and osteoblastic MC3T3-E1 (OB) cells were plated at $5x10^5$ cells per glass slide and incubated for 24 hr in α-MEM containing 10% fetal bovine serum (FBS). Prior to PFF stimulation, cells were incubated for 1 hr in α-MEM containing 2% FBS with 1 μM of CSK disrupting agents; cytochalasin B and colchicine to disrupt actin and microtubule polymerization, respectively. Untreated, actin-disrupted, or microtubule-disrupted cells were either subjected to 3 or 5 Hz (0.4 – 0.6 Pa) PFF for 10 min in a parallel plate chamber or kept as static controls. After stimulation, cells were stained with FITC-phalloidin, a fluorescent label that binds to an anti-body directed against actin, such that changes in the actin CSK due to PFF and CSK disruption could be visualized. NO accumulated in the medium was measured as nitrite (NO_2^-) using the Griess reagent. PGE_2 release was measured by enzyme immunoassay, using an anti-body raised against mouse PGE_2. Differences between groups were tested using the Mann-Whitney U test.

RESULTS:

Applying PFF to OCYs and OBs (Fig. 1A-D) increased formation of actin bundles/stress fibers (SFs) and parallel alignment of SFs – 36±11% of OCYs, and 73±7% of OBs exhibit this 'combed' appearance (mean ± SEM, n=4). Actin or microtubule disruption reduced SF alignment in OBs (12±4% and 11±5% respectively), but caused actin clustering at adhesion sites. OCY actin disruption reduced cell body size, yielding rounded stellate morphologies extending thinner actin-rich processes and reduced alignment of SFs in PFF (10±0.3%). Disrupting OCY microtubules caused slight ruffling of actin boundaries and caused a slight decrease in number of cells with aligned SFs (26±4%).

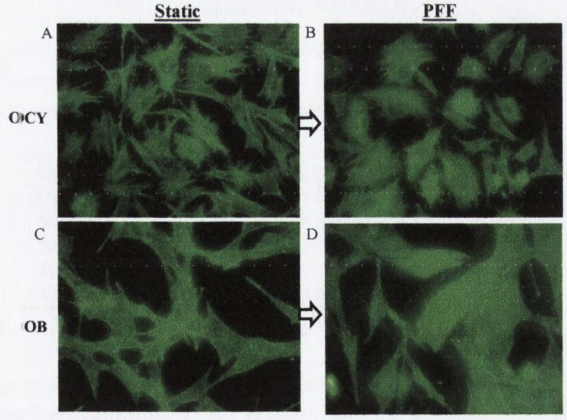

Figure 1: *The effect of PFF on actin CSK in OCY and OB cells (400 x).*

In OCYs, a significant PFF-induced increase in NO release did not require intact actin, and was further increased by disruption of microtubules (Fig. 2A). The PFF-induced PGE_2 response in OCYs required both intact actin and microtubules (Fig. 2B). In OBs, PFF-induced NO release was inhibited by disrupting actin only (Fig. 2C). PFF-induced PGE_2 release in OBs was only observed when either the actin or microtubule CSK was disrupted (Fig. 2D).

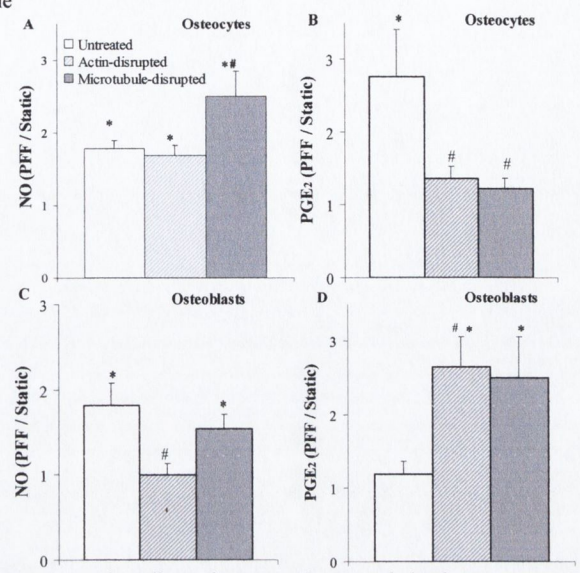

Figure 2: *The effect of actin and microtubule disruption on PFF-induced NO and PGE_2 release in osteocytes (A,B) and osteoblasts (C,D). *significantly > 1, # different from untreated, mean ± SEM, $p<0.05$.*

DISCUSSION:

Many of these OB and OCY early responses to PFF agree with earlier findings [3-5]. However, the effect of actin and microtubule disruption reveal: (i) differences in NO and PGE_2 release in both cell types; and, interestingly, (ii) opposite CSK effects on OB and OCY responses.

While we can say that SF formation and alignment may be involved in PFF-induced NO response, this can not explain the 'mechanism' by which the CSK modulates OCY and OB responses. For example, SF alignment may be required for NO release in OBs, but PGE_2 release appears independent of alignment. Rather, the increased PFF-induced PGE_2 in OBs is more likely related to actin clustering at focal adhesions upon CSK disruption (also seen in [6]). Also, the differences in CSK modulation of OCY and OB responses may be related to CSK composition. The significant effect of actin disruption in OCYs (also observed in [7]) indicates that OCY structure is largely dependent on actin, the disruption of which can render the membrane incapable of maintaining tension [7]. This in turn can adversely affect ion channel activity [8]. Indeed, stretch-activated cation channels are involved in mechanically-induced PGE_2 release in OCYs [9], which may explain inhibition of PGE_2 in OCYs but not OBs, as we have observed.

The opposite effects of CSK disruption on PGE_2 response in OBs and OCYs can also be related to the fact that blocking shear/stretch cation channels abolishes mechanically-induced responses (e.g. PGE_2) release in OCYs, but only slightly reduces PGE_2 release in OBs [9]. The greater dominance of these channels in OCYs suggests that a consequence of CSK disruption may be altered shear/stretch cation channel activity, leading to the differences in PGE_2 response in OBs and OCYs as observed here. Additionally, the fact that blocking these channels also alters NO release [9] points to the same mechanism, i.e. CSK disruption may modulate NO release via PFF-stimulated shear/stretch cation channels. Hence, while remaining mindful of the different signaling pathways involved in PGE_2 and NO response, we suggest that CSK disruption modulates OCY and OB responses to PFF by altering mechanosensitivity [10], in particular shear/stretch ion channel activity.

REFERENCES:

[1] Turner, *AJP* 270,'96; [2] Forwood, *AJP* 11,'96; [3] Burger, *FASEB J* 13,'99; [4] Ajubi, *BBRC* 225,'96; [5] Norvell, *J Appl Physiol* 96,'04; [6] Ponik, *J Appl Physiol* 97,'04; [7] Kamioka, *JBMR* 13,'98; [8] Duncan, *AJP* 267,'94; [9] Rawlinson, *Bone* 19,'96; [10] Wang, *Science* 260,'93.

**ACTA-Vrije Universiteit, The Netherlands.

A BIOMECHANICAL CELL MODEL REVEALS THE IMPORTANCE OF DEFORMATION IN THE RESPONSE OF BONE CELLS TO MECHANICAL STIMULI

*McGarry, J G; **Klein-Nulend, J; **Mullender, M G; +*Prendergast, P J
+Centre for Bioengineering, Trinity College Dublin, Ireland

Introduction

Several studies have reported that bone cells respond differently to physiological levels of fluid flow and strain mechanical stimuli *in vitro*. In particular, osteoblasts respond to physiological fluid shear stress with increased PGE_2 and NO release [1]. In contrast, applying physiological strains was found to increase collagen I production, but does not alter PGE_2 or NO release. Further explanation of the origins of these differences is hampered by the fact that the biomechanical effects of both stimuli on a cellular level remain unknown. To investigate if the cellular deformation as a result of both stimuli is related to differences in bone cell responses, we developed a novel computational cell model, and used this model to compute cellular deformation under both fluid flow and strain loading conditions.

Materials and Methods

The volume and contact radius of the model (fig. 1) are 3,000 μm^3 and 19.2 μm respectively. The cytoskeleton is modelled as an interconnected network of 6 compressive struts and 24 tensile cables, representing the aggregate behaviour of microtubules and microfilaments. Cytoskeletal elements alter in position and length from a rounded tensegrity structure to merge with nodes of the membrane and underlying cytoplasm.

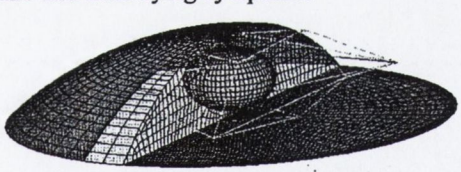

Figure 1: Three-dimensional computational model of an adherent cell comprising nucleus, microfilament, microtubule, cytoplasm and membrane components.

Component	Elasticity (N/μm^2)	Poisson ratio
Cytoplasm [2]	$1x10^{-10}$	0.37
Nucleus	$4x10^{-10}$	0.37
Membrane [2]	10^{-9}	0.3
Microtubules [3]	$1.2x10^{-3}$	0.3
Microfilaments [3]	$2.6x10^{-3}$	0.3

Table 1: Material properties of cell model components.

Assuming rigid cellular attachments at the cell-substrate interface, boundary conditions to model the effect of substrate strain involve displacing each node at the lower membrane surface axially by 0.01% and laterally by 0.003%. To model fluid flow effects it is assumed that flow acts tangentially along the cell surface. The total shear stress (0.6 pN/μm^2) is distributed by applying forces to modes based on the surface area of each membrane element.

Results

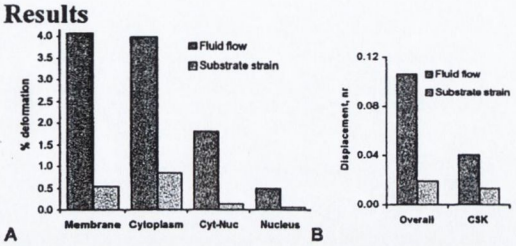

Figure 2: Comparisons of (A) deformation, and (B) displacement due to physiological strain and fluid flow.

Fluid flow loading conditions cause higher stresses (expressed as % deformation; fig. 2A) in all cellular components, as compared to strain. Similarly, displacement of the membrane and cytoskeleton components is also higher in fluid flow (fig. 2B).

Discussion

Our novel cell model is a fusion of contrasting tensegrity and continuum approaches [4]. When related to the experimental findings [1] our model results indicate that increases in PGE_2 and NO release are caused by higher cellular deformation and hence stimulation in fluid flow. If, as our findings suggests, signaling molecule production is deformation-dependent, then higher magnitudes of strain could elicit equivalent responses to those caused by physiological fluid flow. Indeed, bone cells have been shown to respond with significant increases in NO release at 3,800 $\mu\varepsilon$, and in PGE_2 release at 4,000 $\mu\varepsilon$.

Conclusion

Our findings reveal that cellular deformation caused by physiological fluid flow and strain can not be considered equivalent. Assuming the physiological estimates are reasonable, our finding that NO and PGE_2 release is deformation-dependent indicates that threshold levels of stimulation provided only by fluid flow are required for activating mechanosensory function in bone remodeling.

References

[1] Mullender *et al*, Med. Biol Eng. Comp.,42:14-21, 2004.
[2] Kamm *et al*, ASME Mechanics in Biology 242: 2000.
[3] Gittes *et al*, J. Cell Biol. 120, 4: 923-934, 1993.
[4] Stamenovic *et al*, J. Appl. Physiol. 89: 2085-90, 2000.

Acknowledgement
Funded by EU BITES project (QLK3-1999-00559).

Affiliations: +P.J. Prendergast, *Centre for Bioengineering, Dept. of Mechanical Engineering, Trinity College, Dublin; Email: pprender@tcd.ie
**Dept. Oral Cell Biology, ACTA-Vrije Univeriteit, Amsterdam.
Keywords: bone biology; bone biomechanics